

UNITED KINGDOM · CHINA · MALAYSIA

Division of Drug Delivery and Tissue Engineering

School of Pharmacy

Synthesis, Characterisation and Applications of New Polyesters for Drug Delivery

Deepak Kakde

Thesis submitted to the University of Nottingham for the degree of Doctor of Philosophy

OCTOBER 2016

Abstract

In recent years, a number of reports have focused on the use of polyesters in drug delivery due to their intrinsic biocompatibility and biodegradability. In this thesis, aliphatic polyesters were synthesized by polycondensation reaction and ring opening polymerization reactions. The properties of the polymers and drug delivery potential of the resultant materials were evaluated.

In the polycondensation reactions, a series of aliphatic polyesters of similar molecular weight were synthesized by reacting 1,10-decanediol with different ratios of succinic acid/phenylsuccinic acid and the effects of phenyl group side-chain substitution on polymer properties was investigated. A solvent-free melt polycondensation method using scandium (III) triflate as catalyst at an industrially relevant temperature (120 °C) was used. As the phenyl content increased, the polymers changed from semicrystalline to amorphous in state. The loading capability of polymers was checked by formulating nanoparticles containing coumarin 6 as a fluorescent dye analogue of active drugs. A polymer with a 70/30 ratio of succinic acid and phenylsuccinic acid showed the highest dye loading among the set of materials synthesised. This polymer was found to be degradable over time under selected experimental conditions. Amphiphilic block co-polymers from the Pluronic^{TM} class were used to stabilize, in PBS, nanoparticles formed

from these polyesters by nanoprecipitation routes. The metabolic activity, cell membrane integrity and lysosomal functions of C3A cells dosed with the polymers were determined to observe the cytocompatibility of the highest dye-loaded nanoparticles. Activity relative to undosed C3A cells was retained at more than 80% in the all of the assays. Imaging of Pluronic coated and uncoated nanoparticles in C3A cells suggested that both types of the nanoparticles were endocytosed in the early stage of the study (within 10 min). The internalization of nanoparticles was increased progressively over the study time. These results indicated the possible utility of the selected polymers in diagnostic and delivery applications.

Ring opening polymerization (ROP) reactions were used for the synthesis of a diblock (mPEG-b-PεDL) and a triblock (PεDL-b-PEG-b-PεDL) copolymer from a seven membered ε-decalactone (ε-DL) monomer obtained from renewable sources. A diblock (mPEG-b-PεDL) copolymer was compared with structurally similar mPEG-b-PCL copolymer synthesized via ROP of ε-caprolactone (ε-CL) monomer, which can be considered as a non-renewable monomer. A six membered δ-decalactone (δ-DL) was also used for the synthesis of a diblock copolymer (mPEG-b-PδDL) to compare the reaction kinetics and properties of the copolymers. The copolymers were prepared via bulk polymerisation using 1,5,7-Triazabicyclo[4.4.0]dec-5-ene (TBD) as a metal-free catalyst to replace the conventionally used stannous octoate [$Sn(Oct)_2$]. A higher polymerization efficiency was achived with TBD

compared to $Sn(Oct)_2$ catalyst. However, a notable difference in the reaction temperature required for ε-DL and δ-DL polymerization was observed. The comparison with a structural analogue, i.e. ε-CL, demonstrated that the ε-DL polymerization was inhibited due to the presence of the alkyl chain of ε-DL monomer. However, a higher reaction time (12 h for TBD and 24 h for $Sn(Oct)_2$) in CROP of ε-DL was addressed by using microwave based ring opening polymerization (MROP) reaction.

The MROP was adopted as a 'green' and cheap heating method alternative to conventional heating (CROP) for the synthesis of mPEG-b-PεDL diblock copolymers using TBD as a catalyst. All the reactions were conducted in bulk. The MROP was designed based on the dielectric properties of all the reacting materials, as it was found that ε-DL monomers showed good absorption of MW radiation ($\tan\delta>0.5$). Accordingly, MROP resulted in a higher rate of ε-DL polymerization compared to CROP but comparison of the synthesis of mPEG-b-PCL copolymer by MROP indicated that the presence of the alkyl chain in ε-DL monomer significantly reduced the rate of polymerization.

The synthesized mPEG-b-PεDL copolymer was investigated as a potential drug delivery vehicle for solubilization and controlled delivery of indomethacin. The indomethacin loading and release from mPEG-b-PεDL micelles (amorphous core) was compared against well-established mPEG-b-PCL micelles (semicrystalline core). The drug-polymer compatibility was also

determined through a predictive computational approach to access the drug solubilisation (or drug loading) into hydrated micelles. The micelles were prepared by solvent evaporation method and characterized for size, morphology, indomethacin (IND) loading and release. Both of the micelle formulations showed a uniform distribution of spherical micelles with size <60 nm. However, a significantly higher size of empty mPEG-b- PεDL micelle was observed compared to mPEG-b-PCL micelles. A higher compatibility of the drug was predicted with PCL core as determined by modified Flory-Huggins interaction parameters (χ_{sp}) using the Hanson solubility parameter (HSP) approach. The compatibility of the drug was determined for both of the segments (hydrophilic and hydrophobic) of the copolymers and found to be in the order of χ_{sp} (PεDL)> χ_{sp} (mPEG)> χ_{sp} (PCL). The predictions suggested that more IND should encapsulate within the micelles with PCL core compared to PDL core, but the IND loading experiments revealed an overall higher loading in PεDL core (6.55 wt%) compared to PCL core (5.39 wt%) ($P < 0.05$, unpaired student's t-test). However, consideration of the IND loading per unit volume of the micelles revealed that the PCL cored micelles was able to load 1.5 times more compared to the PεDL cored micelles. This result illustrated the higher compatibility of the IND with PCL core in accordance with the solubility parameter calculations. These data also suggested that the overall higher IND loading in PεDL core was attributable to the amorphous nature of the core which increased the core

volume by 1.81 times compared to the PCL core. Drug release studies showed the sustained release pattern from both of the micelle systems although the semicrystalline PCL core (80% drug release in 110 h) was able to release the drug for a longer period compared to PεDL core (80% drug release in 72 h). Cell viability tests demonstrated the cytocompatibility of the mPEG-b-PεDL polymer. The micelles were internalized effectively in the early stages of the study and progressively increased with time.

The results of the present thesis suggested that novel aliphatic polyester can be good candidates for the drug delivery applications and further studies can explore the possible applications of these polymers in the biomedical field.

Contents

Abstract ..... **i**

List of Figures ..... **xi**

List of Tables ..... **xxi**

List of Schemes ..... **xxiii**

Acknowledgement ..... **xxiv**

Abbreviation List ..... **xxv**

1. Introduction

1.1 Introduction 1

1.2 Synthesis of Polymers 4

1.2.1 Polycondensation 4

1.2.2 Ring Opening Polymerization (ROP) 9

1.2.3 Microwave based Synthesis of Polyesters 12

1.3 Polymeric Micelles in Drug Delivery 21

1.3.1 Micelles Preparation Procedures 23

1.3.2 Factors Affecting Drug Loading 28

1.3.3 Drug Release from Micelles 34

1.3.4 Stability of Micelles 37

1.3.5 Pharmaceutical Applications 39

1.4 Aim and Objectives 43

1.5 References 45

2. Materials and Methods

2.1 Materials 53

2.2 Instruments and Methods 54

2.2.1 Fourier Transform Infrared (FTIR) Spectroscopy 54

2.2.2 Nuclear Magnetic Resonance (NMR) 54

2.2.3 Size Exclusive Chromatography (SEC) 55

2.2.4 Differential Scanning Colorimeter (DSC) 55

2.2.5 Dynamic Light Scattering (DLS) and Zeta Potential 55

2.2.6 Transmission Electron Microscopy (TEM) 56
2.2.7 Fluorescence Spectroscopy 57
2.2.8 Ultraviolet-Visible Spectroscopy (UV/Visible) 57
2.2.9 CEM Discover Microwave Reactor 57
2.3 Critical Micelle Concentration (CMC) Determination 57
2.4 Drug Content and Encapsulation Efficiency 59
2.5 References 60

3. Synthesis, Characterisation and Evaluation of Novel Linear Polyesters

3.1 Introduction 62
3.2 Methods 65
3.2.1 Synthesis and Characterisation of Polymers 65
3.2.2 Empty and Dye-Loaded Nanoparticle Formulations 72
3.2.3 Characterisation of Nanoparticle Formulations 74
3.2.4 Degradation Study of P02 Polymeric Nanoparticle 75
3.2.5 C3A Cell Culture 75
3.2.6 Cell Viability Assessment 75
3.2.7 Cell Uptake Study 77
3.3 Results 79
3.3.1 Synthesis and Characterisation of Polymers 79
3.3.2 Preparation and Characterisation of Nanoparticles 88
3.3.3 Degradation Study of P02 Nanoparticle Formulation 92
3.3.4 Impact of Nanoparticles on C3A Cell Activity 93
3.3.5 Cellular Uptake of Nanoparticles by C3A Cells 94
3.4 Discussion 99
3.5 Conclusion 109
3.6 References 110

4. Synthesis and Characterisation of Homopolymers and Block Copolymers of ε-Decalactone (ε-DL) by Ring Opening Polymerisation (ROP)

4.1 Introduction..... 114
4.2 General Synthesis Method for ε-Decalactone (ε-DL) Polymers..... 119
4.2.1 Synthesis of ε-Decalactone (ε-DL) Homopolymers..... 119
4.2.2 Synthesis of ε-Decalactone (ε-DL) Copolymers..... 120
4.2.3 Synthesis of δ-Decalactone (δ-DL) Copolymers..... 122
4.2.4 Synthesis of ε-Caprolactone (ε-CL) Copolymer..... 123
4.2.5 Copolymerisation of ε-Decalactone and ε-Caprolactone with mPEG (ABC type copolymer)..... 124
4.3 Results..... 125
4.3.1 Homopolymers of ε-Decalactone (ε-DL)..... 125
4.3.2 Copolymers of ε-Decalactone (ε-DL)..... 134
4.3.3 Copolymers of δ-Decalactone (δ-DL)..... 143
4.3.4 Copolymers of ε-Caprolactone (ε-CL)..... 149
4.3.5 mPEG-b-PCL-b-PεDL (ABC) Copolymer by Sequential Addition of ε-Caprolactone (ε-CL) and ε-Decalactone (ε-DL)..... 155
4.4 Discussion..... 159
4.5 Conclusion..... 166
4.6 Reference..... 166

5. Microwave Assisted Synthesis of ε-Decalactone based Copolymers and Evaluation of the Properties of the Copolymers

5.1 Introduction..... 170
5.2 Experimental Methods..... 173
5.2.1 Measurement of Dielectric Properties..... 173
5.2.2 Microwave Assisted Ring Opening Polymerisation (MROP)..... 174
5.2.3 Determination of Critical Micelle Concentration (CMC) of Copolymers..... 176
5.2.4 Preparation of Blank and Coumarin 6 loaded mPEG-b-PεDL and mPEG-b-PCL Micelles..... 177
5.2.5 Characterization of the Micelles..... 178
5.2.6 Cytotoxicity and Cell Uptake Study..... 179
5.3 Results..... 179

5.3.1 Measurement of Dielectric Properties of the Reagents 179
5.3.2 Microwave Assisted Ring Opening Polymerisation (MROP) 183
5.3.3 Determination of CMC of the Block Copolymers 191
5.3.4 Preparation and Characterization of Blank and Loaded Micelles 193
5.3.5 Cytotoxicity and cell uptake study..... 196
5.4 Discussion 199
5.5 Conclusions 206
5.6 References 207

6. Self-Assembly of Poly (ε-decalactone) based Copolymer Micelles for Delivery of Indomethacin

6.1 Introduction..... 211
6.2 Methods 213
6.2.1 Determination of Solubility Parameters of Drug and Copolymers 213
6.2.2 Preparation of Blank and Indomethacin Loaded Micelles 215
6.2.3 Characterization of the Micelles 218
6.2.4 Stability Studies of the Micelles 219
6.2.5 Degradation Study of Micelles 219
6.2.6 *In Vitro* Indomethacin Release Study 220
6.3 Results..... 221
6.3.1 Solubility Parameters of Drug and Copolymers 221
6.3.2 Preparation and Characterization of Blank and Indomethacin Loaded Micelles 222
6.3.3 *In Vitro* Indomethacin Release..... 229
6.4 Discussion 231
6.5 Conclusions 238
6.6 Appendix..... 239
6.7 References 240

7. Conclusions and Future Work

7.1 Conclusions 244
7.2 Future Work 246

List of Figures

Figure 1-1 Types of polyester polymers (A) linear diblock, (B) linear triblock, (C) branched, (D) multiblock block and (E) dendritic polyester.....2

Figure 1-2 Preparation of polyesters by stepwise polycondensation method. Reproduced from reference[1] 5

Figure 1-3 Chemoselective polycondensation of diols and diacids under mild condition. Reproduced from reference [17].....7

Figure 1-4 Mechanism of acid catalyzed Fischer esterification reaction of diacid and diol. Reproduced from reference [22] 8

Figure 1-5 Ring opening polymerization of lactone ring by anionic mechanism. Reproduced from reference[6].....10

Figure 1-6 Organometallic (M) catalyzed ring opening polymerization of lactones in the presence of nucleophiles (Nu). Reproduced from reference[24] 10

Figure 1-7 Ring opening polymerization in presence of stannous octoate (A) and (B) stannous octoate initiator (C) Deactivation of catalyst by water (D) coordination insertion of monomer into stannous alkoxide and (E) chain transfer to unreacted alcohol. Reproduced from reference.[29].....12

Figure 1-8 Microwave based synthesis of poly(butylene succinate) polymer. Reproduced from reference.[37] 14

Figure 1-9 Polycondensation of lactic acid by Microwave and conventional methods. Reproduced from reference.[38] 15

Figure 1-10 Reaction rate constant (kp) determination for microwave and conventional (FCH) method. Reproduced from reference.[44] 17

Figure 1-11 MROP of ε-CL catalyzed by zinc oxide in the presence of ionic liquid. Reproduced from reference [49] 19

Figure 1-12 Synthesis of PLLA-PEG-PLLA triblock copolymer by MROP. Reproduced from reference [50] 19

Figure 1-13 Synthesis of mPEG-PLLA diblock copolymers by MROP. Reproduced from reference [51] 20

Figure 1-14 Synthesis of PHA-b-PLA diblock copolymer by MROP. Reproduced from reference.[55] 21

Figure 1-15 Micelles preparation by flash nanoprecipitation method using impinging jets mixer (CIJM) and the multi-inlet vortex mixer (MIVM). Reproduced from reference[77] 26

Figure 2-1 Fluorescence spectra of pyrene in (A) different polarity solvents (water and hexane) (B) in presence of block copolymer with different concentrations in water 59

Figure 3-1 Pictorial representation of preparation and characterisation of nanoparticles 74

Figure 3-2 Comparative ^{1}H NMR spectra of monomers and synthesised polyesters with different phenyl contents (1) P01 polymer (2) P02 polymer (3) P03 polymer (4) P04 polymer (5) P05 polymer (6) 1, 10-Decanediol (7)

Succinic acid (8) Phenylsuccinic acid. *Chloroform residue, **Methanol residue, *** Water residue, ****DMSO residue. 82

Figure 3-3 Comparative ^{1}H-^{1}H COSY NMR spectra of (A) Polymer with no phenyl contents (P01) and (B) Polymer with highest phenyl content (P05). 83

Figure 3-4 Comparative ^{13}C NMR spectra of synthesised polyesters with different phenyl contents (1) P01 polymer (2) P02 polymer (3) P03 polymer (4) P04 polymer (5) P05 polymer 84

Figure 3-5 Comparative FTIR spectra of synthesised polyesters with different phenyl contents (1) P01 polymer (2) P02 polymer (3) P03 polymer (4) P04 polymer (5) P05 polymer 85

Figure 3-6 DSC graph showing (A) glass transition temperature (T_g) (B) melting temperature (T_m) (C) crystallization temperature (T_c) of synthesised polyester polymers from P01 to P05..... 87

Figure 3-7 Coumarin 6 loading (wt% to polymer) in different copolymers. Each point represents mean ± SD (n=3). A significant difference ($P < 0.05$, unpaired student's t test) was observed. P02*: Pluronic coated P02 nanoparticles 90

Figure 3-8 Stability of nanoparticle in HPLC water and PBS (A) Uncoated P02 nanoparticle in HPLC water (B) Uncoated P02 nanoparticle in PBS (C) Pluronic coated P02 nanoparticle in HPLC water (D) Pluronic coated P02 nanoparticle in PBS..... 91

Figure 3-9 TEM images of uncoated (A) and pluronic coated nanoparticles (B). The images were taken without staining. Scale bar – 1000nm. 91

Figure 3-10 Loss in molar mass (M_n) of P02 nanoparticles (A) and polydispersity index (B) with time (days) in presence and absent of *Pseudomonas cepacia* lipase (0.2 mg/mL) at 37 °C..... 92

Figure 4-1 Structure of lactone monomers derived from renewable materials 115

Figure 4-2 Structures of epsilon decalactone and epsilon caprolactone monomers 118

Figure 4-3 ^{1}H NMR spectra of Benzyl-PεDL before and after conversion.. 127

Figure 4-4 ^{1}H NMR spectra of Benzyl-PεDL acquired in $CDCl_3$ (**Solvent peak). 129

Figure 4-5 ^{1}H NMR spectra of Propargyl-PεDL acquired in $CDCl_3$ (**Solvent peak). 129

Figure 4-6 ^{13}C NMR spectra of Benzyl-PεDL acquired in $CDCl_3$ (*Solvent peak). 130

Figure 4-7 ^{13}C NMR spectra Propargyl-PεDL acquired in $CDCl_3$ (*Solvent peak). 130

Figure 4-8 Differential scanning calorimetry (DSC) plot of Benzyl-PεDL homopolymer. 131

Figure 4-9 SEC traces of (A) Propargyl-PεDL homopolymer and (B) Benzyl-PεDL homopolymer 132

Figure 4-10 ^{1}H NMR and GPC of unpurified mPEG-b-PεDL copolymer (A and B), GPC of purified mPEG-b-PεDL copolymer (C)..... 137

Figure 4-11 Kinetic analysis of ε-decalactone polymerisation from mPEG5K at 120 °C (A) TBD catalyst (B) $Sn(Oct)_2$ catalyst..... 138

Figure 4-12 ^{1}H NMR spectra of mPEG-b-PεDL copolymer acquired in $CDCl_3$ (*Solvent peak). 139

Figure 4-13 ^{1}H NMR spectra of PεDL-b-PEG-b-PεDL acquired in $CDCl_3$ (*Solvent peak). 139

Figure 4-14 ^{13}C NMR spectra of mPEG-b-PεDL acquired in $CDCl_3$ (*Solvent peak). 140

Figure 4-15 ^{13}C NMR spectra of PεDL-b-PEG-b-PεDL acquired in $CDCl_3$ (*Solvent peak). 140

Figure 4-16 ^{1}H-^{1}H COSY NMR spectra of mPEG-b-PεDL acquired in $CDCl_3$. 141

Figure 4-17 Retention times of the initiators and copolymers of the ε-decalactone. 141

Figure 4-18 Differential scanning calorimetry (DSC) plots of mPEG-b-PεDL and PεDL-b-PEG-b-PεDL (A) T_g (B) T_m. 142

Figure 4-19 ^{1}H NMR spectra of mPEG-b-PδDL copolymer in $CDCl_3$ (**Solvent peak, $^{*}H_2O$). 145

Figure 4-20 ^{13}C NMR spectra of mPEG-b-PδDL copolymer in $CDCl_3$ (*Solvent peak). 145

Figure 4-21 ^{1}H-^{1}H COSY NMR spectra of mPEG-b-PδDL acquired in $CDCl_3$. 146

Figure 4-22 Kinetic analysis of δ-decalactone polymerisation from mPEG5K at 60 °C using TBD catalyst 146

Figure 4-23 SEC graphs of mPEG-b-PδDL copolymer acquired in $CHCl_3$.. 147

Figure 4-24 Differential scanning calorimetry (DSC) plot of mPEG-b-PδDL copolymer (A) T_g (B) T_m. 148

Figure 4-25 Positions of α / ε protons before and after conversion and the position of the methoxy proton with respect to ε' proton used for determination of M_n by ^{1}H NMR 150

Figure 4-26 ^{1}H NMR of mPEG-b-PCL copolymer in $CDCl_3$ (**Solvent peak) 151

Figure 4-27 ^{13}C NMR of mPEG-b-PCL copolymer in $CDCl_3$ (*not detected; **Solvent peak) 151

Figure 4-28 ^{1}H-^{1}H COSY NMR spectra of mPEG-b-PCL acquired in $CDCl_3$. 152

Figure 4-29 SEC graph of mPEG-b-PCL copolymer acquired in $CHCl_3$. 153

Figure 4-30 Differential scanning calorimetry (DSC) plot of mPEG-b-PCL copolymer (A) T_g (B) T_m. 154

Figure 4-31 ^{1}H NMR spectra of mPEG-b-PCL-b-PεDL copolymer acquired in $CDCl_3$ (**Solvent peak, $^{*}H_2O$ peak)..... 157

Figure 4-32 ^{13}C NMR spectra of mPEG-b-PCL-b-PεDL copolymer in $CDCl_3$ (**Solvent peak) 157

Figure 4-33 Differential scanning calorimetry (DSC) plot of mPEG-b-PCL-b-PεDL (A) T_g (B) T_m. 158

Figure 4-34 Dual mechanism of TBD as catalyst and initiator for ε-DL polymerisation[15] 162

Figure 4-35 Generation of primary and secondary alcohol during ROP of ε-DL and ε-CL respectively. 164

Figure 4-36 Structure of ε-decalactone (seven membered ring) and δ-decalactone (six membered ring)..... 165

Figure 5-1 Standard calibration curve of coumarin 6 in methanol at wavelength (λ_{max}) of 460 nm. 178

Figure 5-2 Dielectric constant (ε') of monomer, initiator and catalyst at various temperatures 180

Figure 5-3 Dielectric loss (ε'') of monomer, initiator and catalyst determined at various temperatures 181

Figure 5-4 Loss tangent (tan δ) of monomer, initiator and catalyst at various temperatures 182

Figure 5-5 Microwave heating profile for the reaction mixture (ε-DL, mPEG and TBD) for 50 sec 184

Figure 5-6 Kinetics behaviour of ε-DL polymerisation based on MROP 187

Figure 5-7 Reaction kinetic of ε-DL polymerisation on mPEG initiator using microwave and CH methods..... 188

Figure 5-8 GPC traces of mPEG 5000, and synthesised copolymers made by MROP method 189

Figure 5-9 Comparison of ^{1}H NMR in D_2O and $CDCl_3$ solvent (A) mPEG-b-PεDL copolymer (B) mPEG-b-PCL copolymer 190

Figure 5-10 CMC plot for (A) mPEG-b-PεDL and (B) mPEG-b-PCL obtained by pyrene 1:3 peak ratio method. 192

Figure 5-11 Comparison of 95% confidence interval (IC50) of the CMC. IC50 value was obtained by non-linear curve fitting of CMC plot (sigmoidal, 4PL)..... 193

Figure 5-12 Coumarin 6 loading in different copolymers. Each point represents mean ± SD (n=3). A significant difference ($P < 0.05$, unpaired student's t test) was observed. Picture shows the micelle formulations. No dye was detected in blank where polymer was absent. 194

Figure 5-13 The TEM Images of empty micelles with size distribution histogram (using Image J software) and (A) mPEG-b-PCL micelles, (B) mPEG-b- PεDL micelles. The images were taken without staining. Scale bar – 2000nm. 195

Figure 5-14 The C3A hepatocytes cell viability test following the exposure of mPEG-b-PDL micelles (at concentrations ranging from 4.6 to 300 μg mL^{-1}) for 24 h using Alamar Blue (A), CFDA (B) and Neutral Red (C) assays. Data are expressed as % viability ± SEM (n = 3 minimum). 197

Figure 5-15 The time dependent uptake of coumarin 6 labelled mPEG-b-PεDL micelles by C3A (human hepatocellular carcinoma) cell lines. Cells were treated with cell medium (A) or micelles for 10 min (B), 60 min (C), 240 min and (D) 1440 min and then stained for the tubulin cytoskeleton (red) and nucleus (blue). The green colour showed by coumarin 6 loaded micelles. 198

Figure 6-1 Standard calibration curve of indomethacin in methanol at wavelength (λ_{max}) of 318 nm. 218

Figure 6-2 Effect of different methods on (A) drug loading and (B) average diameter of mPEG-b-PεDL micelles. A significant difference was observed between drug loading and micelle size for nanoprecipitation/Emulsion method and Dialysis/Emulsion method (***= P < 0.001, **= P < 0.01, One way ANOVA). 223

Figure 6-3 Effect of different solvents on (A) nanoprecipitation and (B) dialysis on drug loading in mPEG-b-PεDL micelles. Significant difference was observed between acetone and ethanol solvents (***= P < 0.001, *= P < 0.05, One way ANOVA). 224

Figure 6-4 Effect of different solvents on sizes of the mPEG-b-PεDL micelles made by nanoprecipitation and dialysis methods. A significant difference was observed between solvents during nanoprecipitation (***= P < 0.001, **= P < 0.01, unpaired student's t test). 225

Figure 6-5 Effect of different drug to polymer ratios on drug loading in mPEG-b-PεDL and mPEG-b-PCL micelles. Significant difference in drug

loading was observed for different polymers in different drug/Polymer ratios (***= P < 0.001, **= P < 0.01, unpaired student's t test)..... 225

Figure 6-6 Nanoprecipitation of the copolymers (A) indomethacin loading (weight % to polymer) (B) Z- average size of the micelles. A significant difference (*= P < 0.05, unpaired student's t test) was observed between both of the copolymers for loading and size. 227

Figure 6-7 Loss in molar mass (M_n) of mPEG-b-PεDL copolymer (A) and polydispersity index (B) with time (days) in the presence and absent of *Pseudomonas cepacia* lipase (0.2 mg/mL) at 37 °C..... 228

Figure 6-8 Micelle Size distributions by TEM Image and size distribution histogram (using Image J software) of empty (A) mPEG-b-PεDL micelles, (B) mPEG-b-PCL micelles. The images were taken without staining. Scale bar – 1000nm. 229

Figure 6-9 *In vitro* indomethacin release (%) from different test formulations in pH 7.4 PBS buffer solution at 37 °C. Each point represents mean ± SD (n=3). 231

List of Tables

Table 3-1 Synthesis of polyester with different feed ratio (mol%) of succinic acid, phenylsuccinic acid and 1- 10- Decanediol using scandium (III) triflate as catalyst 65

Table 3-2. Polymer code, composition (mol% of diacid) and molecular weight (g/mol) of polyesters 80

Table 3-3 Thermal and physical properties of the synthesised polyester polymer (n=1). 86

Table 3-4 Characteristics of empty and dye loaded polymeric nanocarrier (n=3)..... 88

Table 4-1 Summary of experimental details and molecular weight obtained after ROP of Decalactones and Caprolactone using TBD as catalyst. [*]Stannous octoate was used as catalyst. [$]Caprolactone and ε-Decalactone monomers added sequentially in equal molar concentration. (ND= not determined)..... 133

Table 5-1 Dielectric properties of all the starting materials at 2.45 GHz frequency at 120 °C..... 182

Table 5-2 Summary of experimental details and molecular weight obtained after ROP of ε-Decalactone and ε-Caprolactone using TBD as a catalyst. . 185

Table 5-3 Intensity ratio values for peak 1 and 3 of fluorescence spectrum of pyrene acquired in different concentrations of polymers..... 191

Table 5-4 Characteristics of empty and Coumarin 6 loaded block copolymer micelles..... 195

Table 6-1 Calculated value of partial solubility parameters and total solubility parameters of copolymer segments and drug 222

Table 6-2 Calculated values of solubility difference (δ_s-δ_p) and interaction parameter χ_{sp} between solute (drug) and polymer segments..... 222

Table 6-3 Characterization data of blank and drug loaded micelles prepared from block copolymers. 226

List of Schemes

Scheme 3-1 Polycondensation of succinic acid and 1, 20-decanediol catalyzed by scandium (III) triflate 66

Scheme 3-2 Polycondensation of phenylsuccinic acid and 1,10-decanediol catalyzed by scandium (III) triflate 67

Scheme 3-3 Polycondensation of succinic acid, phenylsuccinic acid and 1,10-decanediol catalyzed by scandium (III) triflate 69

Scheme 4-1 ROP of ε-DL catalyzed by TBD using different initiators 126

Scheme 4-2 ROP of ε-decalactone on mPEG 5000 and PEG 4000 using TBD catalyst 134

Scheme 4-3 Ring opening polymerisation (ROP) of δ-Decalactone (δ-DL) on mPEG5K using TBD catalyst 143

Scheme 4-4 Ring opening polymerisation (ROP) of ε-caprolactone (ε-CL) on mPEG5K using TBD catalyst 149

Scheme 4-5 Ring opening polymerisation (ROP) of ε-caprolactone (ε-CL) and ε-decalactone (ε-DL) on mPEG5K using TBD catalyst 155

Scheme 5-1 Synthesis of ε-DL homopolymer (A), ε-DL copolymer (B) and ε-CL copolymer (C) catalysed by TBD in bulk using different initiators in MROP. 183

Acknowledgement

I am exceptionally grateful to Prof. Cameron Alexander, for giving me the opportunity to carry out research in his lab and freedom for doing innovative work during my PhD tenure. I am especially indebted to my co-supervisors, Prof. Derek Irvin and Prof. Steve Howdle for all the support, encouragement and help.

This thesis would not have been possible without the help of Mss. Leagh G. Powell who performed the cell studies for me. I also owe my sincere thanks to Dr. Giuseppe Mantovani, Dr. Kuldeep Bansal and all senior scientists (Post-Docs) for being always there to listen and give advice.

I would like to thank members of the administrative staff for their support and patience with the administrative and instrumental matters. I must give special thanks to all former and present students in B-15 lab and my other friends for their help and for providing a warm, friendly atmosphere throughout my stay in Nottingham.

The financial aid provided by Government of India is duly acknowledged. Finally, I would like to show my appreciation to my family members for their continuous moral support, without which this work would not have been possible.

Abbreviation List

^{13}C NMR	Carbon^{13} nuclear magnetic resonance spectroscopy
^{1}H NMR	Proton nuclear magnetic resonance spectroscopy
ANOVA	Analysis of variance
ATCC	American Type Culture Collection
CH	Conventional Heating
CMC	Critical micelle concentrations
CO_2	Carbon dioxide
CROP	Conventional ring opening polymerization
DC	Drug content
DCM	Dichloromethane
DLS	Dynamic light scattering
DMSO	Dimethyl sulfoxide
DP	Degree of Polymerization
DSC	Differential scanning colorimetry
EDTA	Ethylenediaminetetraacetic acid
EE	Encapsulation Efficiency
FCS	Foetal calf serum
FDA	Food and drug administration
FTIR	Fourier Transform Infrared Spectroscopy
GHz	Giga Hertz
HEPES	N-(2-hydroxyethyl) piperazine-N- (2-ethanesulphonic acid)
IND	Indomethacin
KDa	Kilo dalton = 10^3 g/mol
Mn	Number average molecular weight
MROP	Microwave assisted ring opening polymerization
Mw	Weight average molecular weight
MWCO	Molecular weight cut-off
nm/ d.nm	Nanometer/ diameter in nanometer
NMR	Nuclear Magnetic Resonance

^{o}C	Degree Celsius
PBS	Phosphate Buffer Saline (10 milimolar, pH- 7.4)
PCL	Polycaprolactone
PD/PDI	Polydispersity / Polydispersity Index
PEG / mPEG	Poly(ethylene glycol)/ methoxy poly(ethylene glycol)
PLA	Polylactide
PLGA	Poly (lactide-co-glycolide)
PS	Polystyrene
ROP	Ring opening polymerization
SEC	Size exclusion chromatography
$Sn(Oct)_2$	Stannous octoate
tanδ	Dissipation factor
TBD	1,5,7-triazabicyclo[4.4.0]dec-5-ene
TEM	Transmission Electron Microscope
T_g	Glass Transition Temperature
THF	tetrahydrofuran
T_m	Melting Temperture
UV-Vis	Ultraviolet-visible
wt%	Weight %
ε′	Dielectric constant
ε′′	Dielectric loss or loss factor
µg	Micrograms

Chapter

1

Introduction

1.1 Introduction

Most of the polymeric systems used today for drug delivery applications are based on biodegradable and biocompatible materials. These materials include polyesters, polyanhydrides, polyethers, polyamides, polyorthoesters and polyurethanes. Polyesters can be considered as the first family of synthetic condensation polymers. They usually vary in the physical state ranging from amorphous material to fibers and liquid crystals depending on the groups attached to the ester group.[1] Among the various categories, aliphatic polyesters are one of the most important classes of biodegradable polymer because they possess good biocompatibility and tunable biodegradability. Additionally, the possibility to use renewable monomers for polyester synthesis has enhanced interest in these materials in recent years.[2] There are different types of polyesters which include linear, branched, hyper-branched as well as dendritic, as well as polyester (block) copolymers which have enabled the application of these materials in biomedical fields (Figure 1-1). Polyesters have been used in products such as sutures, bone screws, pins, stents, and plates for fracture[3], as artificial skin, tissue engineering scaffolds[4] and drug delivery systems.[5] Polyesters already used for biomedical applications include poly(lactic acid) (PLA), poly (lactic-co-glycolic acid) (PLGA) and poly(ε-caprolactone) (PCL). These polymers are derived from monomers like lactide (LA), glycolide (GA), ε-

caprolactone (ε-CL), β-butyrolactone (β-BL) and 1,5-dioxepan-2-one (DXO).[6]

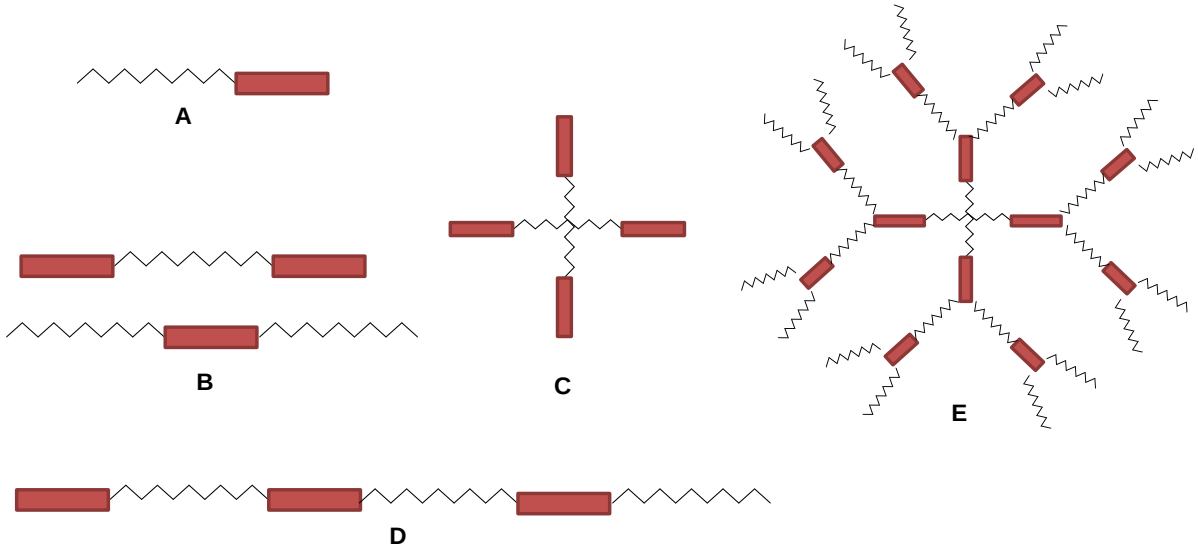


Figure 1-1 Types of polyester polymers (A) linear diblock, (B) linear triblock, (C) branched, (D) multiblock block and (E) dendritic polyester

However, many of the above polyesters are semicrystalline and hydrophobic in nature, and also show nonlinear biodegradation profiles which can limit certain drug delivery applications. For tissue engineering, three-dimensional scaffolds are needed to help cells grow and differentiate and polymer matrices are required that are soft and flexible enough to imitate the mechanical properties of the surrounding tissues. Hence, polyesters with a range of improved properties are needed. One example is to incorporate unsaturated bonds in polyester side chains or main chains to allow cross-linking and thus forming elastomers with higher moduli for tissue engineering applications.[7] Similarly, additional functional groups in the polymer main chain or appended as side groups may enhance drug polymer

interactions to improve drug loading. For instance, Yang *et al.* described the synthesis of acid functionalized copolymers with mPEG as a hydrophilic block for the delivery of doxorubicin (DOX). They showed a higher drug loading due to the strong interaction of amine group of the drug with the acid groups of the polymer.[8] Therefore, many research groups are working on the insertion of different functionalities into polyester chains to modify their physicochemical properties, for example: phenyl groups, carboxylic acid[9], hydroxyl[2], acrylate[10] and alkyne[9] were successfully incorporated into polyester chains. The introduction of phenyl groups can influence the degradability, crystallinity, and polarity of polyesters. For example, Witt *et al.* suggested an improvement in mechanical properties of polymers by incorporating aromatic units into the polyester backbone. However, the biodegradability decreased due to higher crystallinity as aromatic content increased.[11] The incorporation of aromatic units as a side group in the polyester backbone was achieved by copolymerization of mendalic acid with poly(butylene succinate) and poly(ethylene adipate). The increase in the phenyl group caused a decrease in crystallinity hence the biodegradability was increased.[12] These properties are important factors to design controlled drug delivery systems for bioactive molecules.[13, 14]

The incorporation of renewable monomers and selection of suitable synthetic methods (e.g. conventional or microwave heating) can greatly reduce the environmental costs of the final material. Several lactone rings have been

used in the synthesis of copolymers by ring opening polymerization utilising mPEG initiators. This method is less time and energy consuming compared to polycondensation reactions which have been more commonly used in the past for polyester synthesis. However, many lactone monomers are currently obtained from non-renewable sources. Glavas *et al.* used ε-decalactone, which is regarded as a renewable monomer, for the synthesis of the copolymer on mPEG2K. The micelles were compared with the structurally similar ε-caprolactone based copolymer (mPEG-b-PCL) to determine the difference in the core properties of the prepared micelles.[13] In preceding work, Bansal *et al.* used δ-decalactone as a renewable material for copolymer synthesis (mPEG-b-PδDL) and Amphotericin B encapsulation and release. The results were compared against ε-caprolactone based copolymer (mPEG-b-PCL). The mPEG-b-PδDL copolymer with pendant alkyl chains significantly enhanced the loading of the drug compared to a mPEG-b-PCL copolymer with no alkyl chains.[15] These data show that the core properties of polyester drug carriers can be changed by including aromatic units or alkyl chains or attachment of diverse functionalities in the polymers.

1.2 Synthesis of Polymers

1.2.1 Polycondensation

Condensation polymerization involves the reaction of a difunctional monomer of AB type (e.g. hydroxyacid) or reaction of AA (e.g. diacid, diacid chloride or diesters) with BB (e.g. diol) difunctional monomers.[1] The reaction of

diacids with diols produces water as byproduct while the reaction of diols with diacid chlorides produces HCl as a byproduct. Due to the formation of small byproducts, these reactions are called polycondensation. It also involved ester interchange of diols and diesters as outlined in the figure 1-2.

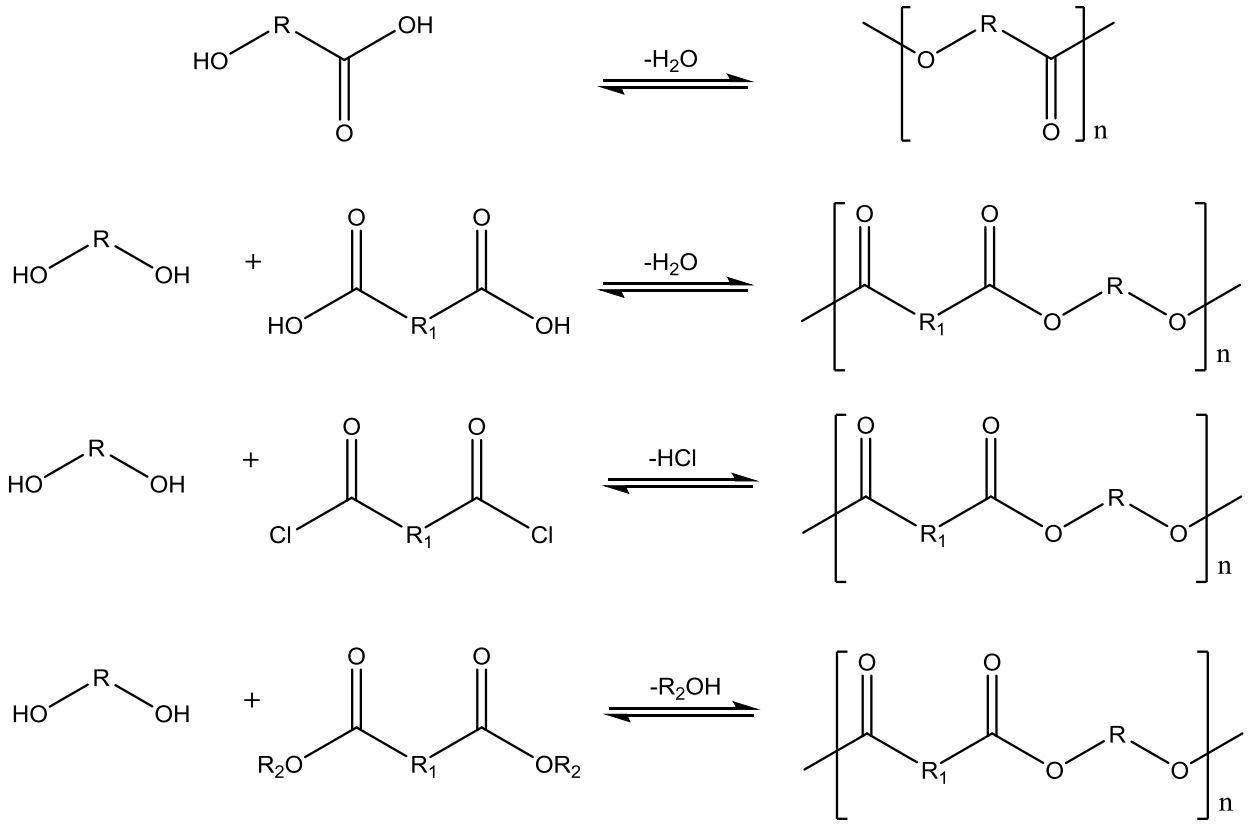


Figure 1-2 Preparation of polyesters by stepwise polycondensation method. Reproduced from reference[1]

Carothers work[16] on polycondensation relates the degree of polymerization to the extent of reaction:

$$\overline{X}_n = 1/(1-p)$$

Where:

$\overline{X}_n$= Degree of polymerization.
p= Extent of reaction (or conversion to polymer)

Such type of reactions includes a number of drawbacks; (1) Polycondensation involves the formation of by-products like water which must be eliminated during the reaction to drive the reaction toward higher conversion; (2) Higher conversion (>98-99%) is essential to get the higher molecular weight of the polyester; (3) A correct stoichiometric balance of monomers is a major factor in the reaction to get higher conversion which although can readily be achieved with purified hydroxylacid but difficult to get with diacids and diols monomers and (4) Long reaction time and higher temperature (>200–250 ^{o}C) with reduced pressure is usually required for the synthesis of polyesters for commercial use which may lead to side reactions. Therefore, several groups are attempting to overcome the shortcomings of polycondensation to synthesize polyester with desired physicochemical properties.

Takasu *et al.* described the one-step chemoselective polycondensation of several diols and dicarboxylic acids having pendent hydroxyl groups under mild conditions, using rare-earth trifluoromethanesulfonates. They showed that under mild conditions (Temperature <100 ^{o}C), the secondary alcohols of diacids (Tartaric acid and Malic acid) did not react hence polyesters with pendent hydroxyl groups were formed which were further modified by glycosidation using glucose pentaacetate as the glycosyl donor (Figure 1-

3).[17] A series of polyester copolymers based on poly (butylene succinate) and poly (ethylene glycol) were synthesised by polycondensation. The authors found that increasing the PEG content decreased the melting temperature (T_m), crystallization temperature (T_c), and crystallinity (χ_c) of these copolyesters.[18]

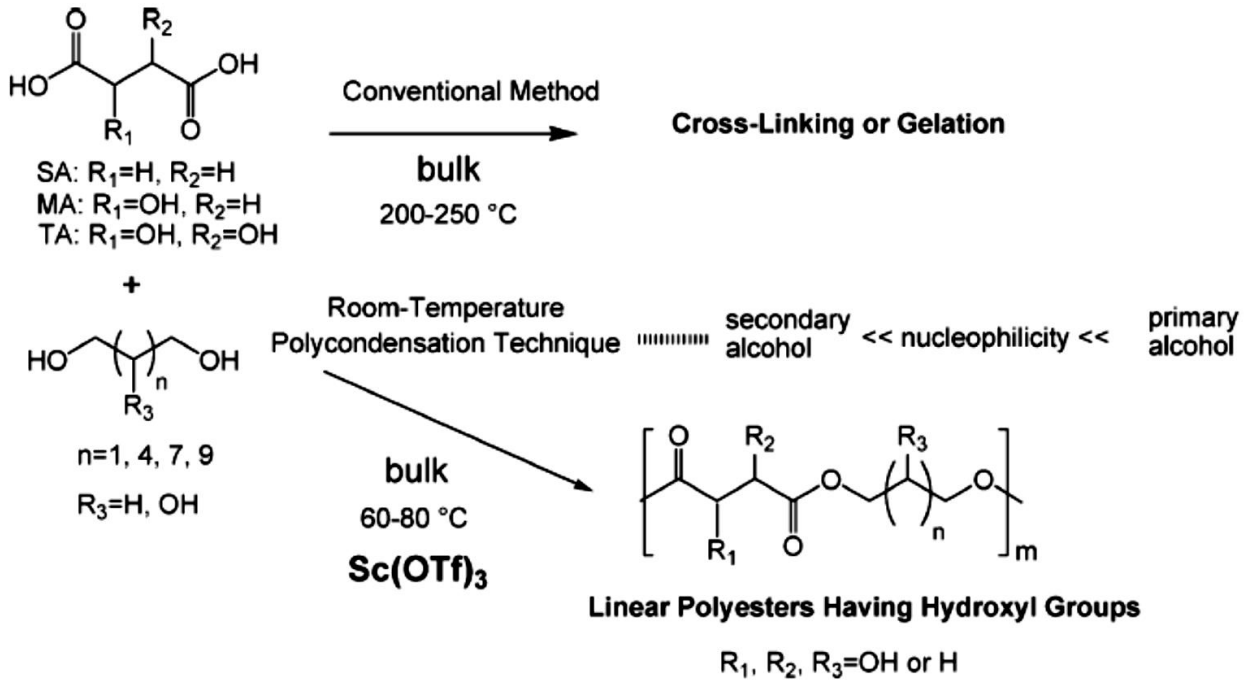


Figure 1-3 Chemoselective polycondensation of diols and diacids under mild condition. Reproduced from reference [17]

Tang *et al.* described the synthesis and characterisation of elastic aliphatic polyesters from sebacic acid, glycol, and glycerol achieved in two step procedures. The prepolymers were formed in the first step by reaction of the sebacic acid with a glycol and then crosslinked with glycerol to obtain the desired elastic polymeric material.[19] Takasu *et al.* investigated the effect of strong Brønsted acids, bis(perfluoroalkanesulfonyl)imide and perfluoroalkanesulfonic acid on dehydration polycondensation of diacids and

diols. They found that these acids had higher reactivity than p-toluenesulfonic acid or rare-earth catalysts at 60 ^{o}C. The used bis(nonafluorobutanesulfonyl)imide (Nf_2NH) was sublimed to recycle the catalyst.[20] Surfactant-combined Bronsted and Lewis acids were used for emulsion polycondensations of 1,9-nonanediol (1,9-ND) and dodecanedioic acid (DDA) at 80 ^{o}C. The hexamethylene diisocyanate was used as a chain extender.[21] Fischer esterification is one of the most common routes for the formation of polyesters. In this route, a carboxylic acid reacts with alcohol in the presence of Lewis or Bronsted acid to give esters (releasing a molecule of water).[22] Figure 1-4 shows the mechanism of acid catalyzed Fischer esterification reaction of diacid and diol.

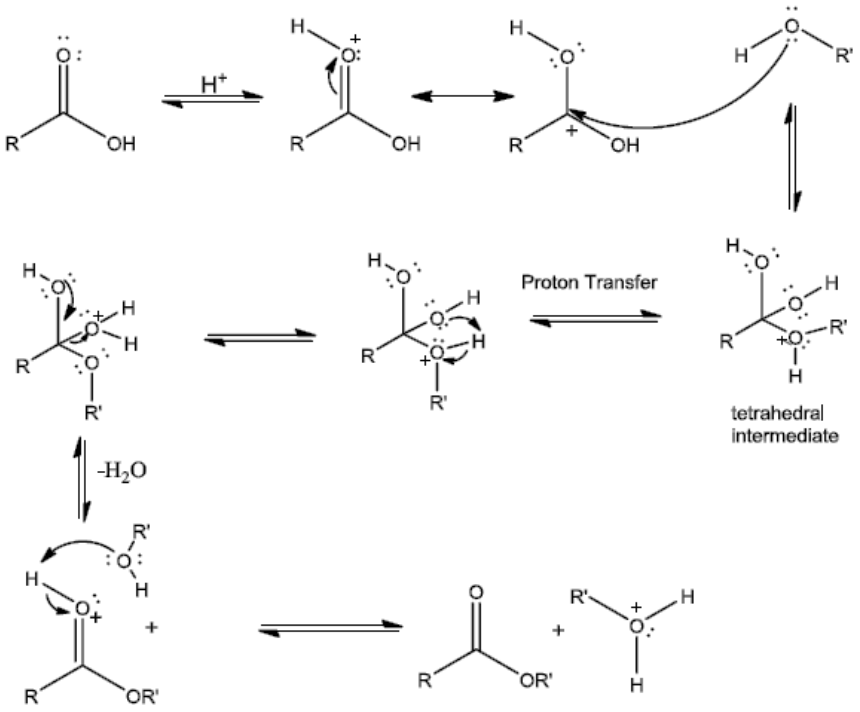


Figure 1-4 Mechanism of acid catalyzed Fischer esterification reaction of diacid and diol. Reproduced from reference[22]

1.2.2 Ring Opening Polymerization (ROP)

The ROP offers a number of advantages over polycondensation to produce polyesters. The low reaction temperature and time, the absence of by-products and better control over the molecular weight are the main advantages.[23, 24] The ROP involves the opening of cyclic monomers (e.g. lactones, lactides, and glycolide) from an initiator (nucleophile) to produce a primary chain molecule (1st mer) with the reactive functional chain end, which reacts with next available cyclic monomer to open it generating a second reactive chain end and this process continues until all monomers are consumed.[25] Anionic, cationic and coordinative insertions have been reported as mechanisms involved in ROP.[24] However, a higher molecular weight polymers are mostly achieved by anionic and coordinative insertion mechanisms.[6]

Anionic Mechanism

This reaction involves the nucleophilic attack of a negatively charged initiator on the carbonyl carbon to break acyl-oxygen bond (acyl-oxygen scission) to form an alkoxide ion as the propagating species. However, in 4-membered rings such as β-butyrolactone, either alkyl or acyl-oxygen cleavage has also been reported giving a carboxylate or alkoxide respectively (Figure 1-5).[6] The initiators used for anionic mechanisms include alkali metals, alkali metal oxides, etc.

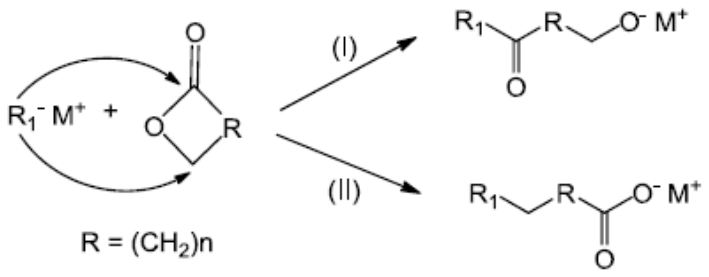


Figure 1-5 Ring opening polymerization of lactone ring by anionic mechanism. Reproduced from reference[6]

Coordination-Insertion Mechanism of ROP

This reaction has been used most extensively for the preparation of aliphatic polyesters with well-defined architecture. It involves the use of aluminum or tin alkoxides and carboxylates with vacant "d" orbitals as coordination initiators. It proceeds via two mechanisms depends on which organometallic species are used. Some organometallics activate the monomer by forming a electron pair donor-acceptor complex with the carbonyl group. The polymerization then precedes by the attack of any nucleophile, e.g., water or alcohol added in the reaction.[24] However, this mechanism has been questioned in recent literature (Figure 1-6)

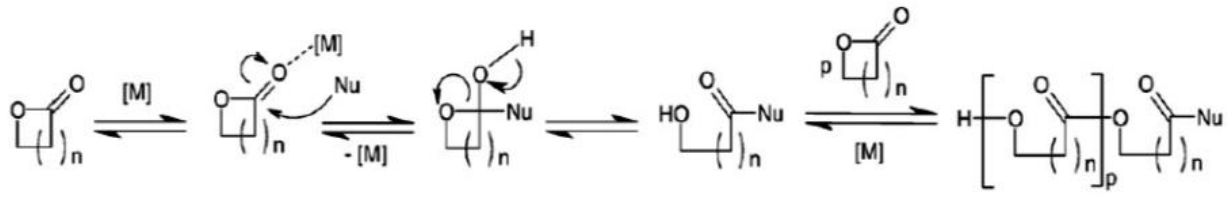


Figure 1-6 Organometallic (M) catalyzed ring opening polymerization of lactones in the presence of nucleophiles (Nu). Reproduced from reference[24]

Another mechanism proposed to occur when metal alkoxides are used as initiator, is 'insertion–coordination' mechanism. Metal carboxylates are weaker nucleophiles, therefore, behave more like a catalyst when compared to metal alkoxides which can be considered to act as an initiator. Therefore, a co-initiator (hydrogen compound, e.g., alcohols) is needed along with metal carboxylates to convert catalyst into active initiator.[6, 24] Tin(II) bis-(2-ethylhexanoate) [metal carboxylate] also known as tin octoate or octanoate [$Sn(Oct)_2$] is one of the most popular catalyst/initiator reagents for ROP. It has been accepted as a food additive by the US Food and Drug Agency (FDA). According to the mechanism, $Sn(Oct)_2$ is converted into a tin alkoxide in the presence of alcohol to form an actual initiator for ROP (Step A and B in Figure 1-7).[28-30] The presence of water in the reaction can deactivate the actual initiator (Step C). The metal in the actual initiator is suggested to coordinate with the carbonyl group of the monomer to cleave the acyl–oxygen bond followed by insertion in the metal alkoxide bond. The coordination of metal with exocyclic oxygen further polarizes the carbonyl carbon-oxygen bond, making this carbon more susceptible to nucleophilic attack (Step D in Figure 1-7).[24, 26-28]

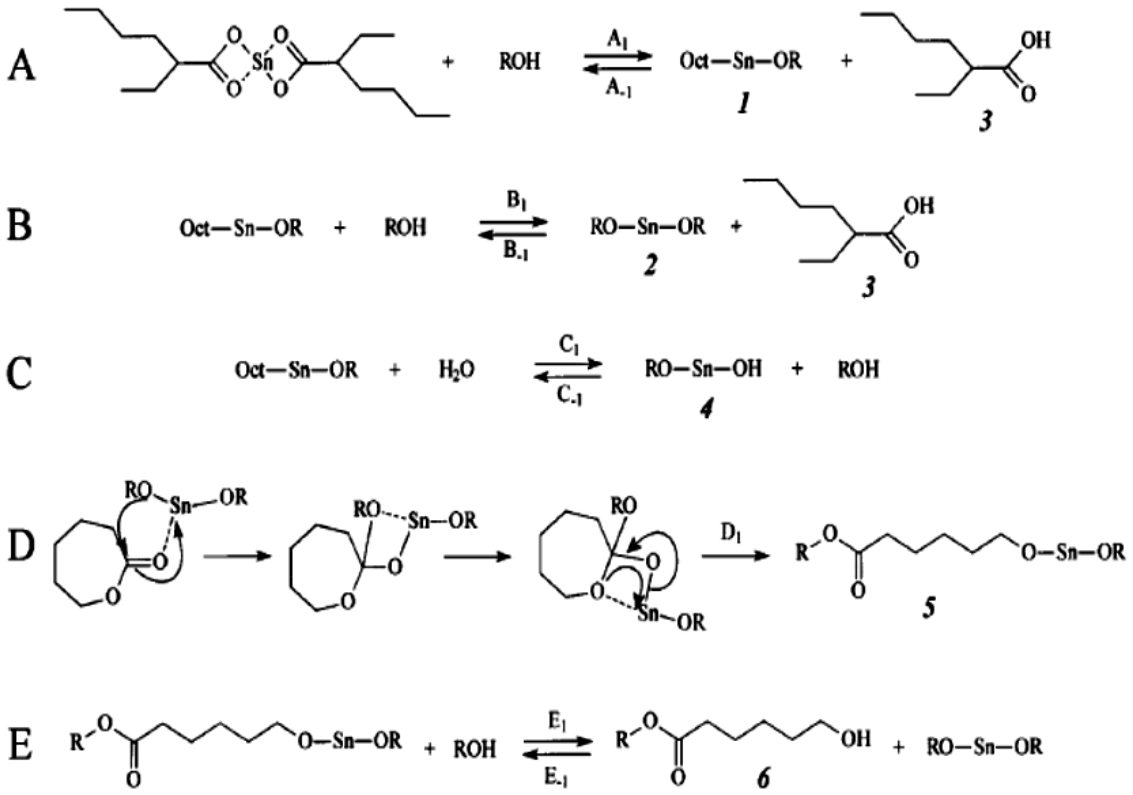


Figure 1-7 Ring opening polymerization in presence of stannous octoate (A) and (B) stannous octoate initiator (C) Deactivation of catalyst by water (D) coordination insertion of monomer into stannous alkoxide and (E) chain transfer to unreacted alcohol. Reproduced from reference.[29]

1.2.3 Microwave based Synthesis of Polyesters

The synthesis of polyester can be improved by the use of Microwave as a energy source for the polycondensation and ring opening polymerization reactions. Microwave is a form electromagnetic radiation (EMR) with a frequency range of 0.3 to 300 GHz. It has been used widely for heating of the materials for industrial and domestic purposes at a frequency of 2.45 GHz (correspond to microwave wavelength of 12.25 cm). The microwave-based synthesis is considered as an environmentally benign method where it

offers several advantages over conventional synthesis. Some of them includes instantaneous and rapid bulk heating, selective and direct heating, temperature homogeneity etc.[31] This advantages lead to reduce the reaction time from h to min, improves the reproducibility, increase the yield and reduce the side reactions.[32] Therefore, many research groups are focusing on microwave based synthesis an effective alternative energy source. These advantages triggered an exponential increase in publications in the last two decades.[32-34] The energy of photon (0.0016 eV) at 2.45 GHz frequency is lower than the Brownian motion energy and the energy required to break a bond and hence it cannot induce any chemical reactions.[33] The microwave heating of the material is based on the ability of a material to absorb microwave radiation and convert it into heat. This phenomenon is known as "microwave dielectric heating''. The irradiation of a sample with microwave causes the molecules to try to align itself with the applied electromagnetic field to cause the molecular friction, rotation and collision to loose energy in the form of heat.[35, 36] Hence, the heating of reaction mixture strongly depends on the dielectric properties of material used.

1.2.3.1 Microwave Assistant Polycondensation

Velmathi *et al.* synthesised poly(butylenesuccinate) (PBS) by an eco-friendly direct polyesterification of a dicarboxylic acid and a diol using distannoxane catalyst under microwave irradiation (Figure 1-8). The method was compared against a conventional heating polycondensation, in which a

polymer of M_w 1.02X10^4 was produced in 5 h at 200 ^oC. In contrast, the microwave-based method produced a polymer with M_w of 1.03X10^4 (at 200 ^oC) in 20 min. The short reaction time at atmospheric pressure, freedom of solvent for the synthesis makes this method ecomonical compared to conventional methods of polyesters synthesis.[37]

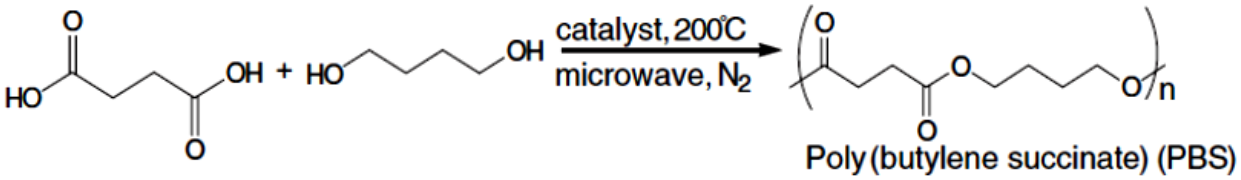


Figure 1-8 Microwave based synthesis of poly(butylene succinate) polymer. Reproduced from reference.[37]

The direct polycondensation of LA (renewable monomer) to PLA in microwave-based method has been studied by Nagahata *et al.* Industrially, PLA is produced by ROP of L-lactide (a cyclic dimer of lactic acid (LA) which itself is formed by conventional polycondensation of LA to form oligo(lactic acid) followed by cyclization depolymerization to produce lactides. This method is time and energy consuming and expensive. The authors showed a higher acceleration of polymerization rate in microwave based synthesis compared to the conventional polycondensation reaction using a binary catalyst of $SnCl_2$/p-TsOH. The microwave-based reaction under reduced pressure (30 mmHg) produced PLA with M_w of 16000 within 30 min (figure 1-9).[38] A large-scale polycondensation of LA was studied by Nakamura *et al.* using microwaves as an energy source in a batch reactor. The microwave method was able to produce PLA with molecular weights exceeding 10,000 in

5 h. The authors also showed that scaling up the reaction saved energy per mole of the substrate in polycondensation reaction.[39]

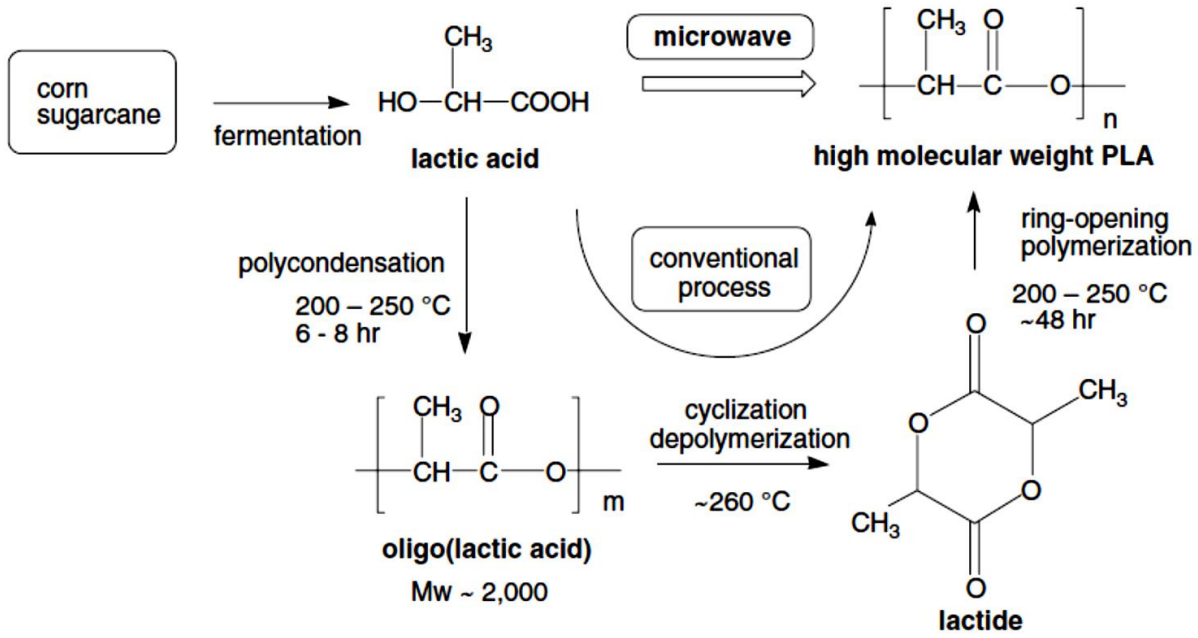


Figure 1-9 Polycondensation of lactic acid by Microwave and conventional methods. Reproduced from reference.[38]

Nakamura *et al.* also studied the dielectric properties of the reacting material (lactic acid, oligo(lactic acid) and water) used for the polycondensation of the lactic acid. They showed a decrease in the dielectric properties as the reaction progressed. The calculated penetration depths also suggested the deep penetration of the microwaves in the reaction system.[40]

The polycondensation of sebacic acids and ω-amino alcohols was studied by Borriello *et al.* They compared the conventional and microwave irradiation based polycondensation reaction for poly(amide-ester)s synthesis and found that the microwave-based method showed a higher reaction rate and yield

while retaining physical-chemical properties, compared to the conventional polycondensation reaction.[41]

1.2.3.2 Microwave Assistant Ring Opening Polycondensation (MROP)

Albert and co-workers studied the ROP of ε-caprolactone (ε-CL) under microwave irradiation using titanium tetrabutylate as a catalyst in 1996. They compared the results of microwave ROP against conventional ROP for conversion and reaction kinetics using different monomer:catalyst molar ratios at 180 ^{o}C. They showed a similar M_n with no significant difference in the conversion rate, hence did not indicate any advantages of microwave-based method over conventional ROP.[42]

The ROP of ε-caprolactam and ε-caprolactone using microwave irradiation was studied by Fang *et al.* The PCL was produced using stannous octoate as a catalyst at the forward power of about 70–100W for 2 h. The author suggested a higher yield and shorter processing time in microwave made it a promising method than the conventional method of synthesis.[43]

The non-thermal microwave effect of the stannous octoate-catalyzed ROP of ε-CL was investigated by Li *et al.* They used different microwave power levels of 400, 500, 600, 700 and 800 W, and corresponding polymerization mixture equilibrium temperatures of 165, 180, 197, 213 and 228 ^{o}C for polymerization of ε-CL. The microwave-based results were compared against the conventional heating method. The Arrhenius's Law was followed by the

conventional method. Hence, the polymerization was considered to follow purely by thermal effect. On the other hand, Arrhenius's Law was not followed by microwave heating. The reaction rate constant (k_p) increased anomalously, and an abrupt variation appeared for 500 W (180 ^oC)[44] as shown in figure 1-10.

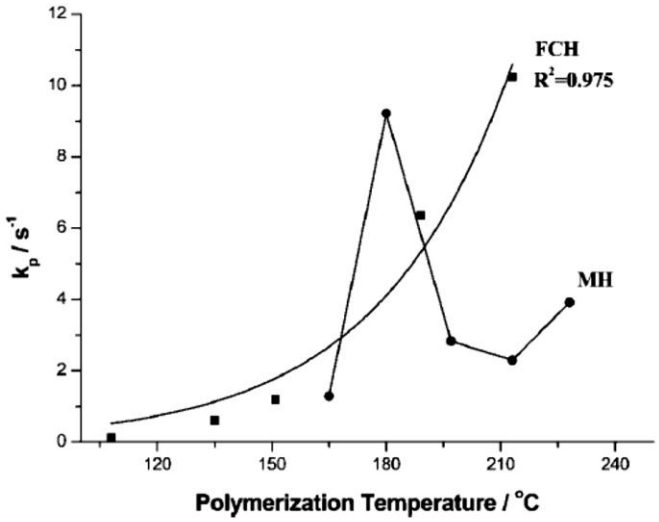


Figure 1-10 Reaction rate constant (kp) determination for microwave and conventional (FCH) method. Reproduced from reference.[44]

Liu *et al.* grafted polycaprolactone chains on chitosan molecules to improve the properties of the resultant copolymer using microwaves as the heating source in ROP. The microwave-based method achieved a very high grafting percentage, particularly when the power output was >450 W in comparison to the conventional method.[45]

A significant improvement in the ROP of ε-caprolactone (ε-CL) was achieved by the microwave method without any metal catalyst using benzoic acid and chlorinated acetic acid as initiators. The microwave irradiation of ε-CL and

benzoic acid (25/1 molar ratio) produced PCL with M_w = 4.48 X 10^4 g/mol and low Đ of 1.6 at 680 W for 240 min. On the other hand, conventional method achieved M_w of 1.21 X 10^4 g/mol with high Đ of 4.2 at 210 ^oC for 240 min.[46]

The ROP of ε-CL has been performed in large scale using an industrial microwave reactor (6000 W) in the presence of stannous octanoate ($Sn(Oct)_2$) (Monomer:Catalyst = 1000) as a catalyst. The reaction proceeded smoothly to give M_w up to 1.22 X 10^5 g/mol within 40 min with over 93% yield at different microwave powers (850, 1700, and 2550 W).[47]

ROP of ε-CL was performed at constant microwave powers of 170, 340, 510, and 680 W at a frequency of 2.45 GHz using a microwave oven in the temperature range from 80 to 210 ^oC. PCL with M_w of 1.24 X 10^5 g/mol was obtained within 30 min at 680 W when 0.1% (mol/mol) stannous octanoate was used as a catalyst. The use of zinc powder (1% w/w) catalyst enabled PCL of M_w of 9.23 X 10^4 g/mol to be produced after microwave irradiation at 680 W for 270 min.[48]

Microwave-assisted ROP of ε-CL has been carried out in an ionic liquid 1-butyl-3- methylimidazolium tetrafluoroborate, (30 wt%) using zinc oxide as a catalyst. An enhanced polymerization rate in the presence of ionic liquid was reported (M_w of 2.85 X 10^4 g/mol was obtained at 85 W for 30 min). Increasing the ionic liquid concentration resulted in higher microwave absorptivity of the medium at two different microwave power levels (85 W

and 170W), resulting in an increase in the reaction temperature and hence the M_w of the resulted polymer (Figure 1-11).[49]



Figure 1-11 MROP of ε-CL catalyzed by zinc oxide in the presence of ionic liquid. Reproduced from reference [49]

The microwave-based ring opening polymerization was used for the synthesis of Poly(L-lactide)-block-poly(ethylene glycol)-block-poly(L-lactide) (PLLA-PEG-PLLA). The results demonstrate the higher conversion of L-lactide (92.4%) from PEG2000 to give a number-average molar mass of 2.82 X 10^4 g/mol when irradiated for 3 min at 100 ^oC. The feed ratio of L-lactide/PEG was suggested to have a strong influence on L-lactide conversions. The higher ratio was found to enhance the copolymer molar masses. The results also suggested a faster copolymerization when compared to the conventional synthesis (Figure 1-12).[50]

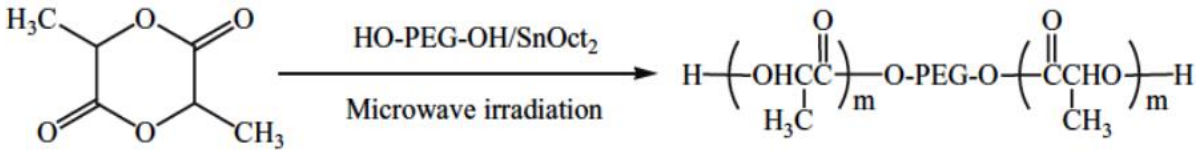


Figure 1-12 Synthesis of PLLA-PEG-PLLA triblock copolymer by MROP. Reproduced from reference [50]

The controlled synthesis of diblock copolymer of L-lactide initiated on MPEG under microwave based ROP was studied by Zhang *et al.* The polymerization took 20 min at 100 ^{o}C to produce polymers with number-average molar mass ranging from 7.33 X 10^3 to 1.18 X 10^5 g/mol while the lactides conversion were in the range of 65.1 to 97.3 %. The authors also showed a strong influence of L-lactide/PEG ratio used in the synthesis. The higher ratio produced polymer with higher molecular weight. The longer PLLA segment in copolymer was suggested to improve the thermal stability of the copolymer (Figure 1-13).[51]

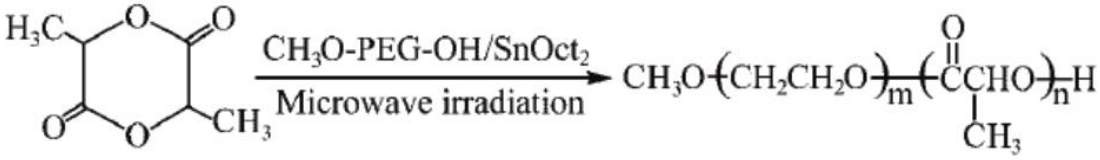


Figure 1-13 Synthesis of mPEG-PLLA diblock copolymers by MROP. Reproduced from reference [51]

Yu *et al.* synthesised PCl-PEG-PCl triblock co-polymers with a number-average molar mass (M_n) over 2.0 X 10^4 g/mol using MROP. They controlled the Mn and composition of the copolymer by varying the molar mass of PEG. The synthesised copolymer showed a sustained release pattern for ibuprofen.[52] Trathnigg and co-workers reported the synthesis of PCL-b-PEG-b-PCL triblock copolymers on difunctional PEG (PEG 200 and PEG 300) using MROP method. The reaction was conducted in bulk varying the ratio of PEG:PCL using stannous octoate as a catalyst at 140 ^{o}C for 30 min. The copolymers showed a higher content of triblock in the product compared to

commercial products as determined by liquid chromatography and MALDI-TOF-MS.[53] The synthesis and characterisation of mPEG-b-PCl and mPEG-b-PLL [methoxy-poly(ethylene glycol)-block-poly(L-lactide)] diblock copolymers were described by Karagoz and Dincer. The copolymers were prepared in the presence of stannous octoate [$Sn(Oct)_2$] as a catalyst by MROP and compared with conventional ROP. The short reaction time with small Đ suggested a higher efficiency of the microwave method compared to conventional heating.[54] The poly(3-hydroxyalkanoate)-b-poly(D,L-lactide) (PHA-b-PLA) diblock copolymers were synthesised by MROP of D, L-lactide (LA) on mono-hydroxylated PHA-based macroinitiators. The authors investigated the effect of irradiation time, monomer/initiator ratio and temperature on LA polymerization. The kinetic investigation revealed the living/controlled characteristics of MROP of LA (Figure 1-14).[55]

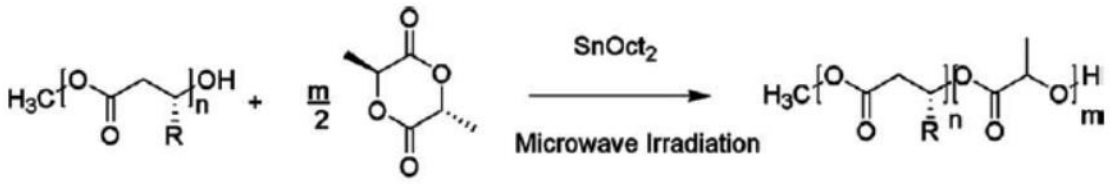


Figure 1-14 Synthesis of PHA-b-PLA diblock copolymer by MROP. Reproduced from reference.[55]

1.3 Polymeric Micelles in Drug Delivery

The synthetic block copolymers (as described above) have numerous applications in the biomedical field particularly in drug delivery. Block

copolymers have emerged as efficient drug delivery vehicles as they can spontaneously self-assemble in solution to form micelles. The block copolymer also allows a better administration, transportation and site-specific localization of the therapeutic drug at the site of action. In an aqueous solution, the hydrophobic block forms the core of the micelles stabilized by an outer corona or hydrophilic shell formed by hydrophilic block.[56] The hydrophobic core is known to act as a reservoir to solubilize hydrophobic moiety in the micelles. In the last few years, hundreds of research groups have contributed in this area.[14, 15, 57-59] In most of the work, micelles of block copolymers were made by synthesizing different hydrophobic blocks on a hydrophilic PEG chain. Some of the examples of the hydrophobic blocks includes poly(aspartic acid), poly(β-benzyl-L-aspartate)(PBLA), PCL, Poly(gamma-benzyl-L-glutamte), poly(D,L-lactic acid) (PDLLA), poly(L-lysine), Poly(propylene oxide)(PPO), polyspermine etc. The different hydrophobic blocks impart different properties in the micelles and hence are effective for some specific drugs than other drugs. For instance, β-carotene was found to be more suitable for PLGA [Poly(lactic-co-glycolic acid)] block compared to PS (Polystyrene), PLA and PCL blocks of copolymers.[60] Therefore, one copolymer cannot be used for delivery of all hydrophobic drugs. The drug-polymer (core) compatibility plays an important role to enhance drug encapsulation in the micelles.

1.3.1 Micelles Preparation Procedures

1.3.1.1 Direct Dissolution

The direct dissolution involves the addition of copolymer directly into the water which leads to the micellization. The encapsulation can be achieved by transferring the drug stock solution (in acetone) to an empty vial followed by evaporation in which copolymer micelle solution is added. For instance, the formation of pyrene or DPH loaded PEO-b-PPO-b-PEO copolymeric micelles by direct dissolution method.[61] In some cases, an elevated temperature can be used to promote micellization in water.

1.3.1.2 Oil-in-Water Emulsion Method

The method involves the dissolution of polymer and drug in a water immiscible organic solvent followed by a fast addition of water. The mixture is then emulsified by sonication/stirring to form an oil-in-water emulsion. The copolymers, in the disperse droplets containing drug, self-associate such that the hydrophobic portion remains in the oil phase whereas the hydrophilic portion extends into the water phase. The subsequent stage requires the removal of organic solvent by evaporation and results in the formation of drug loaded micelles.[57, 62] The organic solvent used for the method most commonly includes ethyl acetate[63], dicloromethane[64] and chloroform.[65]

1.3.1.3 Dialysis Method

This method is mainly used when the copolymer is not very soluble in water. The method requires the dissolution of the polymer and drug in a water miscible organic solvent (such as ethanol,[66] acetone,[67] tetrahydrofuran,[68] dimethyl sulfoxide,[69] or *N*, *N*-dimethyl formamide).[69] The obtained solution is then dialyzed against water and the slow replacement of organic solvent results in association of hydrophobic portions of the polymer chains along with the hydrophobic drug to form micelles.[14, 58] It has been suggested that the addition of water (at a slow rate) into the organic phase before dialysis yields reproducible micelles with narrow size distribution.[14] The choice of the solvent and rate of addition of water determines the size, size distribution, morphology, and yield of the micelles. La *et al.* studied the effect of solvents (DMSO and DMAc) on PEO-b-PBLA micelles size, distribution, and yield. The authors suggested a higher yield and narrow size distribution of micelles when DMAc was used as an organic solvent compared to DMSO .[70] The free drug (unencapsulated drug) can be removed during the dialysis process. Hence, no additional method is needed for purification of the formulation. The use of non-chlorinated solvents makes this approach superior over oil-in-water emulsion method.

1.3.1.4 Solution Casting Method

This method requires the dissolution of the block copolymer and drug in a suitable volatile organic solvent. This is followed by the evaporation of the

solvent to leave a polymer-drug film. Hot water is then added to the film with stirring which causes the polymer to self-assemble in the presence of the drug. The hydrophobic interaction between drug and polymers during the process leads to the formation of drug loaded micelles.[62, 71] This method is mainly used for copolymers with high hydrophilic to hydrophobic ratio to achieve complete reconstitution.[57]

1.3.1.5 Nanoprecipitation Method

The nanoprecipitation method involves the dissolution of the block copolymer and drug in a water-miscible volatile organic solvent. This is followed by the dropwise addition of the organic phase into water under stirring. The solvent diffusion in water with simultaneous evaporation drives the self-assembly of the copolymer to produce drug loaded polymeric micelles.[57, 72] The obstructions in the self-assembly due to mass-transfer limitations can be overcome by sonication/stirring or both. Different solvents can be used for nanoprecipitation methods, although acetone is preferred due to its higher water miscibility and low vapor pressure which makes it easier to remove from formulations.[63, 73] Process parameters can significantly affect the loading capability of polymers assembled by nanoprecipitation. For instance, increasing the hydrophobic block length (hydrophobic ratio) or decreasing the organic to aqueous phase ratio resulted in higher cyclosporine (CyA) loading in mPEG-PCL copolymeric micelles.[74] The co-solvent method was also compared with O/W emulsion

method at the same concentration of drug (Amiodarone) and polymer (mPEG-b-PCL). A higher loading and encapsulation was found with co-solvent method. This indicates that the preparation method also affects the loading capability of the micelles.[65]

1.3.1.6 Flash Nanoprecipitation Method

This method requires a rapid mixing of the organic solvent stream (contain drug and polymer) and antisolvent stream in a common mixer chamber (in the order of millisecond) to obtain a homogeneous supersaturation conditions to precipitate the copolymer to form micelles/nanoparticles (Figure 1-15). [75-78]

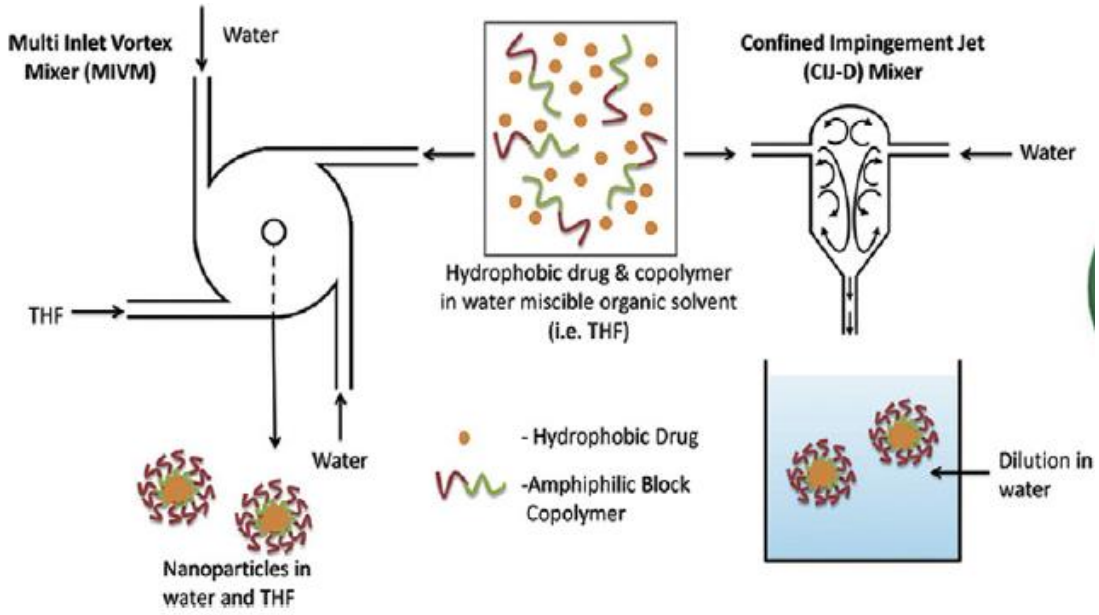


Figure 1-15 Micelles preparation by flash nanoprecipitation method using impinging jets mixer (CIJM) and the multi-inlet vortex mixer (MIVM). Reproduced from reference[77]

The physical property of the nanoparticles (size, distribution, morphology) can be changed by tuning the kinetics of micromixing (flow rates and mixer geometry).[79] The mixers developed for the flash nanoprecipitation process include the confined impinging jets mixer (CIJM)[75] and the multi-inlet vortex mixer (MIVM). [76, 80] The method is simple, continuous, and scalable while at the same time high yield, high drug loading and controlled size can also be obtained.[79]

1.3.1.7 Salting Out Method

The method also involves the dissolution of the drug and copolymer in the water miscible organic phase (e.g. acetone) followed by the addition of concentrated aqueous electrolyte solution (up to 60 wt% salt).[81] The high concentration of salt prevents the mixing of acetone with water. The resultant mixture is then emulsified by stirring or by sonication to make fine droplets of the organic phase in water. The rapid addition of large volume of water forces acetone to diffuse into the water resulting in the precipitation of copolymer in the form of micelles.[81-83] A stabilizer such as polyvinyl alcohol (PVA) can also be added during the method to produce stable nanoparticles.[84]

1.3.1.8 Freeze-Drying Method

This method involves the use of *tert*-butanol as a solvent to solubilize the polymer and drug. The resultant solution is mixed with water and freeze dried. The reconstitution freeze dried solid with water makes the micelles

again. The freeze-drying provides the higher stability of the micelles, and the method can be used for large-scale production. However, the limited availability of freeze-dryable organic solvent prevents the method for regular use. Also, the insolubility of PEO in *tert*-butanol prevents the use of this method for block copolymers containing PEO chains. The method has been successfully adopted for paclitaxel loading in poly(N-vinylpyrrolidone)-b-poly(D,L lactide) (PVP-b-PDLLA) copolymer.[85, 86]

1.3.2 Factors Affecting Drug Loading

The micellar core of the amphiphilic block copolymers serves as a reservoir for most of the hydrophobic drug molecules. The drug loading efficiency of drug entrapment in micelles depend on several factors. These include drug-core compatibility, type of hydrophobic block, hydrophobic block length, core crystallinity, polymer concentration, solute concentration, solute properties and method of preparation. A higher drug loading content (ratio of drug encapsulated to total amount of micelles) permits the use of lower amount of polymer for delivery of the desired dose, hence, can reduce the side effects associated with polymers. On the other hand, drug loading efficiency (ratio of drug encapsulated to total amount of drug used) is an important term to evaluate the overall process cost and effectiveness of the micelle preparation methods.[81]

1.3.2.1 Drug–Micellar Core Compatibility

The drug–micellar core compatibility is one of the major factors which influence the drug encapsulation and drug loading capacity. A good compatibility can be expected if drug and hydrophobic block exhibit structural similarity and similar polarity. Therefore, different functional groups have been incorporated into block co-polymers to increase favorable interactions with drugs (e. g. amphotericin B[59], cisplatin[87] and DOX[88, 89]) to improve the drug loading, stability and release property. The drug–micellar core compatibility can be calculated by a term denoted as the Flory-Huggins interaction parameter given by:

$$X_{sp} = (\delta_s - \delta_p)^2 V_s / RT \quad (1)$$

Where X_{sp} = Interaction parameter of solubilizate (drug) and core forming block (polymer hydrophobic block); δ_s = Solubility parameter of solubilizate (drug); δ_p = Solubility parameter of the polymer (core block); V_s = Molar volume of solubilizate (drug); R = Gas constant and T temperature in Kelvin. Lower the value of $X_{sp.}$ indicates the higher compatibility between drug and micelle core. In the same way, compatibility will be highest when solubility parameters of drug and polymer become equal ($\delta_s = \delta_p$).

The phenomenon of drug-polymer compatibility is complex. However, a good approximation can be obtained via the Flory-Huggins interaction parameter. For instance, the Flory-Huggins interaction parameter between a drug

(cucurbitacin I (Cut) and selected different polymers were determined by Lavasanifer *et al.* They used PCL, poly(α-benzylcarboxylate-ε-caprolactone) (PBCL) and poly(α-cholesterylcarboxylate-ε-caprolactone) (PChCL) as the hydrophobic blocks in copolymers to determine the compatibility with the cucurbitacin I. The structural similarity of this drug with the PChCL core compared to the PCL and PBCL cores resulted in higher compatibility which was consistent with the Flory-Huggins interaction parameter value.[90]

1.3.2.2 Effect of Core Block Length

Increasing the hydrophobic length of the copolymer can influence various factors affecting drug loading. This includes drug partition coefficient, micelle size, core hydrophobicity, critical micelles concentration (CMC), aggregation number of micelles and a total number of micelles in the formulation. All these parameters are correlated, hence, should be considered during formulation to achieve higher encapsulation efficiency. Micelles with a longer hydrophobic block can lead to an increase in a solvent (water)-micelle core partition coefficient of the hydrophobic drugs. This can result in a higher drug loading content in the micelles. A possible explanation might be related to the higher hydrophobicity of the core which can reduce the CMC of micelles, thus, also increasing the stability of the micelles. The longer hydrophobic blocks (thus the hydrophobicity) also increase the aggregation number (number of block copolymer molecules required to form micelles). Hence, larger size micelles with higher accessible volume can be produced.

However, this can also reduce the total number of micelles in the formulation. The larger hydrophobic volume can act as a reservoir to encapsulate a higher level of drug within the micelle core. For instance, amiodarone (a class III antiarrhythmic agent used for various types of cardiac dysrhythmias), formulations with PEG5K-PCL5K, PEG5K-PCL13K, and PEG5K-PCL24K were prepared and evaluated for size and drug contents. Increasing the hydrophobic block length resulted in increasing the size and drug loading the micelles.[65] The same group also synthesised PEG5K-PCL5K, PEG5K-PCL13K, PEG5K-PCL24.5K copolymers and used these for the preparation of curcumin loaded micelles. The authors suggested the highest encapsulation efficiency in PEG5K-PCL24.5K micelles.[91] The opposite trend can be obtained by reducing the hydrophobic block length or increasing the hydrophilic block length. This not only increases the CMC of the micelles (thus reduces the stability) but also reduces the micelles size and core volume. This can lead to a reduced loading capability of the copolymer.[92]

1.3.2.3 Micelle Core Crystallinity

The amorphous content and crystallinity of the hydrophobic block can affect the physical state of the micelles core. This factor mainly depends on the the glass transition temperature (T_g) of the hydrophobic block at physiological conditions (37 ^oC). Micelles with higher amorphous content possess fluid like cores where the hydrophobic chains can easily move hence displaying higher volumes which can encapsulate a higher amount of drug. On the other hand,

crystalline polymers (hydrophobic block) possess solid like cores where polymeric chains are 'frozen' hence displaying smaller volumes for the drug to be encapsulated. However, the presence of drug may decrease the crystallinity of the core. For semicrystalline polymers (for example PCL), the crystallinity of the core increases with increasing molecular weight of the hydrophobic chain which can have an adverse impact on the drug loading capability. Glavas *et al.* synthesised copolymers (of same molecular weight) with semicrystalline (mPEG-PCL) or amorphous (mPEG-PεDL) hydrophobic blocks. The author reported a higher critical micelle concentration (CMC) of micelles having amorphous cores compared to those with semicrystalline cores. The sizes of the micelles with amorphous cores were shown to be increased by enhancing the hydrophobic:hydrophilic ratio of the copolymer. An opposite trend in size was observed for the micelles with semicrystalline cores[13]. In a previous publication, Bansal *et al.* reported a higher amphotericin B loading in mPEG-b-PDL (amorphous core) micelles compared to mPEG-b-PCL (semicrystalline core) micelles.[15] In another paper, a copolymer of poly (2-hydroxyethyl aspartamide) was prepared and used for the loading of the anticancer drug methotrexate. The authors modified the core by varying the degree of substitution of octadecyl (C18) side chains in the hydrophobic block. They suggested a higher volume of the core by increasing hydrophobic block length which should increase the loading capability. However, increasing substitution also increased the core

crystallinity, which resulted in less accessible volume for the drug to encapsulate in the micelles.[93]

1.3.2.4 Effect of Polymer and Drug Concentration

The maximum drug loading capacity can be achieved by optimization of polymer concentration for a specific polymer–drug system. At the maximum loading point, micelle cores are suggested to be completely saturated with the drug. Increasing the polymer concentration above the maximum capacity (or saturation point) may lead to precipitation of the drug and thus, can decrease the loading capability of a polymer.[14, 81] This depends on the interaction of the drug and hydrophobic block where stronger interaction enables saturation of core at low polymer concentration. For instance, naphthalene loading in less hydrophobic Pluronic copolymer micelles was found to be dependent on the polymer concentrations. However, increasing the hydrophobicity of the copolymer resulted in less sensitivity of naphthalene to copolymer concentration. At the highest hydrophobic content, the naphthalene loading became independent of copolymer concentration.[94-96] In another study, increasing the hydrophobic molecule (drug) concentration was suggested to enhance the aggregation of the copolymer in water and at the same time, reducing the CMC of the micelles (thus increasing the stability) and increasing the solubilization capacity.[92] The polymer/drug ratio also affects the drug loading capability. For instance, decreasing the polymer:drug ratio increased the drug loading capability of

the mPEG-b-PCL copolymer. In this case, the drug displayed an excellent compatibility with the polymer.[65] In the case of low compatibility, it can be suggested that the polymer:drug ratio should be increased to obtain sufficient drug loading in the micelles.

1.3.3 Drug Release from Micelles

Micelles have been used for solubilization (or loading) of many hydrophobic drugs. However, it is equally important to release the drug when desired in a controlled manner. Micelles are thermodynamic aggregates of block copolymers hence the stability of micelles is an important aspect which can affect the release of encapsulated drug molecules. Micelles with low stability can break up into unimers upon dilution after intravenous injection resulting in burst release characteristics. For stable micelles, drug release is mainly controlled by the rate of diffusion of the drug from micelles core to external media. The rate of diffusion is influenced by the drug-micelle core interaction where favorable interaction not only enhances the drug loading but also prevents the drug release from the micelle core. Therefore, it is important to maintain a balance between the loading and release characteristics required for specific drug delivery applications. A higher release rate of indomethacin from PEO-b-poly(β-benzyl-L-aspartate) (PEG –PBLA) micelles was suggested by increasing the pH of the release media which caused ionization of carboxyl groups of the drug hence reducing the hydrophobic interaction with the core.[70] In the same way, doxorubicin has been suggested to release at a

faster rate in acidic media (pH 5) compared to normal physiological conditions (pH 7.4). The possible reason might be the ionization of the amino group in doxorubucin due to re-protonation in acidic media which not only reduces the hydrophobic interaction with the micelle core but also increases the drug solubility in the aqueous media. This type of the system is particularly important for anticancer drug delivery where drug should be retained inside the micelles in blood (pH 7.4) but released once the micelles reach at the cancer site (low pH condition).[89] The length of the hydrophobic block not only increases the interaction with the drug but also enhances the size of the micelles. Both of these factors are known to reduce the release rate of the drug. For instance, Shuai *et al.* reported an increase in the size of micelles by increasing the hydrophobic block length in PEG-b-PCL copolymer. The micelles with longer PCL chain were reported to reduce the doxorubicin release rate. The authors also investigated the effect of pH (pH 7.4 and pH 5) on doxorubicin release. A faster release was observed in acidic media whereas, at physiological pH, a sustained release was observed for a longer period.[97]

The physical state of the micelle core at physiological pH can influence the release rate. The micelles with amorphous cores can release faster as compared to a crystalline core. Pyrene release occurred slowly from the polystyrene cores (T_g~100 ^oC) which are glassy at room temperature compared to poly(tert-butyl acrylate) core (T_g~42 ^oC).[98] The location of the

drug molecules in the micelles also influences the release characteristics of the micelles. The drug can be present either in the corona, core-corona interface or deep inside the core of the micelles. The localization of drug molecules depends on the interaction of the drug with the copolymers. A drug with higher hydrophilic characteristics can stay either in the core-corona interface or at the corona itself. On the other hand, more hydrophobic molecules usually stay in the core. Drugs can easily come out in the release media from the corona or core-corona interface, and these drug distributions mostly account for the burst release observed from polymer micelles. The drug molecules present in the core have to cross the core barrier before reaching the core-corona interface, hence taking a longer time to release. The drug molecules present at the periphery of the core need to cross a smaller distance than the drug molecules present deep inside the core. Therefore, drug release occurs at a faster rate when present in periphery compared to drug present deep inside the core.[98] The diffusion rate of the drug from the core also depends on the molecular volume of the drug. Drugs with a larger molecular volume diffuse at a slower rate than those with a smaller volume hence are released at a slower rate. Drugs present at core-corona interface or corona diffuse at rates less strongly dependent on the molecular drug volume.[98]

1.3.4 Stability of Micelles

The stability is an important aspect of the micelles system to be used as a drug delivery vehicle. A micelle is said to be thermodynamically stable when the concentration of the copolymer lies above CMC. The CMC is a concentration above which the copolymeric chains come together to form thermodynamic aggregates called micelles. Hence, CMC represents the concentration above which the single chains and micelles both coexist in the aqueous solution. The low CMC value shows the high stability of the micelles compared to high CMC of copolymer micelles.[14] Some factors influence the value of CMC like nature of hydrophobic block, length of the hydrophobic block, presence of solubilizate. Although, the type and length of hydrophobic block are one of the most important factors which influences the CMC most significantly. For instance, increasing the PCL chain length in mPEG-b-PCL copolymers (using a constant hydrophilic chain) increased the physicochemical stability by reducing the CMC, dissociation/aggregation and hydrolytic degradation of the micelles.[99] In the same study, author modified the copolymer by attaching benzyl carboxylate (mPEG-b-PBCL), or free carboxyl (mPEG-b-PCCL) on the backbone of PCL chain. The pendent benzyl carboxylate (aromatic) groups decreased the CMC considerably probably by enhancing the hydrophobic interactions. However, these micelles showed a higher adsorption of serum protein. On the other hand, the presence of a more hydrophilic free carboxyl group substituted on the PCL chain led to the

increase in the CMC while at the same time adsorbing less serum protein compared to the mPEG-b-PCL copolymer.[99] The other factor which influences the micelles stability includes the T_g of the hydrophobic block. Micelles with high T_g disassemble slowly compared to those with T_g.[14] The stability of the micelles may also be increased by incorporation of hydrophobic compounds in the micelles core which can enhance the hydrophobic interactions. For instance, Yokoyama et at studied the physical entrapment and chemical conjugation of Adriamycin (ADR) in poly(ethylene glycol)–poly(aspartic acid) (PEG–P(Asp)) micelles. They showed an enhanced stability of micelles by physical/chemical entrapment of drug in micelles probably due to increase the hydrophobic interactions within the core.[88] A long circulation time is a prerequisite condition for a delivery system to improved tissue accumulation and delivery of drug at the site of action. Nanoscale (10 – 200 nm in diameter) micelles are less susceptible to uptake by reticuloendothelial system (RES) system and also bypass the filtration of inter-endothelial cells in the spleen.[100] Particle sizes below 100 nm also help in extravasations of micelles at tumor sites. The presence of a hydrophilic surface (e.g. PEG) in micelles prevents the adsorption of plasma proteins (opsonin) by providing steric hindrance at the core-corona interface.[101, 102] Hence, the micelles can more easily escape the RES uptake. Despite the small size, the micelles are sufficiently large to avoid renal excretion which ultimately enhance the circulation time. There are several factors which control the size of the

micelles. However, the length of the hydrophobic block and physical state of the core (crystallinity) appears to have a profound effect on the micelles size.[14] For instance, increasing the PCL chain lengths in mPEG-b-PCL copolymer enhances the size of the micelles.[99] On the other hand, the size of the micelles was found to be increased by increasing the hydrophobic ratio of mPEG-b-PεDL (amorphous core) copolymer while for mPEG-b-PCL (semicrystalline core), the size was decreased by increasing the hydrophobic ratio.[13] The small size of certain micelles (<100nm) also facilitates their extravasation from the leaky site of capillaries e.g. tumor and inflammation. The other advantages of small size include enhancing uptake by the cells, ease of administration and sterilization by filtration.[103]

1.3.5 Pharmaceutical Applications

The applications of the polymeric micelles are mainly concentrated in the areas of drug solubilization, controlled drug release, and drug targeting. The ability to solubilize hydrophobic drugs (e.g. mainly anticancer drugs) is a key challenge in the field of drug delivery. The currently used solubilizing agents mostly consist of small molecular weight surfactant molecules to solubilize hydrophobic drugs. However, upon dilution in blood, they can easily break up to give a burst release in the body. Also, many current solubilizing agents are not inert in nature and possess side effects. For instance, the use of Cremophor EL for solubilization of paclitaxel (PTX) can result in neurotoxicity, hyperlipidemia and hypersensitivity reactions. Drugs such as

amiodarone and amphotericin B are usually solubilized by Tween 80 and sodium deoxycholate respectively. Both of these solubilizers are suggested to have hemolytic toxicity.[57] Therefore, polymeric micelles can be used as an alternative to solubilizing agents to solubilize different hydrophobic agents.[68, 74, 97, 104-108]

Solubilization is particularly important for chemotherapy as most current anticancer drugs are hydrophobic in nature hence requires solubilization in aqueous media (to make them administrable in the body). The application of the PEO-*b*-PDLLA micelles was reported to enhance the paclitaxel (PTX) and doxorubicin (DOX) solubility up to 5000 and 12000 times respectively.[109, 110] The use of micelles not only enhances the solubility but also prevents the degradation by improving the stability of the drugs.[62, 111, 112] For instance, camptothecin loaded N-phthaloylchitosan-grafter PEG methyl ether (PLC-g-MPEG) micelles were reported to prevent the hydrolysis of the lactone group (active form) of the drug.[113] Apart from the solubilization, controlling the release is an important characteristic for the controlled drug delivery system. The micelles system not only solubilizes the drug but also sustain the release. For instance, amphotericin was not only solubilized in polyethylene glycol-b-poly(δdecalactone) (mPEG-b-PDL) micelles but also provide sustained release for the extended period of time.[114]

Polymeric micelles provide numerous potential advantages for drug targeting, particularly to cancer sites. Most cancer therapeutics need carrier

systems to deliver the drug at the target site at a controlled rate while at the same time preventing the drug release in non-target sites to maximize therapeutic benefits. Micellar systems can be designed to exploit the opportunities provided by certain cancer physiologies which include the EPR effect, high interstitial pressure, low pH condition, over expressed receptors, angiogenesis etc. However, these opportunities can be utilized only if the micelle remains intact in the circulation for sufficiently long duration of time so that the system can target to the cancer site. The smaller size and surface hydrophilicity of micelles makes them less susceptible to RES system uptake hence an increased half-life of drug can be achieved.[111] Additionally, the enhanced permeability and retention (EPR) effect[115] (due to leaky vasculature at cancer site) allows the passive targeting of the micelles in the tumor site.[116, 117] PTX loaded PEG-poly(aspartic acid) micelles, where 50% carboxy groups were modified by 4-phenyl-1-butanol, showed a higher paclitaxel loading (23% w/w approx) and high tumor uptake efficiency due to the EPR effect. The product is under phase III clinical trial in breast cancer patients.[118, 119]

The selectivity of the drug targeting can be enhanced by attaching target-specific ligands on the surface of the micelles. The attachment of the ligand not only improves the selectivity but also enhances the intracellular uptake of the micelles which consequently improves the intracellular drug delivery.[111, 120] At the target site, a micelle tagged with a ligand may interact

with the specific receptor present in tumor cells and cause the micelle to be internalized by receptor-mediated endocytosis.[62, 111, 120-122] A number of ligand molecules such as specific antibodies, peptides, proteins, carbohydrates, small organic molecules and aptamers have been extensively reported in the literature for ligand-mediated targeting.[62, 111, 120, 123-128] For example, a PEG–PLA copolymer was conjugated with a APRPG (Ala-Pro-Arg-Pro-Gly) peptide at the PEG end to target $\alpha_v\beta_3$ integrin receptors which are often over-expressed during angiogenesis. The micelles were encapsulated with angiogenesis inhibitor (TNP-470). Inhibition of proliferation, migration, and tube formation was observed by drug-loaded micelles in human umbilical vein endothelial cells (HUVECs).[129] PEG–PLA nanoparticles were also conjugated with the CLT-1 peptide for targeting fibronectin (FN) overexpressed in the tumor. The micelles were loaded with paclitaxel. The drug loaded targeted micelles efficiently penetrated glioma cells to deliver the drug and extended the median survival time of the mice.[130]

Folate receptors are known to be over-expressed in many tumors particularly in breast and ovarian cancer. A folate-modified poly (2-ethyl-2-oxazoline)-b-poly (ε-caprolactone) (FA-PEOz-PCL) block copolymer loaded with doxorubicin (DOX) was synthesised for cellular uptake study. The formulation was tested in folate receptor positive (FR+) Human HeLa cervical carcinoma cell lines (HeLa), folate receptor negative (FR-) human A549 lung adenocarcinoma cell lines; human KB nasopharyngeal epidermal

carcinoma cell lines (KB) and Multidrug-Resistant human breast cancer MCF-7/ADR cell lines. The folate conjugated micelles (FA4) showed an enhanced cellular uptake in FR+ cell lines compared to non-folate micelles. Also, the addition of free folate along with the folate-conjugated micelles (FA4) showed a decreased uptake suggesting that the internalization was mainly driven by the folate receptor-mediated endocytosis mechanism.[131] In another study, transferrin (protein) was conjugated with mPEG-b-PLA copolymer. The micelles of the copolymer loaded with paclitaxel were tested for uptake on SGC-7901 (gastric carcinoma), SKOV-3 (ovarian carcinoma), and MCF-7 (breast carcinoma) cell lines. A higher uptake of transferrin conjugated micelles was observed with MCF-7 and SGC-7901 cell lines possess higher level of transferrin receptors. A lower difference in uptake was observed in SKOV-3 cell line as it expressed a lower level of transferrin.[132]

1.4 Aim and Objectives

The aim of this PhD project was to develop a novel polyester based delivery system to address specific drug delivery problems as discussed earlier. Based on the aim, the objectives of the work are:

- Synthesis of polyesters via polycondensation reactions with different aromatic side-chain contents to understand the effect on polymer properties. The addition of phenyl groups in the polymer was anticipated to enhance the hydrophobic interactions between aromatic

ring based drugs and the polymer to increase the loading capability. The polymer selected for highest loading capability was proposed to be utilized for stability, degradability, cytocompability and cell uptake capability studies.

- Synthesis of polyester copolymers from ROP reactions using renewable decalactone monomer to reduce the dependency on fossil feedstocks. The ROP route was selected as a comparator against polycondensation reactions. The metal-based catalyst normally used was proposed to be replaced with a more efficient organocatalyst (TBD) which can easily be separated from the desired copolymer product for subsequent re-use.
- Synthesis of polyester copolymers based on dielectric properties of the starting materials using microwave-based ring opening polymerization (MROP) for comparison with conventional ROP methods. Microwave irradiation was adopted as a clean, 'green' and cheap heating method.
- The utilization of polyester based micelles as a drug delivery vehicle for hydrophobic drugs and comparison with the structurally similar well-established Polycaprolactone (PCL) based micelle system. Indomethacin (IND) was utilized as model hydrophobic molecules for drug loading and release study. The novel formulation was also utilized for stability, degradability, cytocompatibility, and cell uptake studies.

1.5 References

1. U. Edlund and A. C. Albertsson, *Advanced Drug Delivery Reviews*, 2003, **55**, 585-609.
2. C. Hahn, S. Wesselbaum, H. Keul and M. Moller, *European Polymer Journal*, 2013, **49**, 217-227.
3. S. Slomkowski, *Macromolecular Symposia*, 2010, **288**, 121-129.
4. S. Slomkowski, *Macromolecular Symposia*, 2007, **253**, 47-58.
5. H. Zhang, A. Patel, A. K. Gaharwar, S. M. Mihaila, G. Iviglia, S. Mukundan, H. Bae, H. Yang and A. Khademhosseini, *Biomacromolecules*, 2013, **14**, 1299-1310.
6. A. C. Albertsson and I. K. Varma, *Biomacromolecules*, 2003, **4**, 1466-1486.
7. S. Vlad, S. Oprea, A. Stanciu, C. Ciobanu and V. Bulacovschi, *European Polymer Journal*, 2000, **36**, 1495-1501.
8. C. Yang, A. B. E. Attia, J. P. K. Tan, X. Ke, S. Gao, J. L. Hedrick and Y.-Y. Yang, *Biomaterials*, 2012, **33**, 2971-2979.
9. X. D. Lou, C. Detrembleur and R. Jerome, *Macromolecular Rapid Communications*, 2003, **24**, 161-172.
10. C. Vaida, M. Takwa, M. Martinelle, K. Hult, H. Keul and M. Moller, *Macromolecular Symposia*, 2008, **272**, 28-38.
11. U. Witt, R. J. Muller and W. D. Deckwer, *Macromolecular Chemistry and Physics*, 1996, **197**, 1525-1535.
12. H. J. Jin, B. Y. Lee, M. N. Kim and J. S. Yoon, *Journal of Polymer Science Part B-Polymer Physics*, 2000, **38**, 1504-1511.
13. L. Glavas, P. Olsen, K. Odelius and A.-C. Albertsson, *Biomacromolecules*, 2013, **14**, 4150-4156.
14. C. Allen, D. Maysinger and A. Eisenberg, *Colloids and Surfaces B-Biointerfaces*, 1999, **16**, 3-27.
15. B. Kuldeep, K. Deepak, P. Laura, I. Derek, H. Steven, M. Giuseppe and A. Cameron, *Journal*, 2015, **6**, 7196-7210.
16. W. H. Carothers, *Journal*, 1929, **51**, 2548-2559.
17. A. Takasu, Y. Shibata, Y. Narukawa and T. Hirabayashi, *Macromolecules*, 2007, **40**, 151-153.
18. X.-M. Zhou, *Materials Science & Engineering C-Materials for Biological Applications*, 2012, **32**, 2459-2463.
19. J. Tang, Z. Zhang, Z. Song, L. Chen, X. Hou and K. Yao, *European Polymer Journal*, 2006, **42**, 3360-3366.
20. T. Moyori, T. Tang and A. Takasu, *Biomacromolecules*, 2012, **13**, 1240-1243.
21. A. Takasu, A. Takemoto and T. Hirabayashi, *Biomacromolecules*, 2006, **7**, 6-9.
22. D. C. Forbes and K. J. Weaver, *Journal of Molecular Catalysis a-Chemical*, 2004, **214**, 129-132.

23. C. Detrembleur, M. Mazza, X. Lou, O. Halleux, P. Lecomte, D. Mecerreyes, J. L. Hedrick and R. Jerome, *Macromolecules*, 2000, **33**, 7751-7760.
24. C. Jerome and P. Lecomte, *Advanced Drug Delivery Reviews*, 2008, **60**, 1056-1076.
25. A. C. Albertsson and I. K. Varma, *Degradable Aliphatic Polyesters*, 2002, **157**, 1-40.
26. A. Duda, A. Kowalski, S. Penczek, H. Uyama and S. Kobayashi, *Macromolecules*, 2002, **35**, 4266-4270.
27. J. Libiszowski, A. Kowalski, R. Szymanski, A. Duda, J. M. Raquez, P. Degee and P. Dubois, *Macromolecules*, 2004, **37**, 52-59.
28. J. Libiszowski, A. Kowalski, A. E. Duda and S. Penczek, *Macromolecular Chemistry and Physics*, 2002, **203**, 1694-1701.
29. R. F. Storey and J. W. Sherman, *Macromolecules*, 2002, **35**, 1504-1512.
30. A. Kowalski, J. Libiszowski, T. Biela, M. Cypryk, A. Duda and S. Penczek, *Macromolecules*, 2005, **38**, 8170-8176.
31. F. Fischer, *Chemie in Unserer Zeit*, 2002, **36**, 240-244.
32. A. Sosnik, G. Gotelli and G. A. Abraham, *Progress in Polymer Science*, 2011, **36**, 1050-1078.
33. C. O. Kappe, *Angewandte Chemie-International Edition*, 2004, **43**, 6250-6284.
34. C. O. Kappe and D. Dallinger, *Molecular Diversity*, 2009, **13**, 71-193.
35. R. Hoogenboom and U. S. Schubert, *Macromolecular Rapid Communications*, 2007, **28**, 368-386.
36. K. Kempe, C. R. Becer and U. S. Schubert, *Macromolecules*, 2011, **44**, 5825-5842.
37. S. Velmathi, R. Nagahata, J. Sugiyama and K. Takeuchi, *Macromolecular Rapid Communications*, 2005, **26**, 1163-1167.
38. R. Nagahata, D. Sano, H. Suzuki and K. Takeuchi, *Macromolecular Rapid Communications*, 2007, **28**, 437-442.
39. T. Nakamura, R. Nagahata, K. Kunii, H. Soga, S. Sugimoto and K. Takeuchi, *Organic Process Research & Development*, 2010, **14**, 781-786.
40. T. Nakamura, R. Nagahata, S. Suemitsu and K. Takeuchi, *Polymer*, 2010, **51**, 329-333.
41. A. Borriello, L. Nicolais, X. Fang, S. J. Huang and D. A. Scola, *Journal of Applied Polymer Science*, 2007, **103**, 1952-1958.
42. P. Albert, H. Warth, R. Mulhaupt and R. Janda, *Macromolecular Chemistry and Physics*, 1996, **197**, 1633-1641.
43. X. M. Fang, C. D. Simone, E. Vaccaro, S. J. Huang and D. A. Scola, *Journal of Polymer Science Part a-Polymer Chemistry*, 2002, **40**, 2264-2275.

44. H. Li, L. Liao and L. Liu, *Macromolecular Rapid Communications*, 2007, **28**, 411-416.
45. L. Liu, Y. Li, Y. Fang and L. X. Chen, *Carbohydrate Polymers*, 2005, **60**, 351-356.
46. Z. J. Yu, L. J. Liu and R. X. Zhuo, *Journal of Polymer Science Part a-Polymer Chemistry*, 2003, **41**, 13-21.
47. Q. Xu, C. Zhang, S. Cai, P. Zhu and L. Liu, *Journal of Industrial and Engineering Chemistry*, 2010, **16**, 872-875.
48. L. Q. Liao, L. J. Liu, C. Zhang, F. He, R. X. Zhuo and K. Wan, *Journal of Polymer Science Part a-Polymer Chemistry*, 2002, **40**, 1749-1755.
49. L. Liao, L. Liu, C. Zhang and S. Gong, *Macromolecular Rapid Communications*, 2006, **27**, 2060-2064.
50. C. Zhang, L. Liao and S. Gong, *Macromolecular Rapid Communications*, 2007, **28**, 422-427.
51. C. Zhang, L. Liao and S. Gong, *Macromolecular Chemistry and Physics*, 2007, **208**, 1122-1128.
52. Z. J. Yu and L. J. Liu, *Journal of Biomaterials Science-Polymer Edition*, 2005, **16**, 957-971.
53. H. Ahmed, B. Trathnigg, C. O. Kappe and R. Saf, *European Polymer Journal*, 2010, **46**, 494-505.
54. A. Karagoz and S. Dincer, in *New Frontiers in Macromolecular Science*, eds. V. Cimrova and F. Rypacek, 2010, vol. 295, pp. 131-137.
55. J. Ramier, E. Renard and D. Grande, *Journal of Polymer Science Part a-Polymer Chemistry*, 2012, **50**, 1445-1455.
56. M. L. Adams, A. Lavasanifar and G. S. Kwon, *Journal of Pharmaceutical Sciences*, 2003, **92**, 1343-1355.
57. H. M. Aliabadi and A. Lavasanifar, *Expert opinion on drug delivery*, 2006, **3**, 139-162.
58. M. C. Jones and J. C. Leroux, *European Journal of Pharmaceutics and Biopharmaceutics*, 1999, **48**, 101-111.
59. A. Lavasanifar, J. Samuel, S. Sattari and G. S. Kwon, *Pharmaceutical Research*, 2002, **19**, 418-422.
60. Z. Zhu, *Biomaterials*, 2013, **34**, 10238-10248.
61. A. V. Kabanov, I. R. Nazarova, I. V. Astafieva, E. V. Batrakova, V. Y. Alakhov, A. A. Yaroslavov and V. A. Kabanov, *Macromolecules*, 1995, **28**, 2303-2314.
62. U. Kedar, P. Phutane, S. Shidhaye and V. Kadam, *Nanomedicine-Nanotechnology Biology and Medicine*, 2010, **6**, 714-729.
63. R. Gref, Y. Minamitake, M. T. Peracchia, V. Trubetskoy, V. Torchilin and R. Langer, *Science*, 1994, **263**, 1600-1603.
64. H. Miura, H. Onishi, M. Sasatsu and Y. Machida, *Journal of Controlled Release*, 2004, **97**, 101-113.
65. S. Elhasi, R. Astaneh and A. Lavasanifar, *European Journal of Pharmaceutics and Biopharmaceutics*, 2007, **65**, 406-413.

66. V. P. Sant, D. Smith and J.-C. Leroux, *Journal of Controlled Release*, 2004, **97**, 301-312.
67. W. J. Lin, L. W. Juang and C. C. Lin, *Pharmaceutical Research*, 2003, **20**, 668-673.
68. S. Y. Kim and Y. M. Lee, *Biomaterials*, 2001, **22**, 1697-1704.
69. P. Vangeyte, S. Gautier and R. Jerome, *Colloids and Surfaces a-Physicochemical and Engineering Aspects*, 2004, **242**, 203-211.
70. S. B. La, T. Okano and K. Kataoka, *Journal of Pharmaceutical Sciences*, 1996, **85**, 85-90.
71. J.-P. Jee, A. McCoy and S. Mecozzi, *Pharmaceutical Research*, 2012, **29**, 69-82.
72. M. Gou, K. Men, H. Shi, M. Xiang, J. Zhang, J. Song, J. Long, Y. Wan, F. Luo, X. Zhao and Z. Qian, *Nanoscale*, 2011, **3**, 1558-1567.
73. S. Galindo-Rodriguez, E. Allemann, H. Fessi and E. Doelker, *Pharmaceutical Research*, 2004, **21**, 1428-1439.
74. H. M. Aliabadi, S. Elhasi, A. Mahmud, R. Gulamhusein, P. Mahdipoor and A. Lavasanifar, *International Journal of Pharmaceutics*, 2007, **329**, 158-165.
75. B. K. Johnson and R. K. Prud'homme, *Australian Journal of Chemistry*, 2003, **56**, 1021-1024.
76. H. Shen, S. Hong, R. K. Prud'homme and Y. Liu, *Journal of Nanoparticle Research*, 2011, **13**, 4109-4120.
77. K. M. Pustulka, A. R. Wohl, H. S. Lee, A. R. Michel, J. Han, T. R. Hoye, A. V. McCormick, J. Panyam and C. W. Macosko, *Molecular Pharmaceutics*, 2013, **10**, 4367-4377.
78. Z. Zhu, *Molecular Pharmaceutics*, 2014, **11**, 776-786.
79. S. F. Chow, K. Y. Wan, K. K. Cheng, K. W. Wong, C. C. Sun, L. Baum and A. H. L. Chow, *European Journal of Pharmaceutics and Biopharmaceutics*, 2015, **94**, 436-449.
80. Y. Liu, C. Cheng, R. K. Prud'homme and R. O. Fox, *Chemical Engineering Science*, 2008, **63**, 2829-2842.
81. Z. L. Tyrrell, Y. Shen and M. Radosz, *Progress in Polymer Science*, 2010, **35**, 1128-1143.
82. M. L. T. Zweers, G. H. M. Engbers, D. W. Grijpma and J. Feijen, *Journal of Controlled Release*, 2006, **114**, 317-324.
83. M. L. T. Zweers, D. W. Grijpma, G. H. M. Engbers and J. Feijen, *Journal of Biomedical Materials Research Part B-Applied Biomaterials*, 2003, **66B**, 559-566.
84. M. L. T. Zweers, G. H. M. Engbers, D. W. Grijpma and J. Feijen, *Journal of Controlled Release*, 2004, **100**, 347-356.
85. E. Fournier, M. H. Dufresne, D. C. Smith, M. Ranger and J. C. Leroux, *Pharmaceutical Research*, 2004, **21**, 962-968.

86. D. Le Garrec, S. Gori, L. Luo, D. Lessard, D. C. Smith, M. A. Yessine, M. Ranger and J. C. Leroux, *Journal of Controlled Release*, 2004, **99**, 83-101.
87. N. Nishiyama, Y. Kato, Y. Sugiyama and K. Kataoka, *Pharmaceutical Research*, 2001, **18**, 1035-1041.
88. M. Yokoyama, S. Fukushima, R. Uehara, K. Okamoto, K. Kataoka, Y. Sakurai and T. Okano, *Journal of Controlled Release*, 1998, **50**, 79-92.
89. K. Kataoka, T. Matsumoto, M. Yokoyama, T. Okano, Y. Sakurai, S. Fukushima, K. Okamoto and G. S. Kwon, *Journal of Controlled Release*, 2000, **64**, 143-153.
90. A. Mahmud, S. Patel, O. Molavi, P. Choi, J. Samuel and A. Lavasanifar, *Biomacromolecules*, 2009, **10**, 471-478.
91. Z. Ma, A. Haddadi, O. Molavi, A. Lavasanifar, R. Lai and J. Samuel, *Journal of Biomedical Materials Research Part A*, 2008, **86A**, 300-310.
92. L. Xing and W. L. Mattice, *Macromolecules*, 1997, **30**, 1711-1717.
93. H. Kang, J. D. Kim, S. H. Han and I. S. Chang, *Journal of Controlled Release*, 2002, **81**, 135-144.
94. P. N. Hurter and T. A. Hatton, *Langmuir*, 1992, **8**, 1291-1299.
95. P. N. Hurter, J. Scheutjens and T. A. Hatton, *Macromolecules*, 1993, **26**, 5592-5601.
96. P. N. Hurter, J. Scheutjens and T. A. Hatton, *Macromolecules*, 1993, **26**, 5030-5040.
97. X. T. Shuai, H. Ai, N. Nasongkla, S. Kim and J. M. Gao, *Journal of Controlled Release*, 2004, **98**, 415-426.
98. Y. Teng, M. E. Morrison, P. Munk, S. E. Webber and K. Prochazka, *Macromolecules*, 1998, **31**, 3578-3587.
99. S. M. Garg, M. R. Vakili and A. Lavasanifar, *Colloids and Surfaces B-Biointerfaces*, 2015, **132**, 161-170.
100. A. Lavasanifar, J. Samuel and G. S. Kwon, *Advanced Drug Delivery Reviews*, 2002, **54**, 169-190.
101. S. M. Moghimi, A. C. Hunter and J. C. Murray, *Pharmacological Reviews*, 2001, **53**, 283-318.
102. I. Brigger, C. Dubernet and P. Couvreur, *Advanced Drug Delivery Reviews*, 2002, **54**, 631-651.
103. Y. Lu and K. Park, *International Journal of Pharmaceutics*, 2013, **453**, 198-214.
104. H. M. Aliabadi, A. Mahmud, A. D. Sharifabadi and A. Lavasanifar, *Journal of Controlled Release*, 2005, **104**, 301-311.
105. M. Shahin, N. Safaei-Nikouei and A. Lavasanifar, *Journal of Drug Targeting*, 2014, **22**, 629-637.
106. X.-B. Xiong and A. Lavasanifar, *Acs Nano*, 2011, **5**, 5202-5213.
107. I. L. G. Shin, S. Y. Kim, Y. M. Lee, C. S. Cho and Y. K. Sung, *Journal of Controlled Release*, 1998, **51**, 1-11.

108. J. J. Yu, H. A. Lee, J. H. Kim, W. H. Kong, Y. Kim, Z. Y. Cui, K. G. Park, W. S. Kim, H. G. Lee and S. W. Seo, *Journal of Drug Targeting*, 2007, **15**, 279-284.
109. X. C. Zhang, H. M. Burt, G. Mangold, D. Dexter, D. VonHoff, L. Mayer and W. L. Hunter, *Anti-Cancer Drugs*, 1997, **8**, 696-701.
110. E. Piskin, X. Kaitian, E. B. Denkbas and Z. Kucukyavuz, *Journal of Biomaterials Science-Polymer Edition*, 1995, **7**, 359-373.
111. C. Oerlemans, W. Bult, M. Bos, G. Storm, J. F. W. Nijsen and W. E. Hennink, *Pharmaceutical Research*, 2010, **27**, 2569-2589.
112. V. P. Torchilin, *Cellular and Molecular Life Sciences*, 2004, **61**, 2549-2559.
113. P. Opanasopit, T. Ngawhirunpat, A. Chaidedgumjorn, T. Rojanarata, A. Apirakaramwong, S. Phongying, C. Choochottiros and S. Chirachanchai, *European Journal of Pharmaceutics and Biopharmaceutics*, 2006, **64**, 269-276.
114. K. K. Bansal, D. Kakde, L. Purdie, D. J. Irvine, S. M. Howdle, G. Mantovani and C. Alexander, *Polymer Chemistry*, 2015, **6**, 7196-7210.
115. H. Maeda, J. Wu, T. Sawa, Y. Matsumura and K. Hori, *Journal of Controlled Release*, 2000, **65**, 271-284.
116. H. Maeda, G. Y. Bharate and J. Daruwalla, *European Journal of Pharmaceutics and Biopharmaceutics*, 2009, **71**, 409-419.
117. V. Torchilin, *Advanced Drug Delivery Reviews*, 2011, **63**, 131-135.
118. T. Hamaguchi, Y. Matsumura, M. Suzuki, K. Shimizu, R. Goda, I. Nakamura, I. Nakatomi, M. Yokoyama, K. Kataoka and T. Kakizoe, *British Journal of Cancer*, 2005, **92**, 1240-1246.
119. K. Kato, K. Chin, T. Yoshikawa, K. Yamaguchi, Y. Tsuji, T. Esaki, K. Sakai, M. Kimura, T. Hamaguchi, Y. Shimada, Y. Matsumura and R. Ikeda, *Investigational New Drugs*, 2012, **30**, 1621-1627.
120. D. Sutton, N. Nasongkla, E. Blanco and J. Gao, *Pharmaceutical Research*, 2007, **24**, 1029-1046.
121. F. Danhier, O. Feron and V. Preat, *Journal of Controlled Release*, 2010, **148**, 135-146.
122. D. Peer, J. M. Karp, S. Hong, O. C. FaroKhzad, R. Margalit and R. Langer, *Nature Nanotechnology*, 2007, **2**, 751-760.
123. A. M. Jhaveri and V. P. Torchilin, *Frontiers in pharmacology*, 2014, **5**, 77-77.
124. Y. Miura, T. Takenaka, K. Toh, S. Wu, H. Nishihara, M. R. Kano, Y. Ino, T. Nomoto, Y. Matsumoto, H. Koyama, H. Cabral, N. Nishiyama and K. Kataoka, *Acs Nano*, 2013, **7**, 8583-8592.
125. N. Nasongkla, X. Shuai, H. Ai, B. D. Weinberg, J. Pink, D. A. Boothman and J. M. Gao, *Angewandte Chemie-International Edition*, 2004, **43**, 6323-6327.
126. P. a. Ma, S. Liu, Y. Huang, X. Chen, L. Zhang and X. Jing, *Biomaterials*, 2010, **31**, 2646-2654.

127. R. Yang, F. Meng, S. Ma, F. Huang, H. Liu and Z. Zhong, *Biomacromolecules*, 2011, **12**, 3047-3055.
128. W. Xu, I. A. Siddiqui, M. Nihal, S. Pilla, K. Rosenthal, H. Mukhtar and S. Gong, *Biomaterials*, 2013, **34**, 5244-5253.
129. Y. Wang, P. Liu, Y. Duan, X. Yin, Q. Wang, X. Liu, X. Wang, J. Zhou, W. Wang, L. Qiu and W. Di, *Biomaterials*, 2014, **35**, 983-992.
130. B. Zhang, S. Shen, Z. Liao, W. Shi, Y. Wang, J. Zhao, Y. Hu, J. Yang, J. Chen, H. Mei, Y. Hu, Z. Pang and X. Jiang, *Biomaterials*, 2014, **35**, 4088-4098.
131. L.-Y. Qiu, L. Yan, L. Zhang, Y.-M. Jin and Q.-H. Zhao, *International Journal of Pharmaceutics*, 2013, **456**, 315-324.
132. J. Yue, S. Liu, R. Wang, X. Hu, Z. Xie, Y. Huang and X. Jing, *Molecular Pharmaceutics*, 2012, **9**, 1919-1931.

Chapter

2

Materials and Methods

2.1 Materials

General Chemicals

All chemicals were purchased from Sigma-Aldrich unless specifically stated. A list of chemicals with their purity given by manufacturer has been described below.

Succinic acid (≥99.0%), phenylsuccinic acid (98%), 1,10-decanediol (98%), scandium(III) triflate (99%), Pluronic (F-68), ε-decalactone (ε-DL) (≥99%), δ-decalactone (δ-DL) (≥98%), ε-caprolactone (ε-CL) (97%), 1,5,7-triazabicyclo[4.4.0]dec-5-ene (TBD) (98%), poly(ethylene glycol) monomethyl ether (mPEG) (M_n-5000), benzoic acid (≥99.5%), pyrene (≥99%), indomethacin (IND) (≥99%), coumarin 6 (≥99.5%), 1 mM sodium pyruvate, 1% non- essential amino acids, phosphate buffer solution, CFDA-AM, Neutral Red, acetic acid, 95% ethanol, ammonium chloride, Triton-X100, DAPI, H_2O_2, HBSS, low melting point agarose, agarose , lysis buffer base, dimethyl sulfoxide (DMSO), HEPES, potassium chloride, Ethylenediaminetetraacetic acid [EDTA], Bovine Serum Albumin, sodium hydroxide, Tris base and GelRed were purchased from Sigma-Aldrich.

Cell culture reagents including MEM medium, foetal calf serum (FCS), 2 mM L-glutamine, 100 U/ml penicillin/streptomycin, phenol red free MEM medium, 10 x trypsin (2.5%) and 0.4% v/v Trypan Blue were purchased

from Gibco, Invitrogen. The human hepatocyte cell line C3A was purchased from ATCC, Manassas, VA, USA.

Poly(ethylene glycol) monomethyl ether (M_n-5000), ε-DL, δ-DL and ε-CL were dehydrated by azeotropic distillation using anhydrous toluene. All other materials were used as received unless otherwise stated. All other solvents were purchased from Fischer Scientific UK. The deuterated solvents for NMR spectroscopy were purchased from Sigma-Aldrich.

2.2 Instruments and Methods

2.2.1 Fourier Transform Infrared (FTIR) Spectroscopy

Fourier transform infrared (FTIR) spectroscopy analysis was performed using a Cary 630 FTIR spectrophotometer. For all analyses, a background spectrum was collected before placing the sample of interest on a clean crystal present in the sample holder. The collected sample spectrum was analysed using MicroLab software.

2.2.2 Nuclear Magnetic Resonance (NMR)

Bruker NMR spectrometers operating at 400 MHz (^{1}H) and 101 MHz (^{13}C) were used to perform nuclear magnetic resonance (NMR) analysis in deuterated solvents. Chemical shifts were recorded in ppm and MestReNova 6.0.2 copyright©2009 software was used for analyzing the spectra. Residual solvent peaks were used as an internal standard ($CDCl_3$: δ_H 7.26, δ_C 77.16, DMSO-d_6: δ_H 2.50, δ_C 39.52).

2.2.3 Size Exclusive Chromatography (SEC)

Size exclusive chromatography (SEC) was used to determine number-average molar mass (M_n), weight average molar mass (M_w) and mass distribution (polydispersity, Đ, M_w/M_n). A Polymer Laboratories GPC 50 instrument fitted with a differential refractive index detector was used for chromatography. A Polymer Labs PLgel guard column (50 × 7.5 mm, 8 μm) and a pair of PLgel Mixed-D columns (300 × 7.5 mm, 8 μm) were also present in the instrument. HPLC grade $CHCl_3$ was used as an eluent at 1 mL min^{-1} flow rate. Column calibration was performed using narrow molar mass distribution polystyrene standards. Polymer Labs Cirrus 3.0 software was used for data analysis.

2.2.4 Differential Scanning Colorimeter (DSC)

Melting temperature (T_m) and glass transition temperature (T_g) of the polymers were determined using a TA-Q2000 DSC (TA Instruments) under nitrogen atmosphere. The sample (5–10 mg) was weighed into a T_{zero} DSC pan. A T_{zero} DSC lid was placed on the top and then sealed with a T_{zero} press (TA Instruments) using a Black T_{zero} lower die and a flat upper die. Typically, the samples were exposed to two cooling-heating cycles from –90 to 150 °C at a rate of 10 °C/min. The results of the second cycle were reported.

2.2.5 Dynamic Light Scattering (DLS) and Zeta Potential

Dynamic light scattering (DLS) was used for measuring the size and size distribution of nanoparticles/micelles samples. DLS measures the intensity

fluctuations of scattered light caused by Brownian motion of the nanoparticles, which can be converted into a measure of particle size using the Stokes-Einstein relationship.

The z-average diameter and the Polydispersity Index (PDI) of nanoparticles were determined by DLS using a NanoZS instrument (Malvern, UK) at 25 °C using 633 nm (4 mW) wavelength laser. The scattered light was detected at an angle of 173° and analysis was performed using zetasizer software version 7.03.

NanoZS instrument (Malvern, UK) was used for measuring zeta Potential via a Laser Doppler Micro-electrophoresis technique. An electric field was applied to the formulation containing particles, which caused a movement of particles at a certain velocity. The velocity was measured by phase analysis light scattering to give electrophoretic mobility. This electrophoretic mobility value was used for the calculation of zeta potential and zeta potential distribution. Data analysis was performed using zetasizer software version 7.03. The mean values were reported which obtained from three measurements.

2.2.6 Transmission Electron Microscopy (TEM)

The size and morphology of the nanoparticles and micelles were determined using Transmission Electron Microscopy (TEM). The samples were imaged using an FEI Tecnai G2 electron microscope. A droplet of

nanoparticle/micelles solution (10 µL) containing 0.1 mg/mL of the polymer was placed on the copper grid and allowed to dry in air. Samples were then imaged without staining at 100 KV and analysed using TIA imaging software.

2.2.7 Fluorescence Spectroscopy

A Cary Eclipse Fluorescence spectrophotometer (Varian) was used to record the fluorescence spectra. The excitation and emission slit widths were set at 5 nm. The intensities were measured against appropriate blank at room temperature.

2.2.8 Ultraviolet-Visible Spectroscopy (UV/Visible)

A Beckman Coulter DU 800 UV spectrophotometer was used for measurements of the samples using a capped quartz cuvettes. The samples (700 µL) were measured using appropriate dilution against the blank at room temperature (RT).

2.2.9 CEM Discover Microwave Reactor

The reactions under microwave irradiation were performed in a CEM Discover Microwave Reactor. Reactions were controlled under a preset program of the CEM reactor computer. All the reactions were performed under nitrogen atmosphere.

2.3 Critical Micelle Concentration (CMC) Determination

Pyrene was used as a fluorescent probe for determination of CMC values of amphiphilic block copolymers by pyrene 1:3 peak ratio method.[1, 2] The

fluorescence spectra of pyrene show five different peaks. The intensities of these peaks are dependent on the surrounding environment (i.e. polarity) experienced by the pyrene molecule (Figure 2-1). When the pyrene molecules move from the polar to non-polar regions, the peak intensity at 373 nm (I_1) reduces while that of the third peak (I_3) at 384 nm increases. When micelles start to form in an experimental solution, they provide a hydrophobic environment for pyrene. Consequently, the pyrene molecules move from water (polar phase) to micelle cores (nonpolar phase) which lead to a decrease in the intensity of peak 1 or the ratio of peak 1st to 3rd.

Briefly, pyrene was dissolved in acetone to make a stock solution. A pre-calculated quantity of pyrene in a solution of known concentration ($6x10^{-7}$ M) was transferred into vials. It was followed by evaporation of acetone under a slow stream of nitrogen. Different concentrations of micelles solutions (0.001 to 50 µg/mL) were added to each vial and agitated overnight in the dark to equilibrate. The fluorescence spectra of samples were then recorded in the range of 350 to 420 nm at an excitation wavelength of 335 nm. The pyrene 1:3 ratio was then calculated using intensities of emitted light at 373 nm (I_1) and 384 nm (I_3). The pyrene 1:3 ratio was plotted against the concentration of polymer used (log scale) to determine CMC. All measurements were performed in triplicate at room temperature and mean value was reported.

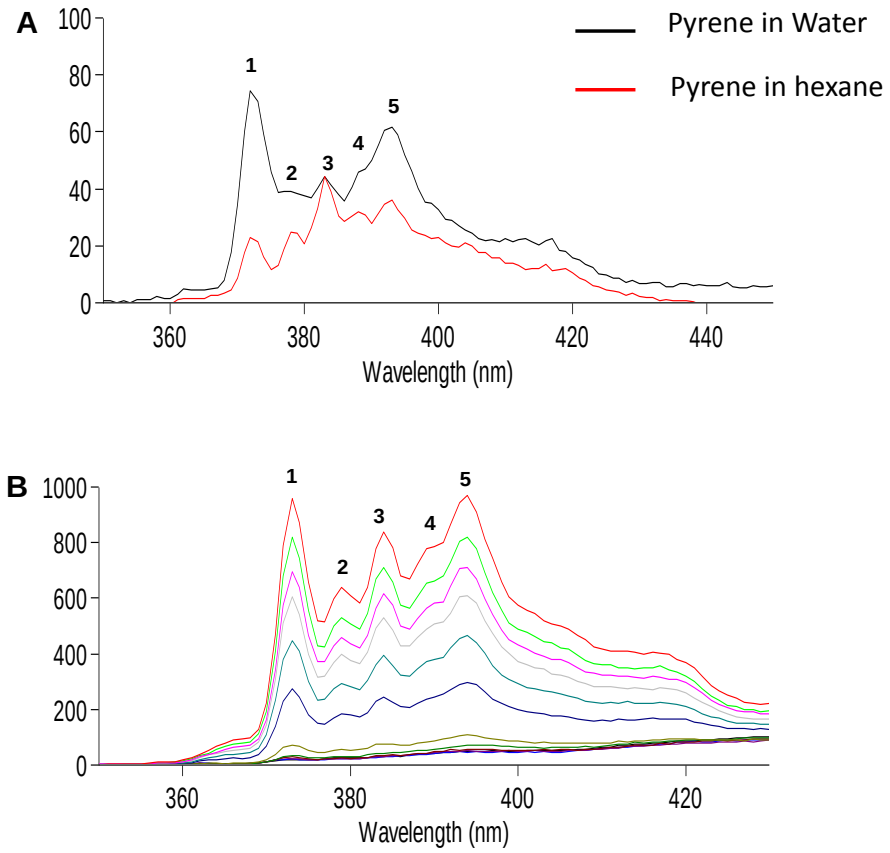


Figure 2-1 Fluorescence spectra of pyrene in (A) different polarity solvents (water and hexane) (B) in presence of block copolymer with different concentrations in water

2.4 Drug Content and Encapsulation Efficiency

Drug content weight percent (DC wt%) and percent encapsulation efficiency (EE %) in the samples were calculated using the formula below:

$$\text{DC (wt\%)} = \frac{\text{Amount of drug loaded}}{\text{Amount of polymer used}} \text{X100}$$

$$\text{EE \%} = \frac{\text{Amount of drug loaded}}{\text{Amount of drug used}} \text{X100}$$

2.5 References

1. J. Aguiar, P. Carpena, J. A. Molina-Boĺıvar and C. Carnero Ruiz, *Journal of Colloid and Interface Science*, 2003, **258**, 116-122.
2. G. Basu Ray, I. Chakraborty and S. P. Moulik, *Journal of Colloid and Interface Science*, 2006, **294**, 248-254.

Chapter

3

Synthesis, Characterisation and Evaluation of Novel Linear Polyesters

3.1 Introduction

In recent times, drug delivery systems have been modified in a number of ways to improve controlled release of active moieties at disease sites. Polymeric systems have many potential advantages to control the release of drugs and hence are extensively used in emerging drug delivery technologies.[1-3] Out of the various types of polymers, polyesters are considered as one of the most important classes because of their intrinsic biocompatibility.[4, 5] The ester bonds in the polymeric backbone of polyesters can be tuned to be hydrolytically labile to base or acid, and also to provide an opportunity for hydrolytic enzymes to cleave polymers into smaller, more easily cleared, fragments.[6, 7] Therefore, polyesters have become a material of choice for various biomedical applications including drug delivery [2, 8-11] and tissue engineering.[12-16] The commonly used polyesters for biomedical applications include poly (lactic acid) (PLA), poly (lactic-co-glycolic acid) (PLGA) and poly (ε-caprolactone) (PCL). However, they have limitations of use, for instance, the release of excessive acid upon degradation[17] for PLGA or long degradation time[12] for PCL polymers. Non-linear biodegradability and release profiles also limit their use in certain drug delivery applications. Furthermore, the brittle and rigid nature of the above polyesters limits their use as tissue engineering scaffolds when a soft and flexible matrix with similar mechanical properties of the surrounding tissues is required.[18] Hence, there is a need to develop novel polyesters with enhanced properties.

A careful selection of the monomers in the synthesis of polyesters can address the issues of crystallinity, hydrophobicity, degradability, loading capability and biocompatibility.[19] The introduction of aromatic rings in polyesters can change physical properties like crystallinity.[20] However, the position of the aromatic ring (within the polymer backbone or as a side group appended to the backbone) in the polyester can markedly affect the characteristics of the polymers. For instance, Witt *et al.* studied the incorporation of aromatic units into the polyester main chain where they suggested an improvement in mechanical properties. However, the biodegradability decreased due to higher crystallinity as the aromatic content increased.[21] In another study poly(butylene succinate) and poly-(ethylene adipate) were copolymerised with mendalic acid to evaluate the effect of aromatic content on thermal and mechanical properties of polymers. It was observed that increasing the phenyl content in polymers as side chain decreased the melting temperature and crystallinity but increased the glass transition temperature. The biodegradability was increased with higher content of phenyl side chain at the same time as a decrease in crystallinity.[20] These two studies suggested two important factors (1) phenyl groups within the polyester backbone cause higher crystallinity hence slower biodegradability, whereas (2) phenyl groups as side chains on polyester backbones cause decreases in crystallinity and hence higher biodegradability. These two properties are important to design controlled

drug delivery systems for bioactive molecules. Therefore, we hypothesized that the introduction of phenyl group as side chain will change the properties of the polymers (mainly hydrophobicity and crystallinity) and hence will affect the drug loading capability of the polymer. Thus, the first part of this study deals with the synthesis, characterisation, and evaluation of properties of polyester polymers. It includes the synthesis of polymers containing different ratios of succinic acid, phenylsuccinic acid and 1, 10-decanediol to obtain a small polymer library ranging in different phenyl contents as a side group in the polyester backbone. Hence, the difference in the physical properties of the synthesised polyesters ranging from crystalline (no phenyl content) to amorphous material (high phenyl content) was expected. The second part of the study describes the effect of phenyl content on coumarin 6 dye loading in nanoparticles made by nanoprecipitation methods. The selected best polymer (regarding size and dye loading) was also used to make Pluronic F68 (stabilizer) coated nanoparticles. The formulations were evaluated for dye loading, nanoparticle size, particle stability (in water and PBS), and polymer stability (with and without *Pseudomonas cepacia* lipase). The determination of cytotoxicity and cell uptake study were also conducted to determine the safety aspects of the nanoparticle to be used for biomedical applications.

3.2 Methods

3.2.1 Synthesis and Characterisation of Polymers

Poly(decamethylenesuccinate) [PDeMS], Poly(decamethylene phenylsuccinate) [PDsMPS] and their copolymers Poly(decamethylene succinate-co-phenylsuccinate) [PDeMS-co-PS] were synthesised by solvent-free melt polycondensation at 125 °C. The diacid and diol ratio was maintained at 1:1 in all polycondensation reactions. The concentration of scandium (III) triflate was 0.05 mol% of diol component for all the reactions. The polymer name, abbreviation and code along with feed composition are given in Table 3-1.

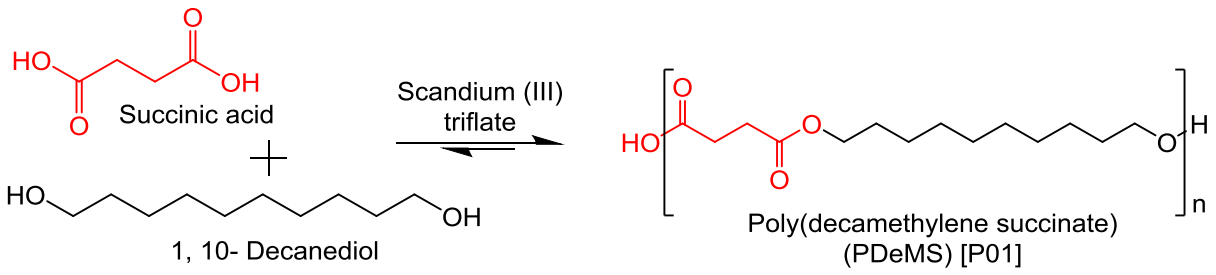
Table 3-1 Synthesis of polyester with different feed ratio (mol%) of succinic acid, phenylsuccinic acid and 1- 10- Decanediol using scandium (III) triflate as catalyst

Polymer[$]	Code	Feed ratio (mol%)			Scandium (III) triflate[*]
		Succinic acid	Phenylsuccinic acid	1, 10-Decanediol	
Poly(decamethylene succinate) (PDeMS)	P01	100 (0.61 g, 5.15 mmol)	0	100 (0.90 g, 5.15 mmol)	0.05 (1.27 mg, 2.58 µmol)
Poly(decamethylene succinate-co-phenylsuccinate) (PDeMS-co-PS)	P02	70 (0.42 g, 3.60 mmol)	30 (0.30 g, 1.54 mmol)	100 (0.90 g, 5.15 mmol)	0.05 (1.27 mg, 2.58 µmol)
	P03	50 (0.30 g, 2.57 mmol)	50 (0.50 g, 2.57 mmol)	100 (0.90 g, 5.15 mmol)	0.05 (1.27 mg, 2.58 µmol)
	P04	30 (0.18 g, 1.54 mmol)	70 (0.70 g, 3.60 mmol)	100 (0.90 g, 5.15 mmol)	0.05 (1.27 mg, 2.58 µmol)
Poly(decamethylene - phenylsuccinate) (PDeMPS)	P05	0	100 (1 g, 5.15 mmol)	100 (0.90 g, 5.15 mmol)	0.05 (1.27 mg, 2.58 µmol)

[$] 21 h in bulk 125 °C under reduced pressure; [*] Scandium (III) triflate was 0.05 mol% of diol (1, 10- Decanediol).

3.2.1.1 Synthesis of Poly(decamethylenesuccinate) [PDeMS] Polymer (P01)

The synthetic route for the Poly(decamethylenesuccinate) polymer (P01) has been given in scheme 3-1.



Scheme 3-1 Polycondensation of succinic acid and 1, 20-decanediol catalyzed by scandium (III) triflate

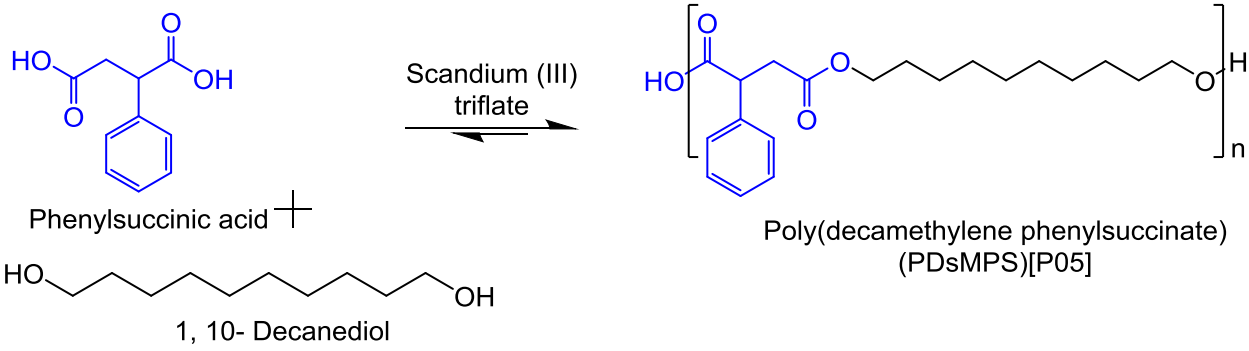
The polymer was synthesised by mixing succinic acid (0.61 g, 5.15 mmol, 1 eq) and 1, 10-decanediol (0.90 g, 5.15 mmol, 1 eq) in the reaction vessel at 80 °C for 30 min under stirring for melting and mixing of the monomers. Scandium (III) triflate (1.27 mg, 2.58 µmol, 0.05 eq) was added followed by purging of the reaction mixture with nitrogen. The reaction was continued for 3 h after increasing the temperature to 125 °C. The pressure was then reduced to 10^{-2} mbar, and the reaction was further continued for 18 h after which, the reaction was stopped, and the mixture was allowed to cool. The resultant polymer was purified by dissolving in a small volume of acetone (1 mL) and precipitated in stirred cold methanol for three times. The precipitate was filtered and dried under vacuum to obtain a white solid powder in 94 % yield.

^{1}H NMR (400 MHz, $CDCl_3$) δ (ppm) 4.07 (CO-O-$\underline{CH_2}(C_8H_{18})\underline{CH_2}$, t, 4.00H), 2.62 (CO-$\underline{CH_2}$-$\underline{CH_2}$-CO, s, 4H), 1.61 ($CH_2$-$\underline{CH_2}(C_6H_{12})\underline{CH_2}$-$CH_2$, m, 4.00H), 1.28 ($C_2H_4(\underline{C_6H_{12}})C_2H_4$, m, 12.00H).

^{13}C NMR (101 MHz, $CDCl_3$) δ (ppm) 172.53 ($\underline{C}O$-CH_2-CH_2-$\underline{C}O$), 65.02 (CO-O-$\underline{C}H_2$), 29.57 (CO-O-CH_2-$\underline{C}H_2$), 29.37 (CO-$\underline{C}H_2$-$\underline{C}H_2$-CO), 29.33 (CO-O-CH_2CH_2-$\underline{C}H_2$), 28.73 (CO-O-$CH_2CH_2CH_2$-$\underline{C}H_2$), 26.02 (CO-O-$CH_2CH_2CH_2CH_2$-$\underline{C}H_2$).

FTIR wavenumber (cm^{-1}): 3446 (O-H, stretching), 2920 (C-H, asymmetric stretching), 2852 (C-H, symmetric stretching), 1722 (C=O, stretching), 1421 (C-H, bending), 1153 (C-O, stretching).

3.2.1.2 Synthesis of Poly(decamethylene phenylsuccinate) [PDsMPS] Polymer (P05)



Scheme 3-2 Polycondensation of phenylsuccinic acid and 1,10-decanediol catalyzed by scandium (III) triflate

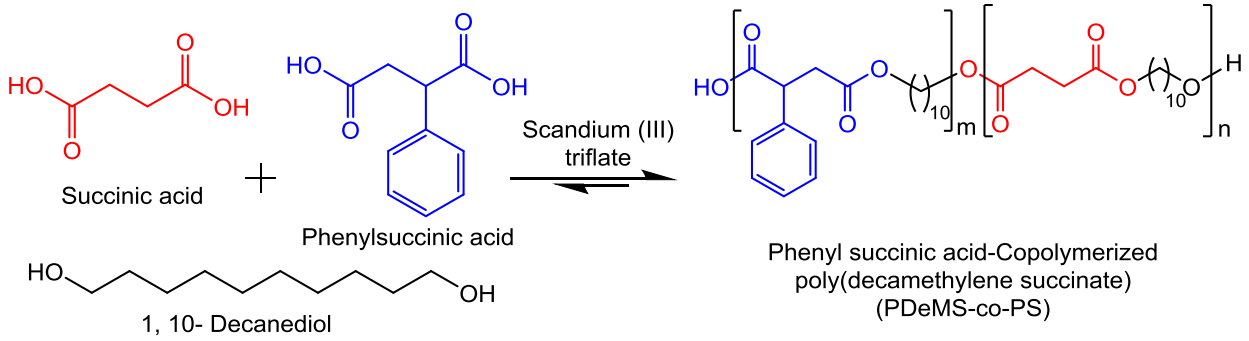
The polymer was synthesised by the same procedure as described above except instead of succinic acid, phenyl succinic acid (1 g, 5.15 mmol, 1eq) was incorporated as the diacid component reacting with 1, 10- decanediol (0.90 g, 5.15 mmol, 1 eq) using scandium (III) triflate (1.27 mg, 2.58 µmol, 0.05 eq) as a catalyst (Scheme 3-2). The resultant polymer was purified by the precipitating in cold methanol three times followed by drying under vacuum to obtain a light brown viscous liquid material in 90% yield.

^{1}H NMR (400 MHz, $CDCl_3$) δ (ppm) 7.28 ($\underline{C_6}\underline{H_5}$, ring protons, m, 5H), 4.06 (CO-O-$\underline{CH_2}(C_8H_{18})\underline{CH_2}$ and CO-$\underline{CH}(C_6H_5)$, m, 5H), 3.17 ($CH(C_6H_5)$-$\underline{CH_2}$-CO, m, 1H), 2.68 ($CH(C_6H_5)$-$\underline{CH_2}$-CO, m, 1H), 1.55 (CH_2- $\underline{CH_2}(C_6H_{12})\underline{CH_2}$-$CH_2$, m, 4.00H), 1.26-1.19 ($C_2H_4(\underline{C_6}\underline{H_{12}})C_2H_4$, m, 12.00H).

^{13}C NMR (101 MHz, $CDCl_3$) δ (ppm) 173.07 ($\underline{C}$O-$CH(C_6H_5)$-CH_2-CO), 171.69 (CO-$CH(C_6H_5)$-CH_2-$\underline{C}$O), 138.03, 128.86, 127.86, 127.63 (Ring carbon peaks), 65.00 (CH_2-CO-O-$\underline{C}H_2$), 47.43 (O-CO-$\underline{C}H(C_6H_5)$-CH_2-CO-O) , 37.84 (O-CO-$CH(C_6H_5)$-$\underline{C}H_2$-CO-O), 29.49 (CO-O-CH_2-$\underline{C}H_2$), 29.22 (CO-O-CH_2CH_2-$\underline{C}H_2$), 28.57 (CO-O-$CH_2CH_2CH_2$-$\underline{C}H_2$), 25.78 (CO-O-$CH_2CH_2CH_2CH_2$-$\underline{C}H_2$).

FTIR wavenumber (cm^{-1}): 3452 (O-H, stretching), 2925 (C-H, asymmetric stretching), 2854 (C-H, symmetric stretching), 1729 (C=O, stretching), 1612 (aromatic C=C stretching), 1455 (C-H, bending), 1159 (C-O, stretching).

3.2.1.3 Synthesis of Poly(decamethylene succinate-co-phenylsuccinate) [PDeMS-co-PS] (P02,P03 and P04)



Scheme 3-3 Polycondensation of succinic acid, phenylsuccinic acid and 1,10-decanediol catalyzed by scandium (III) triflate

The copolymers were synthesised by reacting succinic acid, phenylsuccinic acid and 1, 10-decandiol (Scheme 3-3). The feed ratio of succinic acid and phenylsuccinic acid has been given in table 3-1. The diacids and diol ratio was maintained at 1:1 in all polycondensation reactions.

As an example, the synthesis of polymer with 70 mol% of succinic acid and 30 mol% of phenylsuccinic acid (P02 polymer) is described here. The succinic acid (0.42 g, 3.60 mmol), phenylsuccinic acid (0.30 g, 1.54 mmol) and 1,10-decanediol (0.90 g, 5.15 mmol) were charged in a reaction vessel and heated to 80 °C for 30 min under stirring for melting and mixing of the monomers. Scandium (III) triflate (1.27 mg, 2.58 µmol) was then added, and the reaction was purged with nitrogen followed by increasing the reaction temperature to 125 °C. After 3 h of reaction, the pressure was reduced to 10^{-2} mbar, and the reaction was continued for 18 h after which the reaction was stopped and the mixture was allowed to cool. The resultant

polymer was dissolved in a small volume of acetone and precipitated in stirred cold methanol for three times. The precipitate was filtered, washed with methanol and dried under vacuum.

The different feed ratios generated polymers with different physical properties ranging from off-white solid powders to light brown viscous liquids with yields from 90-95%.

PDeMS-co-PS (P02)

^{1}H NMR (400 MHz, $CDCl_3$) δ (ppm) 7.28 ($\underline{C_6}\underline{H_5}$, ring protons, m, 2.22H), 4.07 (CO-O-$\underline{CH_2}(C_8H_{18})\underline{CH_2}$ and CO-$\underline{CH}(C_6H_5)$, m, 4.23H), 3.19 (CH(C_6H_5)-$\underline{CH_2}$-CO, m, 0.30H and 2.68 (CH(C_6H_5)-$\underline{CH_2}$-CO), m, 0.30H), 2.62 (CO-$\underline{CH_2}$-$\underline{CH_2}$-CO), s, 2.80H), 1.61 (CH_2-$\underline{CH_2}(C_6H_{12})\underline{CH_2}$-$CH_2$, m, 4.00H), 1.28 ($C_2H_4(\underline{C_6}\underline{H_{12}})C_2H_4$, m, 12.00H).

^{13}C NMR (101 MHz, $CDCl_3$) δ (ppm) 172.95 ($\underline{C}$O-CH(C_6H_5)-CH_2-CO), 172.38 ($\underline{C}$O-CH_2-CH_2-$\underline{C}$O), 171.57 (CO-CH(C_6H_5)-CH_2-$\underline{C}$O), 137.92, 128.74, 127.75, 127.52 (Ring carbon peaks), 64.87 (CH_2-CO-O-$\underline{C}H_2$), 47.32 (O-CO-$\underline{C}$H(C_6H_5)-CH_2-CO-O), 37.73 (O-CO-CH(C_6H_5)-$\underline{C}H_2$-CO-O), 29.43 (CO-O-CH_2-$\underline{C}H_2$), 29.22 (CO-$\underline{C}H_2$-$\underline{C}H_2$-CO), 29.19 (CO-O-CH_2CH_2-$\underline{C}H_2$), 28.59 (CO-O-$CH_2CH_2CH_2$-$\underline{C}H_2$), 25.87 (CO-O-$CH_2CH_2CH_2CH_2$-$\underline{C}H_2$).

FTIR wavenumber (cm^{-1}): 3450 (O-H, stretching), 2920 (C-H, asymmetric stretching), 2852 (C-H, symmetric stretching), 1723 (C=O, stretching),

1609 (aromatic C=C stretching), 1420 (C-H, bending), 1154 (C-O, stretching).

PDeMS-co-PS (P03)

^{1}H NMR (400 MHz, $CDCl_3$) δ (ppm) 7.28 ($\underline{C_6}\underline{H_5}$, ring protons, m, 2.92H), 4.07 (CO-O-$\underline{CH_2}(C_8H_{18})\underline{CH_2}$ and CO-$\underline{CH}(C_6H_5)$, m, 4.45H), 3.19 ($CH(C_6H_5)$-$\underline{CH_2}$-CO, m, 0.50H and 2.68 ($CH(C_6H_5)$-$\underline{CH_2}$-CO), m, 0.50H), 2.62 (CO-$\underline{CH_2}$-$\underline{CH_2}$-CO), s, 2.00H), 1.61 (CH_2-$\underline{CH_2}(C_6H_{12})\underline{CH_2}$-$CH_2$, m, 4.00H), 1.27 ($C_2H_4(\underline{C_6}\underline{H_{12}})C_2H_4$, m, 12.05H).

^{13}C NMR (101 MHz, $CDCl_3$) δ (ppm) 172.94 ($\underline{C}$O-$CH(C_6H_5)$-CH_2-CO), 172.37 ($\underline{C}$O-CH_2-CH_2-$\underline{C}$O), 171.57 (CO-$CH(C_6H_5)$-CH_2-$\underline{C}$O), 137.92, 128.74, 127.74, 127.51 (Ring carbon peaks), 64.86 (CH_2-CO-O-$\underline{C}H_2$), 47.32 (O-CO-$\underline{C}H(C_6H_5)$-CH_2-CO-O), 37.73 (O-CO-$CH(C_6H_5)$-$\underline{C}H_2$-CO-O), 29.42 (CO-O-CH_2-$\underline{C}H_2$), 29.21 (CO-$\underline{C}H_2$-$\underline{C}H_2$-CO), 29.19 (CO-O-CH_2CH_2-$\underline{C}H_2$), 28.58 (CO-O-$CH_2CH_2CH_2$-$\underline{C}H_2$), 25.87 (CO-O-$CH_2CH_2CH_2CH_2$-$\underline{C}H_2$).

FTIR wavenumber (cm^{-1}): 3453 (O-H, stretching), 2925 (C-H, asymmetric stretching), 2854 (C-H, symmetric stretching), 1731 (C=O, stretching), 1605 (aromatic C=C stretching), 1423 (C-H, bending), 1159 (C-O, stretching).

PDeMS-co-PS (P04)

^{1}H NMR (400 MHz, $CDCl_3$) δ (ppm) 7.28 ($\underline{C_6}\underline{H_5}$, ring protons, m, 4.15H), 4.06 (CO-O-$\underline{CH_2}(C_8H_{18})\underline{CH_2}$ and CO-$\underline{CH}(C_6H_5)$, m, 4.29H), 3.19 (CH(C_6H_5)-$\underline{CH_2}$-CO, m, 0.70H and 2.68 (CH(C_6H_5)-$\underline{CH_2}$-CO), m, 0.70H), 2.61 (CO-$\underline{CH_2}$-$\underline{CH_2}$-CO), s, 1.30H), 1.55 (CH_2-$\underline{CH_2}(C_6H_{12})\underline{CH_2}$-$CH_2$, m, 4.00H), 1.26-1.20 ($C_2H_4(\underline{C_6}\underline{H_{12}})C_2H_4$, m, 12.00H).

^{13}C NMR (101 MHz, $CDCl_3$) δ (ppm) 172.97 ($\underline{C}$O-CH(C_6H_5)-CH_2-CO), 172.40 ($\underline{C}$O-CH_2-CH_2-$\underline{C}$O), 171.59 (CO-CH(C_6H_5)-CH_2-$\underline{C}$O), 137.92, 128.75, 127.75, 127.53 (Ring carbon peaks), 64.90 (CH_2-CO-O-$\underline{C}H_2$), 47.32 (O-CO-$\underline{C}$H(C_6H_5)-CH_2-CO-O), 37.74 (O-CO-CH(C_6H_5)-$\underline{C}H_2$-CO-O), 29.39 (CO-O-CH_2-$\underline{C}H_2$), 29.22 (CO-$\underline{C}H_2$-$\underline{C}H_2$-CO), 29.20 (CO-O-CH_2CH_2-$\underline{C}H_2$), 28.56 (CO-O-$CH_2CH_2CH_2$-$\underline{C}H_2$), 25.84 (CO-O-$CH_2CH_2CH_2CH_2$-$\underline{C}H_2$).

FTIR wavenumber (cm^{-1}): 3447 (O-H, stretching), 2925 (C-H, asymmetric stretching), 2854 (C-H, symmetric stretching), 1731 (C=O, stretching), 1608 (aromatic C=C stretching), 1428 (C-H, bending), 1159 (C-O, stretching).

3.2.2 Empty and Dye-Loaded Nanoparticle Formulations

Nanoparticles of synthesised polymers were prepared by nanoprecipitation methods with some modification.[22] Briefly, polymer (20 mg) was dissolved in 5 mL of organic solvent (acetone) to make a homogeneous organic phase. The organic phase was added drop-wise into 10 mL of HPLC grade water under stirring (1000 rpm) and stirred for 4 h at room temperature. Syringe

pump was used to control the dropping rate (0.5 mL/min). The formulation was then left overnight (open vial) to ensure the complete removal of organic solvent. The nanoparticle solution was then passed through a membrane syringe filter (pore size: 220 nm) (Millex-LG, Millipore Co., USA) to obtain a clear formulation. The size and zeta potential of the formulations were measured after appropriate dilutions.

Coumarin 6 dye-loaded nanoparticles were prepared by a similar method as with blank nanoparticles by adding dye in the organic phase along with polymer. Briefly, coumarin 6 (1 mg) was dissolved along with the polymer (20 mg) in acetone (5 mL) and added at a fixed rate (0.5 mL/min) into the HPLC grade water (10 mL). After 4 h of stirring, the formulations were stored overnight (open vials) to allow the traces of acetone to evaporate. The process was performed in the dark to prevent the degradation of light sensitive coumarin 6 dye (vials covered by aluminum foil). The precipitated polymer and dye were removed by filtration through a membrane filter (pore size: 220 nm). Coumarin 6 loaded nanoparticles were passed through PD10 Desalting Column (Sephadex G-25 Medium, GE Healthcare Life Sciences) to separate the unencapsulated dye from the formulations. Purified nanoparticle solution was used for further characterisation. The drug content was determined after freeze drying a part of nanoparticle solution. The poloxamer (Pluronic F68) coating was achieved by the same method, i.e. where poloxamer (Pluronic F68) was dissolved in an aqueous medium

(0.2%w/v) to make dye loaded and empty nanoparticles. A pictorial presentation of the process is shown in figure 3-1.

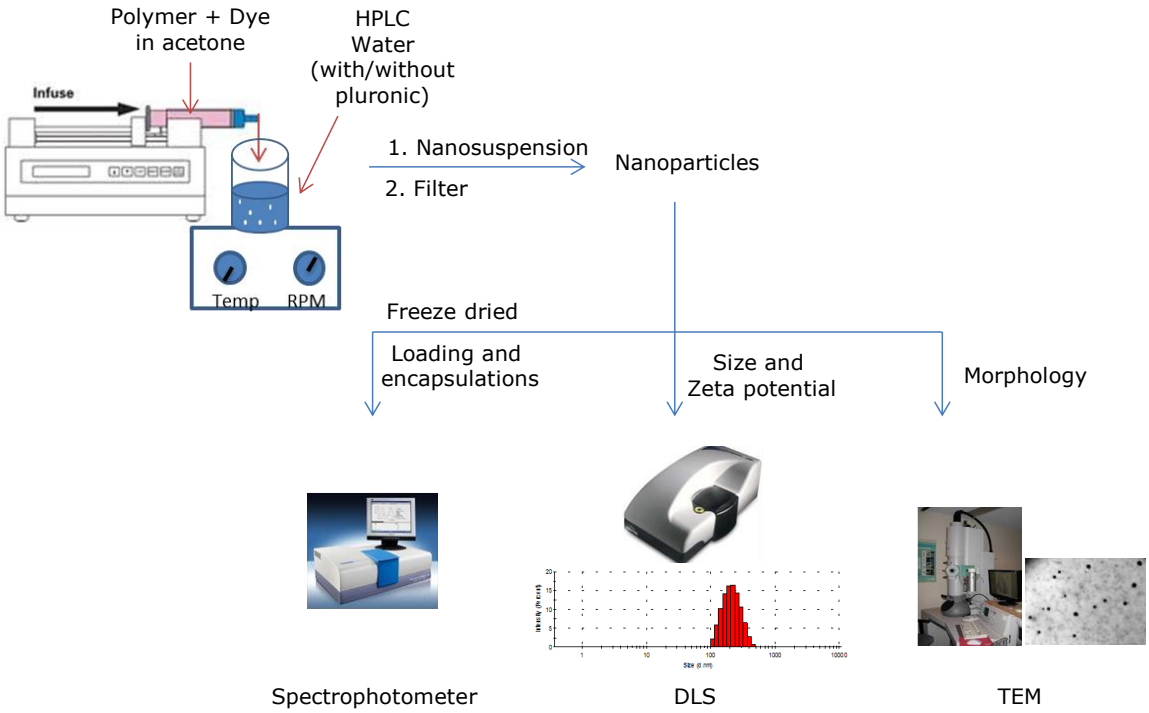


Figure 3-1 Pictorial representation of preparation and characterisation of nanoparticles

3.2.3 Characterisation of Nanoparticle Formulations

The nanoparticles samples (50 µg/mL) in HPLC grade water were analyzed using a Malvern NanoZS instrument for size and polydispersity measurements. Surface zeta potential was measured in HEPES 10 mM buffer (pH 7.4) using Malvern NanoZS instrument. The surface morphology and size were confirmed by TEM analysis performed on TEM grids without staining. Chapter 2 reports the full experimental procedures for these methods.

3.2.4 Degradation Study of P02 Polymeric Nanoparticle

The degradation profile was assessed for the empty P02 nanoparticle formulation in HPLC water (pH 7.4) and nanoparticle formulation (in HPLC water) with *Pseudomonas cepacia* lipase (0.2 mg mL^{-1}). The nanoparticle formulations were incubated at 37 °C. One vial from each set was collected at a predetermined time (30 days) and freeze-dried. The freeze-dried samples were then dissolved in chloroform, filtered, and analyzed by GPC to determine the change in molecular weight.

3.2.5 C3A Cell Culture

C3A human hepatocellular carcinoma cells were cultured in MEM medium supplemented with 10% heat-inactivated foetal calf serum (FCS), 2 mM L-glutamine, 100 U/mL penicillin/streptomycin, 1 mM sodium pyruvate and 1% on-essential amino acids (termed MEM complete medium) and incubated at 37 °C and 5% CO_2.

3.2.6 Cell Viability Assessment

The cytotoxicity of the coumarin 6 labelled uncoated and Pluronic F68 coated P02 nanoparticles was determined by a fluorescence-based 3 in 1 assay.[23] This approach allows the simultaneous assessment of cell viability using the Alamar Blue (for metabolic activity), CFDA-AM (for cell membrane integrity) and Neutral Red (for lysosomal function) assays. C3A cells were seeded at a concentration of 1.56 $x10^5$ cells/cm^2 into a 96 well plate and incubated at 37 °C and 5% CO_2 for 24 h. Cells were then exposed to MEM complete medium

(control), 1% triton X100 (positive control) or nanoparticles at concentrations of 4.68, 9.37, 18.75, 37.50, 75, 150 and 300 μg mL^{-1} (100 uL/well) and incubated at 37 °C 5% CO_2 for 24 h. Nanoparticles were prepared via dilution in complete MEM medium and gently vortexed prior to cell exposure. After 24 h the supernatants were removed (and stored at -80 ^{o}C) and the cells were washed twice with phosphate buffered saline (PBS). A solution of both 1.25% v/v Alamar Blue (TREK Lab Services) and 4 μM CFDA-AM was prepared in phenol red free MEM medium and added to cells (100 μL) before incubating the cells in the dark at 37 °C and 5% CO_2 for 1 h. Fluorescence was measured on a SpectraMax M5 Microplate Reader (Molecular Devices) at an excitation/emission of 532/590 nm for Alamar Blue and an excitation/emission of 485/535 nm for CFDA-AM. Next, for the Neutral Red uptake assay, cells were washed twice using PBS, and Neutral Red (33 μg mL^{-1}) prepared in phenol red free MEM medium was added (100 μL) to cells, which were then incubated in the dark at 37 °C and 5 % CO_2 for 1 h. Following incubation, cells were washed 3 times with PBS and then acidified (1% acetic acid) 50% EtOH (in water) (100 μL). Cells were then incubated in the dark at room temperature for 20 minute (with shaking). Fluorescence was measured in a SpectraMax M5 Microplate Reader at an excitation/emission of 532/645 nm. All experiments were repeated on different days, on at least 3 separate occasions and data reported as mean

% viability (compared to the control) +/- standard error mean. GraphPad Prism 6 was used to analyze the statistical significance of the data.

3.2.7 Cell Uptake Study

3.2.7.1 Confocal Microscopy

C3A cells were seeded (6.58 x10^4 cells/cm^2) on 12 mm glass cover slips at 37 °C and 5% CO_2 in 24 well plates (Falcon) for 24 h. Cells were then exposed to Pluronic F68 coated and uncoated P02 nanoparticles at a sub lethal concentration (100 µg/mL) or MEM complete medium (control) for 10, 60, 240 and 1440 minutes at 37 °C and 5% CO_2. Following exposure, cells were washed twice with PBS and fixed in 3% formaldehyde (in PBS, 250 µL) for 30 minutes in the dark at room temperature. Subsequently, the plates were washed twice with PBS and incubated with 50 mM ammonium chloride (250 µL) for 10 minutes in the dark, at room temperature. Cells were then washed twice with PBS before permeabilizing with 0.1% Triton-X100 (250 µL) for 20 minutes at room temperature. The cells were washed twice with PBS and then exposed to primary antibody monoclonal anti α tubulin mouse ascites fluid clone DM1A (1:200 in PBS, Molecular Probes, 250 µL) for 1 h at room temperature. Cells were then washed twice with PBS and incubated with secondary antibody Rhodamine Red goat anti mouse IgG (1:100 in PBS, Molecular Probes, 250 µL) for 1 h at room temperature. The cells were then washed twice in PBS and incubated for 5 minutes in the dark with 1 µg mL^{-1} DAPI (250 µL) at room temperature to stain the nucleus. Finally, cells were

washed twice with PBS and coverslips were mounted onto glass slides with Vector shield (Vector –H1000) and edges sealed with varnish. Cells were imaged using a Zeiss LSM880 confocal microscope using the Zen program for data analyses.

3.2.7.2 Quantification of Cell Uptake Study

C3A cells were seeded into 96 well plates at a concentration of 1.56 $x10^5$ cells/cm^2 and incubated for 24 h. Cells were exposed to uncoated and coated P02 nanoparticles (4.68-300 µg mL^{-1}) or MEM complete medium (control) in duplicate for 10, 60, 240 and 1440 minutes at 37 °C and 5% CO_2. Following treatment cell supernatants were removed and cells were washed twice using PBS and 0.4% v/v Trypan Blue (50 µL) was added for 10 minutes at room temperature. Cells were washed twice using PBS and then lysed with 0.2% Triton X100 in the dark at room temperature for 20 minutes. Fluorescence was measured using a SpectraMax M5 Microplate Reader at an excitation/emission of 488/550 nm. All experiments were repeated on at least 3 separate occasions.

A standard curve of fluorescence for each NP (4.68-300 µg mL^{-1}) was generated to enable uptake to be quantified which was expressed as the percentage (%) of applied dose.

3.3 Results

3.3.1 Synthesis and Characterisation of Polymers

The synthesis of polyesters by one pot polycondensation took place in two steps. In the first step, diacid monomers slowly dissolved in melted diol monomer in a solvent free reaction. The reaction was then continued for 3 h after the addition of scandium triflate (which catalysed the reaction) and produced a light brown viscous material. In the second stage of reaction, a highly viscous brown material was produced after the reduction of pressure for 18 h. The colour intensity of the material was reduced after the purification of the materials with methanol. The colour and the physical state of the materials were dependent on the composition of the polymer. The polymer from succinic acid/decanediol gave white solid polymer while the polymer prepared with phenylsuccinic acid/decanediol gave a light brown viscous material. Combining the succinic acid and phenylsuccinic acid in reactions produced polymers ranging from solid to viscous materials according to phenyl content. The yields of the polymers were in the range of 90-95%. The polymers were characterised by GPC, ^{1}H NMR, ^{13}C NMR and ^{1}H-^{1}H NMR spectroscopy. The characterisation data of the synthesis and polymers are given in table 3-2.

Table 3-2. Polymer code, composition (mol% of diacid) and molecular weight (g/mol) of polyesters

Polymer Code	Feed ratio (mol%)		Product ratio (mol%)*		Molecular Weight ($gmol^{-1}$)			Yield (%)
	SA	PSA	SA	PSA	^1M_n	^2M_w	^{3}PDI	
P-01	100	0	100	0	1.15×10^4	4.22×10^4	3.7	94
P-02	70	30	70	30	1.15×10^4	3.76×10^4	2.9	93
P-03	50	50	50	50	1.01×10^4	3.42×10^4	3.4	92
P-04	30	70	30	70	1.10×10^4	3.44×10^4	3.1	91
P-05	0	100	0	100	1.16×10^4	3.76×10^4	3.2	90

*Product ratio determined by ^{1}H NMR spectroscopy; SA: Succinic acid, PSA: Phenylsuccinic acid; ^{1} Number average molecular weight (M_n) by GPC; ^{2} Weight average molecular weight (M_w) by GPC and ^{3} Polydispersity index (PDI = M_w/M_n) determined by GPC.

The polymers with similar molecular weight were selected for comparative study. The polymers showed number molecular weight (M_n) ranges from 1.01×10^4 to 1.16×10^4 $gmol^{-1}$ determined by GPC. The polydispersities of the polymers were nearly the same for all the polymers and hence the polymers were considered suitable for the comparative studies. The composition of the polyesters was determined by ^{1}H NMR spectroscopy. The methylene proton adjacent to the hydroxyl of 1, 10- decanediol resonated at δ3.40 ppm [Peak A*, Figure 3-2 (6)], but upon reaction of hydroxyl group with carboxyl acid, it got shifted to lower field [Peak A, Figure 3-2 (1 to 5) δ4.10 ppm) and hence the integration of these peaks were used to determine the amount of reacted and unreacted diol in the polymer sample. The incorporation of succinic acid and phenyl succinic acid was determined by checking methylene protons of diacids before and after reaction. These protons (before reaction) are usually resonate at high field

[Figure 3-2 Peaks D* (7) D1* and D2* (8)] in the monomer while resonate at lower field in the polymer [Figure 3-2 Peaks D, D1 and D2 (1 to 5)]. All other peaks of the corresponding products are well identified. The ^{1}H NMR showed that all monomers have been incorporated into the polymeric chain (Figure 3-2).

The peak positions and the interaction between different protons of polyesters with and without phenylsuccinic acid (P-01 and P-05) were also confirmed by ^{1}H-^{1}H COSY NMR spectroscopy. Some of the peaks were found to be overlapped with others, for instance, proton peaks at position A and E in P-05 polymer (Figure 3-3). The success of the synthesis was also supported by ^{13}C NMR where all the expected peaks are well identified and showed in figure 3-4. A carbonyl resonance in the P01 polymer, containing succinic acid, appeared at 172.53 ppm. On the other hand, two carbonyl peaks of P05 polymer, containing phenylsuccinic acid, appeared at 172.07 and 171.69 ppm. The polymers made by mixing both of the diacids showed all the three distinct peaks with different intensities. The methylene groups of diol units in the polymers containing phenylsuccinic acids were splited due to the presence of phenyl groups.

Figure 3-5 shows the FTIR spectrum of the polymers in the 500–4000 cm^{-1} region. The formation of polymer generated a number of ester groups within the polymer chains which gave a strong band for carbonyl stretching mode around 1727 cm^{-1}.

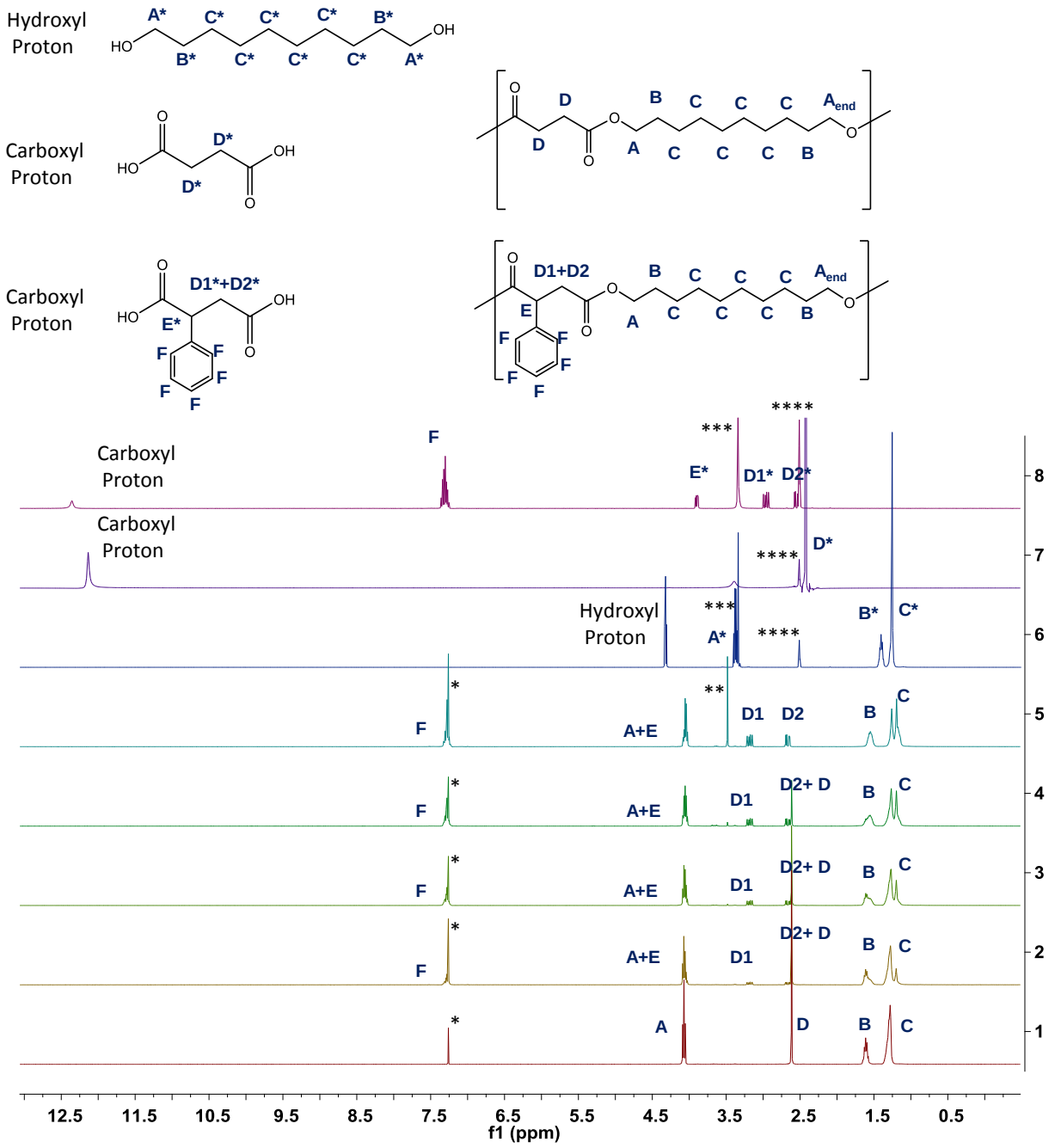


Figure 3-2 Comparative ^{1}H NMR spectra of monomers and synthesised polyesters with different phenyl contents (1) P01 polymer (2) P02 polymer (3) P03 polymer (4) P04 polymer (5) P05 polymer (6) 1, 10-Decanediol (7) Succinic acid (8) Phenylsuccinic acid. *Chloroform residue, **Methanol residue, *** Water residue, ****DMSO residue.

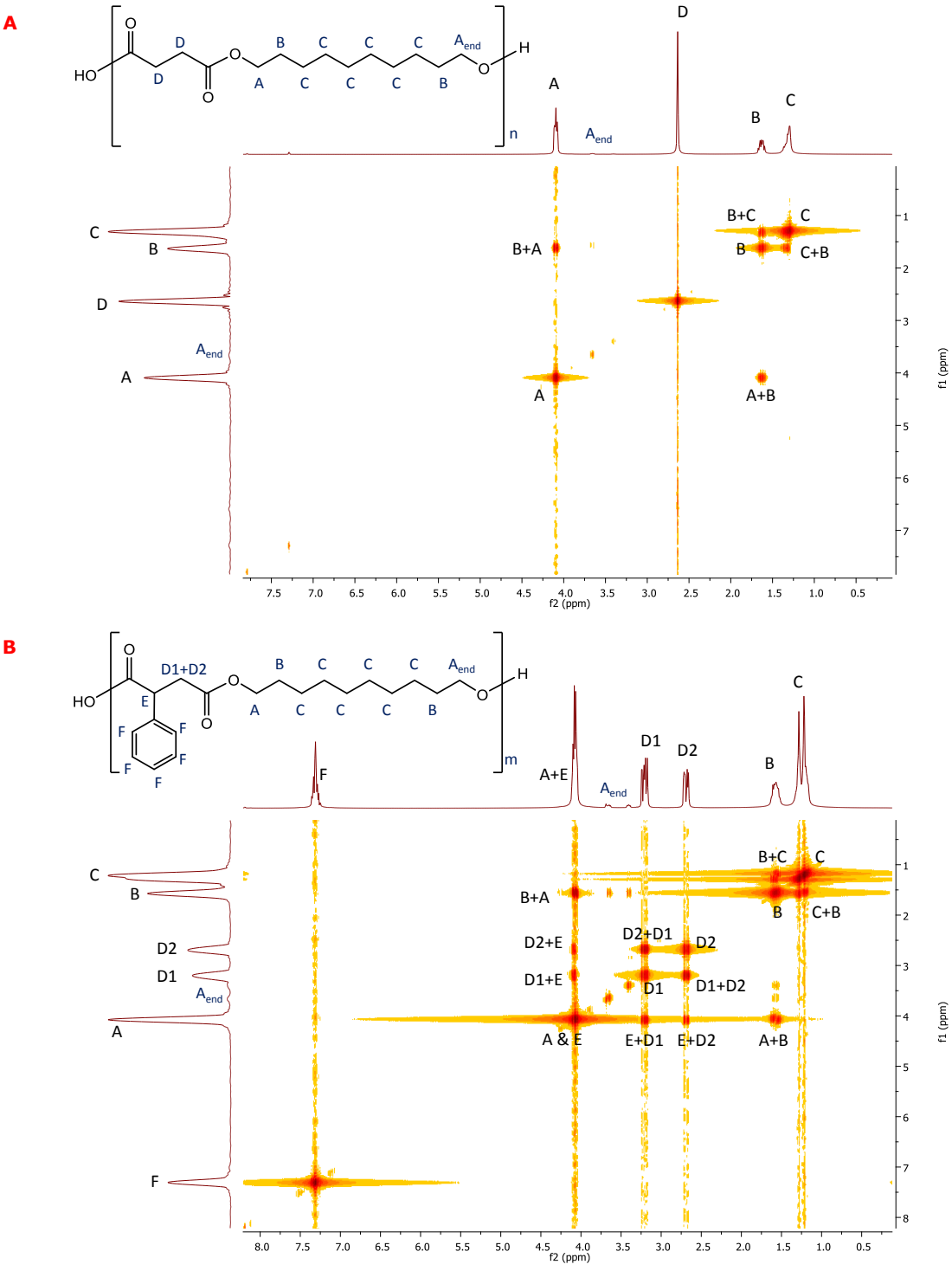


Figure 3-3 Comparative ^{1}H-^{1}H COSY NMR spectra of (A) Polymer with no phenyl contents (P01) and (B) Polymer with highest phenyl content (P05)

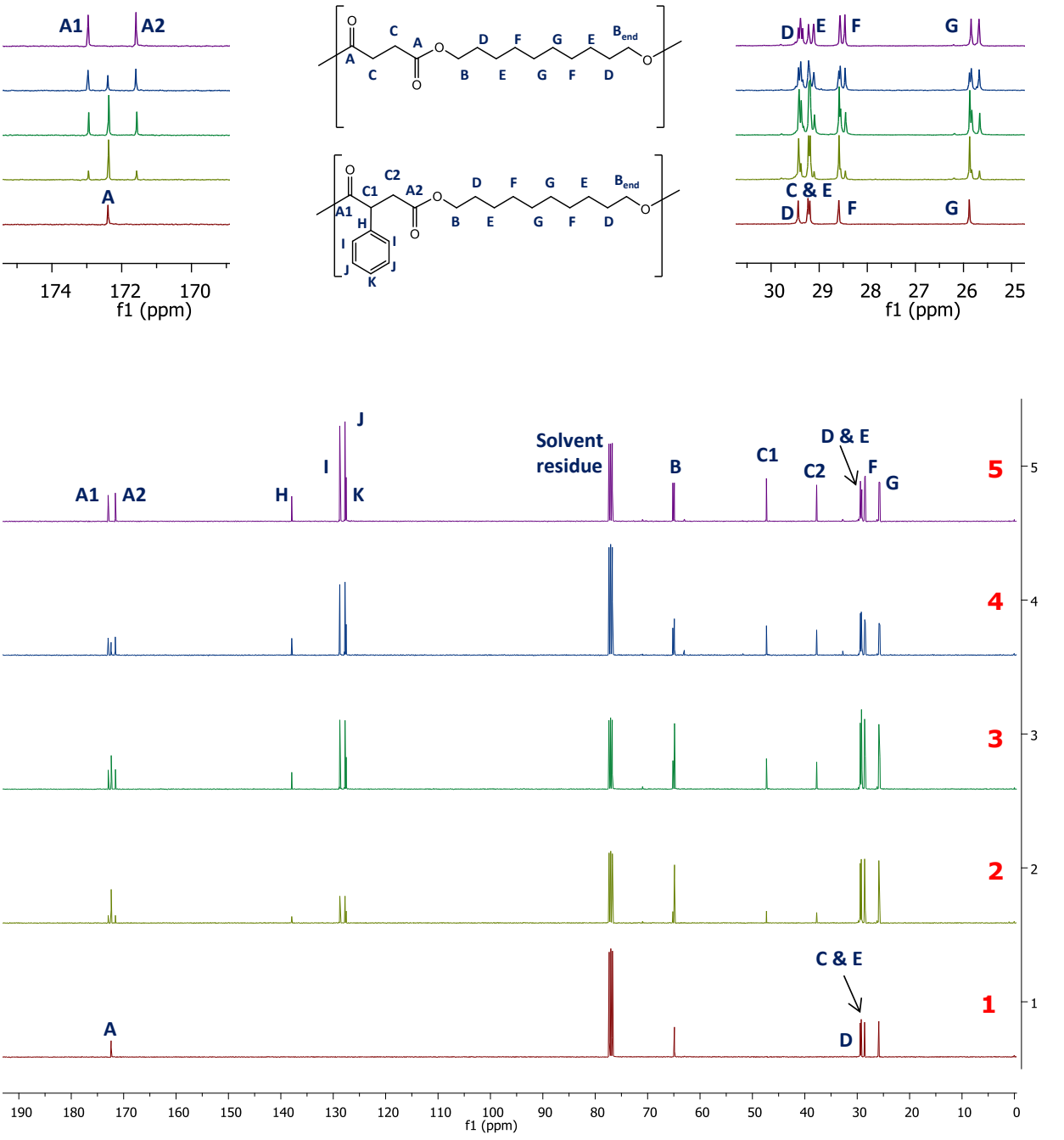


Figure 3-4 Comparative ^{13}C NMR spectra of synthesised polyesters with different phenyl contents (1) P01 polymer (2) P02 polymer (3) P03 polymer (4) P04 polymer (5) P05 polymer

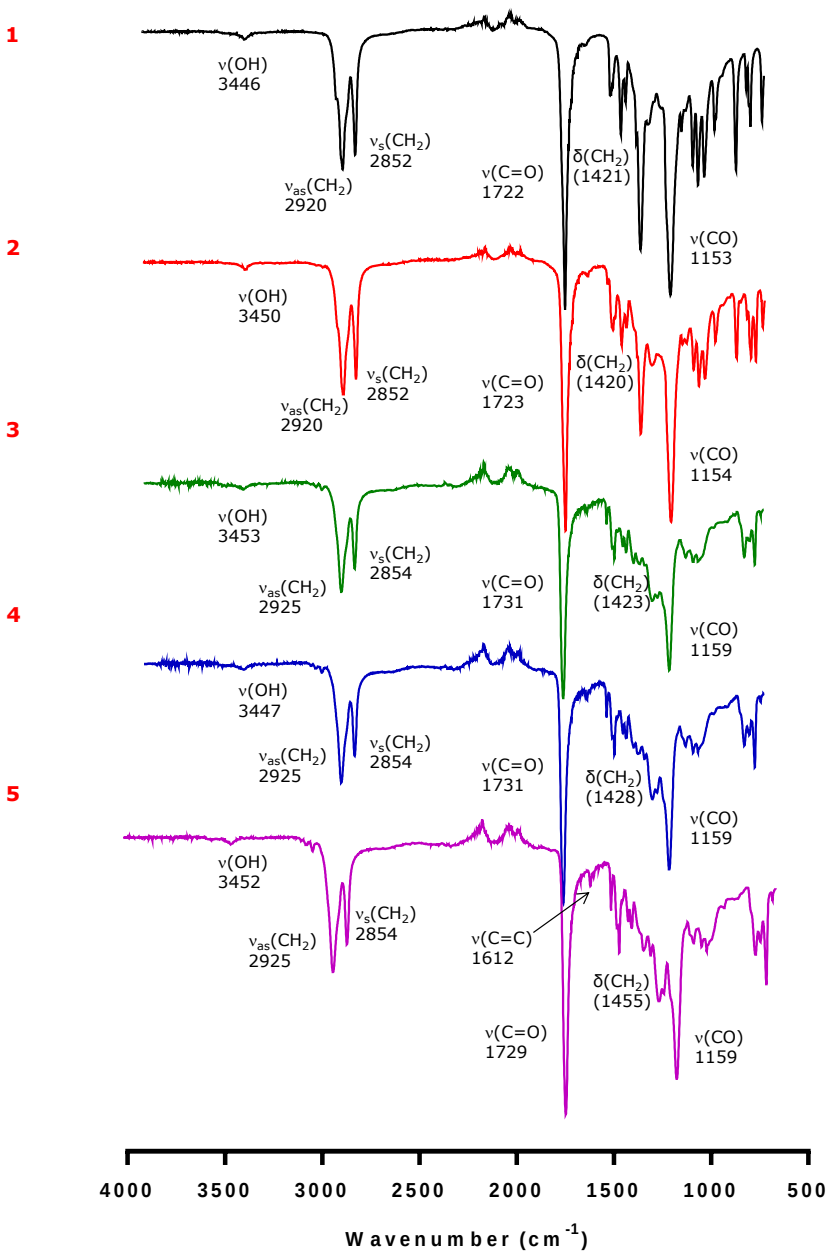


Figure 3-5 Comparative FTIR spectra of synthesised polyesters with different phenyl contents (1) P01 polymer (2) P02 polymer (3) P03 polymer (4) P04 polymer (5) P05 polymer

The DSC data showed a pattern for the thermal properties of the polymers (Table 3-3). The melting temperature (T_m), crystallization temperature (T_c) and melting enthalpy (ΔH) were found to be decreased by increasing phenyl

contents. The values for the above parameters were not detected for polymer P04 and P05. However, a glass transition temperature (T_g) was detected for P04 and P05 polymer. The glass transition temperatures were observed in between -40 to -30 °C. It was expected that increasing the phenyl content will further decrease the T_g of the polymers. However, the T_g was comparable for all the polymers (P04 to P05) indicating that the phenyl content has not influencing the T_g significantly. The P01 polymer with no phenyl content showed a sharp melting temperature while the glass transition temperature was absent for this polymer. The physical properties of the polymer changed from solid to viscous liquid by increasing the phenyl content in the polymer chain. Figure 3-6 shows the trend in the melting temperatures (T_m), glass transitions temperatures (T_g) and crystallization temperature (T_c) of various synthesised polyesters.

Table 3-3 Thermal and physical properties of the synthesised polyester polymer (n=1).

Polymer Code	Product ratio (mol%)		Thermal Property				Physical Property
	SA	PSA	T_g (℃)	T_m (℃)	Melting Enthalpy (ΔH) J/g	T_C (℃)	
P01	100	0	ND	71	124	49	Crystalline (White solid)
P02	70	30	-39	45	44	19	Semicrystalline (Off white solid)
P03	50	50	-38	35	32	4	Semicrystalline (Light brown solid)
P04	30	70	-40	ND	ND	ND	Amorphous (Viscous liquid)
P05	0	100	-34	ND	ND	ND	Amorphous (Viscous liquid)

ND:Not detected;SA:Succinic acid; PSA:Phenylsuccinic acid
T_g: glass transition temperature; T_m: melting temperature; T_c: crystallization temperature

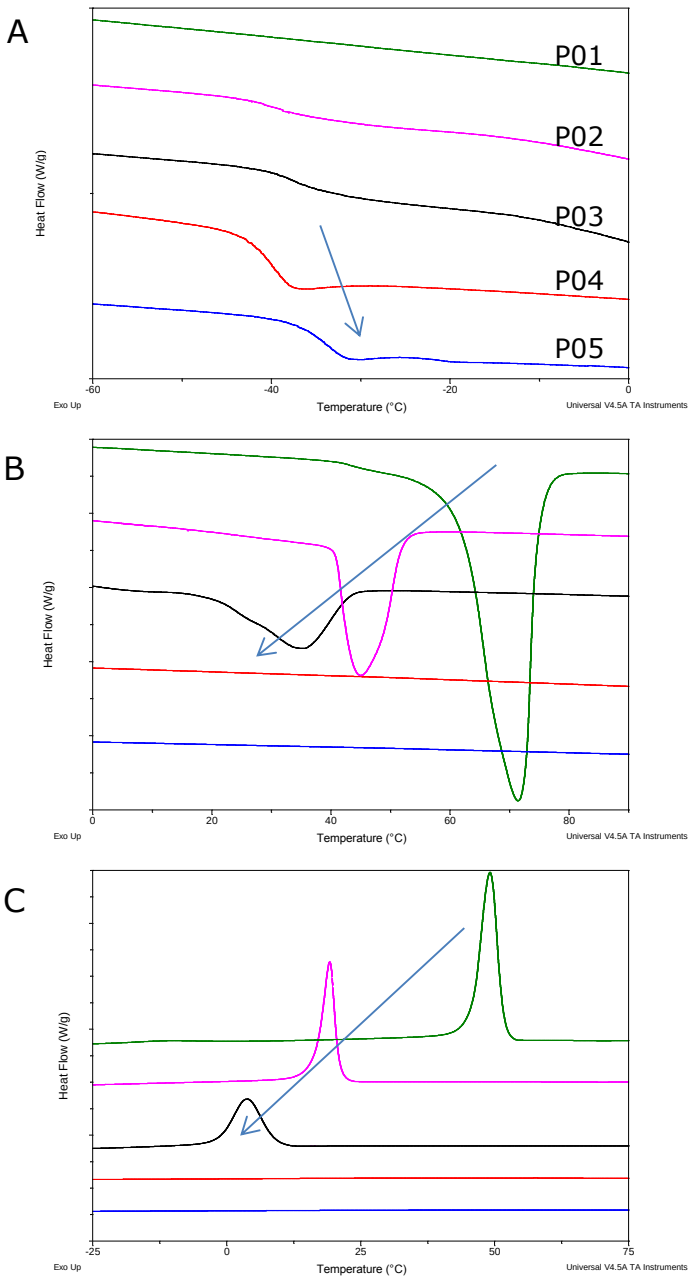


Figure 3-6 DSC graph showing (A) glass transition temperature (T_g) (B) melting temperature (T_m) (C) crystallization temperature (T_c) of synthesised polyester polymers from P01 to P05.

3.3.2 Preparation and Characterisation of Nanoparticles

Polymers of similar molecular weight but with differences in their phenyl content were investigated to determine if side-chain content and T_g/T_m variation had any effect on the ability to encapsulate model drugs. The polymers were mixed with a model drug, coumarin 6, prior to nanoprecipitation from a common solvent to a non-solvent. The results of the nanoprecipitation for dye loading are given in table 3-4.

Table 3-4 Characteristics of empty and dye loaded polymeric nanocarrier (n=3).

Code		Empty Nanoparticles[£]		Dye Loaded Nanoparticles[£]		Zeta potential (mV) (±SD)	Drug Content (%) ± SD
Polymer	NP	Average Size (nm)	PDI	Average Size (nm)	PDI		
P01	NP01	144 ± 6	0.09 ± 0.02	146 ± 9	0.10 ± 0.02	-39 ± 9	ND
P02	NP02	160 ± 7	0.03 ± 0.01	168 ± 7	0.05 ± 0.01	-40 ± 7	0.28 ± 0.01
P03	NP03	163 ± 8	0.06 ± 0.02	166 ± 5	0.07 ± 0.02	-38 ± 5	0.23 ± 0.02
P04	NP04	165 ± 6	0.10 ± 0.03	172 ± 6	0.09 ± 0.02	-39 ± 6	0.12 ± 0.01
P05	NP05	164 ± 4	0.09 ± 0.02	167 ± 7	0.08 ± 0.02	-41 ± 6	0.05 ± 0.01
P02	NP02[*]	185 ± 5	0.07 ± 0.02	206 ± 6	0.08 ± 0.02	-21 ± 6[$]	0.23 ± 0.02

NP: Nanoparticle, [*] Pluronic coated P02 nanoparticles. [£] Determined from Dynamic Light Scattering (DLS) Technique. [$] Significant difference from uncoated NP02 nanoparticles ($P < 0.05$, unpaired student's t test).

The P02 polymer showed a low solubility in acetone which was used as organic phase during nanoprecipitation. However, a small increase in temperature of the organic phase dissolved the polymer. The method of nanoprecipitation was optimized for solvent to non-solvent and polymer to

coumarin 6 dye ratios. A difference in the colour intensity (yellow) was observed when a nanosuspension was passed through a 0.22 μm filter to remove aggregates. The formulation containing coumarin 6 dye in water (no polymer) showed aggregates of dye which upon filtration became a clear transparent solution. In general, the dye content was decreased as the phenyl content was increased in the polymer. No dye was detected in the nanoparticles made from P01 polymer. The dye loading was found to be highest with PDeMS-co-PS (P02) polymer compared to other synthesised polymers. Hence, P02 polymer was utilized for the nanoparticle preparation for further studies. The nanoparticles made from P02 polymer were also stabilized by the adsorption of Pluronic F68 on the surface of the nanoparticles. The effect was observed on size, zeta potential and dye loading. The adsorption of pluronic on the surface of the nanoparticle significantly changed the zeta potential from -40 mV to -21 mV. The dye loading was significantly decreased ($P < 0.05$, unpaired student's t test) when P02 nanoparticle formulations were compared against the Pluronic-coated P02 nanoparticle formulation. The dye loading along with colour intensity of the different formulations are given in figure 3-7.

The sizes of the nanoparticles were observed in the range of 150 to 200 nm. There was no significant difference in the sizes observed between empty and dye-loaded nanoparticles. However, a significant difference was observed for Pluronic coated empty and dye-loaded nanoparticles. A significant difference

in the size of P02 nanoparticle and Pluronic coated P02 nanoparticles were also observed in both empty and dye loaded formulations (table 3-4).

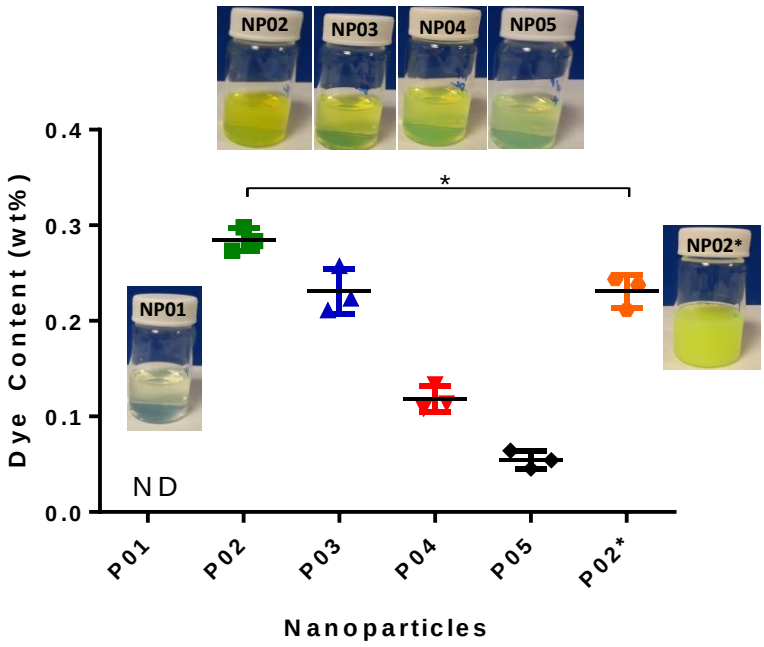


Figure 3-7 Coumarin 6 loading (wt% to polymer) in different copolymers. Each point represents mean ± SD (n=3). A significant difference ($P < 0.05$, unpaired student's t test) was observed. P02*: Pluronic coated P02 nanoparticles

The data for coated and uncoated P02 nanoparticles indicated that the Pluronic coating stabilized the nanoparticles in PBS. The dilution of P02 nanoparticle with HPLC water showed a single sharp peak while two distinct peaks were observed when nanoparticles were diluted with PBS. On the other hand, no significant change in the size was observed for pluronic coated P02 nanoparticle after dilution with PBS (Figure 3-8). The TEM image of uncoated and pluronic coated P02 nanoparticles showed a uniform distribution of spherical nanoparticles in the formulation (Figure 3-9).

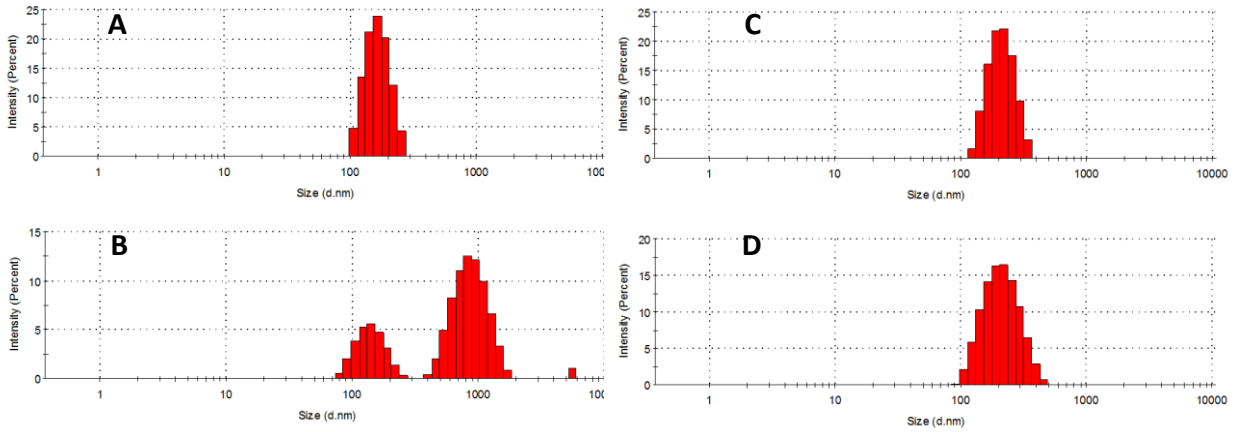


Figure 3-8 Stability of nanoparticle in HPLC water and PBS (A) Uncoated P02 nanoparticle in HPLC water (B) Uncoated P02 nanoparticle in PBS (C) Pluronic coated P02 nanoparticle in HPLC water (D) Pluronic coated P02 nanoparticle in PBS.

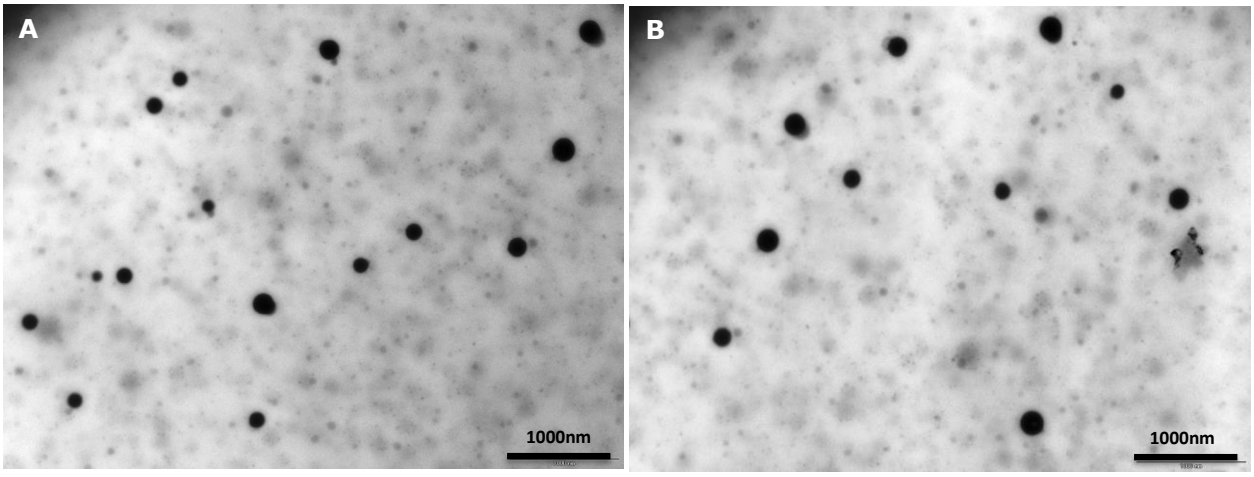


Figure 3-9 TEM images of uncoated (A) and pluronic coated nanoparticles (B). The images were taken without staining. Scale bar – 1000nm.

However, it was hard to observe the Pluronic coating on nanoparticles with the TEM image due to instrument limitations. Nevertheless, the adsorption of pluronic was strongly implied by the reduction in negative zeta potential of the pluronic coated nanoparticles.

3.3.3 Degradation Study of P02 Nanoparticle Formulation

Figure 3-10 shows the degradation profile of the P02 nanoparticle in different conditions.

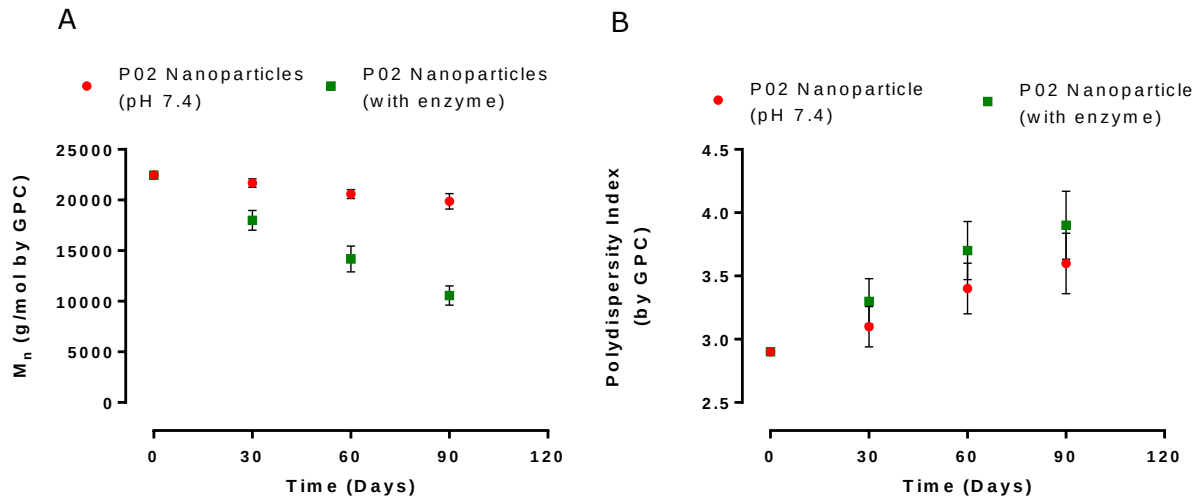


Figure 3-10 Loss in molar mass (M_n) of P02 nanoparticles (A) and polydispersity index (B) with time (days) in presence and absent of *Pseudomonas cepacia* lipase (0.2 mg/mL) at 37 °C

Polymer degradation profiles are important in polyesters designed for sustained release, as these data provide valuable information related to *in vivo* fate and long term solution storage. Degradation of the selected P02 formulation was monitored at specific time intervals (30 days) in the presence and absence of a model hydrolytic enzyme, *Pseudomonas cepacia* lipase (0.2 mg mL^{-1}). The presence of the lipase resulted in a reduction in the polymer M_n to 53% of its original value after 3 months. Conversely, a drop of only 12% in M_n was observed in the absence of enzyme.

3.3.4 Impact of Nanoparticles on C3A Cell Activity

The toxicity of P02 nanoparticles (in the presence and absence of a Pluronic F68 coating) was assessed *in vitro*, using the human C3A hepatocyte cell line. Hepatocytes were selected as the liver is the primary site of nanoparticle accumulation following exposure via different routes (e.g. intratracheal instillation, ingestion, intravenous injection), and existing evidence suggests that C3A cells respond similarly to primary human hepatocytes.[24-27] The effects on C3A hepatocyte cell were assessed using the Alamar Blue, CFDA-AM, and Neutral Red assays. For all assays, cell viability (as a proxy for a specific activity) was more than 80% for both coated and uncoated P02 nanoparticles, at the concentration range tested (4.6 to 300 μg mL^{-1}), 24 h post exposure. Although results at 150 and 300 μg ml^{-1} for coated P02 (Figure 3-11) using the Neutral Red assay indicated a statistically significant decrease in cell viability, this was not considered to be biologically relevant as these were doses well above those likely to be used in a clinical setting and even at these concentrations, the overall viability decrease was no more than 20 %. However this viability decrease could indicate effects on the lysosomal function of C3A cells which might occur after accumulation of these polyester NPs.

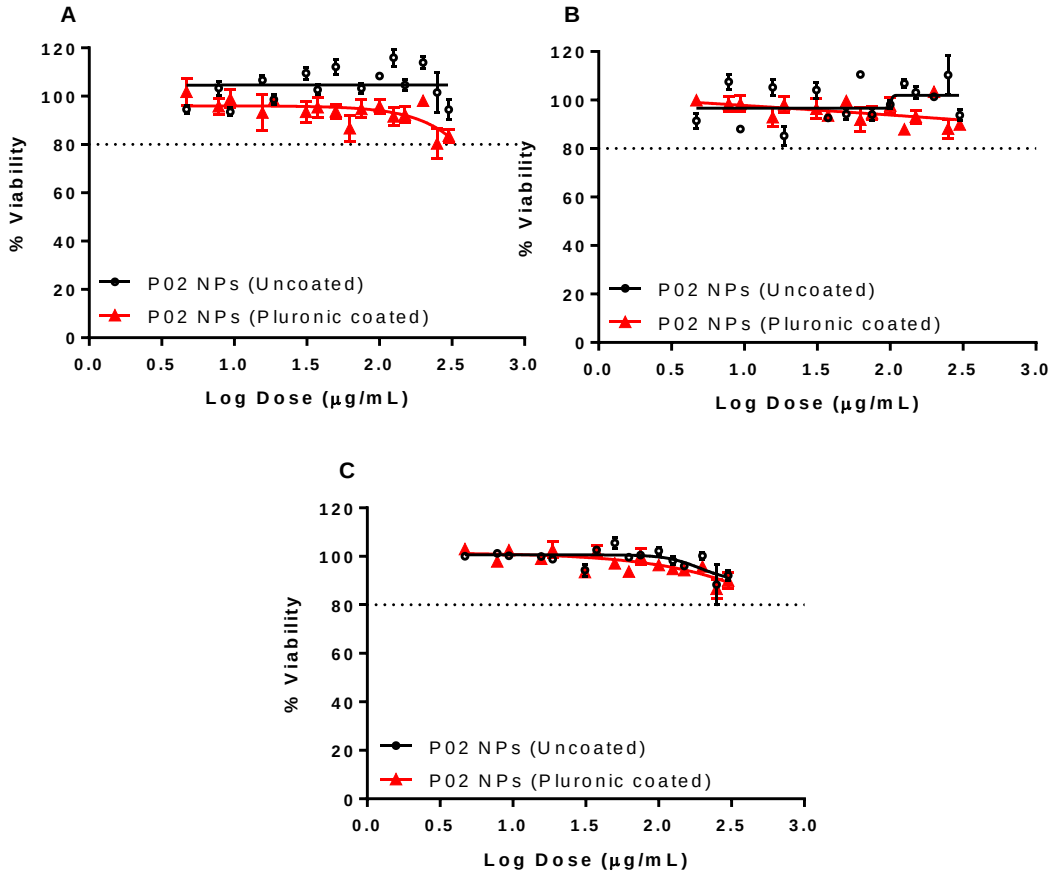


Figure 3-11 Viability of C3A hepatocytes following exposure to Pluronic F68 coated (red) and uncoated (black) P02 NPs. Cells were exposed to NPs (at concentrations ranging from 4.6 to 300 µg mL^{-1}) for 24 h with cell viability assessed via Alamar Blue (A), CFDA (B) and Neutral Red (C) assays. Data are expressed as the average percentage of cell viability (% of the control (MEM complete medium exposed cells) ± SEM (n = 3 minimum).

3.3.5 Cellular Uptake of Nanoparticles by C3A Cells

Imaging of the uptake of coated and uncoated P02 nanoparticles by C3A cells suggested that both types of the nanoparticles were avidly taken up within 10 min. The NPs were present both on the surface of the cells and were internalized into the cell interior (confirmed via z stacks). The internalization of both types of P02 nanoparticles increased progressively

over the study time. NPs were predominately located in the cytoplasm of cells.

Initially (10 minutes post exposure) both types of NPs were observed to be compartmentalized inside and between the cells, although a more diffuse pattern of uptake was observed at 1440 mins (Figures 3-12 and 3-13). For uncoated NPs, vacuoles containing fluorescence adjacent to the nucleus could be seen from 10 min. Internalization of NPs into the cell interior were confirmed via z stacks (Figure 3-14). It is worth noting that due to the resolution (approximately 200 nm) of the microscope it was not possible to distinguish individual nanoparticles.

Quantification of coated and uncoated P02 nanoparticle uptake confirmed the findings obtained from confocal microscopy. The extent of NP uptake by cells was concentration and time dependent (Figure 3-15). The level of uptake of both NP types occurred to a similar extent. For both NP types the greatest level of uptake was observed at 1440 min. The uncoated P02 NPs showed the highest level of uptake at 3.8% of the applied dose internalized at 150 μg mL^{-1} after 1440 min treatment. The greatest level of uptake for Pluronic F68 coated P02 NPs was observed at 1440 min, with 2.7% of the applied dose internalized at a concentration of 300 μg mL^{-1}.

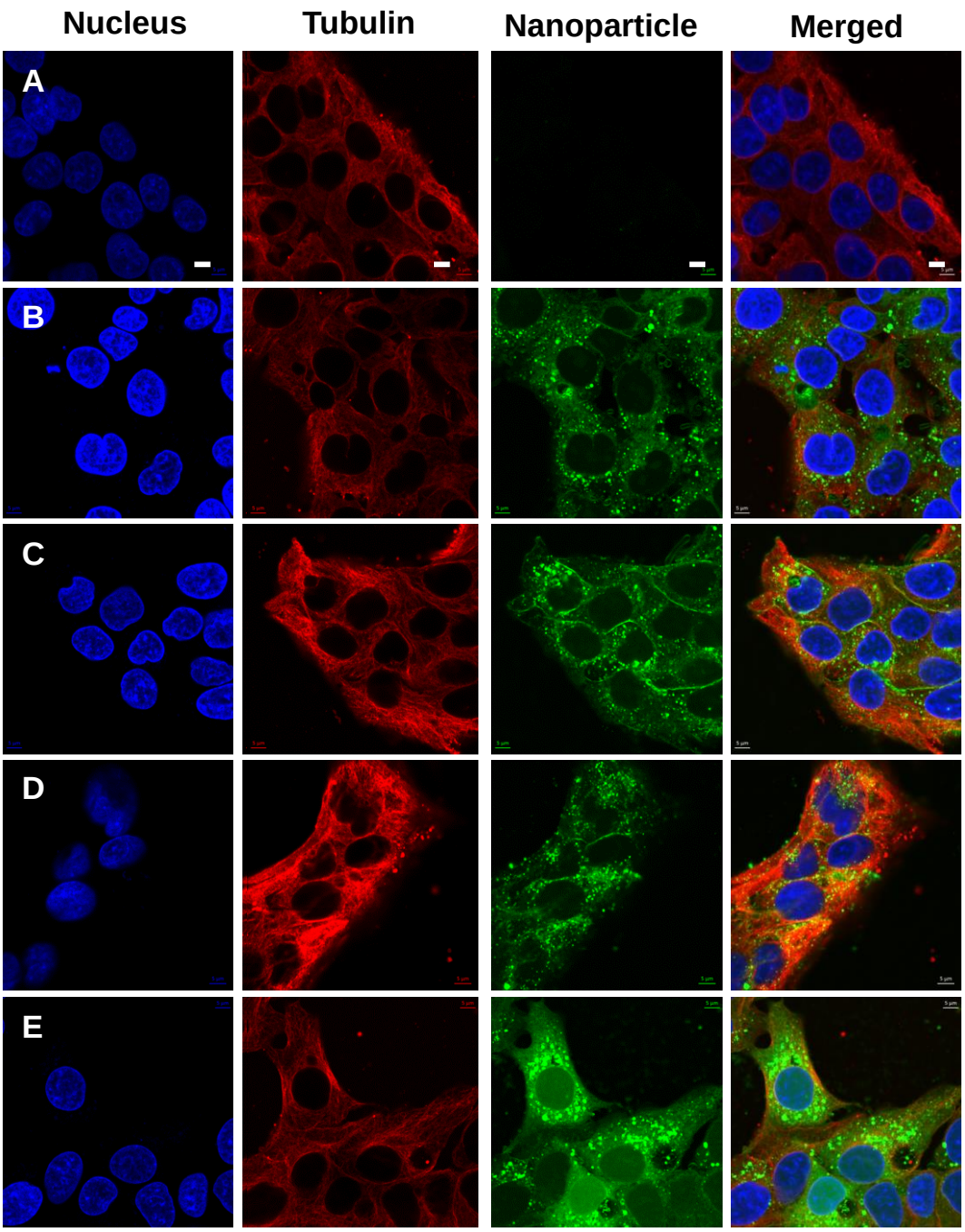


Figure 3-12 The time dependent uptake of coumarin-6 labelled uncoated P02 nanoparticles by C3A cells. Cells were treated with MEM complete medium (A) or NPs (100 μg mL^{-1}) for 10 min (B), 60 min (C), 240 min or (D) 1440 min. Following exposure cells were fixed and stained for the tubulin cytoskeleton (red) and nucleus (blue). The green color represents coumarin 6 loaded NPs. Any yellow color observed indicates co-localization of tubulin and NPs. The scale bars represent 5 μm.

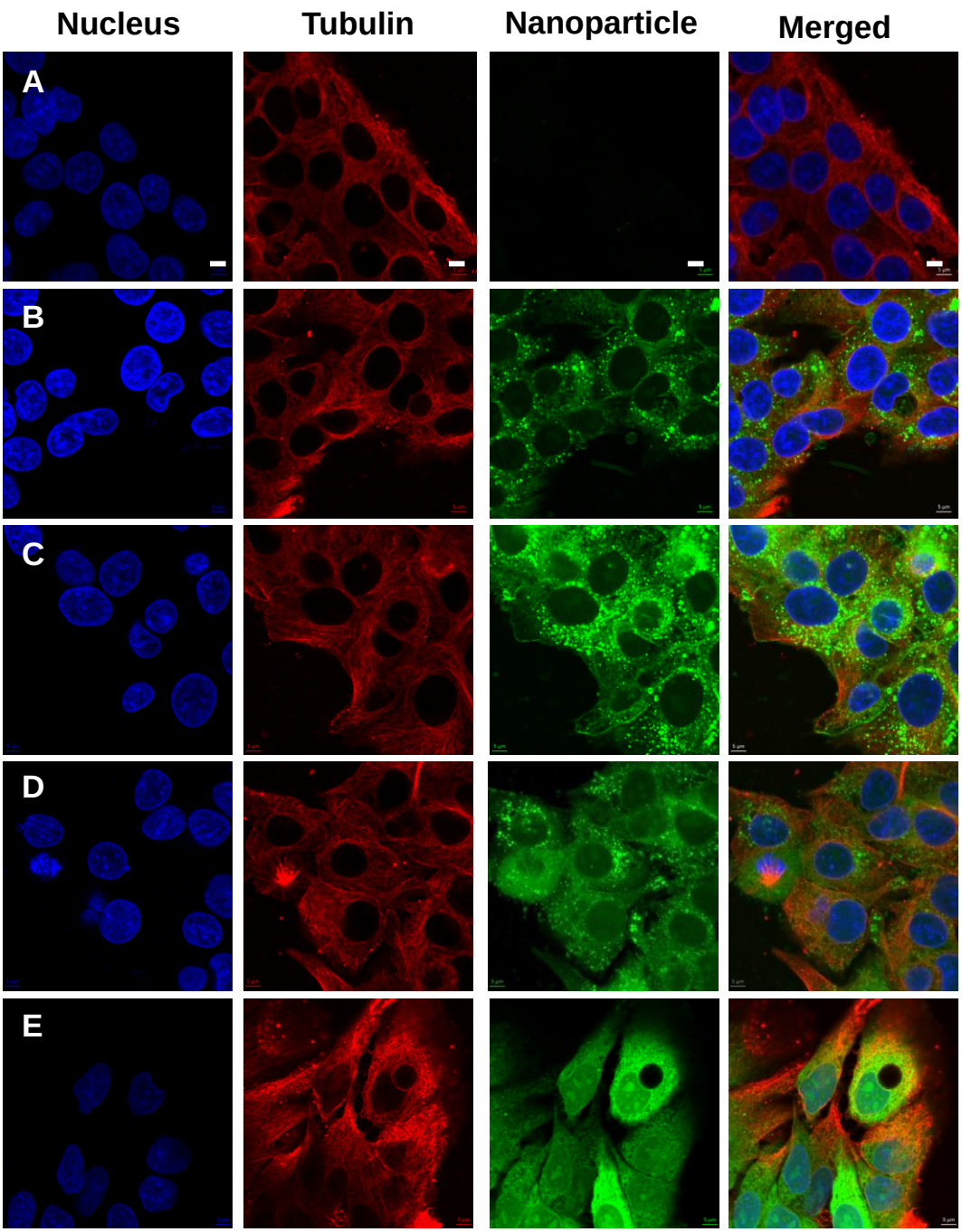


Figure 3-13 The time dependent uptake of coumarin-6 labelled Pluronic F68 coated P02 nanoparticles by C3A cells. Cells were treated with MEM complete medium (A) or NPs (100 μg mL^{-1}) for 10 min (B), 60 min (C), 240 min or (D) 1440 min. Following exposure cells were fixed and stained for the tubulin cytoskeleton (red) and nucleus (blue). The green color represents coumarin 6 loaded NPs. Any yellow color observed indicates co-localization of tubulin and NPs. The scale bars represent 5 μm.

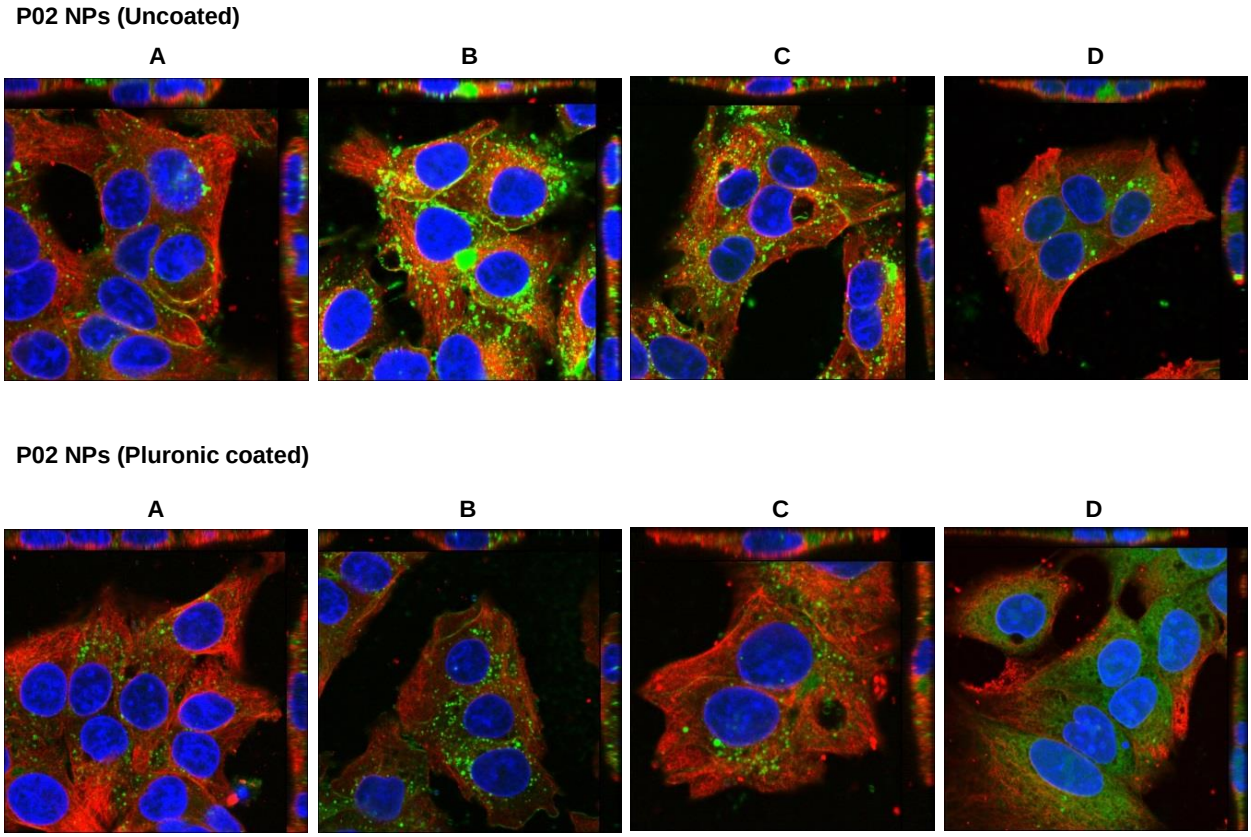


Figure 3-14 Internalization of uncoated P02 and Pluronic F68-coated P02 fluorescent NPs over time by C3A cells. Images represent Z-stacks from which xy and yz micrographs were generated to confirm internalization of NPs. Cells were treated with 100 µg mL^{-1} NPs for 10 min (A), 60 min (B), 240 min (C) and 1440 min (D) and then fixed. Tubulin cytoskeleton is represented by red, the nucleus by blue and the NPs by green. Co-localization of NPs and tubulin is represented by yellow.

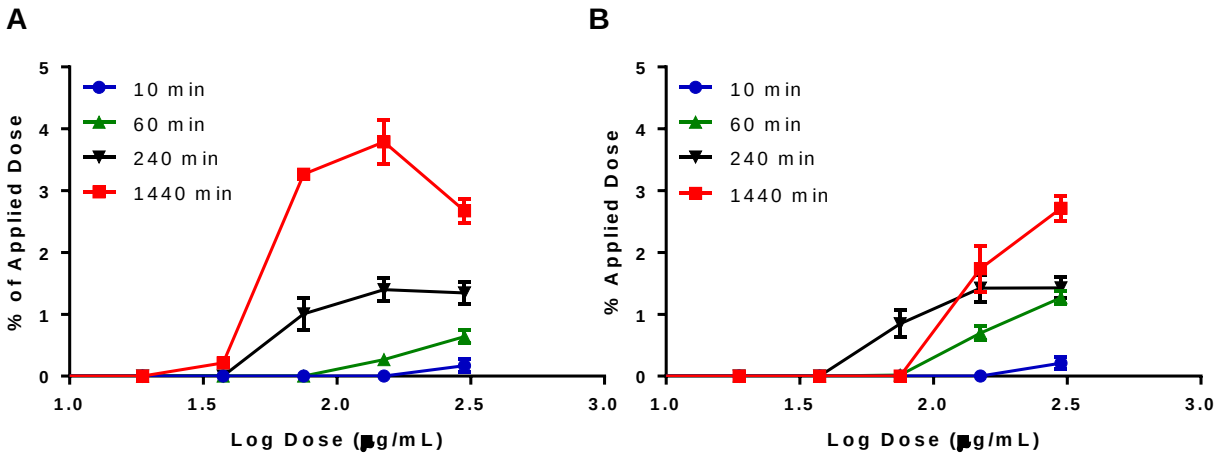


Figure 3-15 Quantification of the uptake of coated and uncoated P02 NPs in C3A cells over time at a range of concentrations (4.6-300 µg mL^{-1}). Cells were treated for 10 min, 60 min, 240 min and 1440 min with uncoated P02 (A) or coated P02 (B). The Percent (%) applied dose was calculated from the relevant standard curves.

3.4 Discussion

For polymer synthesis, polycondensation generally requires high temperatures (above 200 °C) and long reaction times to reach conversion.[28, 29] We selected scandium (III) triflate as a Lewis acid catalyst, to accelerate the reaction under solvent-free melt conditions.[30] In our synthetic strategy, succinic acid and phenyl succinic acid were used as diacids to incorporate different ratio of phenyl contents. However, the high melting temperature (>150 °C) of these monomers limits the use of melt polycondensation. Hence, 1-10- decanediol was used as a reactive 'solvent', as it melts at 80 °C and was able to dissolve diacids in the melted mixture. Therefore, after proper mixing, scandium (III) triflate was added to catalyze the reaction at 125 °C. The use of the organic solvent was avoided to increase the reaction

rate and make synthesis more sustainable. A brown colored viscous material was produced after 3 h of reaction indicating the formation of small oligomers. Conversion to high molecular weight was achieved by carrying out the reaction under reduced pressure, in order to remove water molecules continuously from the reaction. The formed products were precipitated in cold methanol and vacuum dried to give property ranging from solids to viscous liquid depending upon the phenyl content in the polymer backbones.

The reaction was observed by ^{1}H NMR and the peak positions were confirmed by ^{1}H-^{1}H COSY NMR spectroscopy. The methylene protons adjacent to the hydroxyl of 1, 10- decanediol are usually shielded to give peaks at lower frequency (δ3.40 ppm). However, upon reaction of hydroxyl groups with diacid components, deshielding occurs to shift the peaks to higher frequency (δ4.10 ppm). The disappearance of the peak at δ3.40 ppm in the final product indicated that all the diol monomers reacted with diacids during the polycondensation. The success of the syntheses was also supported by the peak positions shown in the ^{13}C NMR spectra (Figure 3-4). The presence of phenyl groups in the phenylsuccinate co-polymers generated two peaks in the carbonyl region of the spectra (Figure 3-4). The appearance of carbonyl stretching modes at 1727 cm^{-1} in the FTIR spectrum also confirmed the synthesis of the polyesters.

In order to compare the polymer properties, it was essential to produce polymers of similar molecular weight. Therefore, the polymers were synthesised and fractionated into those with similar molar masses for further study. Although high polydispersities were expected for polycondensation reactions, the similar values of polydispersity for the range of synthesised polymers indicated the presence of similar chain lengths across the different samples. It should also be noted that the presence of ionisable carboxyl groups on the polymer chain end group might interact with the GPC column to result in the widening of the peak.

The absence of T_g and presence of T_m (49 °C) for P01 polymer (white solid material) indicated the crystalline nature of the polymer. A similar result was also obtained for the same type of polymer previously.[31] Increasing the phenyl content in the polymer resulted in the appearance of a T_g while the T_m and T_c were decreased. The presence of T_g and T_m in the phenyl-substituted polymers indicated the semicrystalline nature of these materials (P02-P03). The polymers with high phenyl content (P04-P05) showed only a T_g while the absence of T_m and T_c indicated that these polymers were amorphous. Linear polymeric chains without bulky side groups can more easily form crystal structures as there is more possibility for the polymer chains to remain close in a regular packed arrangement, generating the high intermolecular forces which cause crystallite formation. On the other hand,

bulky side groups, in this case phenyl, can prevent chain packing and thus these polymers are more amorphous in nature.

The crystallinity in the polymers can affect a number of other properties such as drug loading, release and biodegradability. In order to test the abilities of the polymers to act as carriers for drugs, nanoparticles were prepared by a nanoprecipitation method in the presence of a dye molecule (coumarin 6). Coumarin 6 was chosen because of its (1) high hydrophobicity and (2) highly fluorescence nature. The hydrophobic nature makes it an idea compound to use as an alternative to the hydrophobic drugs while highly fluorescence nature make it traceable during dye loading and cell uptake studies. Also, its high fluorescence makes it possible to track transport during cell uptake studies. Coumarin 6 is not very water soluble, but when nanoprecipitated in the presence of the polymers, the yellow colour of the formulations indicated that the dye was entrapped within the polymeric nanoparticles. The highest loading was observed for P02 polymeric nanoparticles. However, the dye content was decreased as the phenyl content was increased in the polymer. These results were unexpected as the ring systems of the dye were expected to interact more favorably with polymers containing high phenyl content through mutual π-π interactions. Also, the polymers with high phenyl content were amorphous hence were expected to encapsulate more dye due to the higher free volumes in amorphous core regions. These seemingly contradictory results can be

explained by considering three major factors (1) polymer-polymer interaction (2) dye-dye interaction (3) dye-polymer interaction during nanoprecipitation method. For a higher loading, a favorable dye-polymer interaction is important to maintain a close proximity of dye and polymer during the late stages of nanoprecipitation. However, a higher polymer-polymer interaction and dye-dye interaction can cause reduction in the dye loading during nanoprecipitation. For the P01 polymer, a high polymer-polymer and dye-dye interaction caused the molecules to precipitate resulting in a low yield of well-defined nanoparticles and with no detectable dye content. This might have been be due to the low solubility of P01 polymer in the organic phase used (acetone). Upon addition of this phase into water, it is likely that the acetone molecules diffused at a high rate into water with ultra-rapid precipitation of polymer chains and dye molecules with little chance for polymer-dye associations to form. As the phenyl content was increased for P02 polymer, a more favorable interaction between dye and polymer may have resulted hence the higher dye loading. This might have been caused by favorable π-π interactions between dye and phenyl rings in polymer. However, upon further increase of phenyl content in the polymer (P03, P04 and P05), the higher π-π interactions between polymer molecules, rather than dye-polymer molecules, resulted in lower loading capabilities.

Addition of Pluronic F68 during P02 nanoparticle formation resulted in reduction of zeta potential and dye loading, while the sizes of the nanoparticles were increased significantly ($P < 0.05$, unpaired student's t test) compared to those of the parent P02 polyester alone. Spherical particles with uniform size distributions were observed in TEM images although, it was not possible to observe the Pluronic coating directly in these micrographs. However, the presence of a neutral polymer coating at the surface of the nanoparticles was confirmed by the reduction in zeta potential. The adsorption of non-ionic Pluronic on the surface of the negative charged particles enhanced particle stability in aqueous solution upon dilution with PBS. The stability in PBS was important so that formulations could be used during cell uptake studies. A lower dye loading in the coated nanoparticles suggested that the Pluronic polymer altered the structural arrangement of the polymer chains or their association with the dye. However, precipitation of dye in Pluronic solutions and the absence of dye in Pluronic micelles suggested that the dye did not strongly interact with Pluronic F68. Therefore, it is likely that the Pluronic amphiphilic co-polymer associated more strongly with the polyester than the dye, thus reducing the dye loading capability.

The degradation study of the polymer (P02) aimed to provide information related to the fate of these materials inside the body and in long term solution storage conditions.[32] The molar mass profile over time revealed that

the polymer was degradable. However, a low degradation rate of the polymer at pH 7.4 indicated that the polymer was quite resistant to hydrolytic cleavage. The presence of enzymes increased the degradation rate suggesting that the polymer could be degraded in the body more rapidly due to enzymatic-mediated hydrolysis.

A 3 in 1 assay (Alamar Blue, CFDA-AM and Neutral Red) was used to assess viability of cells exposed to the polymer NPs. These assays were selected as it is established that NPs can interfere with biochemical assays used to assess their toxicity,[33] and therefore it is advisable to assess the impact of NPs on cell viability using more than one approach. Furthermore, using 3 different assays which assess different cell responses as indicators of cytotoxicity can provide information on the mechanism of NP toxicity. All three assays indicated that the coated and uncoated P02 NPs exhibited low acute toxicity in the experimental conditions tested. A greater sensitivity was observed with the Neutral Red assay showing statistically significant effects on normal lysosome function at high concentrations of Pluronic F68 coated P02 NPs, although the small changes in cell viability observed were not considered to be of potential clinical significance. In order to evaluate the toxic potency of NPs, the inhibitory concentration $(IC)_{50}$ can be calculated, which identifies the concentration of NPs required to kill 50% of cells. No reliable IC_{50} values could be calculated for the NPs tested in this study despite concentrations up to 300 μg mL^{-1} being tested. Previous studies

which have investigated the response of C3A cells to engineered NPs (e.g. silver, zinc oxide) at a similar concentration range tested in this study, have calculated IC_{50} values of approx. 2 μg ml^{-1},[34] demonstrating the relatively low toxicity of the polymeric NPs tested in this study.

Evaluation of the uptake and intracellular fate of nanoparticles intended for medical use is important as carrier materials are often required to enter the cell in order to deliver a therapeutic or identify a diseased phenotype.[35] Previous studies have indicated that uptake efficiency and subcellular localisation can influence material cytotoxicity.[36] Therefore, it is important to elucidate the uptake pattern of the polyester NPs, particularly in hepatic cell lines, as it is well established that the liver is a site of accumulation for many nanoparticles following exposure via various routes (e.g. intravenous injection, ingestion, inhalation/intratracheal instillation).[24, 25, 27] The uptake of coated and uncoated P02 NPs in C3A cells suggested that the NPs were taken up by the cells in a time and concentration dependent manner. Previous studies have indicated that the uptake of polymer NPs by cells increased with time in other cell lines (e.g. hepatocytes, macrophages), although these studies did not look at the impact of NP concentration on uptake and assessed uptake over a shorter time frame.[37, 38]

In this study NPs were primarily compartmentalized within and between C3A cells as early as 10 min post exposure. At the later time point of 1440 min NPs were observed throughout the cytoplasm of the C3A cells. The

subcellular fate of internalized NPs was not investigated in this study, however the pattern of uptake observed suggests that NPs were initially located within the cell organelles such as endosomes or lysosomes. P02 NPs were observed to accumulate in lysosomes of the J774 macrophage cell line 1 h post exposure (data not shown) and polystyrene NPs and quantum dots have been observed to accumulate in lysosomes and mitochondria of macrophages *in vitro*.[39] Furthermore poly (lactic-co-glycolic) acid (PLGA) NPs coated with Hyaluronan and Polyethyleneimine were co-localized with the lysosome of A549 alveolar epithelial cells after 24 h. Future studies could therefore investigate the subcellular localization to better understand the fate of internalized NPs. Of particular interest may be assessment of accumulation in lysosomes via the use of fluorescent probes such as LysoTracker.[38] Alternatively, transmission electron microscopy could be used to investigate the sub-cellular fate of the NPs in hepatocytes, although it may be challenging to distinguish NPs from sub-cellular structures due to their similarity in size and appearance.

NPs were also seen to accumulate between cells, which may be representative of accumulation in bile canaliculi. These structures are responsible for the formation and secretion of bile by hepatocytes and could be indicative of NP removal from the cells. Interestingly, the elimination of polystyrene NPs (20 nm) in bile has been observed previously *in vitro* and *in vivo*.[38]

The co-localization of NPs with tubulin was also observed in this study, particularly within the perinuclear region of the cell. Research has shown that tubulin may be involved with the directional transport of NPs within the cell and this transport can be targeted towards the nucleus.[40] NPs in vacuoles in close proximity to the nucleus could also suggest targeted delivery to the nucleus, although the size of these particular NPs would likely prohibit them crossing an undamaged nuclear membrane. At 24 h post exposure, coated NPs appeared to become diffuse throughout the cell, whilst the majority of uncoated NPs remained compartmentalized, suggesting that the Pluronic coating may have had an impact on the intracellular fate of NPs. NPs may thus have been partially degraded within certain cell organelles (e.g. lysosomes) via hydrolytic enzymes known to degrade polyesters,[41] and thus any dye associated near the NP surfaces may have been released into the cytoplasm. It is also possible that the P02 NPs escaped the organelles to distribute throughout the cytoplasm. An increase in the number and size of vacuoles within cells treated with coated P02 was also apparent which may indicate damage to the cells had occurred over time.

Commonly, hydrophilic particles are less efficiently internalized compared to hydrophobic nanoparticles.[42] The Pluronic F68 coating provided a hydrophilic layer, and made the particles less negative in terms of zeta potential compared to the uncoated P02 NPs. However, the Pluronic coated NPs were typically internalized to the same extent as that of the uncoated

nanoparticles. At 1440 min the uptake of uncoated P02 NPs was higher than coated P02 NPs. This small difference between the NPs might be related to the coating density and chain length of Pluronic F68 since the coated NPs were still not overall neutral – indicating only a partial coverage of the underlying surface. This factor may thus account for the rapid internalization of all the NPs and their subsequent effects on cellular activity.

3.5 Conclusion

In this study, the synthesis of a new series of polyesters by melt polycondensation under solvent-free conditions has been described and the effects of co-monomer content on polymer properties (e.g. crystallinity) and nanoparticle properties (e.g. size, dye loading) relevant to controlled release applications have been evaluated. The study suggested that side chain phenyl content changed the loading capability of NPs for a model dye, but the overall level of incorporation remained very low. The study provided information about the stability, and degradability of a selected P02 polymer when formulated into Pluronic coated and uncoated nanoparticles. The cellular studies revealed that P02 NPs displayed low cell toxicity and were effectively taken up by the cells. However, the Pluronic coating appeared to enhance some aspects relating to the toxicity of the NPs, and this information should be used to inform the design of formulated NPs in the future.

However, the high polydispersity of the polyesters, the difficulty in generating polymers of similar molar mass repeatedly by this method of synthesis and the overall low loading of the dye persuaded us to consider other strategies for the synthesis of polyester polymers. Therefore, the next chapter deals with the synthesis of polyester polymers by ring opening polymerisation (ROP) reactions of renewable ε-decalactone (ε-DL) and other cyclic ester monomers.

3.6 References

1. I. K. Varma, A. C. Albertsson, R. Rajkhowa and R. K. Srivastava, *Progress in Polymer Science*, 2005, **30**, 949-981.
2. H. M. Aliabadi and A. Lavasanifar, *Expert opinion on drug delivery*, 2006, **3**, 139-162.
3. X.-B. Xiong, Z. Binkhathlan, O. Molavi and A. Lavasanifar, *Acta Biomaterialia*, 2012, **8**, 2017-2033.
4. A. C. Albertsson and I. K. Varma, *Degradable Aliphatic Polyesters*, 2002, **157**, 1-40.
5. S. Slomkowski, *Macromolecular Symposia*, 2007, **253**, 47-58.
6. H. Seyednejad, A. H. Ghassemi, C. F. van Nostrum, T. Vermonden and W. E. Hennink, *Journal of Controlled Release*, 2011, **152**, 168-176.
7. T. Ishigaki, W. Sugano, M. Ike, Y. Kawagoshi, I. Fukunaga and M. Fujita, *Journal of Basic Microbiology*, 2000, **40**, 177-186.
8. M. L. Adams, A. Lavasanifar and G. S. Kwon, *Journal of Pharmaceutical Sciences*, 2003, **92**, 1343-1355.
9. H. Cho, C. S. Cho, G. L. Indig, A. Lavasanifar, M. R. Vakili and G. S. Kwon, *Figshare*, 2014, **1**.
10. S. Elhasi, R. Astaneh and A. Lavasanifar, *European Journal of Pharmaceutics and Biopharmaceutics*, 2007, **65**, 406-413.
11. Z. Ma, A. Haddadi, O. Molavi, A. Lavasanifar, R. Lai and J. Samuel, *Journal of Biomedical Materials Research Part A*, 2008, **86A**, 300-310.
12. M. A. Woodruff and D. W. Hutmacher, *Progress in Polymer Science*, 2010, **35**, 1217-1256.
13. Y. D. Wang, G. A. Ameer, B. J. Sheppard and R. Langer, *Nature Biotechnology*, 2002, **20**, 602-606.

14. H. Seyednejad, D. Gawlitta, W. J. A. Dhert, C. F. van Nostrum, T. Vermonden and W. E. Hennink, *Acta Biomaterialia*, 2011, **7**, 1999-2006.
15. R. N. Shirazi, W. Ronan, Y. Rochev and P. McHugh, *Journal of the Mechanical Behavior of Biomedical Materials*, 2016, **54**, 48-59.
16. H. Kenar, G. T. Köse and V. Hasirci, *Biomaterials*, 2006, **27**, 885-895.
17. J. C. Kang and S. P. Schwendeman, *Biomaterials*, 2002, **23**, 239-245.
18. A. H. Brown and V. V. Sheares, *Macromolecules*, 2007, **40**, 4848-4853.
19. Z. Gan, H. Abe and Y. Doi, *Biomacromolecules*, 2001, **2**, 313-321.
20. H. J. Jin, B. Y. Lee, M. N. Kim and J. S. Yoon, *Journal of Polymer Science Part B-Polymer Physics*, 2000, **38**, 1504-1511.
21. U. Witt, R. J. Muller and W. D. Deckwer, *Macromolecular Chemistry and Physics*, 1996, **197**, 1525-1535.
22. U. Bilati, E. Allemann and E. Doelker, *European Journal of Pharmaceutical Sciences*, 2005, **24**, 67-75.
23. M. Connolly, M.-L. Fernandez-Cruz, A. Quesada-Garcia, L. Alte, H. Segner and J. M. Navas, *International Journal of Environmental Research and Public Health*, 2015, **12**, 5386-5405.
24. C. Schleh, M. Semmler-Behnke, J. Lipka, A. Wenk, S. Hirn, M. Schaeffler, G. Schmid, U. Simon and W. G. Kreyling, *Nanotoxicology*, 2012, **6**, 36-46.
25. S. Hirn, M. Semmler-Behnke, C. Schleh, A. Wenk, J. Lipka, M. Schaeffler, S. Takenaka, W. Moeller, G. Schmid, U. Simon and W. G. Kreyling, *European Journal of Pharmaceutics and Biopharmaceutics*, 2011, **77**, 407-416.
26. E. Sadauskas, N. R. Jacobsen, G. Danscher, M. Stoltenberg, U. Vogel, A. Larsen, W. Kreyling and H. Wallin, *Chemistry Central Journal*, 2009, **3**.
27. M. Semmler-Behnke, W. G. Kreyling, J. Lipka, S. Fertsch, A. Wenk, S. Takenaka, G. Schmid and W. Brandau, *Small*, 2008, **4**, 2108-2111.
28. A. Takasu, T. Makino and S. Yamada, *Macromolecules*, 2010, **43**, 144-149.
29. S. Yamada and A. Takasu, *Polymer Journal*, 2011, **43**, 1003-1007.
30. M. Oshimura, A. Takasu and K. Nagata, *Macromolecules*, 2009, **42**, 3086-3091.
31. C. Hahn, S. Wesselbaum, H. Keul and M. Moller, *European Polymer Journal*, 2013, **49**, 217-227.
32. B. Kuldeep, K. Deepak, P. Laura, I. Derek, H. Steven, M. Giuseppe and A. Cameron, *Journal*, 2015, **6**, 7196-7210.
33. J. M. Worle-Knirsch, K. Pulskamp and H. F. Krug, *Nano Lett*, 2006, **6**, 1261-1268.
34. A. Kermanizadeh, B. K. Gaiser, M. B. Ward and V. Stone, *Nanotoxicology*, 2013, **7**, 1255-1271.

35. Y. Liu, H. Miyoshi and M. Nakamura, *International Journal of Cancer*, 2007, **120**, 2527-2537.
36. J. Lovric, H. S. Bazzi, Y. Cuie, G. R. A. Fortin, F. M. Winnik and D. Maysinger, *Journal of Molecular Medicine-Jmm*, 2005, **83**, 377-385.
37. R. Firdessa, T. A. Oelschlaeger and H. Moll, *European Journal of Cell Biology*, 2014, **93**, 323-337.
38. H. J. Johnston, M. Semmler-Behnke, D. M. Brown, W. Kreyling, L. Tran and V. Stone, *Toxicology and Applied Pharmacology*, 2010, **242**, 66-78.
39. M. J. Clift, C. Brandenberger, B. Rothen-Rutishauser, D. M. Brown and V. Stone, *Toxicology*, 2011, **286**, 58-68.
40. H. Akita, K. Enoto, H. Tanaka and H. Harashima, *Molecular Therapy*, 2013, **21**, 309-317.
41. M. S. Shive and J. M. Anderson, *Adv Drug Deliv Rev*, 1997, **28**, 5-24.
42. N. S. Melik-Nubarov, O. O. Pomaz, T. Y. Dorodnych, G. A. Badun, A. L. Ksenofontov, O. B. Schemchukova and S. A. Arzhakov, *FEBS Letters*, 1999, **446**, 194-198.

Chapter

4

Synthesis and Characterisation of Homopolymers and Block Copolymers of ε-Decalactone (ε-DL) by Ring Opening Polymerisation (ROP)

Chapter 4

4.1 Introduction

An increasing environmental concern requires new synthetic strategies and renewable materials to reduce the dependency on fossil resources for the synthesis of polymers. In the last few decades, ring opening polymerisation (ROP) has emerged as a major route for the synthesis of biobased aliphatic polyesters.[1] Unlike polycondensation, ROP does not require strict reaction conditions like exact stoichiometry, very high temperature, high vacuum and long reaction times.[2] Also, polymers from ROP can easily be synthesised under mild conditions, generating materials with high molecular weight and low polydispersity index. Hence, ROP has widely been adopted as an important industrial methodology for polyester synthesis. The use of biobased cyclic lactides and lactones in ROP provide an opportunity to switch from nonrenewable (petroleum based) class of monomers to renewable monomers. Some of the examples of bioderived lactone monomers are lactide, 1,5-dioxepan-2-one, δ-decalactone, ε-decalactone, menthide, α-angelica lactone, ethylene brassylate and ω-pentadecalactone (Figure 4-1).[3-13] The ring opening of these monomers mainly depends on the size of the ring. It has been commonly accepted that the release of ring-strain is a major driving force for ROP of small size lactone rings. Small ring systems (<6 atoms) possess higher strain compared to larger rings.[14] Polymerisation of large size lactone rings is not favored by a strain release mechanism, but polymerisation reactions are also driven by entropy.[15-17]

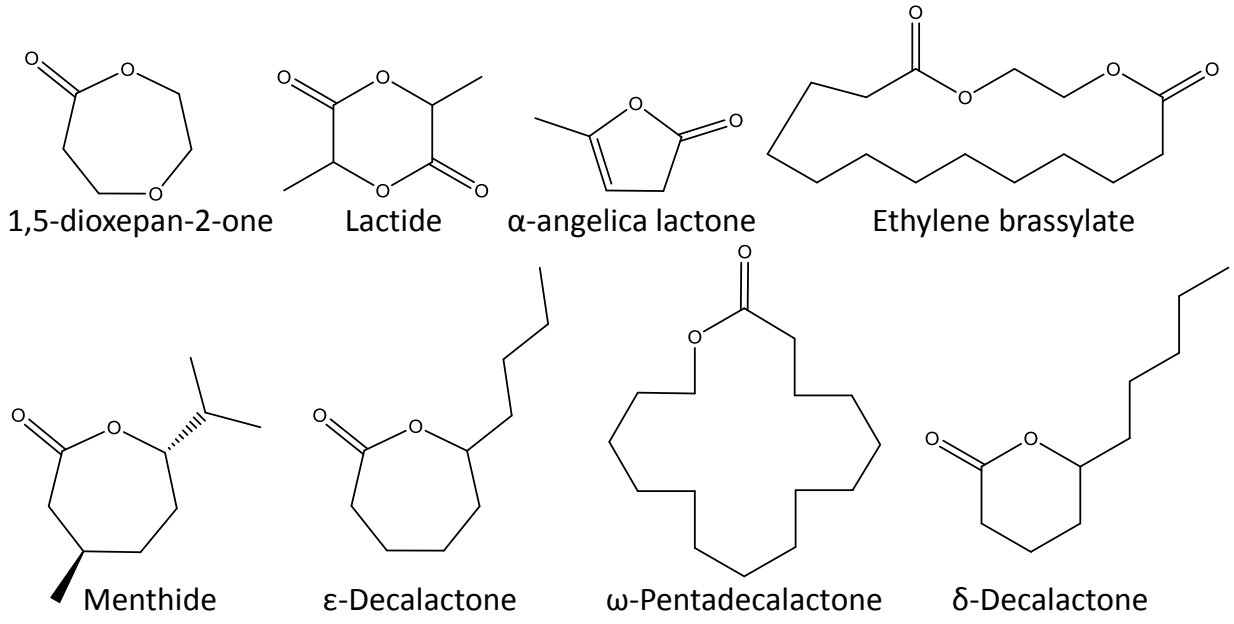


Figure 4-1 Structure of lactone monomers derived from renewable materials

Certain metallic catalysts have shown activity for polymerisation of small ring lactones, for example stannous octoate [$Sn(Oct)_2$], in fact, stannous 2-ethylhexanoate), which is one of the most commonly used catalysts for ROP.[18] Stannous octoate is already registered for use in synthesis of polymers by the FDA and its control over molecular weight and end group functionality makes it suitable as a catalyst for ROP.[19, 20] However, for applications in biomedicine and food packaging, the presence of metal traces are nevertheless undesirable.[14] Alternatively, enzymes (like Candida antarctica lipase B,) have been used to replace metallic catalysts. The preference of lipases for hydrophobic substrates is a driving force for ROP of large size lactones[21], where, the reactivity does not depend on the ring strain.[22] Hence, most of the studies of ROP of large lactones have reported

enzymes as a catalyst. However, high purity enzymes are expensive and most cannot be used at elevated temperatures.[21] Also, some do not offer sufficient control over polymerisation.[22] These disadvantages limit their use in ROP. To overcome the limitations of metal and enzyme catalysts, organic catalysts like triazabicyclo[4.4.0]dec-5-ene (TBD) have been investigated in ROP.[23-25] TBD is a bicyclic guanidine base used for various reactions like acyl transfer,[26] aldol reaction,[27] Michael reactions,[28] ring opening polymerisation[29] etc. Many studies have demonstrated the applicability of TBD in ROP due to its high efficiency and easy separation from products.

The decalactones are renewable class of monomer containing 10 carbon atoms, with or without variable alkyl side chains at carbon adjacent to the ring closing position of the lactones.[9] These lactones are available commercially with ring sizes of five (γ-Decalactone), six (δ-Decalactone) and seven (ε-Decalactone), are categorized as naturally occurring monomers and are widely used in the flavoring and fragrance industries.[30, 31] The reactivity of these monomers is affected by size. Thermodynamically, ε-decalactone can easily polymerize due to difference in ceiling temperature between six and seven membered lactones.[9] The ε-decalactone is a structural analogue of ε-caprolactone with an additional butyl chain at the epsilon position. It is derived from castor oil but, to date, has not been widely exploited for drug delivery applications.[10] Homo and block copolymerisation of ε-decalactone with l-lactides has been investigated by Lin *et al.* The authors showed the

amorphous nature of the homopolymer of ε-decalactone. Further, ε-decalactone was copolymerised with l-lactides to reduce the inherent drawbacks of polylactide homopolymer such as low thermal stability, hardness and brittleness. The final copolymer consisting of ε-decalactone and l-lactide contained soft and hard segments respectively.[10] Olsen *et al.* also copolymerised l-lactide with ε-decalactone to make elastomeric materials. They synthesised the polymer using $Sn(Oct)_2$ and TBD as catalyst.[9] Glavas *et al.* synthesised copolymers of ε-decalactone and ε-caprolactone with mPEG 2000 initiator to control the crystallinity of the hydrophobic segment. This group conducted reaction at 110 ^{o}C in bulk using $Sn(Oct)_2$ as catalyst. Due to the amorphous nature of the synthesised poly(ε-decalactone) (PεDL) block, the micelles of mPEG-b-PεDL were found to have higher CMC. The micelle sizes were also increased with increasing the hydrophobic ratio. In this way it was shown possible to control not only the CMC but also the size of the micelles.[32]

In this chapter, ROP of ε-decalactone and δ-decalactone has been reported using PEG 4000 and mPEG 5000 as initiators. The reactions were conducted in bulk in order to avoid the use of undesirable solvents. The reaction conditions were also optimized in terms of types and concentrations of catalyst used. The PEG was used as a hydrophilic block from which ε-decalactone was polymerised to obtain amphiphilic copolymers. These amphiphilic macromolecules can easily self-assembles in the water to give

micelles which can be used in a number of pharmaceutical applications. The homopolymers of ε-decalactone initiated with benzyl alcohol and propargyl alcohol were also synthesized to compare their properties with the block copolymers. The free functional groups on the homopolymer chain ends such as the propargyl group were designed to make this homopolymer more versatile. This can be used to introduce new properties into the homopolymer by post polymerisation modifications methods.

A copolymer of ε-caprolactone, a structural analogue of ε-decalactone, was also synthesized using mPEG 5000 as initiator in order to compare the properties with ε-decalactone copolymers (Figure 4-2). The ε-decalactone monomer was already known to produce amorphous polymers different from those of the semicrystalline ε-caprolactone polymer.[32] Hence to alter the core property of the micelles, a copolymer was also synthesized by incorporating ε-caprolactone and ε-decalactone subunits.

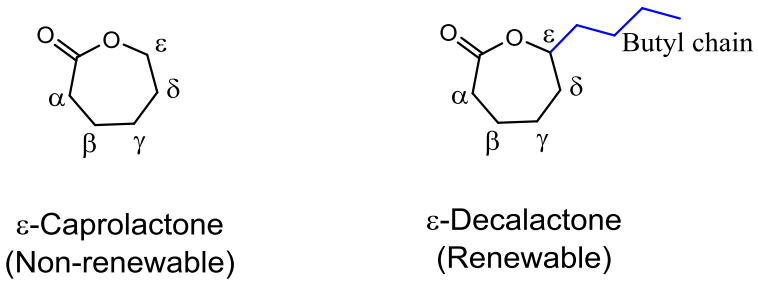


Figure 4-2 Structures of epsilon decalactone and epsilon caprolactone monomers

As it has been suggested that drug incorporation occurs only in amorphous parts of polymer solid-like phases, the copolymers with amorphous blocks

were expected to enhance drug incorporation. Hence, the modification of core crystallinity by mixing co-monomers was also expected to alter the drug loading and release properties.

4.2 General Synthesis Method for ε-Decalactone (ε-DL) Polymers

4.2.1 Synthesis of ε-Decalactone (ε-DL) Homopolymers

The homopolymer was made by ROP of ε-DL from benzyl alcohol/propargyl alcohol using 1,5,7-Triazabicyclo[4.4.0]dec-5-ene (TBD) as catalyst. Briefly, benzyl alcohol (0.04 g, 0.42 mmol) or propargyl alcohol (0.02 g, 0.42 mmol) was transferred into a RBF containing ε-DL (5.00 g, 29.37 mmol). The reaction was mixed until homogeneous. TBD (0.12 g, 0.87 mmol) was then added under a nitrogen atmosphere at the desired reaction temperature of 120 ^{o}C. The reaction was continued for 12 h, and then quenched with benzoic acid (0.21 g, 1.74 mmol) solution in acetone. The resultant product was purified by precipitation in cold methanol followed by evaporation of residual solvent in vacuum. The benzyl-PεDL and propargyl-PεDL were recovered as colorless viscous liquids with percentage yields of 74% (3.73 g) and 76% (3.82 g) respectively.

Benzyl-PεDL:- ^{1}H NMR (400 MHz, $CDCl_3$) δ (ppm) 7.33 (Benzene protons, m, 5H), 5.09 (CH_2-O-CO, s, 2H), 4.84 (CH-O-CO, m, 62H), 4.02 (CH-OH, t, 1H), 2.25 (O-CO-CH_2, t, 133H), 1.60-1.51 (CH_2-CH_2-CH_2-CH (OCO)-CH_2, m,

384H), 1.27 (CH-CH_2-CH_2; CH_3-CH_2-CH_2, m, 382H), 0.86 (CH_2-CH_3, t, 190H).

^{13}C NMR (101 MHz, $CDCl_3$) δ (ppm) 173.25 (O-CO-CH_2), 136.06 (C-CH_2-O, ring carbon), 128.53 (CH-CH-CH-C , ring carbon), 128.16 (CH-CH-CH-C , ring carbon), 73.87(CH_2-CH-O), 66.10 (CH_2-O-CO), 34.48 (CH_2-CH- CH_2), 33.72 (O-CO-CH_2), 27.45 (CH-CH_2-CH_2), 25.00 (CO-CH_2-CH_2), 22.56 (CH-CH_2-CH_2; CH_3-CH_2-CH_2), 13.98 (CH_3-CH_2-CH_2).

Propargyl-PεDL:- ^{1}H NMR (400 MHz, $CDCl_3$) δ (ppm) 4.85 (CH-O-CO, m, 64H), 4.66 (C-CH_2, s, 2H), 4.02 (CH-OH, t, 1H), 2.46 (allyl hydrogen, CH, s, 1H), 2.26 (O-CO-CH_2, t, 131H), 1.61-1.52 (CH_2-CH_2-CH_2-CH (OCO)-CH_2, m, 404H), 1.28 (CH-CH_2-CH_2; CH_3-CH_2-CH_2, m, 400H), 0.88 (CH_2-CH_3, t, 202H).

^{13}C NMR (101 MHz, $CDCl_3$) δ (ppm) 173.41 (O-CO-CH_2), 77.36 (allyl carbon, C-CH_2), 74.03(CH_2-CH-O), 71.80 (allyl carbon, C), 51.93 (C-CH_2-CO), 34.64 (CH_2-CH- CH_2), 33.87 (O-CO-CH_2), 27.60 (CH-CH_2-CH_2), 25.15 (CO-CH_2-CH_2), 22.71 (CH-CH_2-CH_2; CH_3-CH_2-CH_2), 14.13 (CH_3-CH_2-CH_2).

4.2.2 Synthesis of ε-Decalactone (ε-DL) Copolymers

Diblock (AB) and triblock (ABA) copolymers of ε-DL were prepared using mPEG (M_n~5000) and PEG (M_n~4000) as initiators respectively. Briefly, ε-DL (5.00 g, 29.37 mmol) was added in a flask containing mPEG (2.44 g, 0.49 mmol) or PEG (1.69 g, 0.42 mmol). The reaction content was mixed for 15

min at 120 ^{o}C. The required quantity of TBD (0.12 g, 0.87 mmol) was then added into the reaction mixture under a nitrogen atmosphere and the reaction was continued for 12 h. After completion, the reaction mixture was quenched with benzoic acid (0.21 g, 1.74 mmol) solution in acetone. The obtained polymer was precipitated in cold methanol followed by removal of residual solvent in vacuum. The resultant polymer was dissolved in minimum volume of acetone and again precipitated in diethyl ether for three times. The solvent residue was removed by evaporation under vacuum. The copolymers, mPEG-b-PεDL and PεDL-b-PEG-b-PεDL, were wax like materials with 67% (5.02 g) and 69% (4.84 g) yield respectively.

mPEG-b-PεDL (AB diblock copolymer):

^{1}H NMR (400 MHz, $CDCl_3$) δ (ppm) 4.85 (CH-O-CO, m, 36H), 4.21 (CH_2-O-CO, t, 2H), 3.64 (O-CH_2-CH_2-O, s, 487H), 3.37 (O-CH_3, s, 3H), 2.27 (O-CO-CH_2, t, 75H), 1.58-1.52 (CH_2-CH_2-CH_2-CH (OCO)-CH_2, m, 231H), 1.28 (CH-CH_2-CH_2; CH_3-CH_2-CH_2, m, 234H), 0.88 (CH_2-CH_3, t, 116H).

^{13}C NMR (101 MHz, $CDCl_3$) δ (ppm) 173.25 (O-CO-CH_2), 73.86 (CH_2-CH-O), 70.57 (CH_2-CH_2-O), 34.48 (CH_2-O-CO), 33.80 (O-CO-CH_2), 27.44 (CH-CH_2-CH_2), 24.99 (CO-CH_2-CH_2), 22.55 (CH-CH_2-CH_2; CH_3-CH_2-CH_2), 13.97 (CH_3-CH_2-CH_2).

PεDL-b-PEG-b-PεDL (ABA triblock copolymer):

^{1}H NMR (400 MHz, $CDCl_3$) δ (ppm) 4.85 (CH-O-CO, m, 66H), 4.21 (CH_2-O-CO, t, 4H), 3.64 (O-CH_2-CH_2-O, s, 381H), 2.27 (O-CO-CH_2, t, 136H), 1.61-1.52 (CH_2-CH_2-CH_2-CH (OCO)-CH_2, m, 426H), 1.29 (CH-CH_2-CH_2; CH_3-CH_2-CH_2, m, 427H), 0.88 (CH_2-CH_3, t, 211H).

^{13}C NMR (101 MHz, $CDCl_3$) δ (ppm) 173.28 (O-CO-CH_2), 73.89 (CH_2-CH-O), 70.59 (CH_2-CH_2-O), 34.50 (CH_2-O-CO), 33.82 (O-CO-CH_2), 27.47 (CH-CH_2-CH_2), 25.02 (CO-CH_2-CH_2), 22.58 (CH-CH_2-CH_2; CH_3-CH_2-CH_2), 14.01 (CH_3-CH_2-CH_2).

4.2.3 Synthesis of δ-Decalactone (δ-DL) Copolymers

A diblock copolymer of δ-decalactone was prepared by adding δ-DL (5.00 g, 29.37 mmol) in a RBF containing mPEG (5kDa, 2.44 g, 0.49 mmol). The reaction mixture was mixed for 15 min at 50 ^{o}C followed by addition of TBD (0.12 g, 0.87 mmol) under a nitrogen atmosphere. The reaction was continued for 10 h. The reaction mixture was quenched by adding benzoic acid (0.21 g, 1.74 mmol) solution in acetone. The obtained product was precipitated in cold methanol followed by evaporation of residual solvent in vacuum. The dry product was again dissolved in a minimum quantity of acetone and reprecipitated in petroleum ether. The residual solvent was evaporated in vacuum to obtain a wax like purified material with 67% yield (4.98 g).

mPEG-b-PδDL (AB diblock copolymer):

^{1}H NMR (400 MHz, $CDCl_3$) δ 4.86 (CH-O-CO, m, 38H), 4.21 (CH_2-O-CO, t, 2H), 3.63 (O-CH_2-CH_2-O, s, 520H), 3.37 (O-CH_3, s, 3H), 2.28 (O-CO-CH_2, m, 77H), 1.55 (CH_2-CH_2-CH-CH_2, m, 234H), 1.27(CH_2-CH_2-CH_2-CH_3, m, 238H), 0.86 (CH_2-CH_3, t, 136H).

^{13}C NMR (101 MHz, $CDCl_3$) δ 173.17 (O-CO-CH_2), 73.83 (CH_2-CH-O), 70.71 (CH_2-CH_2-O), 63.57 (CH_2-O-CO) 59.16 (O-CH_3), 34.33 (CH_2-CH-O-CO), 34.08 (CH_3-CH_2-CH2-CH_2-CH_2), 33.61 (O-CO-CH_2), 31.78 (CH-CH_2-CH_3), 25.07 (CH-CH_2-CH_2), 22.65 (O-CO-CH_2-CH_2), 20.96 (CH_2-CH_3), 14.17 (CH_2-CH_3)

4.2.4 Synthesis of ε-Caprolactone (ε-CL) Copolymer

A diblock copolymer (AB type) of ε-CL was synthesized by transferring ε-CL (6.84 g, 60 mmol) in RBF containing mPEG (5 kDa, 5 g, 1 mmol). The reaction mixture was heated at 120 °C under a nitrogen atmosphere for 10 min. TBD (0.17 g, 1.2 mmol) solution in anhydrous acetone (0.5 mL) was then added via syringe and the reaction was continued for 10 min under nitrogen atmosphere. After completion, the reaction mixture was quenched with benzoic acid (0.29 g, 2.4 mmol) solution in acetone (0.5 mL). The resultant polymer was precipitated in cold methanol. The residual solvent was evaporated in vacuum. The obtained product was redissolved in a minimum volume of acetone and precipitated again in diethyl ether. The

residual solvent was removed by vacuum to obtain the purified product. The recovered product was off-white in color with 89% (10.54 g) yield.

mPEG-b-PCL (AB diblock copolymer):

^{1}H NMR (400 MHz, $CDCl_3$) δ (ppm) 4.22 ($\underline{CH_2}$-O-CO, t, 2H), 4.06 ($\underline{CH_2}$-O-CO, t, 91H), 3.64 (O-$\underline{CH_2}$-$\underline{CH_2}$-O, s, 462H), 3.38 (O-$\underline{CH_3}$, s, 3H), 2.30 (O-CO-$\underline{CH_2}$, t, 91H), 1.64 ($\underline{CH_2}$-CH_2-$\underline{CH_2}$, m, 207H), 1.38 (CH_2-$\underline{CH_2}$-CH_2, m, 91H).

^{13}C NMR (101 MHz, $CDCl_3$) δ (ppm) 173.65 (O-$\underline{CO}$-CH_2), 70.72 ($\underline{CH_2}$-$\underline{CH_2}$-O), 64.28 ($\underline{CH_2}$-O-CO), 34.26 (O-CO-$\underline{CH_2}$), 28.50 ($\underline{CH_2}$-CH_2-O-CO), 25.68 (CH_2-$\underline{CH_2}$-CH_2), 24.72 (CO-CH_2-$\underline{CH_2}$)

4.2.5 Copolymerisation of ε-Decalactone and ε-Caprolactone with mPEG (ABC type copolymer)

A triblock (mPEG-b-PCL-b-PεDL) copolymer was prepared by sequential addition of ε-CL and ε-DL on mPEG in a 'one pot' method. Briefly, mPEG (5kDa, 2.44 g, 0.49 mmol) was transferred in a RBF containing ε-CL (1.68 g, 14.7 mmol). The reaction mixture was stirred at 120 ^{o}C under a nitrogen atmosphere for 10 min until homogeneous. TBD (0.06 g, 0.44 mmol) solution in anhydrous acetone (0.5 mL) was added via syringe under nitrogen and the reaction was continued for 10 min to make mPEG-*b*-PCL block. The reaction was continued in the same pot by the addition of ε-DL (2.55 g, 14.7 mmol) in the reaction mixture. The reaction was continued for a further 12 h under nitrogen. Benzoic acid (0.11 g, 0.88 mmol) solution in

acetone (0.5 mL) was added to quench the reaction. The obtained product was purified by precipitation in cold methanol followed by evaporation of residual solvent in vacuum. The obtained dry product was redissolved in a small volume of acetone and reprecipitated in diethyl ether to obtain purified product. A wax like material with 76% (5.09 g) yield was obtained.

mPEG-b-PCL-b-PεDL (ABC triblock copolymer):

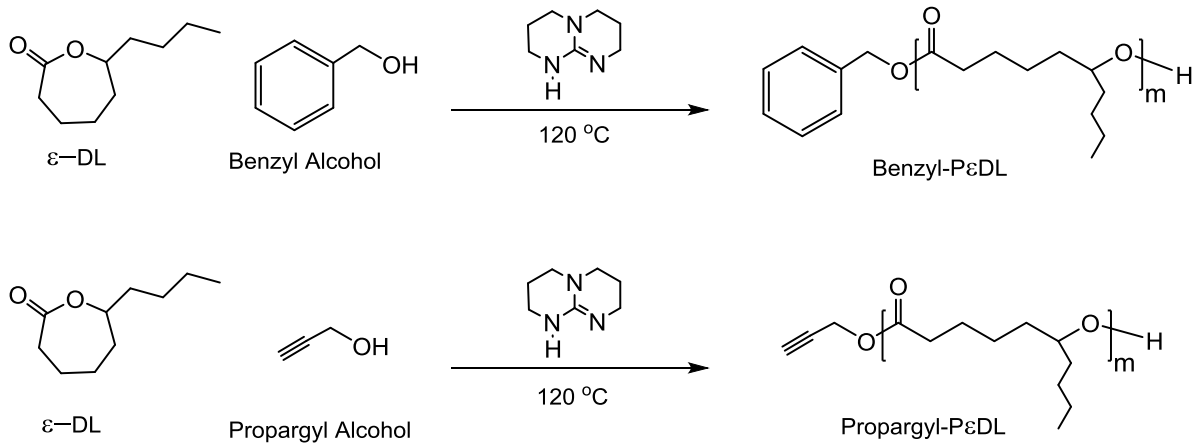
^{1}H NMR (400 MHz, $CDCl_3$) δ (ppm) 4.84 (CH-O-CO, m, 11H), 4.21 (CH_2-O-CO, t, 2H), 4.05 (CH_2-O-CO, t, 14H), 3.63 (O-CH_2-CH_2-O, s, 510H), 3.37 (O-CH_3, s, 3H), 2.28 (O-CO-CH_2, m, 37H), 1.62-1.28 (O-CO-CH_2-CH_2-CH_2-CH_2; CH_3-CH_2-CH_2-CH_2, m, 191H), 0.87 (CH_3-CH_2, t, 116H).

^{13}C NMR (101 MHz, $CDCl_3$) δ 173.46 (O-CO-CH_2), 173.25 (O-CO-CH_2), 73.85 (CH_2-CH-O), 70.58 (CH_2-CH_2-O), 64.12 (CH_2-O-CO), 59.02 (CH_3-O-CH_2) 34.49 (CH_2-CH-O-CO), 34.11 (CH_2-CH-O-CO), 33.80 (O-CO-CH_2), 28.35 (CH_3-CH_2-CH_2), 27.45 (O-CO-CH_2-CH_2-CH_2), 25.53 (CH_2-CH_2-CH_2-O), 25.00 (CH_2-CH_2-CH_2-O), 24.96 (CH_2-CH_2-CH_2-O), 24.57 (CH_2-CH_2-CH_2-O), 22.55 (CH_3-CH_2-CH_2), 13.98 (CH_3-CH_2-CH_2).

4.3 Results

4.3.1 Homopolymers of ε-Decalactone (ε-DL)

The synthetic route for the ROP of ε-DL is given in scheme 4-1.



Scheme 4-1 ROP of ε-DL catalyzed by TBD using different initiators

The results of the polymerisation were given in Table 4.1. No conversion was observed at room temperature irrespective of any catalyst concentrations used. At higher temperature (120 ^{o}C) and low concentration of catalyst (1 mol%), only 18% of conversion was observed after 12 h. On the other hand more than 85% monomer was converted to polymer when the catalyst concentration was increased to 3 mol% hence this stoichiometry was used for subsequent polymer synthesis.

The conversion of the monomer to the polymer was monitored by ^{1}H NMR spectroscopy. The monomer showed distinct shifts upon conversion to polymer especially at the α and ε positions of the ε-decalactone ring. The α proton shifted from 2.57 ppm to 2.27 ppm whereas the ε proton changed from 4.17 ppm to 4.85 ppm (Figure 4-3).

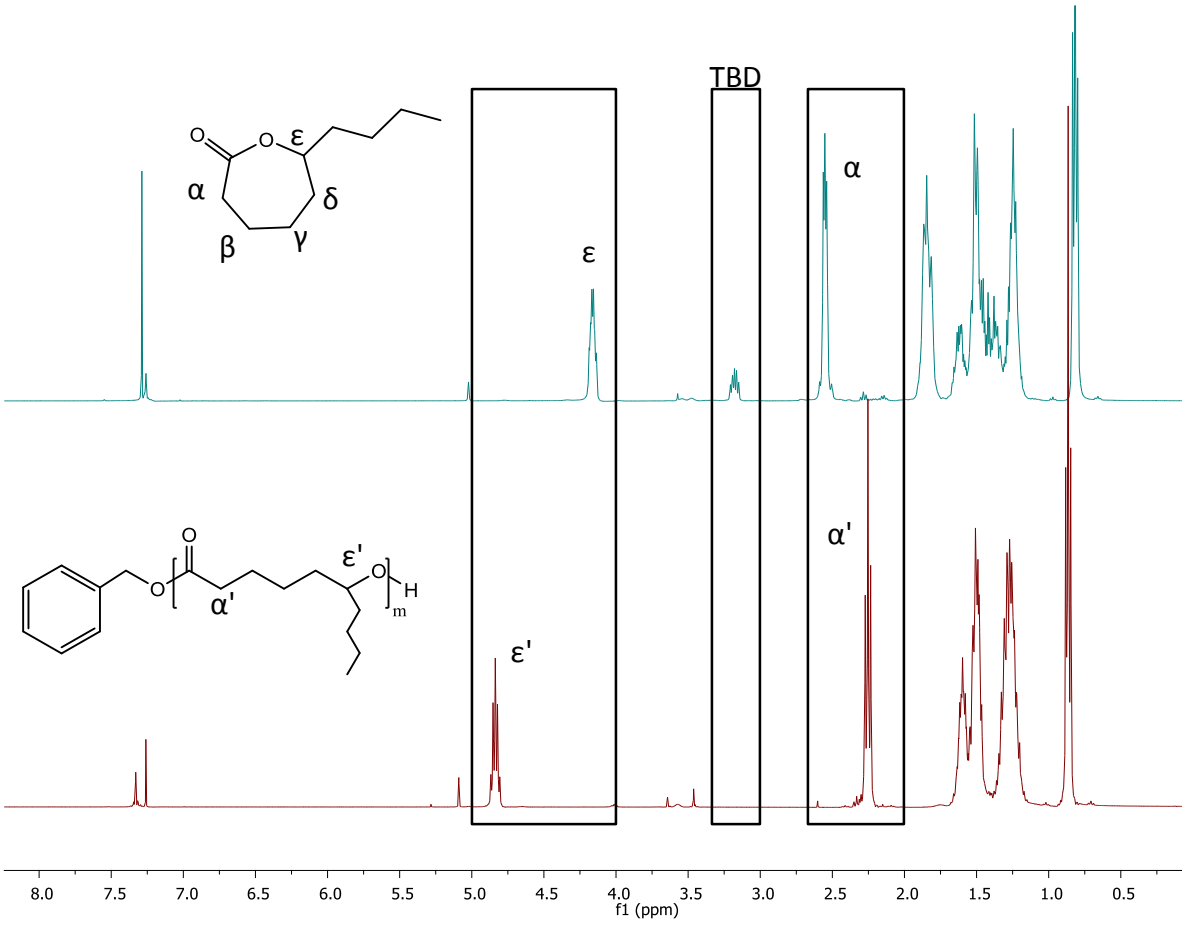


Figure 4-3 ^{1}H NMR spectra of Benzyl-PεDL before and after conversion.

The homopolymer was characterized after purification by precipitation in cold methanol. The homopolymer was separated as a distinct layer upon addition in cold methanol to remove unreacted monomer, initiator and inactivated catalyst. Upon evaporation of the residual solvent, a sticky and viscous colorless purified homopolymer was obtained. ^{1}H NMR spectra of the purified homopolymers with assigned peaks are shown in figure 4-4 and figure 4-5. The molecular weight of the Benzyl-PεDL homopolymer was calculated by integrating 7.33 ppm (peak 1) and 4.84 ppm (peak 3) peaks (Figure 4-4)

whereas for Propargyl-PεDL, peaks at 4.85 ppm (peak 1) and 4.66 ppm (peak 2) were integrated (Figure 4-5). The structure integrity of homopolymers was also determined by ^{13}C NMR. The carbon peaks of the initiators for both of the homopolymers were not prominent compared to carbons peaks of PεDL chain (Figure 4.6 and 4.7). The peak position values were matched with the previous reported values, suggesting the successful synthesis of the homopolymer.[10]

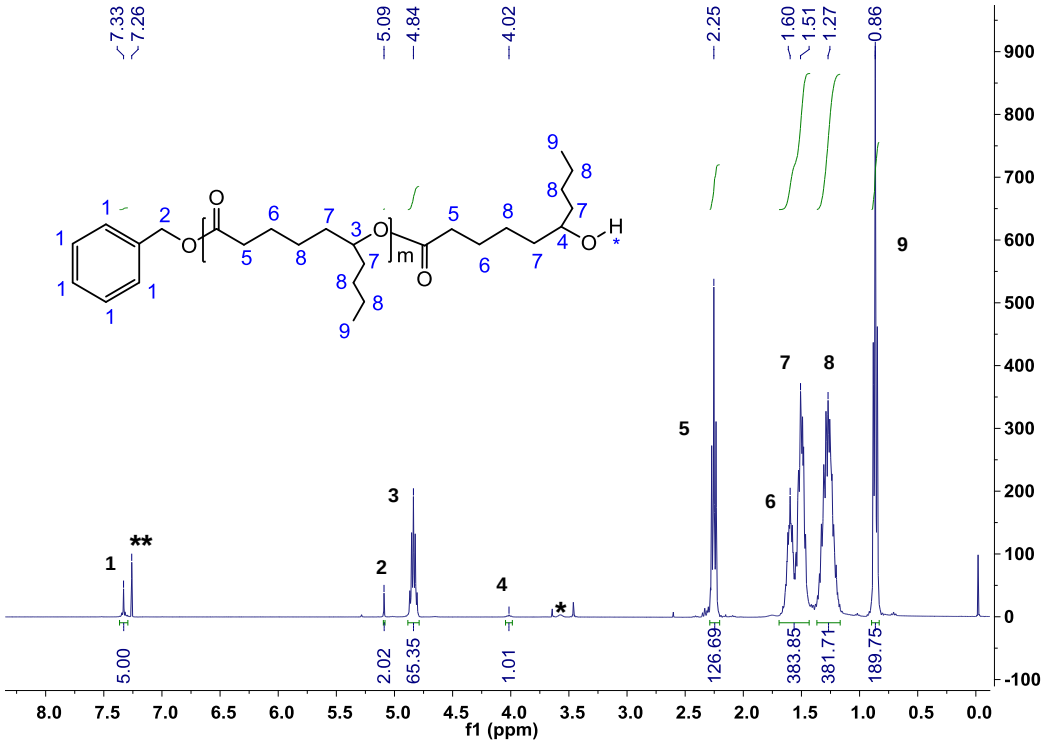


Figure 4-4 ^{1}H NMR spectra of Benzyl-PεDL acquired in $CDCl_3$ (**Solvent peak).

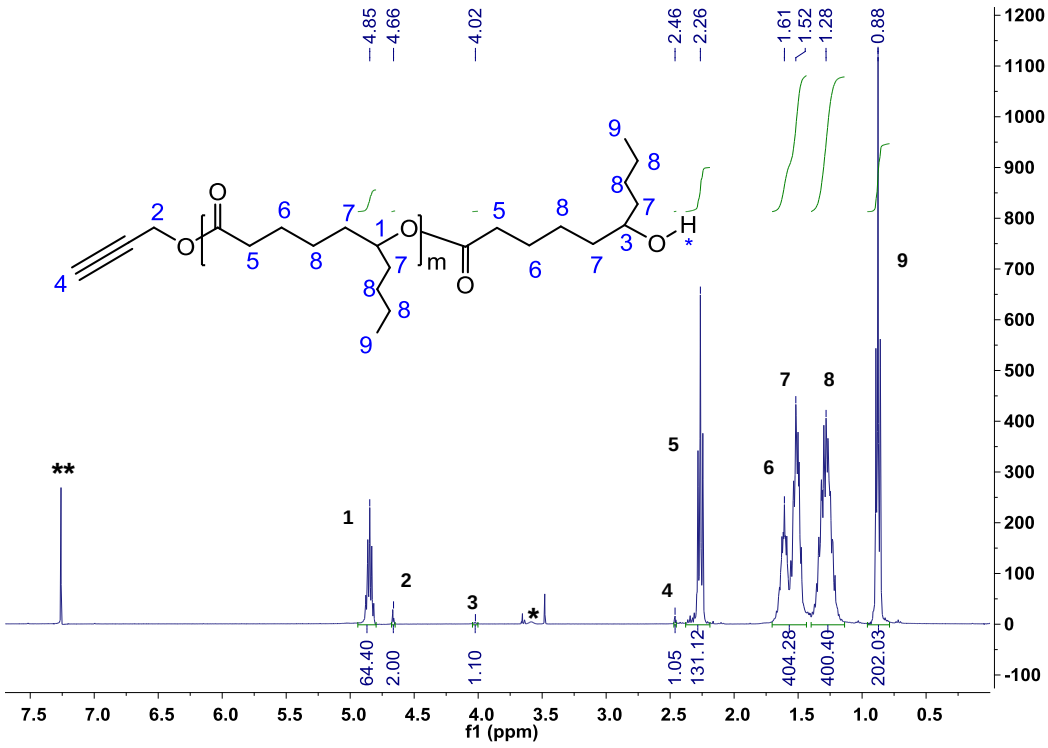


Figure 4-5 ^{1}H NMR spectra of Propargyl-PεDL acquired in $CDCl_3$ (**Solvent peak).

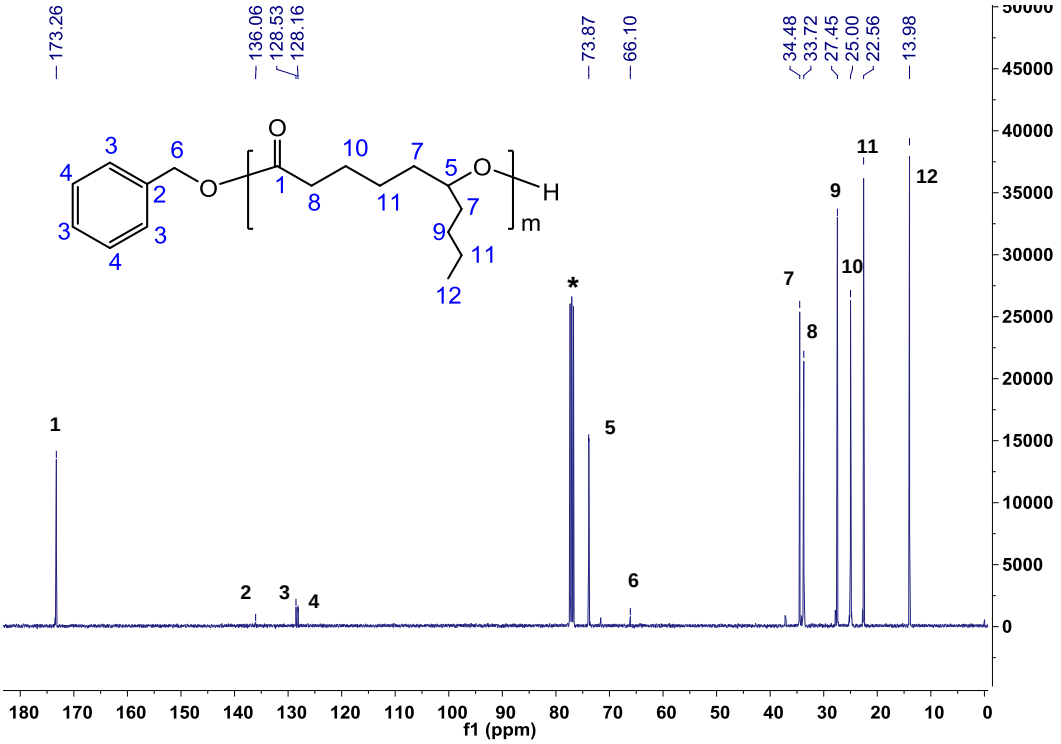


Figure 4-6 ^{13}C NMR spectra of Benzyl-PεDL acquired in $CDCl_3$ (*Solvent peak).

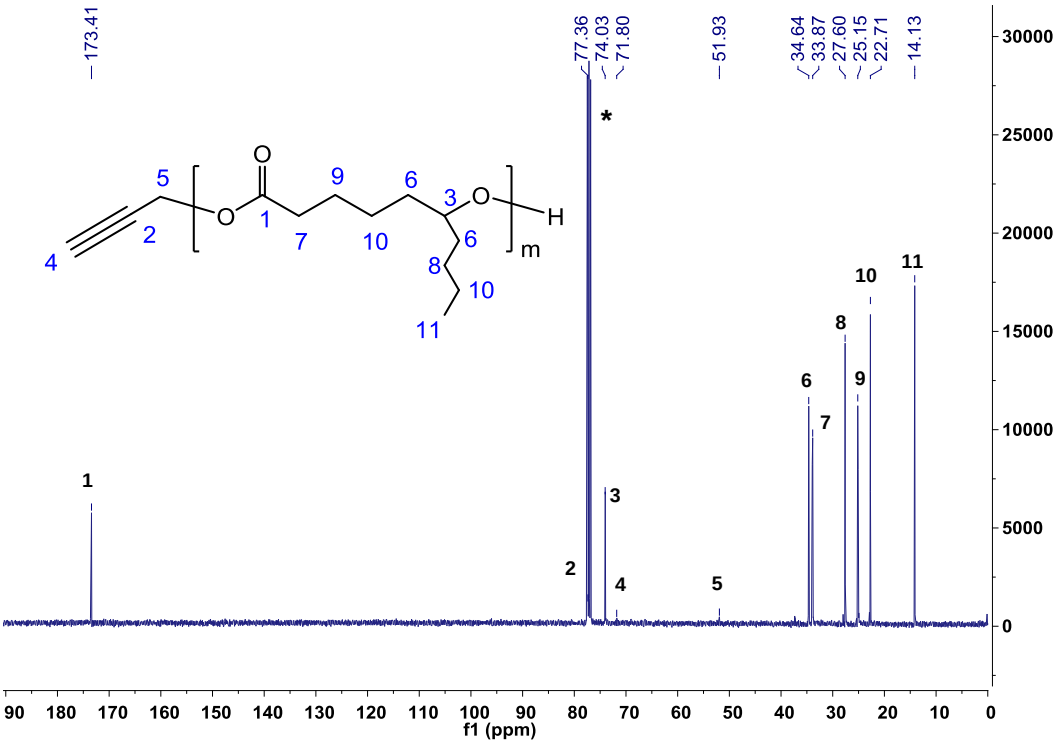


Figure 4-7 ^{13}C NMR spectra Propargyl-PεDL acquired in $CDCl_3$ (*Solvent peak).

The DSC data of the homopolymer revealed the absence of melting temperature (T_m) whereas the presence the glass transition temperature (T_g) at -53.29 ^oC indicates the amorphous nature of the homopolymer (Figure 4-8). The value of the T_g was consistent with the previous reported method.[9]

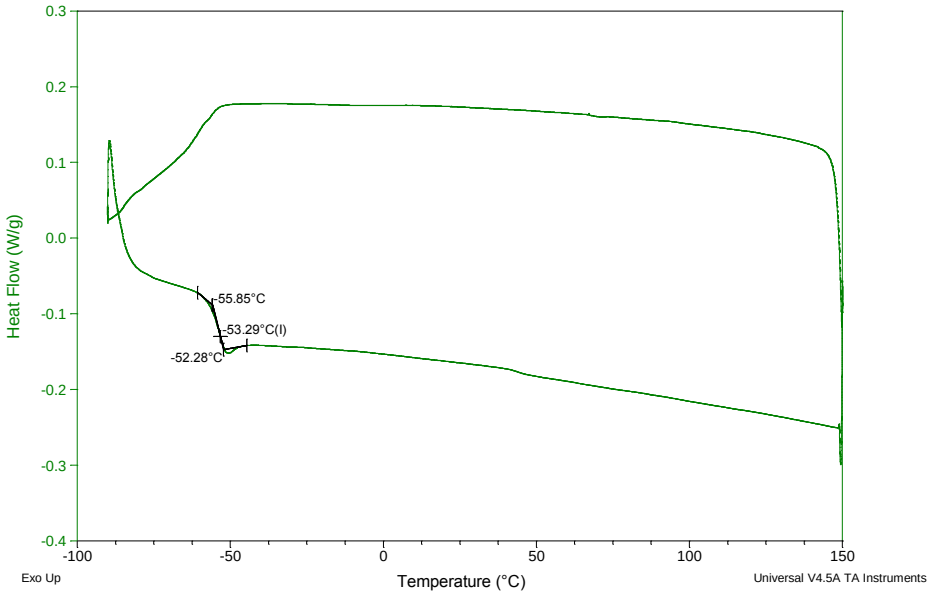
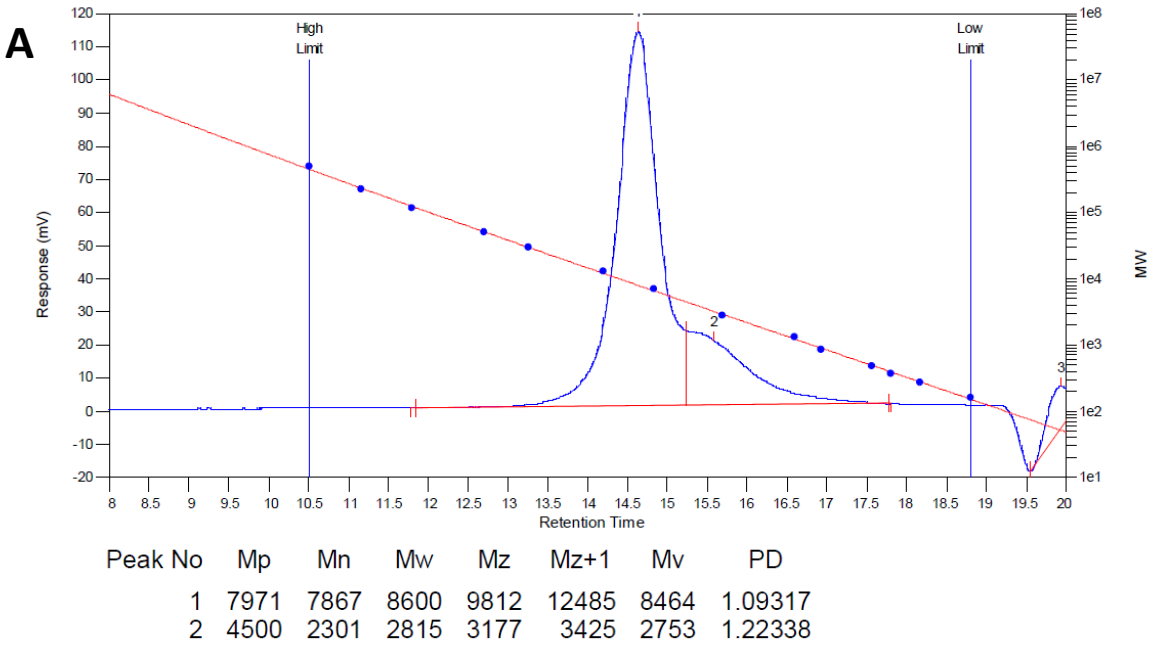
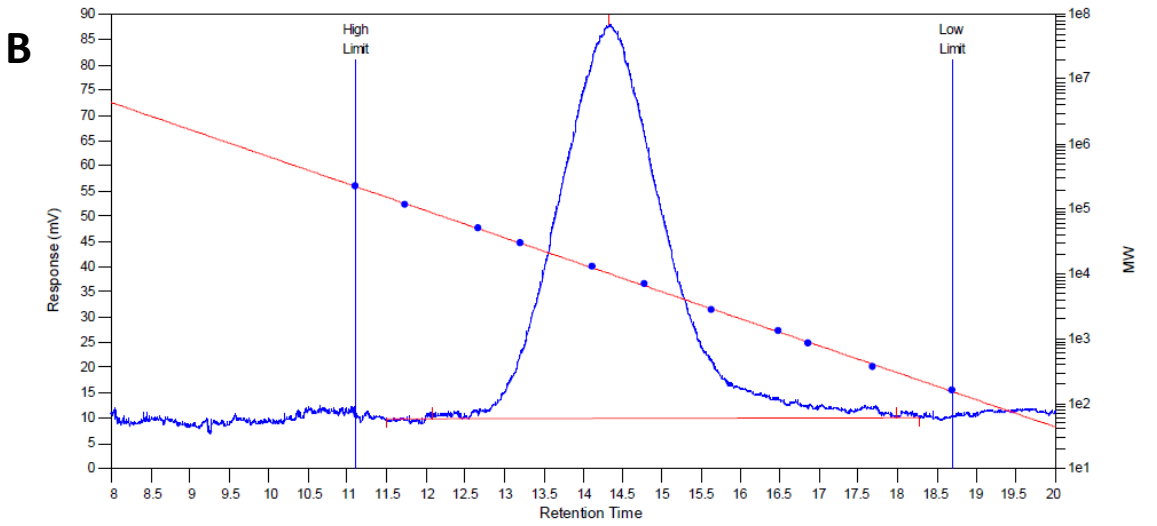


Figure 4-8 Differential scanning calorimetry (DSC) plot of Benzyl-PεDL homopolymer.

Size exclusion chromatography (SEC) performed on the Propargyl tipped-PεDL homopolymer using chloroform as eluent, gave a shoulder in a low molecular weight region along with the main peak of homopolymer. The reasons for the appearance of associated peak have been discussed in the next section. The homopolymers where benzyl alcohol was used as initiator showed a unimodal size distribution but the polydispersity was higher. The SEC underestimated the M_n compared to the calculated M_n by proton NMR (Figure 4-9, Table 4-1).



Peak No	Mp	Mn	Mw	Mz	Mz+1	Mv	PD
1	7971	7867	8600	9812	12485	8464	1.09317
2	4500	2301	2815	3177	3425	2753	1.22338



Peak No	Mp	Mn	Mw	Mz	Mz+1	Mv	PD
1	10052	6068	11321	16886	25230	10620	1.86569

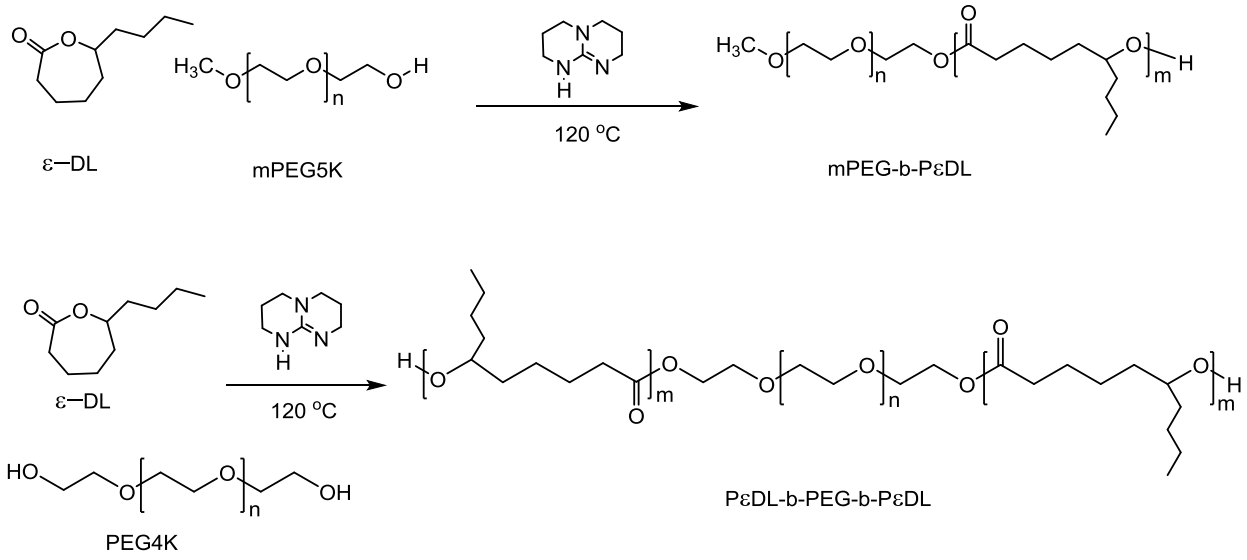
Figure 4-9 SEC traces of (A) Propargyl-PεDL homopolymer and (B) Benzyl-PεDL homopolymer

Table 4-1 Summary of experimental details and molecular weight obtained after ROP of Decalactones and Caprolactone using TBD as catalyst. *Stannous octoate was used as catalyst. $Caprolactone and ε-Decalactone monomers added sequentially in equal molar concentration. (ND= not determined)

Run	Polymer	Initiator	M/I ratio	Temp. (°C)	Time (h)	Catalyst (Mole%)	Conversion by NMR (%)	Theoretical Mol. Wt. (g mol^{-1})	M_n by ^1H NMR	M_n by SEC ($CHCl_3$)	M_w/M_n (Đ)	T_g (°C)	T_m (°C)
1	Benzyl-PεDL	Benzyl Alcohol	70	120	12	3	93	12.0K	11.1K	6.1K	1.86	-53.3	ND
2	Propargyl-PεDL	Propargyl Alcohol	70	120	12	3	92	12.0K	11.0K	7.9K/ 2.3K	1.09/ 1.22	ND	ND
3	PεDL-b-PEG-b-PεDL	PEG4K	70	120	12	3	94	15.9K	15.2K	13.3K	1.05	-62.9	54.4
4	mPEG-b-PεDL	mPEG5K	60	120	12	3	89	15.2K	10.3K	16.2K	1.15	-52.2	56.8
5*	mPEG-b-PεDL	mPEG5K	60	120	24	3	86	15.2K	11.3K	14.8K	1.22	ND	ND
6	mPEG-b-PδDL	mPEG5K	60	50	10	3	88	15.2K	11.4K	15.9K	1.20	-56.9	60.3
7	mPEG-b-PCL	mPEG5K	50	120	10min	2	98	10.7K	10.2K	17.0K	1.48	-56.9	56.6
8$	mPEG-b-PCL-b-PεDL	mPEG5K	60	120	12	3	94	13.5K	7.7K	13.2K	1.05	-59.0	59.8

4.3.2 Copolymers of ε-Decalactone (ε-DL)

The synthetic route for copolymer synthesis is shown in scheme 4-2. The reaction was optimized for different temperatures, concentrations and types of catalysts (TBD and stannous octoate).



Scheme 4-2 ROP of ε-decalactone on mPEG 5000 and PEG 4000 using TBD catalyst

The stannous octoate was also utilized for the synthesis of diblock copolymers in order to compare the efficiency against TBD. The results of the copolymerisation of ε-DL are given in table 4-1. The reaction kinetics was determined by ^{1}H NMR. The percent conversion was estimated by comparing ε and α proton, before and after conversion, as described for homopolymers in the previous section (Figure 4-10 A). The reaction rate was increased by increasing the catalyst concentration and temperature. The conversion at low temperature (~60 ^{o}C) was low, irrespective of any

catalysts (TBD and stannous octoate) used at different concentrations (1 mol% and 3 mol% to monomer). However, the reaction conducted at 120 ^{o}C yielded nearly 90% conversions after 12 h when 3 mol% concentration of the TBD was used. On the other hand, it took 24 h for the stannous octoate to catalyze polymerisation when the same concentrations (3 mol%) and temperatures (120 ^{o}C) were used for the polymerisation. The log of monomer conversion ratio was plotted against time in order to calculate apparent rate constants (k_p) from the slop of the curve. A linear relationship indicates that the reaction is first order with respect to monomer. The apparent rate constant (k_p) of ε-decalactone polymerisation was 0.18 h^{-1} when TBD was used as catalyst which was 2.25 times higher compared to stannous octoate based polymerisation (0.08 h^{-1}). In fact, TBD took half of the time required for the stannous octoate for ε-DL polymerisation at the same temperature and concentration of catalyst (Figure 4-11).

The M_n was determined by integrating the methoxy proton of the mPEG 5000 block at 3.37 ppm (peak 4) relative to the protons adjacent to ester bonds within the PεDL chain at 4.85 ppm (peak 1) (Figure 4-12). For triblock copolymers, protons adjacent to ester bonds in the mPEG 4000 initiator (peak 2) and the protons adjacent to ester bonds within PεDL chain (peak 1) were compared (Figure 4-13).

The copolymers were also characterized with ^{13}C NMR to check the purity and compared with peaks from previous reports to evaluate purity (Figure 4-

14 and 4-15). The diblock copolymer was also characterized by ^{1}H-^{1}H COSY NMR to confirm the detailed structure. All the peaks in ^{1}H-^{1}H COSY NMR were assigned in accordance with the desired structure of the diblock copolymer (Figure 4-16).

The SEC data of the unpurified polymer revealed the presence of homopolymer and unreacted monomers (Figure 4-10 B). The unreacted monomers were removed by precipitation of polymer in cold methanol while the homopolymer was eliminated by precipitation of copolymer in diethyl ether (3 times). The homopolymer was soluble in diethyl ether whereas the copolymer was not, hence reprecipitation gave the pure copolymer (Figure 4-10 C). The comparative retention times determined by SEC of the initiators and the copolymers are given in figure 4-17. A small shoulder in the SEC graph of diblock copolymer indicated the presence of minor impurities. The SEC overestimated the molecular weight (M_n) compared to the molecular weight (M_n) calculated by ^{1}H NMR for diblock copolymers made by both of the catalysts (Table 4-1).

The thermal properties of the copolymers were also characterized by DSC. A T_g and melting temperature were observed for both of the copolymers. The T_g was attributed to the amorphous PεDL chain whereas the melting temperature observed was due to PEG part, hence indicating the formation of semicrystalline polymer (Figure 4-18).

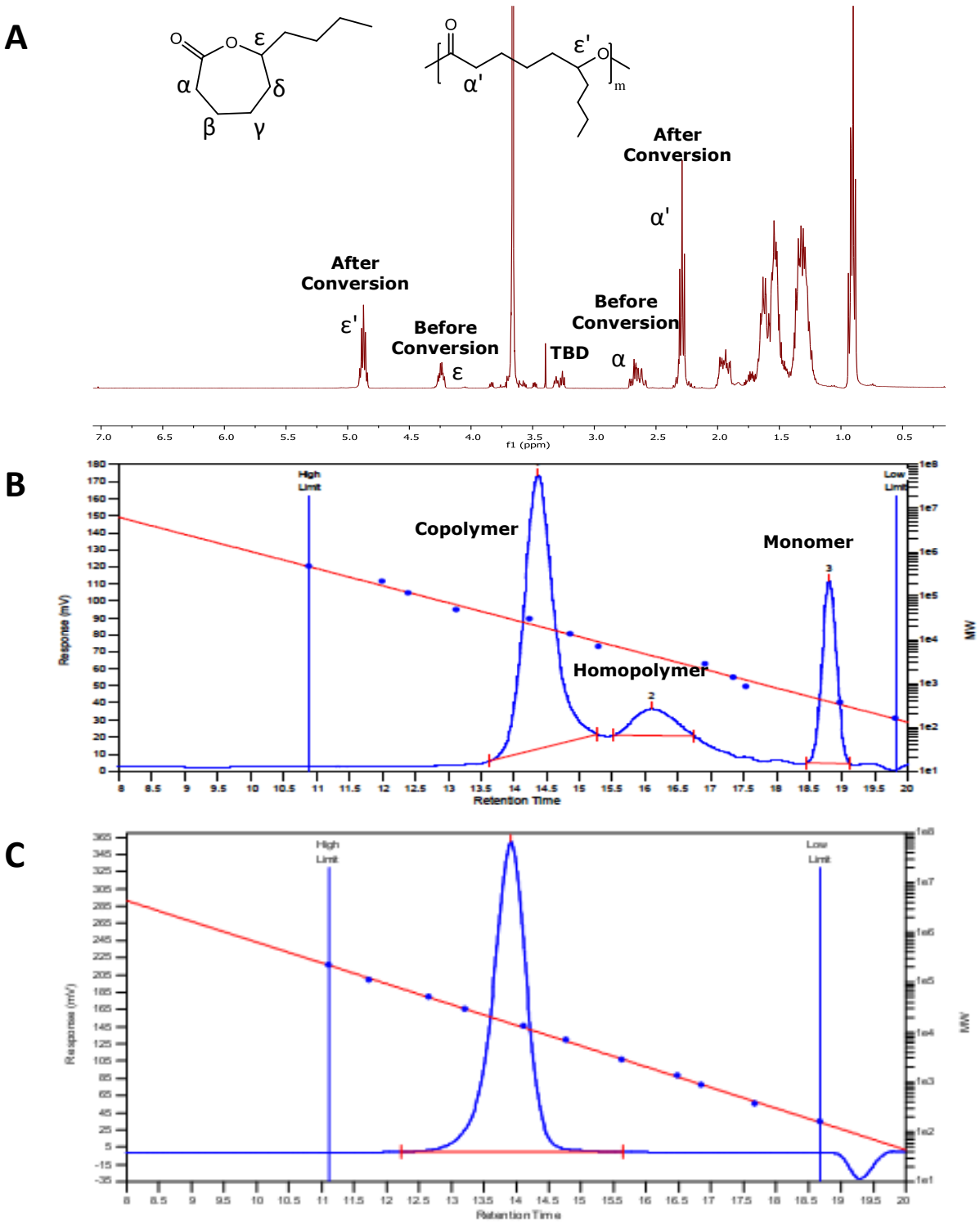


Figure 4-10 ^{1}H NMR and GPC of unpurified mPEG-b-PεDL copolymer (A and B), GPC of purified mPEG-b-PεDL copolymer (C).

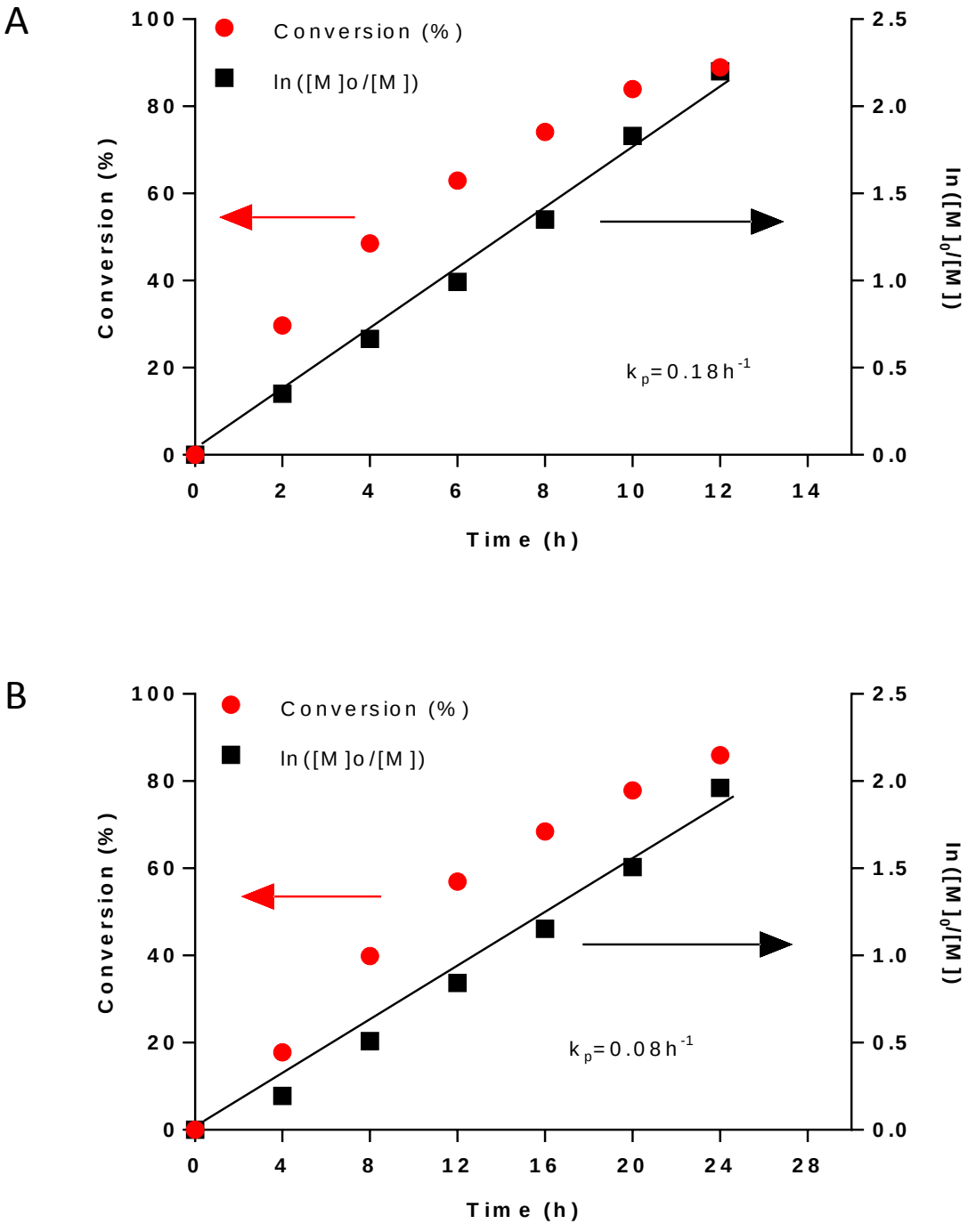


Figure 4-11 Kinetic analysis of ε-decalactone polymerisation from mPEG5K at 120 °C (A) TBD catalyst (B) $Sn(Oct)_2$ catalyst

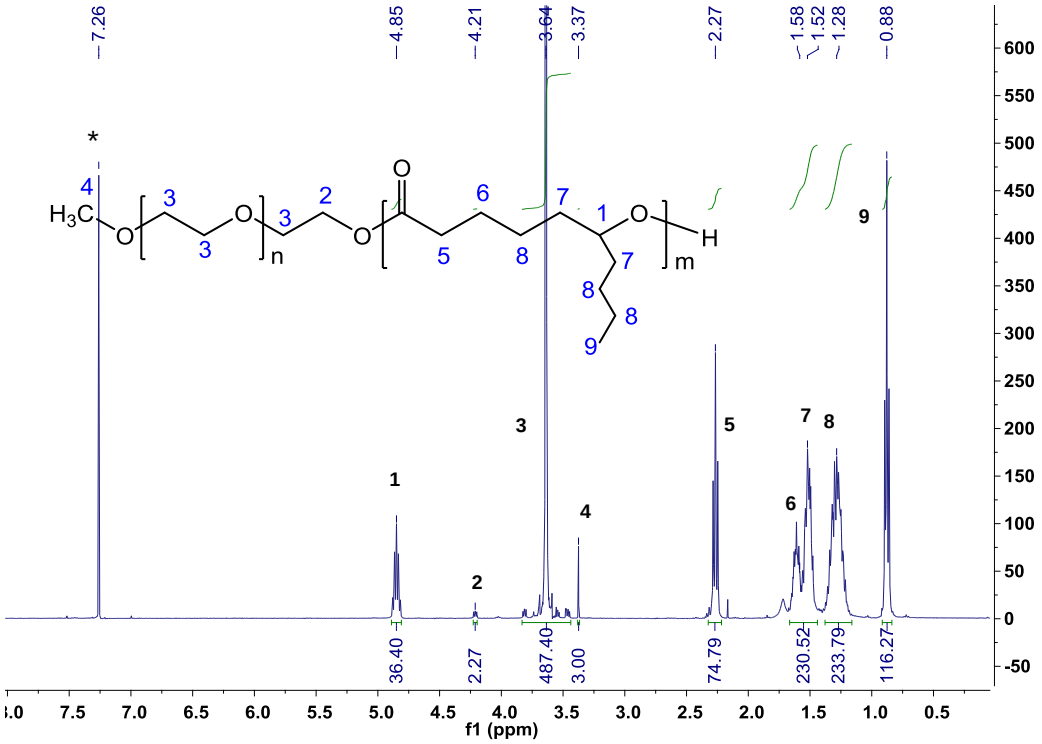


Figure 4-12 ^{1}H NMR spectra of mPEG-b-PεDL copolymer acquired in $CDCl_3$ (*Solvent peak).

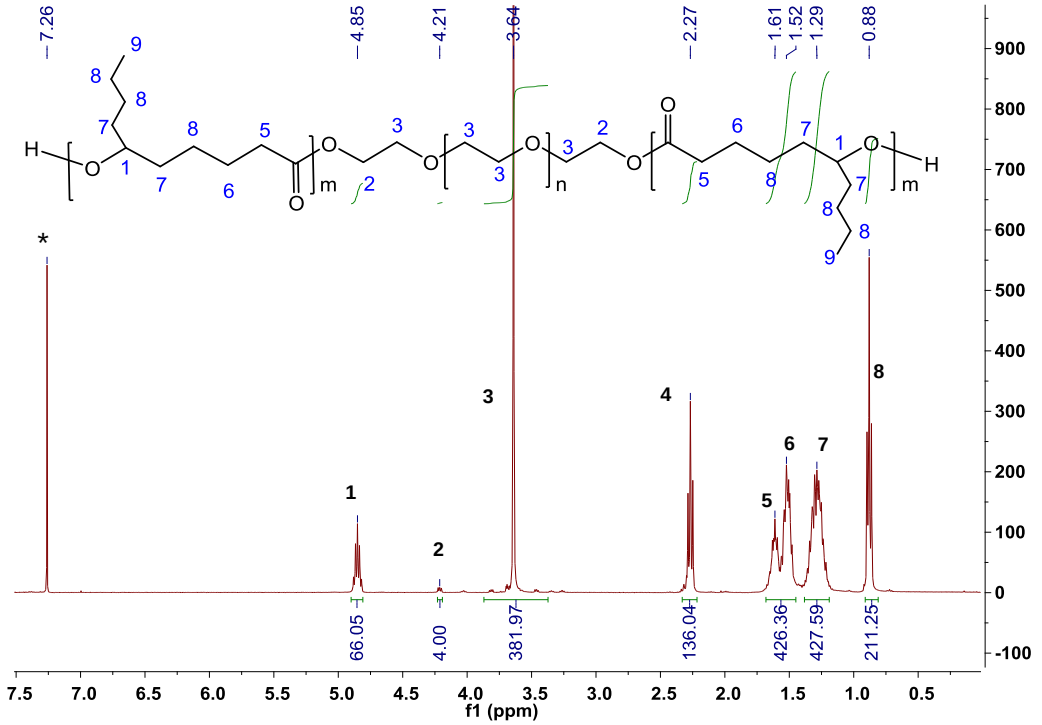


Figure 4-13 ^{1}H NMR spectra of PεDL-b-PEG-b-PεDL acquired in $CDCl_3$ (*Solvent peak).

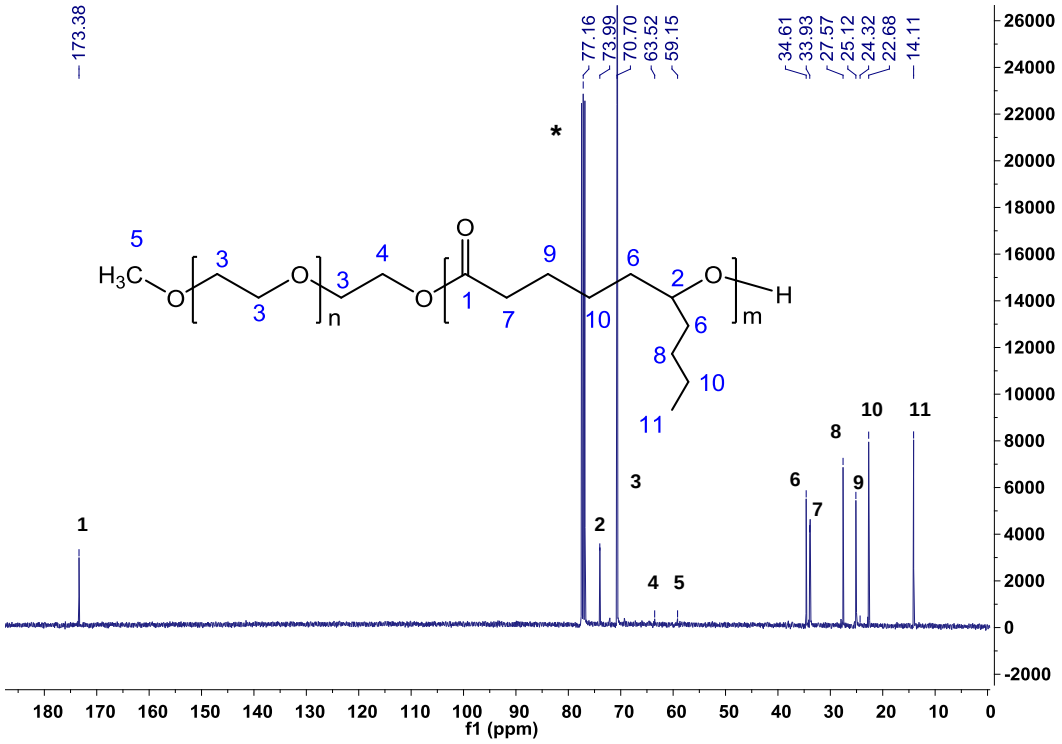


Figure 4-14 ^{13}C NMR spectra of mPEG-b-PεDL acquired in $CDCl_3$ (*Solvent peak).

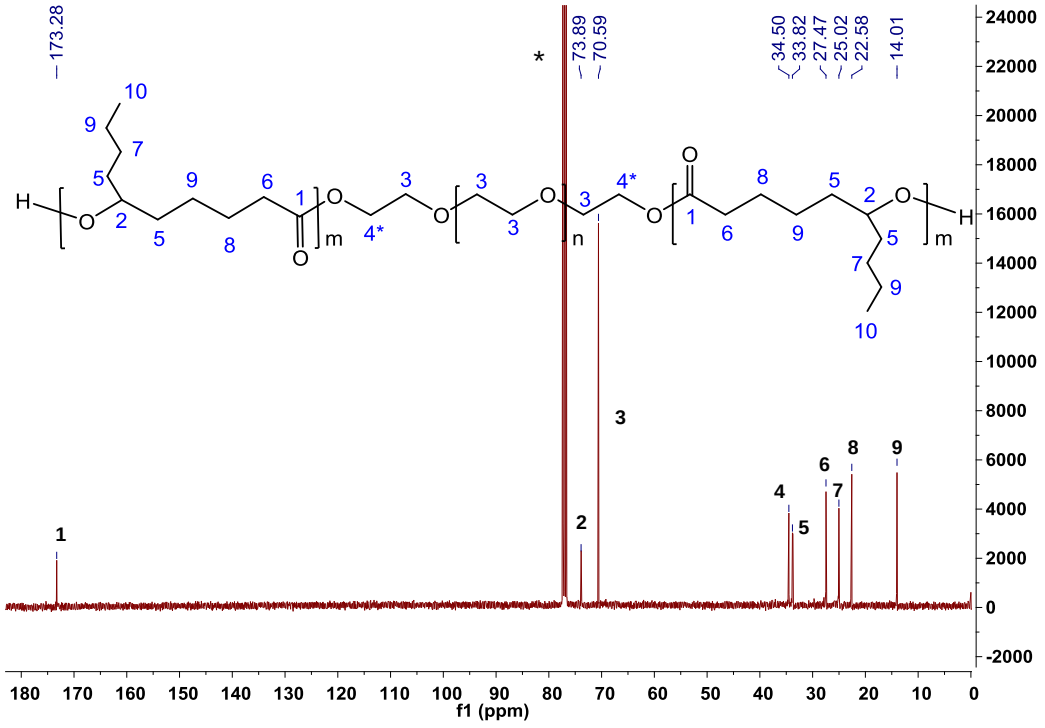


Figure 4-15 ^{13}C NMR spectra of PεDL-b-PEG-b-PεDL acquired in $CDCl_3$ (*Solvent peak).

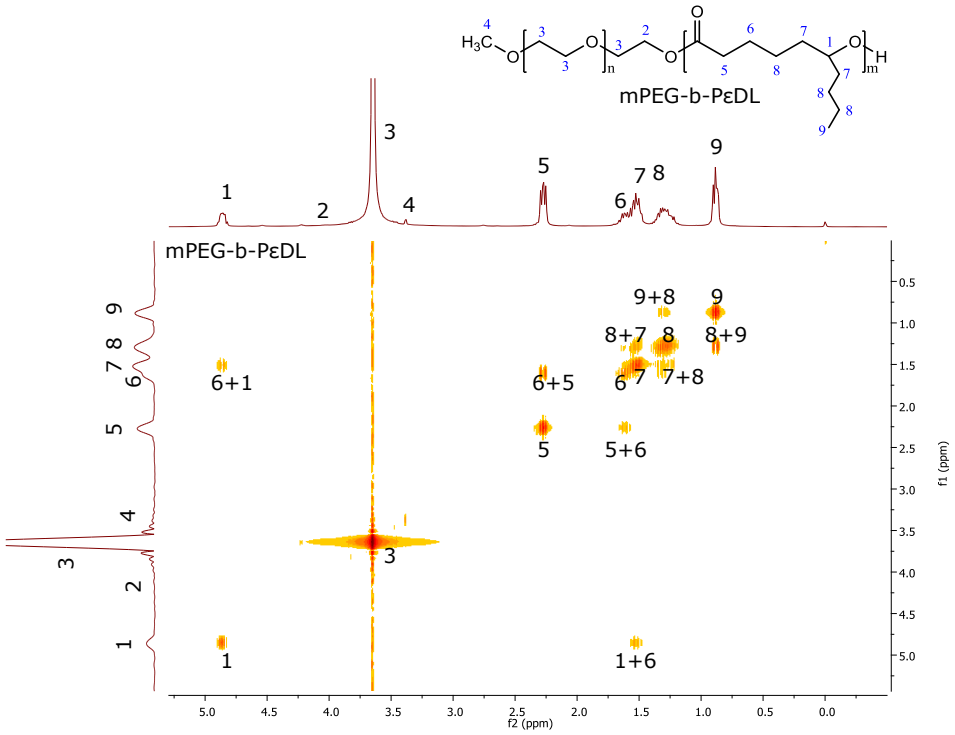


Figure 4-16 ^{1}H-^{1}H COSY NMR spectra of mPEG-b-PεDL acquired in $CDCl_3$.

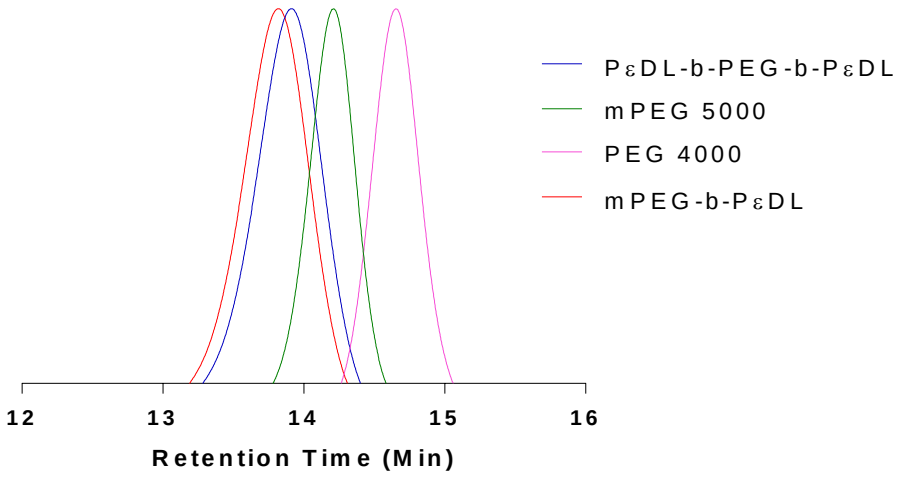


Figure 4-17 Retention times of the initiators and copolymers of the ε-decalactone.

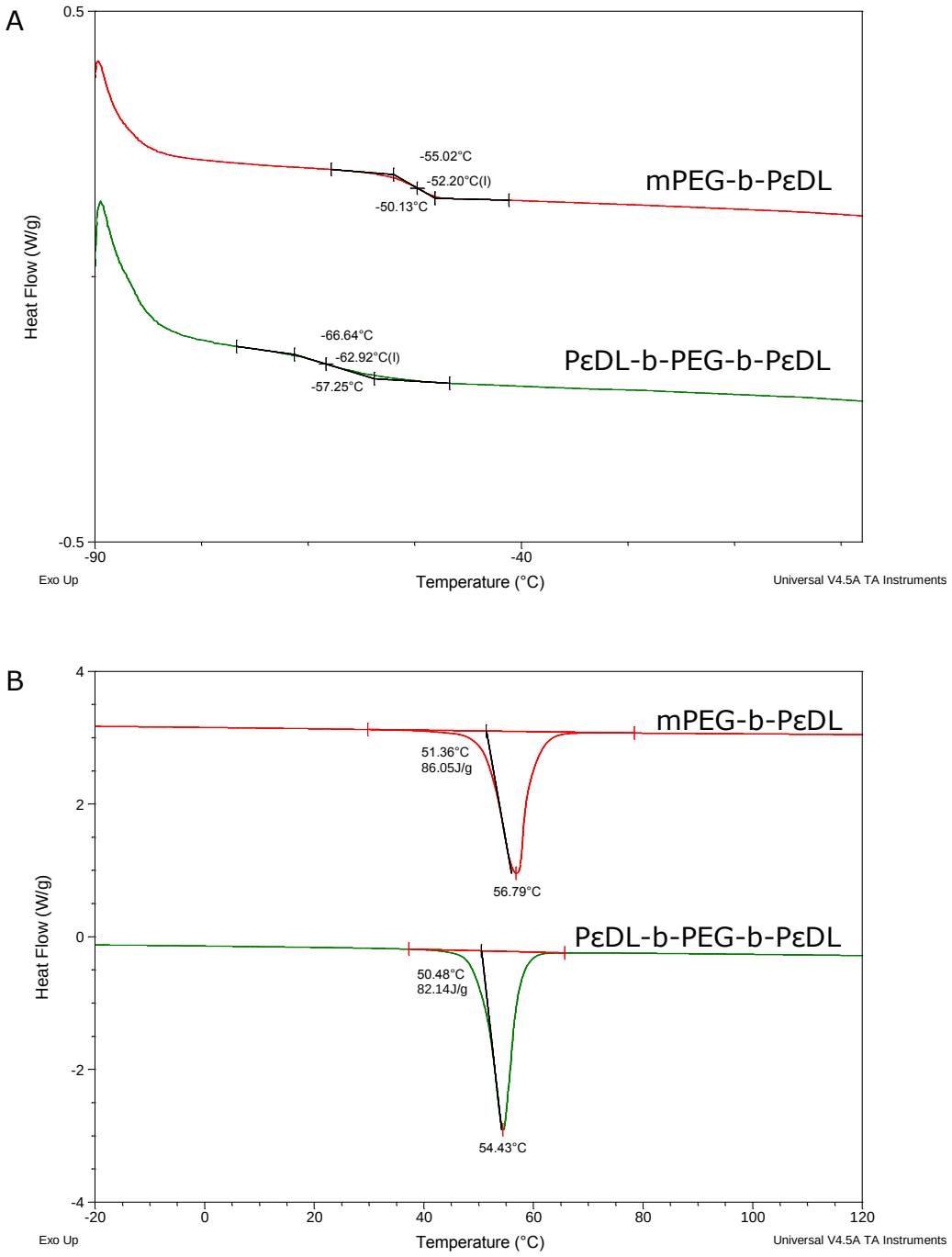
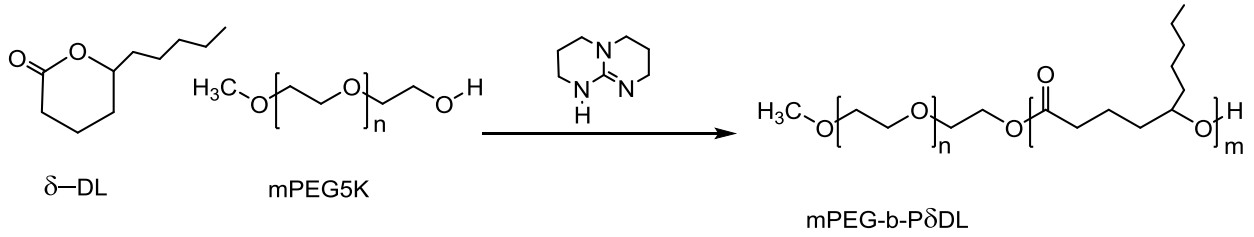


Figure 4-18 Differential scanning calorimetry (DSC) plots of mPEG-b-PεDL and PεDL-b-PEG-b-PεDL (A) T_g (B) T_m.

4.3.3 Copolymers of δ-Decalactone (δ-DL)



Scheme 4-3 Ring opening polymerisation (ROP) of δ-Decalactone (δ-DL) on mPEG5K using TBD catalyst

The synthesis of diblock mPEG-b-PδDL copolymer is shown in the scheme 4-3. The reactions were tried at two different temperatures (120 ^{o}C and 50 ^{o}C) using mPEG5K as initiator at 3 mol% of TBD concentration. The reaction conducted at 120 ^{o}C, resulted in low conversion of δ-DL. On the other hand, more than 85% monomers were consumed when the reaction was carried out at 50 ^{o}C. The kinetics of the reaction was monitored by ^{1}H NMR. The conversion was determined by comparing the δ proton peaks of the monomer before and after polymerisation. The M_n by ^{1}H NMR was determined by comparing the methoxy proton of mPEG at 3.37 ppm (peak 4) to the methine proton adjacent to the ester groups of the polymer chain at 4.86 ppm (peak 1) (Figure 4-19). The synthesis was also confirmed by ^{13}C NMR giving all the corresponding peaks reported previously[33] and as shown in figure 4-20.

The peak positions and the interaction between different protons were detected by ^{1}H-^{1}H COSY NMR spectroscopy and given in figure 4-21. The apparent rate constant (k_p) was determined by plotting a graph of

conversion and time. The slope of the line was measured to obtain the apparent rate constant (k_p) (Figure 4-22). The reaction was shown to following first order kinetics with respect to monomer. The apparent rate constant (k_p) observed for δ-decalactone polymerisation was $0.19h^{-1}$ compared to $0.18h^{-1}$ of ε-decalactone polymerisation. This indicates that the δ-decalactone reacted at a faster rate than ε-decalactone. The copolymer was separated from homopolymer by precipitation in diethyl ether in which the homopolymer was easily solubilized. However, a small shoulder in GPC graph indicated some impurity in the final copolymer (Figure 4-23). The Number average molecular weight (M_n) observed by SEC was higher compared to the molecular weight calculated by ^{1}H NMR.

The thermal properties were characterized by DSC. The semicrystalline nature of the copolymer was indicated by the presence of T_g at -56.9 ^oC and T_m at 60.3 ^oC (Figure 4-24).

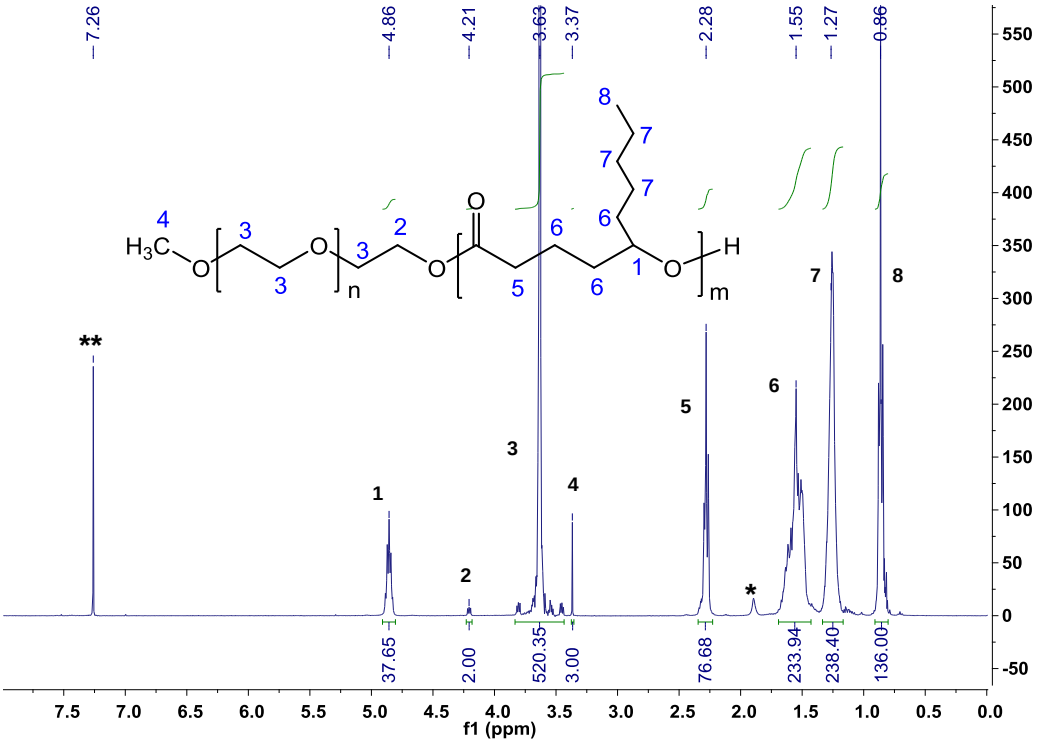


Figure 4-19 ^{1}H NMR spectra of mPEG-b-PδDL copolymer in $CDCl_3$ (**Solvent peak, *H_2O).

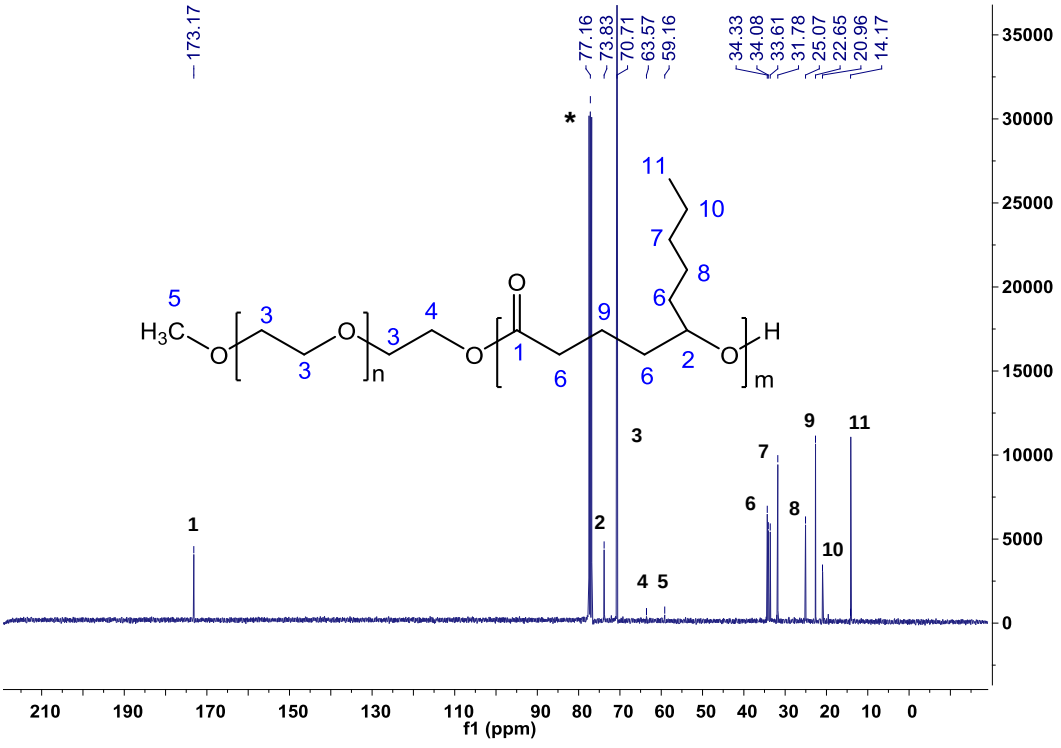


Figure 4-20 ^{13}C NMR spectra of mPEG-b-PδDL copolymer in $CDCl_3$ (*Solvent peak).

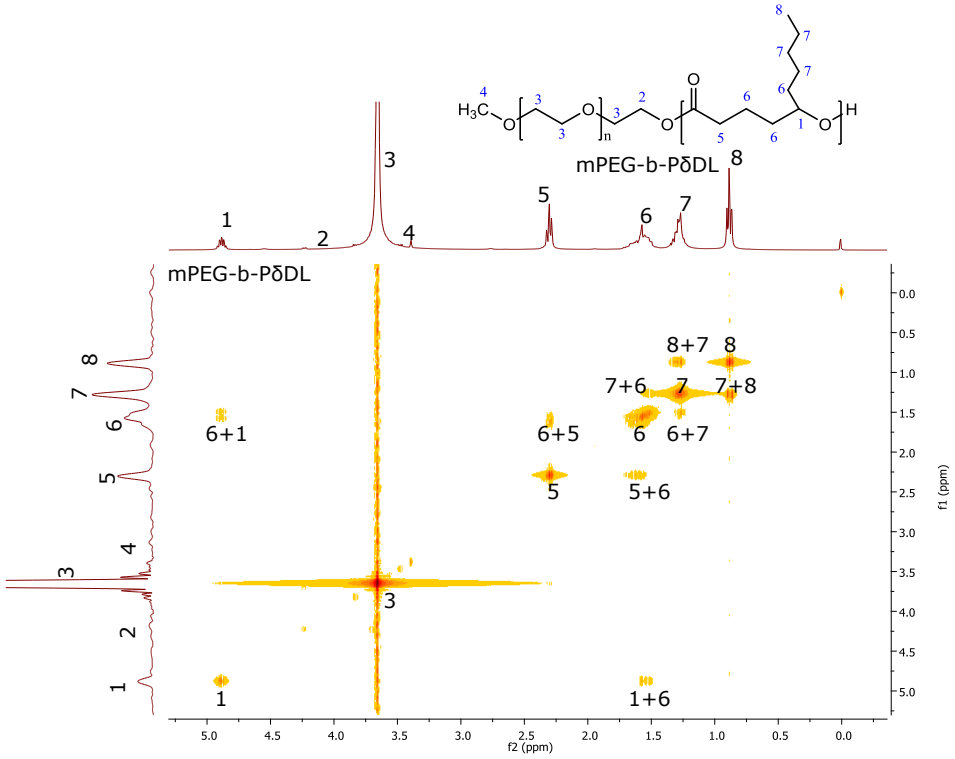


Figure 4-21 ^{1}H-^{1}H COSY NMR spectra of mPEG-b-PδDL acquired in $CDCl_3$.

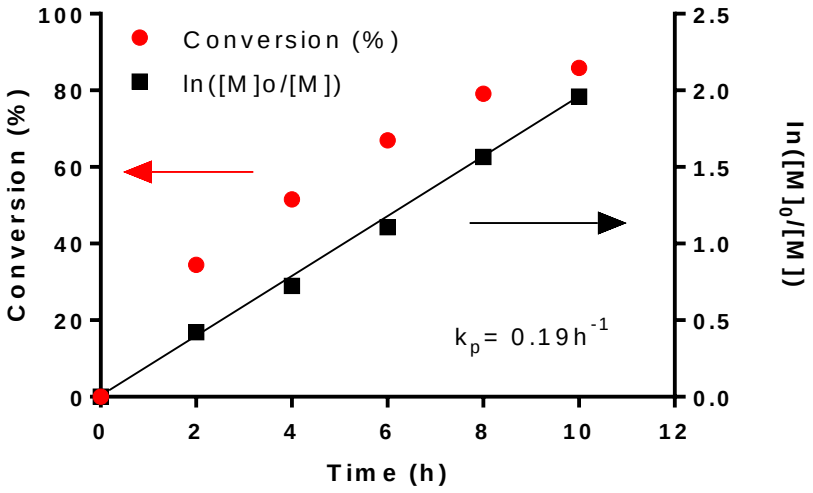
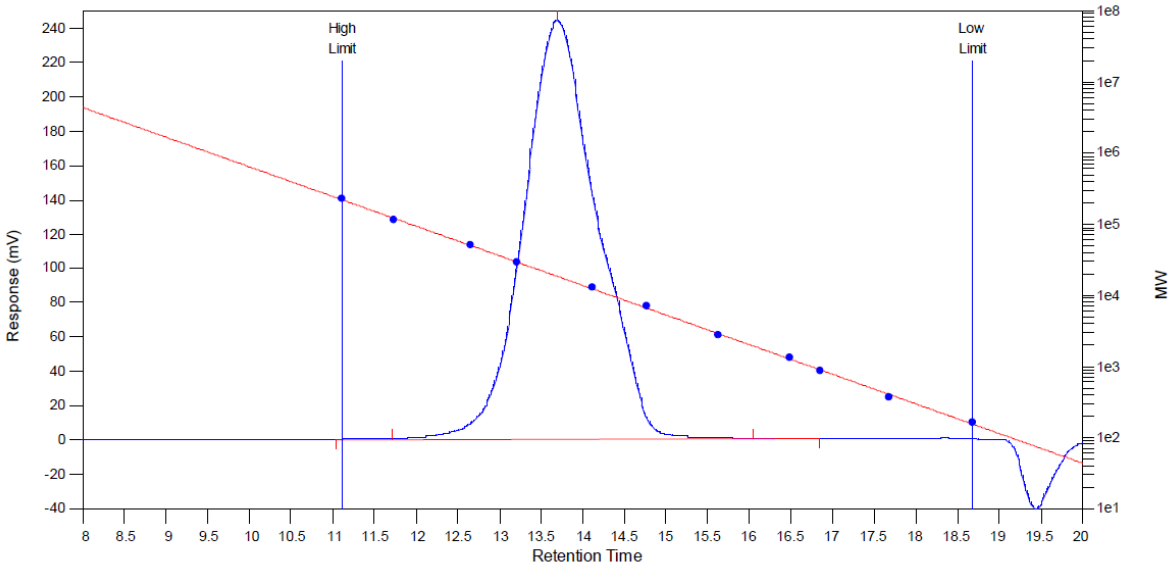
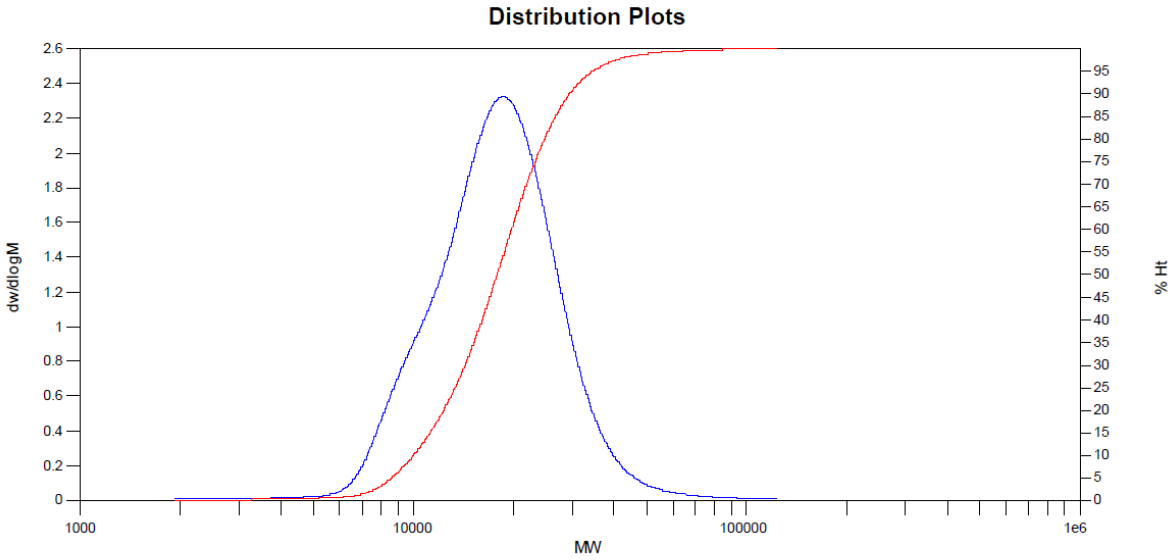


Figure 4-22 Kinetic analysis of δ-decalactone polymerisation from mPEG5K at 60 °C using TBD catalyst





Peak No	Mp	Mn	Mw	Mz	Mz+1	Mv	PD
1	18608	15958	19283	23605	30430	18741	1.20836

Figure 4-23 SEC graphs of mPEG-b-PδDL copolymer acquired in $CHCl_3$.

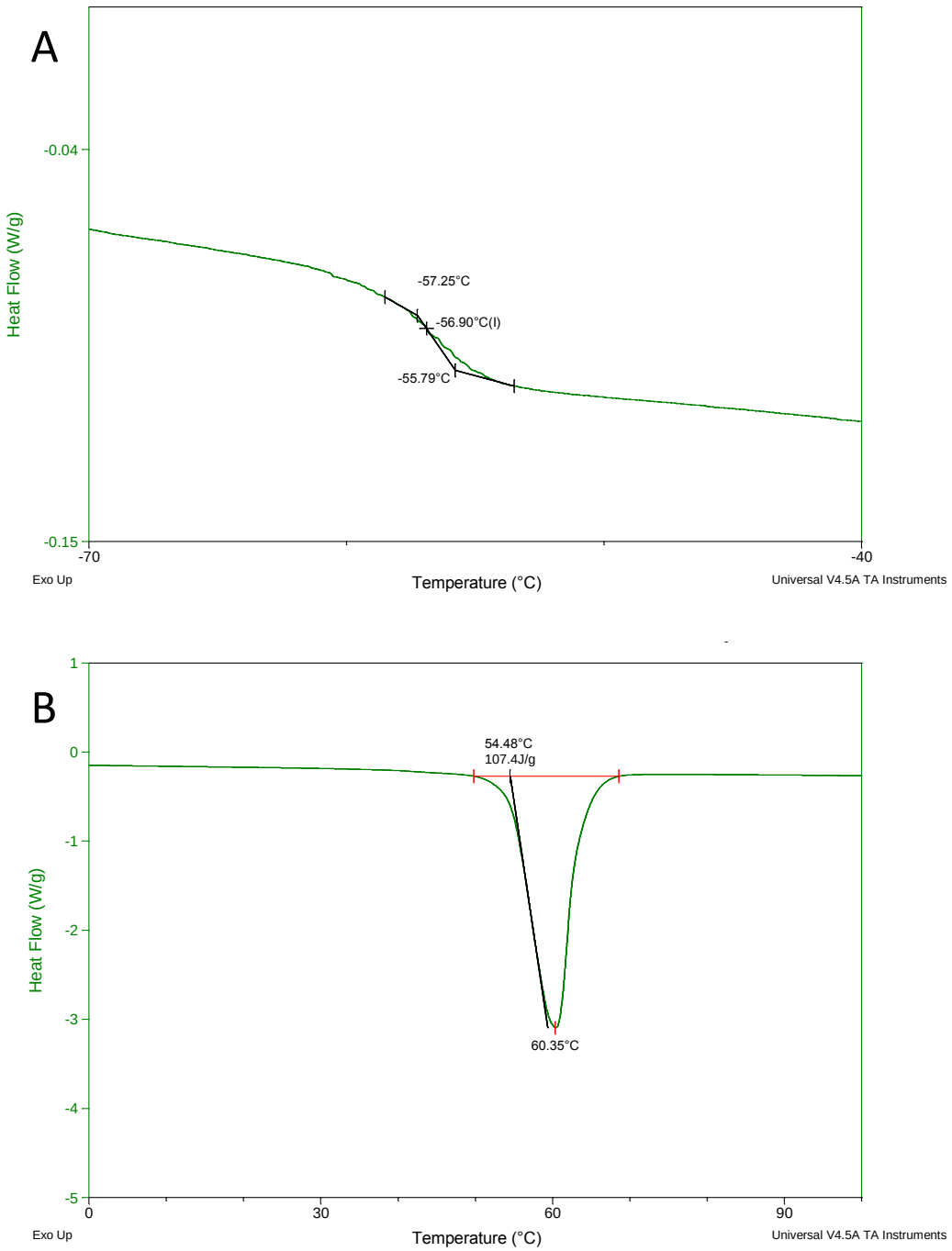
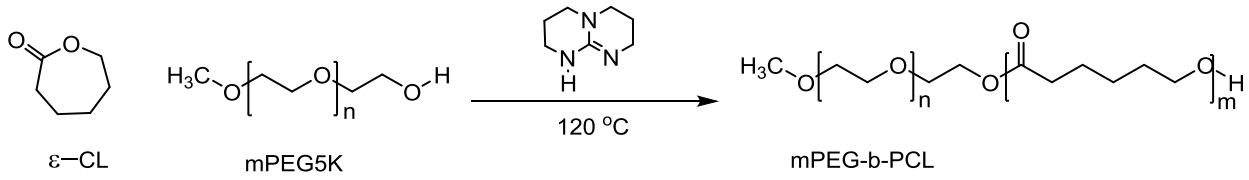


Figure 4-24 Differential scanning calorimetry (DSC) plot of mPEG-b-PδDL copolymer (A) T_g (B) T_m.

4.3.4 Copolymers of ε-Caprolactone (ε-CL)

The synthetic route for the synthesis of mPEG-b-PCL copolymer is shown in the scheme 4-4.



Scheme 4-4 Ring opening polymerisation (ROP) of ε-caprolactone (ε-CL) on mPEG5K using TBD catalyst

The synthesized mPEG-b-PCL was characterized by NMR and SEC after purification to check the purity of the copolymer. The target molecular weight of the copolymer was 10KD in order to compare with the similar molecular weights of the copolymers of ε-decalactone. Approximately, 98% conversion of the monomer was achieved within 10 min, while using a lower concentration of TBD (2 mol%) compared to ε-decalactone polymerisation indicated the higher efficiency of the ε-caprolactone to react. The conversion of monomer was checked by ^{1}H NMR by integrating α or ε peaks of the monomer with respect to α' or ε' peaks of the copolymer. The molecular weight of the copolymer was determined by integrating the methoxy proton of the mPEG with respect to the ε' peaks of the copolymer (Figure 4-25). The proton and carbon NMR peaks of the purified copolymer were matched with the reported peak values[25] (Figure 4-26 and Figure 4-27). The peak positions were also identified by ^{1}H-^{1}H COSY NMR and given in figure 4-28.

The GPC graph indicated a unimodal peak in the final copolymer (Figure 4-29). The DSC graph showed the semicrystalline nature of the copolymer indicated by the presence of a T_g at -52.15 °C and T_m at 56.79 °C (Figure 4-30). Table 4-1 shows all the characteristics data of the copolymer.

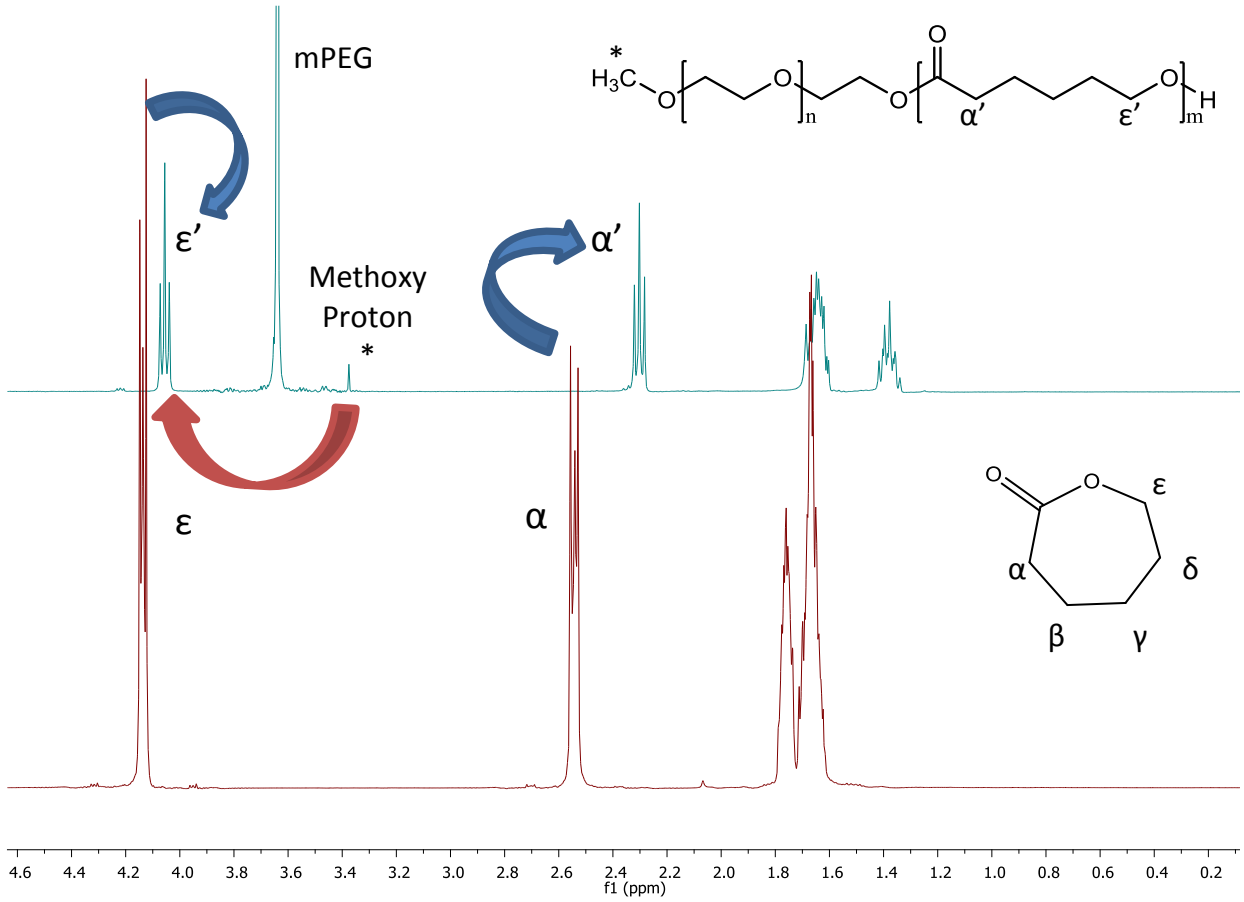


Figure 4-25 Positions of α / ε protons before and after conversion and the position of the methoxy proton with respect to ε' proton used for determination of M_n by ^{1}H NMR

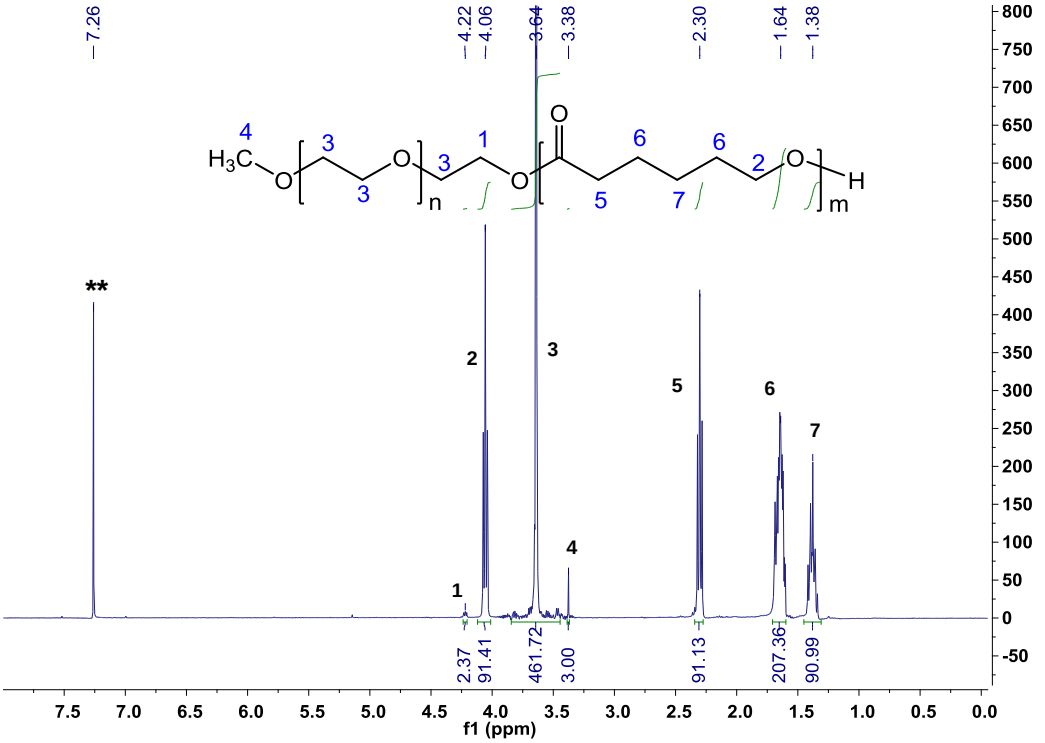


Figure 4-26 ^{1}H NMR of mPEG-b-PCL copolymer in $CDCl_3$ (**Solvent peak)

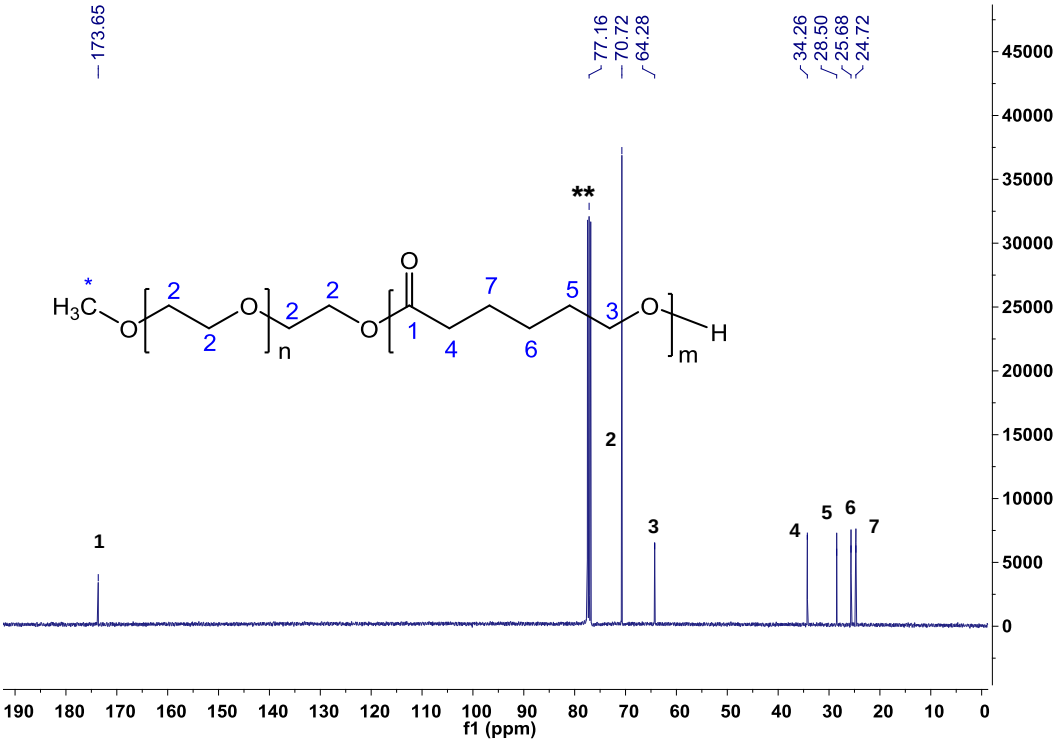


Figure 4-27 ^{13}C NMR of mPEG-b-PCL copolymer in $CDCl_3$ (*not detected; **Solvent peak)

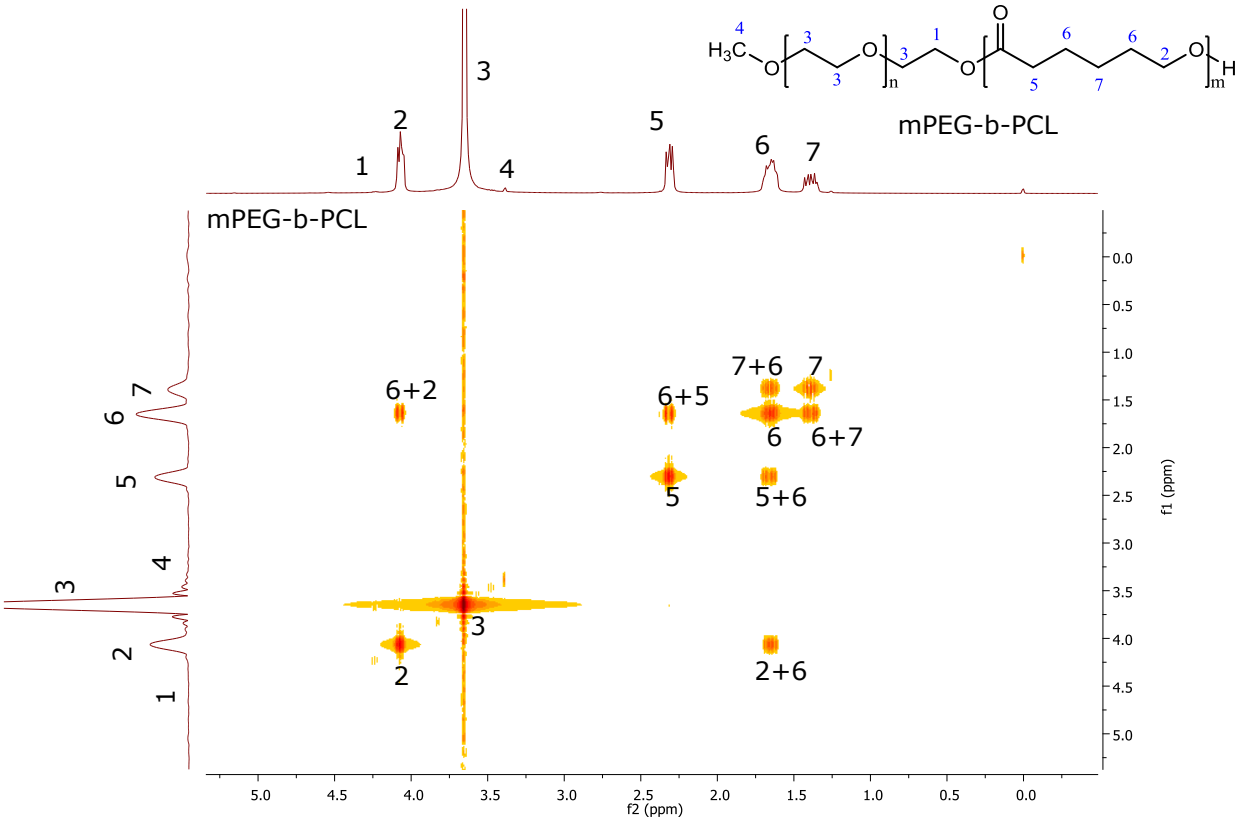
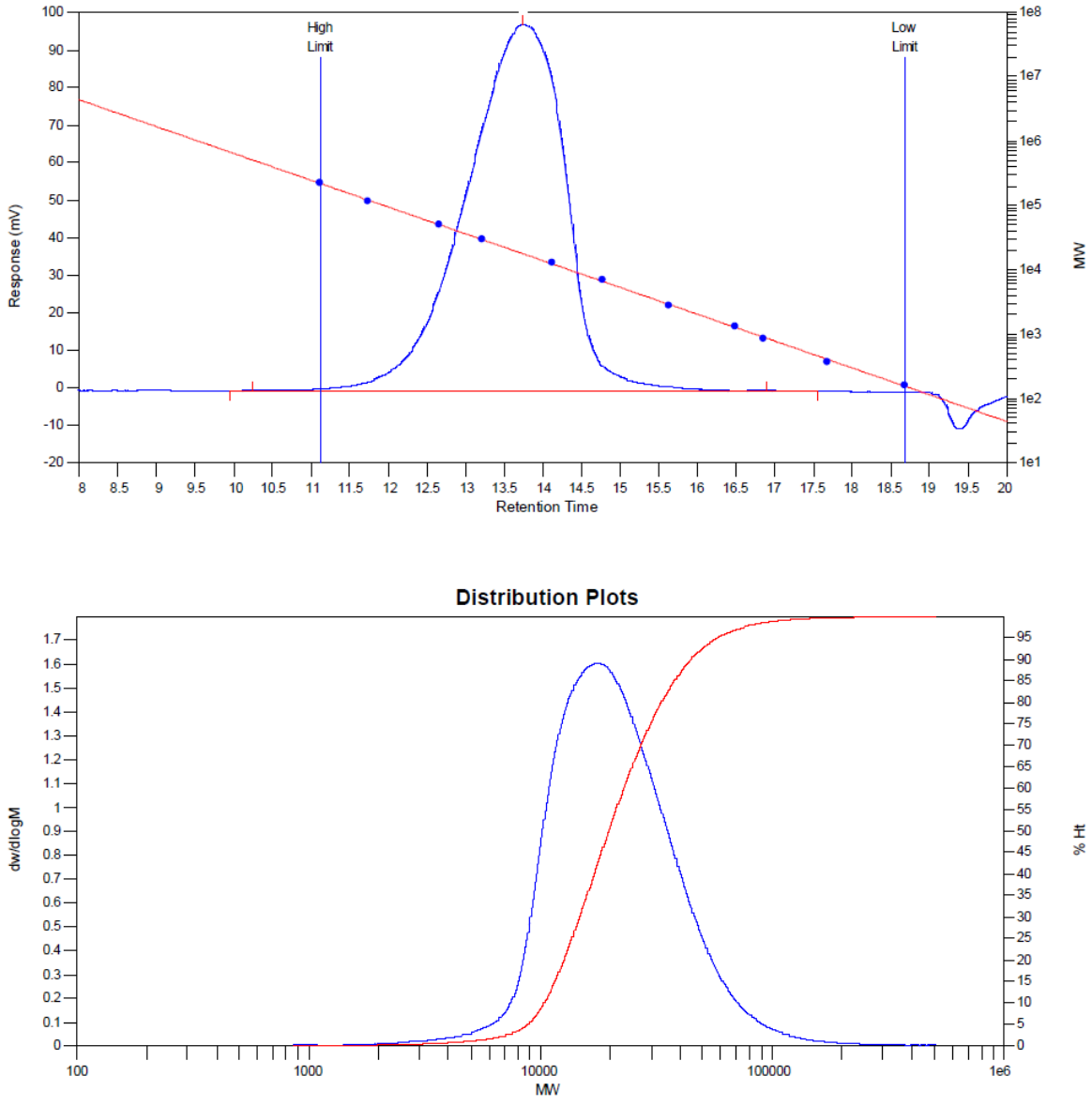


Figure 4-28 ^{1}H-^{1}H COSY NMR spectra of mPEG-b-PCL acquired in $CDCl_3$.



Peak No	Mp	Mn	Mw	Mz	Mz+1	Mv	PD
1	17651	17034	25240	44408	107018	23604	1.48174

Figure 4-29 SEC graph of mPEG-b-PCL copolymer acquired in $CHCl_3$.

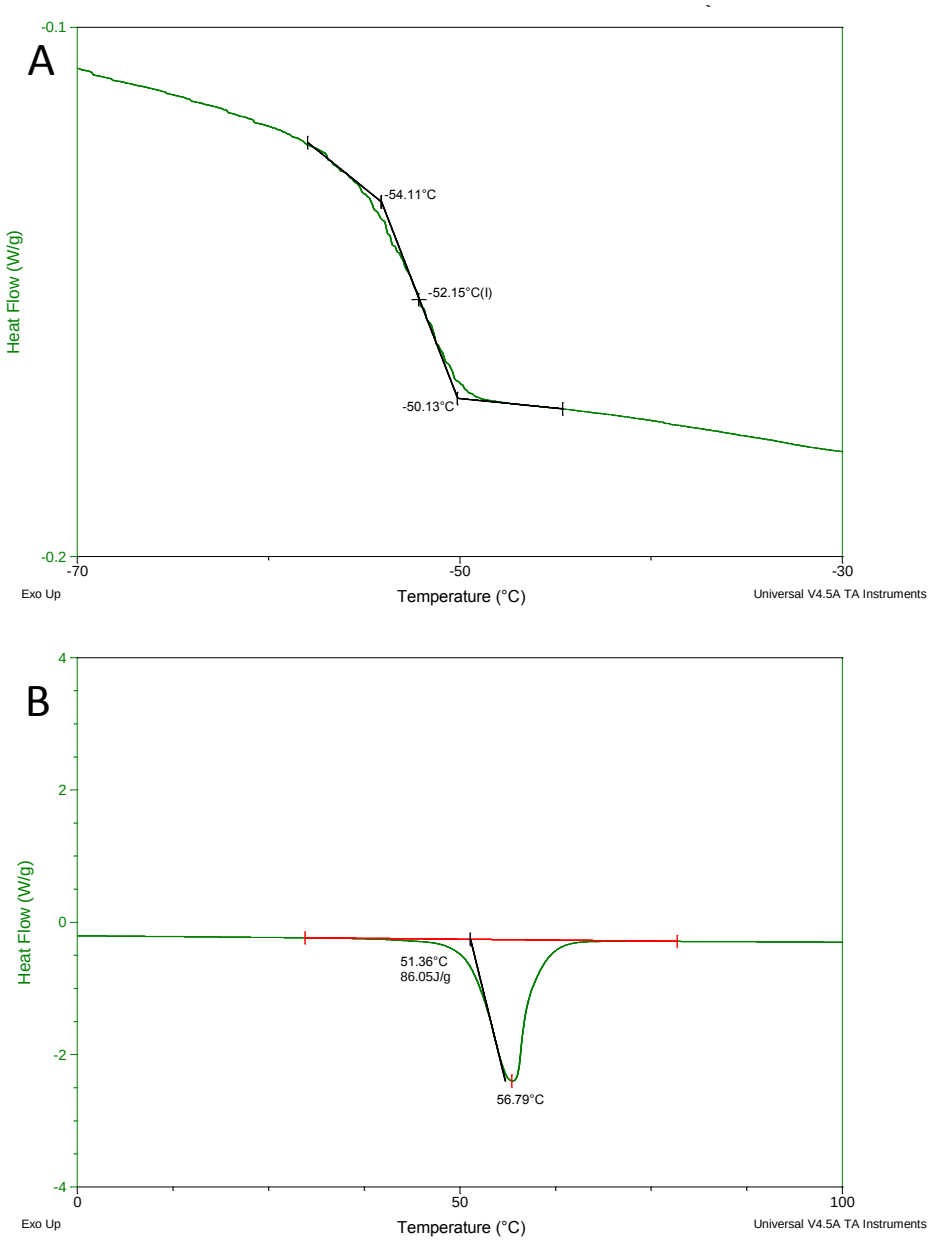
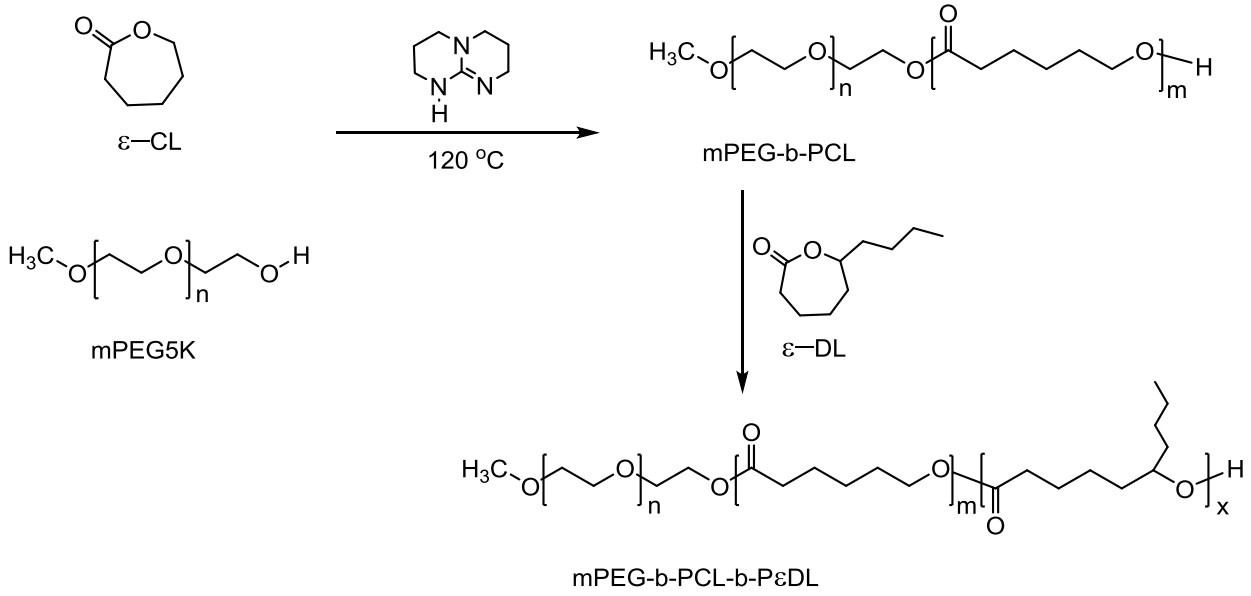


Figure 4-30 Differential scanning calorimetry (DSC) plot of mPEG-b-PCL copolymer (A) T_g (B) T_m.

4.3.5 mPEG-b-PCL-b-PεDL (ABC) Copolymer by Sequential Addition of ε-Caprolactone (ε-CL) and ε-Decalactone (ε-DL)

The ABC type copolymer was synthesized by sequential addition of ε-caprolactone and ε-decalactone as given in scheme 4-5.



Scheme 4-5 Ring opening polymerisation (ROP) of ε-caprolactone (ε-CL) and ε-decalactone (ε-DL) on mPEG5K using TBD catalyst

The ε-caprolactone was polymerised within 10 min as shown by ^{1}H NMR. The reaction was conducted in anhydrous conditions to avoid initiation by water, resulting in >96% conversion determined by ^{1}H NMR. The synthesized material was a white solid at this stage. Addition of ε-decalactone in the same pot for further reaction produced a wax like material after 12 h. An equal molar ratio of both the monomers was taken for the reaction. The copolymer was purified by the same method as described for mPEG-b-PεDL copolymer. The ^{1}H NMR of the copolymer was determined to observe the

conversion of different monomers from mPEG. ^{1}H NMR spectra of the purified copolymers with peaks are given in figure 4-31. The absence of monomers peaks indicated that no monomers were present in the purified polymer. The molecular weight of the mPEG-b-PCL-b-PεDL copolymer was calculated by integrating the methoxy proton of mPEG at 3.37 ppm of (peak 5, **CH_3**-O) against integrals of peaks 4.05 ppm (peak 3) and 4.84 ppm (peak 1) which emerged due to the formation of the hydrophobic chain of PCL (-**CH_2**-OCO) and PεDL (-**CH**(C_4H_9)-OCO) respectively. NMR indicated that 7 monomers of ε-CL and 11 monomers of ε-DL were attached to 1 unit of mPEG. The total molecular weight of mPEG-b-PCL-b-PεDL copolymer obtained from ^{1}H NMR was 7.7 x 10^3 g/mol^{-1} which was lower than the expected theoretical molecular weight of the copolymer. This shows that the hydrophobic chain of the copolymer was small and the obtained molecular weight of the hydrophobic chain was only 2.67 x 10^3 g/mol^{-1}.The structural integrity of copolymers was also determined by ^{13}C NMR and given in figure 4-32 with all assigned peaks. The presence of T_g and T_m indicated the semicrystalline nature of the polymer (Figure 4-33).

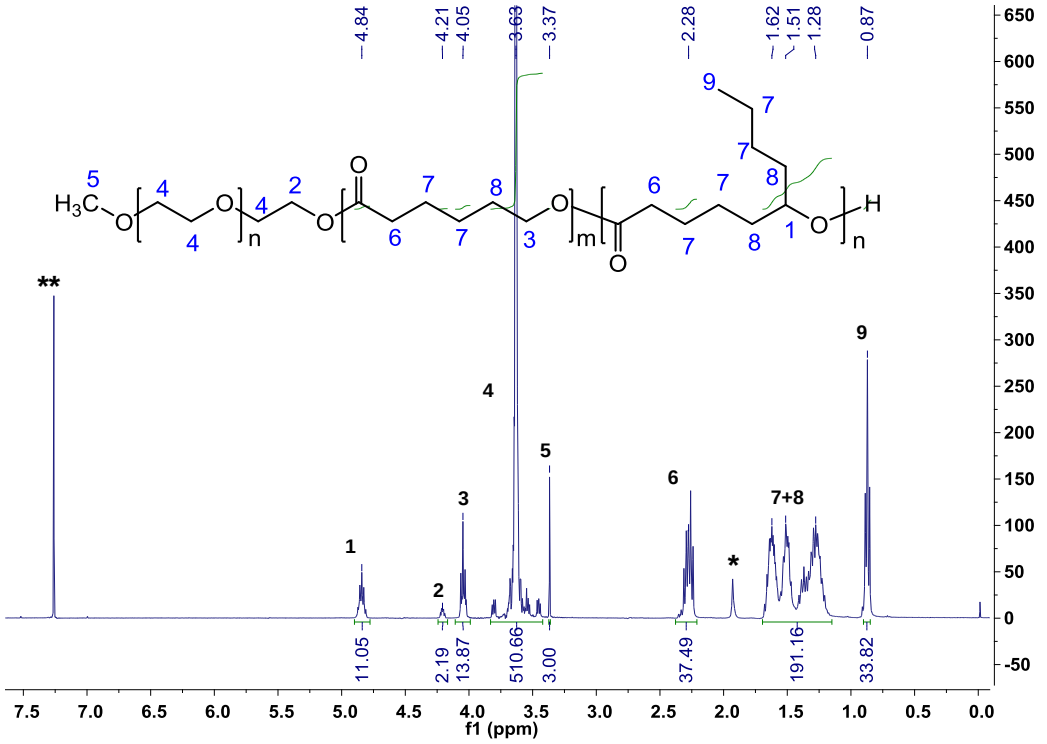


Figure 4-31 ^{1}H NMR spectra of mPEG-b-PCL-b-PεDL copolymer acquired in $CDCl_3$ (**Solvent peak, *H_2O peak).

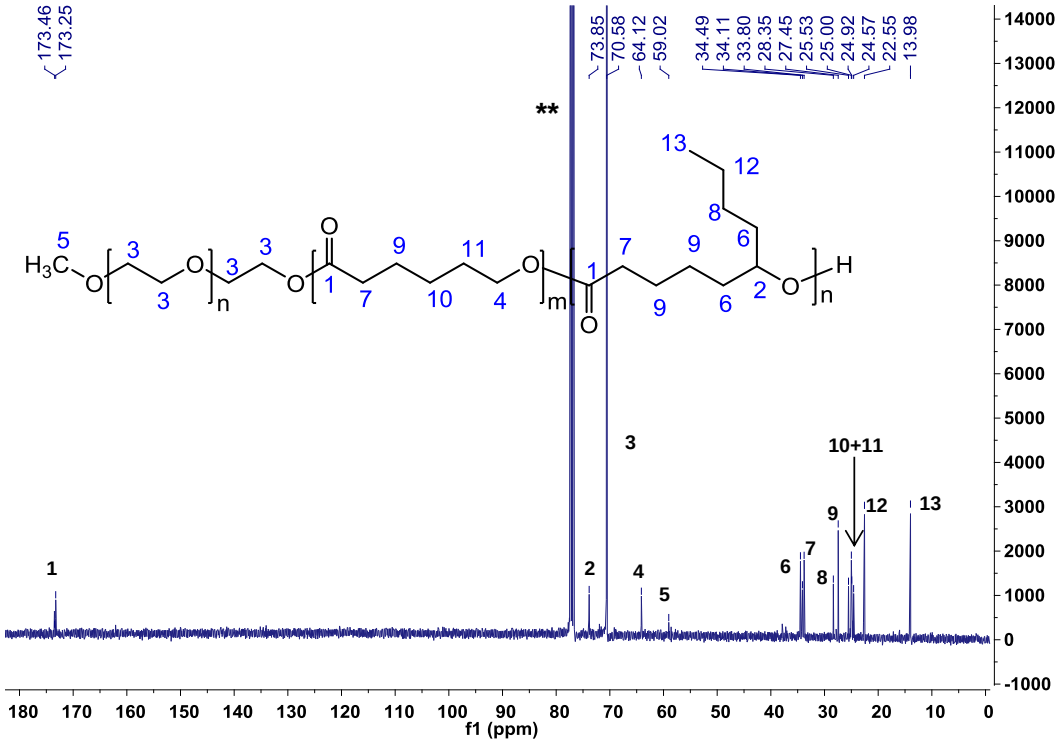


Figure 4-32 ^{13}C NMR spectra of mPEG-b-PCL-b-PεDL copolymer in $CDCl_3$ (**Solvent peak)

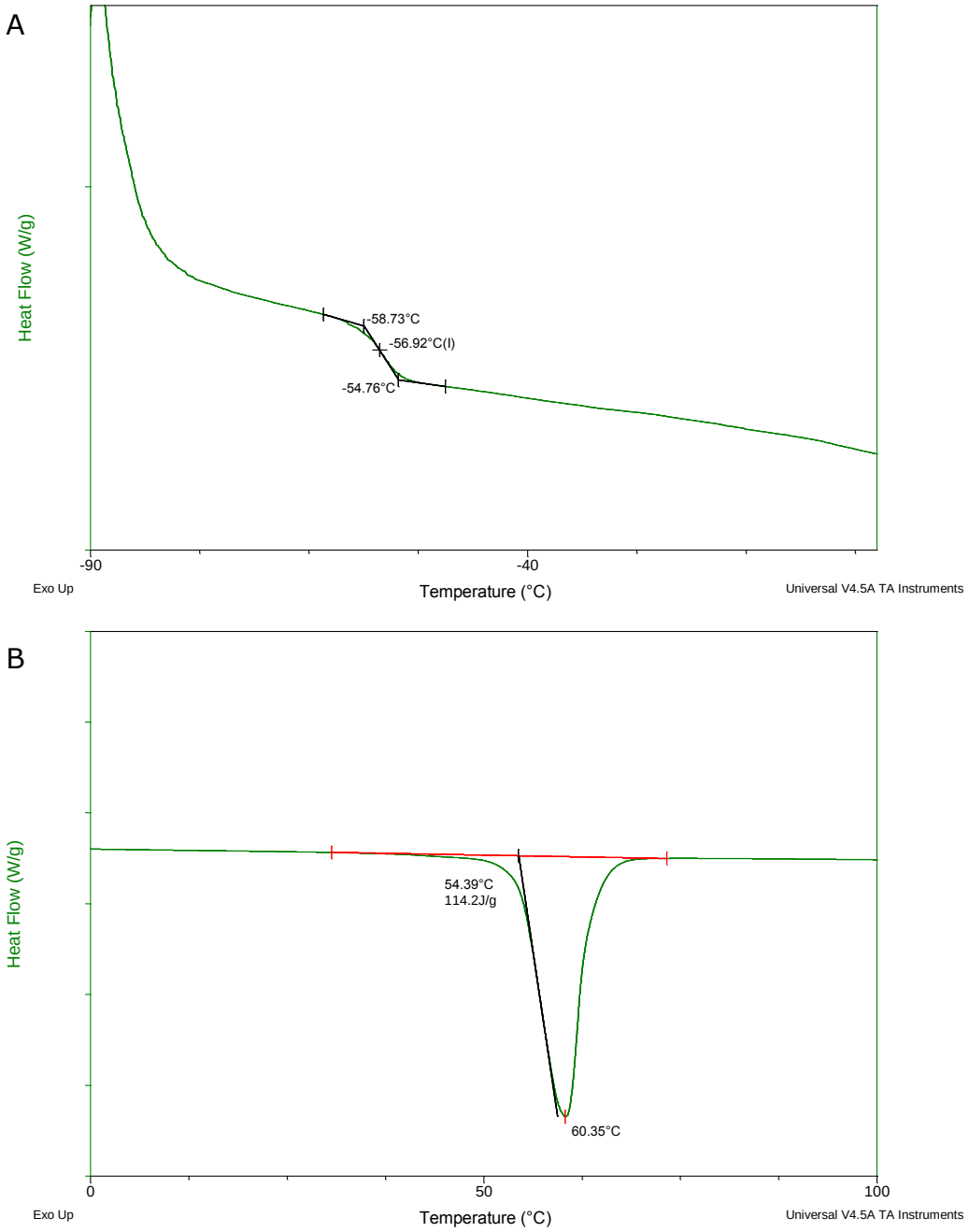


Figure 4-33 Differential scanning calorimetry (DSC) plot of mPEG-b-PCL-b-PεDL (A) T_g (B) T_m.

4.4 Discussion

The homopolymer and copolymers were made by ROP of biobased ε-DL monomer. The seven membered lactone rings with a butyl side chain at the ε position makes this monomer structurally similar to the non-renewable ε-caprolactone (ε-CL) monomer. The homopolymer was synthesized by using TBD as a catalyst with propargyl alcohol and benzyl alcohol as initiators. TBD was chosen as an organocatalyst to replace metal based $Sn(Oct)_2$. Previously, Olsen *et al.* described the synthesis of PεDL using TBD and $Sn(Oct)_2$ as a catalyst.[9] They found a higher reactivity of TBD compared to $Sn(Oct)_2$. The higher reactivity has already been shown by several groups for ROP.[34-36] The benzyl alcohol was used as initiator because it produces a unique ^1H NMR resonance hence was useful for characterization and M_n determination.[37] Propargyl alcohol was also used as an initiator so that further modification of the homopolymer might be achieved by click chemistry.[38] The polymerisation reaction was optimized for TBD concentration and temperature. The reaction rate proceeded very slowly when 1-2 mol% TBD was used at 120 ^oC. Hence, the TBD concentration was increased to 3 mol% for subsequent reactions. The synthesized homopolymers were sticky or oily and amorphous in nature. A higher hydrophobicity and amorphicity was expected for the homopolymers because of the racemic stereochemistry at the attachment point of the butyl chain which prevented the crystallization of the polymer chains.[32] Earlier, the

homopolymer of ε-DL was also synthesized and characterized by Lin *et al.* They showed the complete amorphous nature of the PεDL homopolymer with a T_g value of -53 ^oC with no melting point peak.[10] The synthesized homopolymer with benzyl alcohol also gave the same T_g value of -53 ^oC. A higher DP was achieved for both of the homopolymers (PεDL) after purification. The presence of secondary peaks and high polydispersity of the homopolymers suggested the presence of impurities (impure homopolymer) in the desired homopolymer. The possible reasons might be the presence of nucleophilic impurities or moisture which might have acted as initiator. These impure homopolymer chains were difficult to separate from the intended pure benzylic and Propargyl-terminated homopolymers as there was no solubility difference between them.

A diblock and a triblock copolymer were also made using mPEG5K and PEG 4000 initiators respectively. The efficacy of TBD was determined against stannous octoate by synthesizing diblock copolymers using both of the catalyst at the same temperature and concentration. The reaction was followed by NMR, observing changes at the ε and α positions as described in the result section. The apparent rate constant (k_p) of ε-decalactone polymerisation was 2.25 times higher when TBD was used as catalyst, indicating that TBD was more than twice as active as stannous octoate.

A lower degree of polymerisation (DP) was achieved for diblock copolymers compared to triblock copolymers. The presence of hydroxyl nucleophiles on

both of the ends of the PEG 4000 allowed the lactone monomer to polymerize from both sides. However, it was difficult to purify the triblock copolymer as the solubility difference between the triblock copolymer and homopolymer was low, which resulted in loss of the copolymer during purification step. In contrast to this, diblock copolymers made by higher molecular weight mPEG initiator were easily separated from homopolymers by precipitation in diethyl ether in which the homopolymer was easily solubilized.

The presence of homopolymer was indicated by GPC of the unpurified diblock copolymer which showed a secondary peak. The purification method removed the secondary peak but the presence of a small shoulder in GPC indicated some minor impurity in the final copolymer. Also, a low degree of polymerisation (DP=36) of diblock copolymer despite the higher conversion (90%) indicated the presence of homopolymer. The formation of homopolymer might be due to the presence of moisture or impurities in the starting material which were not removed completely during the initial monomer drying process and hence potentially acted as an initiator. The other probable reason might be associated with the mechanism of TBD catalysis. It can function as a dual activator of monomer and initiator during ROP. The TBD acts by a bifunctional nucleophilic mechanism where the nucleophilic imine nitrogen of TBD attacks the carbonyl carbon of monomer generating an intermediate which reacts with alcohol molecules (initiator) to

liberate polymerised ester and free TBD.[35] In this mechanism the generated intermediate can also act as an initiator to generate homopolymer and free TBD. Figure 4-34 shows the dual activation mechanism of TBD and generation of homopolymer by TBD initiator. Previously, the dual behavior of TBD was also described in the literature, where it was suggested to act not only as a catalyst but also as an initiator during ROP.[15]

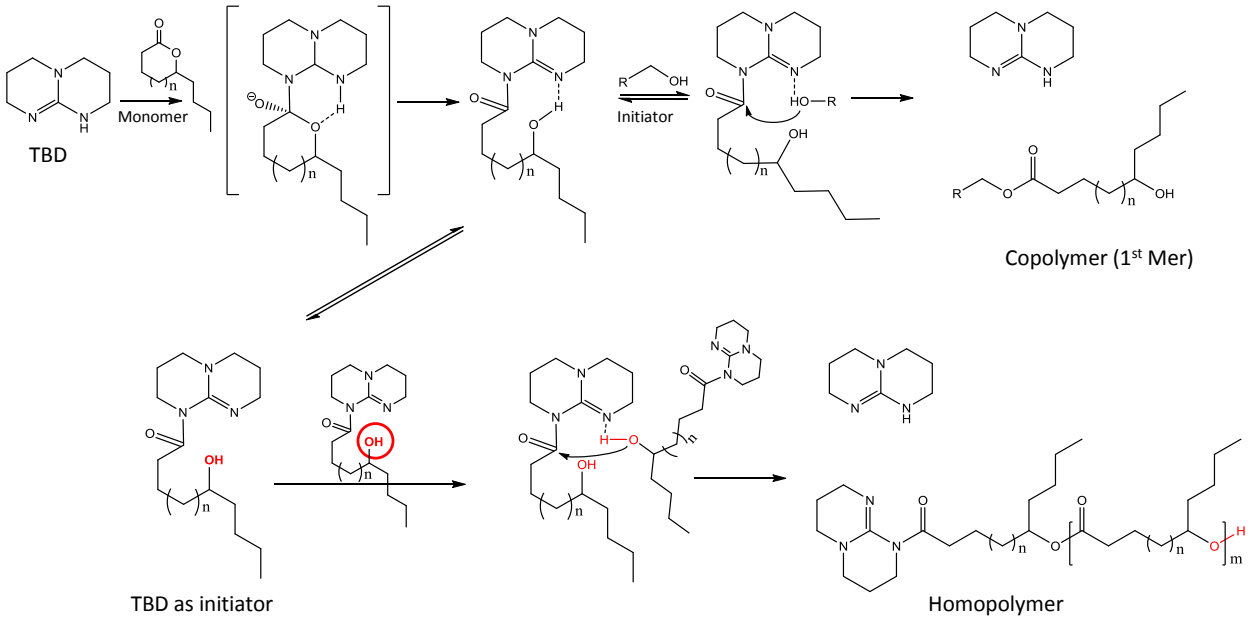


Figure 4-34 Dual mechanism of TBD as catalyst and initiator for ε-DL polymerisation[15]

The GPC data underestimated the M_n of homopolymer and triblock copolymer whereas the M_n of diblock copolymer was overestimated compared to the molecular weight calculated by ^1H NMR. Both of the homopolymers showed nearly half of the M_n (GPC) with high Đ compared to the theoretical molecular eight even when high M/I ratio was used (M/I=70). This might be due to the higher polarity of the chloroform compared to PDL

polymer resulted in suppression of hydrodynamic volume of the polymer. The underestimation of M_n in GPC has already been reported previously.[9] On the other hand, mPEG-b-PεDL copolymer showed a very high M_n with low Đ. In order to explain the difference, mPEG5K was also evaluated by GPC which indicated a M_n of 9.4 X 10^3 $gmol^{-1}$ with a Đ of 1.03. This indicated the different solution properties of the different blocks of polymers under GPC conditions coupled with the limitations of the polystyrene used as a standard for these polymers. The overestimation of the Mn in the GPC compared to the ^1H NMR of the copolymers was consistent with the previous report.[32] Hence, the value of M_n determined from ^1H NMR was used as a standard for further calculations.

The effect of the butyl side chain of ε-DL on ROP was evaluated by comparing the synthesis of mPEG-b-PεDL copolymer against mPEG-b-PCL copolymer made from ε-CL. The ε-CL monomer also was converted to PCL within 10 min (>90% conversion) even with a lower concentration of TBD (2 mol%). On the other hand, ε-DL required 12 h for the same conversion when 3 mol% of TBD was used. These results were expected as upon opening of the ε-DL by mPEG, a secondary alcohol was generated which acted as an initiator for further addition of the monomers during ROP. Additionally, the steric hindrance provided by the butyl side chain of ε-DL prevented the secondary alcohol from reacting further in the ROP. On the other hand, ε-CL reacted faster because of the absence of any alkyl chain.

Also, it generated a primary alcohol on ring opening which could react faster compared to a secondary alcohol (Figure 4-35). The absence of a secondary peak in the GPC of unpurified mPEG-b-PCL copolymer indicated a lower probability of the homopolymer formation. The PCL homopolymer is well known to make semicrystalline to crystalline polymers depending on the molecular weight. These data suggested that the micelles of the mPEG-b-PCL copolymer would have a semicrystalline core which could be compared with the amorphous core of the mPEG-b-PεDL micelles in aqueous solution.

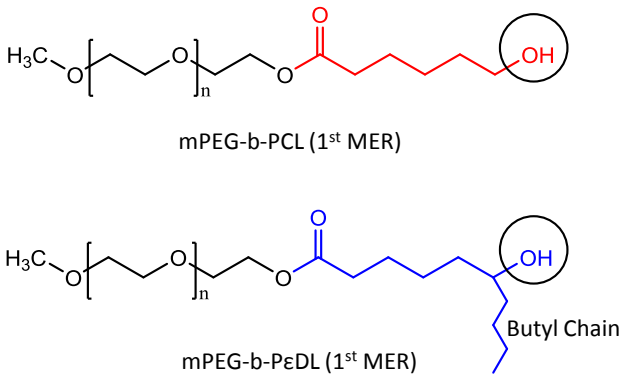


Figure 4-35 Generation of primary and secondary alcohol during ROP of ε-DL and ε-CL respectively.

The polymerisation of seven membered ε-decalactone (ε-DL) was also compared against six membered δ-decalactone (δ-DL) grown from mPEG5K initiator (Figure 4-36).

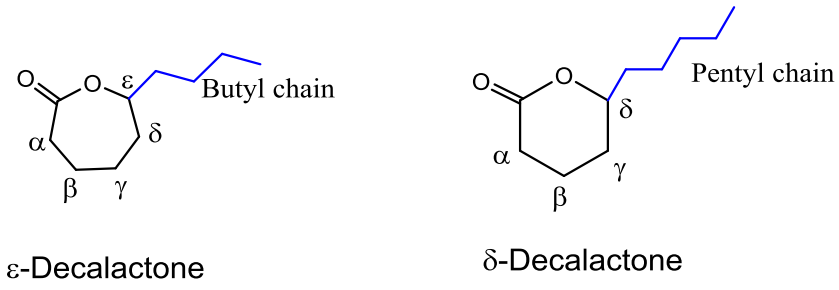


Figure 4-36 Structure of ε-decalactone (seven membered ring) and δ-decalactone (six membered ring)

Both of the monomers are categorized as biobased renewable materials. However, a large difference was observed between the reaction temperatures appropriate for polymerisation. A low temperature was needed for δ-DL polymerisation compared to the high temperature used for ε-DL polymerisation. The different reactivities might have been associated with the ceiling temperature, at which the rate of polymerisation and depolymerisation are equal hence the polymer can revert back to its monomer. The difference in the ceiling temperatures between six and seven membered lactone rings has been shown to be nearly 100 ^{o}C or more. The substitution at the δ position on the six membered ring further reduced the ceiling temperature hence limiting the use of higher temperatures for δ-DL polymerisation. The reaction conducted at higher temperature (120 ^{o}C) yielded a very low δ-DL conversion, which supported the ceiling temperature hypothesis. On the other hand, ε-DL was polymerised at 120 ^{o}C where no sign of depolymerisation was observed, further demonstrating the dependency of the reaction on size of the decalactones.

4.5 Conclusion

A successful synthesis of ε-DL homopolymer and copolymers has been described in the chapter. The synthesis was also compared with δ-DL and ε-CL polymerisation. The synthetic strategy demonstrated the higher polymerisation efficiency of TBD compared to $Sn(Oct)_2$ catalyst. However, a significant difference in the appropriate reaction temperatures of ε-DL and δ-DL polymerisation was observed. The alkyl chains in the substituted lactone monomers provided amorphous content to the resulting polymers. The comparison against the structure analogue ε-CL, revealed that the ε-DL polymerisation was inhibited due to the presence of the alkyl chain of ε-DL monomer. However, a higher reaction time (12 h for TBD and 24 h for $Sn(Oct)_2$) in ε-DL polymerisation persuaded us to attempt to improve the reaction time. Therefore, in the next chapter microwave based ring opening polymerisation (MROP) is described as a tool for conversion of biobased ε-DL monomer.

4.6 Reference

1. A. C. Albertsson and I. K. Varma, *Biomacromolecules*, 2003, **4**, 1466-1486.
2. A. C. Albertsson and I. K. Varma, *Degradable Aliphatic Polyesters*, 2002, **157**, 1-40.
3. M. S. Lindblad, Y. Liu, A. C. Albertsson, E. Ranucci and S. Karlsson, *Degradable Aliphatic Polyesters*, 2002, **157**, 139-161.
4. M. T. Martello, A. Burns and M. Hillmyer, *Acs Macro Letters*, 2012, **1**, 131-135.
5. J. R. Lowe, M. T. Martello, W. B. Tolman and M. A. Hillmyer, *Polymer Chemistry*, 2011, **2**, 702-708.

6. J. R. Lowe, W. B. Tolman and M. A. Hillmyer, *Biomacromolecules*, 2009, **10**, 2003-2008.
7. D. H. Zhang, M. A. Hillmyer and W. B. Tolman, *Biomacromolecules*, 2005, **6**, 2091-2095.
8. C. G. Pitt, M. M. Gratzl, G. L. Kimmel, J. Surles and A. Schindler, *Biomaterials*, 1981, **2**, 215-220.
9. P. Olsen, T. Borke, K. Odelius and A.-C. Albertsson, *Biomacromolecules*, 2013, **14**, 2883-2890.
10. J.-O. Lin, W. Chen, Z. Shen and J. Ling, *Macromolecules*, 2013, **46**, 7769-7776.
11. A. Pascual, H. Sardon, A. Veloso, F. Ruiperez and D. Mecerreyes, *Acs Macro Letters*, 2014, **3**, 849-853.
12. D. McGinty, C. S. Letizia and A. M. Api, *Food and Chemical Toxicology*, 2011, **49**, S193-S201.
13. T. Chen, Z. Qin, Y. Qi, T. Deng, X. Ge, J. Wang and X. Hou, *Polymer Chemistry*, 2011, **2**, 1190-1194.
14. A. Pascual, J. R. Leiza and D. Mecerreyes, *European Polymer Journal*, 2013, **49**, 1601-1609.
15. A. Pascual, H. Sardon, F. Ruiperez, R. Gracia, P. Sudam, A. Veloso and D. Mecerreyes, *Journal of Polymer Science Part a-Polymer Chemistry*, 2015, **53**, 552-561.
16. M. P. F. Pepels, M. Bouyahyi, A. Heise and R. Duchateau, *Macromolecules*, 2013, **46**, 4324-4334.
17. M. P. F. Pepels, P. Soulje, R. Peters and R. Duchateau, *Macromolecules*, 2014, **47**, 5542-5550.
18. K. Takizawa, C. Tang and C. J. Hawker, *Journal of the American Chemical Society*, 2008, **130**, 1718-1726.
19. M. Sinenkov, E. Kirillov, T. Roisnel, G. Fukin, A. Trifonov and J.-F. Carpentier, *Organometallics*, 2011, **30**, 5509-5523.
20. C. Zhang, L. Liao and S. Gong, *Macromolecular Rapid Communications*, 2007, **28**, 422-427.
21. I. K. Varma, A. C. Albertsson, R. Rajkhowa and R. K. Srivastava, *Progress in Polymer Science*, 2005, **30**, 949-981.
22. Y. Yang, Y. Yu, Y. Zhang, C. Liu, W. Shi and Q. Li, *Process Biochemistry*, 2011, **46**, 1900-1908.
23. I. van der Meulen, E. Gubbels, S. Huijser, R. Sablong, C. E. Koning, A. Heise and R. Duchateau, *Macromolecules*, 2011, **44**, 4301-4305.
24. C. G. Jaffredo, J.-F. Carpentier and S. M. Guillaume, *Macromolecules*, 2013, **46**, 6765-6776.
25. M. Bouyahyi, M. P. F. Pepels, A. Heise and R. Duchateau, *Macromolecules*, 2012, **45**, 3356-3366.
26. H. Kim, J. V. Olsson, J. L. Hedrick and R. M. Waymouth, *Acs Macro Letters*, 2012, **1**, 845-847.

27. M. K. Kiesewetter, M. D. Scholten, N. Kirn, R. L. Weber, J. L. Hedrick and R. M. Waymouth, *Journal of Organic Chemistry*, 2009, **74**, 9490-9496.
28. I. Cota, F. Medina, J. E. Sueiras and D. Tichit, *Tetrahedron Letters*, 2011, **52**, 385-387.
29. W. P. Ye, J. Y. Xu, C. T. Tan and C. H. Tan, *Tetrahedron Letters*, 2005, **46**, 6875-6878.
30. A. Endrizzi, Y. Pagot, A. LeClainche, J. M. Nicaud and J. M. Belin, *Critical Reviews in Biotechnology*, 1996, **16**, 301-329.
31. C. Romero-Guido, I. Belo, T. M. N. Ta, L. Cao-Hoang, M. Alchihab, N. Gomes, P. Thonart, J. A. Teixeira, J. Destain and Y. Wache, *Applied Microbiology and Biotechnology*, 2011, **89**, 535-547.
32. L. Glavas, P. Olsen, K. Odelius and A.-C. Albertsson, *Biomacromolecules*, 2013, **14**, 4150-4156.
33. B. Kuldeep, K. Deepak, P. Laura, I. Derek, H. Steven, M. Giuseppe and A. Cameron, *Journal*, 2015, **6**, 7196-7210.
34. A. Chuma, H. W. Horn, W. C. Swope, R. C. Pratt, L. Zhang, B. G. G. Lohmeijer, C. G. Wade, R. M. Waymouth, J. L. Hedrick and J. E. Rice, *Journal of the American Chemical Society*, 2008, **130**, 6749-6754.
35. L. Simon and J. M. Goodman, *Journal of Organic Chemistry*, 2007, **72**, 9656-9662.
36. R. C. Pratt, B. G. G. Lohmeijer, D. A. Long, R. M. Waymouth and J. L. Hedrick, *Journal of the American Chemical Society*, 2006, **128**, 4556-4557.
37. N. T. Nguyen, E. Greenhalgh, M. J. Kamaruddin, J. El Harfi, K. Carmichael, G. Dimitrakis, S. W. Kingman, J. P. Robinson and D. J. Irvine, *Tetrahedron*, 2014, **70**, 996-1003.
38. W. X. Xi, T. F. Scott, C. J. Kloxin and C. N. Bowman, *Advanced Functional Materials*, 2014, **24**, 2572-2590.

Chapter

5

Microwave Assisted Synthesis of ε-Decalactone based Copolymers and Evaluation of the Properties of the Copolymers

5.1 Introduction

In recent decades biodegradable polymers produced from renewable feedstocks have generated a great deal of interest with a key focus on their ability to act as possible substitutes for conventional polymers produced from non-renewable feedstocks. However, whilst use of sustainable feedstocks to produce biodegradable polymers can bring obvious intrinsic environment benefits on both the short and long time scale. To realise this requires improvements in the energy efficiency in the processing steps of their synthesis to be brought forward to make their production competitive with the current commercial petrochemically derived alternatives. In the previous chapters of this thesis, the synthesis of copolymers of ε-decalactone (a renewable feedstock) has been described by using hot plate conventional heating (CH) methods. However, this work has shown that a polymerisation method which requires lower energy consumption and exhibits a shorter reaction time is needed to increase the synthetic routes economic viability and sustainable footprint. Recently, the application of microwave-assisted synthesis has been reported to have a potentially major role in exploitation of green chemistry by presenting a number of advantages over conventional thermal heating methods. Literature reports have detailed that microwave heating/excitation has widely been used for various polymerisation reactions like ROP,[1-3] polycondensation,[4-6] free/controlled radical polymerisation.[7-9] For example and with particular

relevance to this study, it has been claimed to provide a clean (i.e. the use of electricity generated from renewable sources) and economical method of heating (i.e. shorter reaction times and smaller plant footprints as a result of moving from batch to continuous production routes). The other advantages over conventional heating include high yields and limited generation of by-products.[10]

The microwave heating depends on the ability of a material (solvent or reagent) to absorb microwave energy and convert it into heat. Microwave heating/excitation of the material results from the dipoles within a molecule and of the charge separation of ions being affected by the presence of an electric field. In the case of the dipoles, they try to align themselves with applied electric field, whilst in the case of ion pairs the distance between the ions is increased. Furthermore, due to the oscillation of the applied field, the dipoles or ions are continually attempting to realign themselves with phase of the alternating electric field. This causes molecular motion which in turn leads to intermolecular friction with other moieties in the immediate vicinity of the effected molecule. These molecular motions included the rotation and the collision the microwave susceptible molecule, thus loose energy in the form of heat to the materials around them.[10, 11] The level of generated heat observed therefore strongly depends on the ability of the material to align itself with the frequency of the applied field. Thus, molecules with few dipoles, weak dipoles or dipoles that have restricted movement do not align

quickly itself with the applied field, resulted in no or little heating of the material.

Previously, most of the work reported in the literature on ROP reactions using microwave heating source has been conducted using of ε-caprolactone as the monomer.[12-17] All the synthetic procedures attempted showed an improvement in the polymerisation rate and yield when using this heating method compared to equivalent conventionally heated experiments. For examples, poly(ε-caprolactone)-block-poly(ethylene glycol)-block-poly(ε-caprolactone) (PCL-PEG-PCL) triblock copolymers (with M_n 2.0 X 10^4 g/mol) was synthesised within 1 h using microwave heating by Yu and Liu.[2] Similarly, Zhang *et al.* studied the microwave assisted synthesis of poly(L-lactide)-block-poly(ethylene glycol)-block-poly(L-lactide) (PLLA–PEG–PLLA) triblock copolymers using stannous octoate [$Sn(Oct)_2$] as the pre-catalyst and they showed 92% conversion of lactide monomer at 100 °C giving M_n of 2.82 X 10^4 g/mol within 3 min.[18] However, whilst most of the reports showed improvement in reaction rate of ROP, they did not clearly explain the mechanism behind the improvement in ROP kinetics.

Therefore, this chapter reports the synthesis of an amphiphilic copolymer of ε-DL with hydrophilic mPEG *via* microwave assisted ring opening polymerisation (MROP) methods and these results are compared with those achieved with the conventional heating methods described in previous chapter.

The dielectric properties of the reactants were also investigated to determine the capability of the materials to undergo microwave heating. This is because the ability of a material to absorb microwave energy and so undergo microwave heating depends on the dielectric properties of that material and their concentration in the mixture. Moreover, a solvent-free reaction can be conducted in microwave reactor if one of the reactants is liquid and capable of absorbing microwave energy.

The ε-DL monomer is a liquid and expected to absorb microwave energy, therefore, it should polymerize in the microwave heating as an alternative to conventional heating. The self-assembly behaviour of the synthesised copolymers were also investigated. To the best of our knowledge, this is the first report where microwave heating was used for the synthesis of an amphiphilic block copolymer of ε-DL. The TBD has also been used first time as a catalyst for microwave based ROP.

5.2 Experimental Methods

5.2.1 Measurement of Dielectric Properties

The dielectric properties of the reaction components were measured using cavity perturbation technique as described previously in literature publications.[3] The cavity perturbation measures the change in the quality factor and shift in the resonant frequency of the electric field within a resonant cavity upon introduction of the sample in the cavity. A conventional furnace was used as a heating source to pre-heat the samples prior to their

introduction into the cavity to assess the dependency on dielectric properties on temperature. The sample was heated to the set temperature in the furnace before introducing it into the cavity for determination of dielectric property which is known to vary in a non-linear fashion with temperature. The experimental system consists of the cylindrical copper cavity with the furnace (placed above as heat source) connected to Hewlett Packard 875c vector network analyzer.

5.2.2 Microwave Assisted Ring Opening Polymerisation (MROP)

5.2.2.1 Synthesis of Homopolymer of ε-DL (PεDL)

The homopolymer was synthesised by ROP of ε-DL using propargly alcohol as the initiator, TBD as the catalyst and microwave energy as a heating method. Propargyl alcohol (0.04 g, 0.67 mmol) was transferred to a microwave transparent vessel which contained ε-DL (8 g, 46.99 mmol) under nitrogen atmosphere. The reaction vessel was then placed into the microwave reactor cavity of a CEM discovery reactor with a maximum power of 300 Watts and operating at 2.45 GHz. The reactor's temperature program set point was set to 120 °C temperature and the reaction was stirred to ensure that the contents were uniform. Once the reaction had reached the set point temperature, a solution of TBD (0.20 g, 1.40 mmol) in anhydrous acetone (500 µL) was then added *via* syringe to the reaction mixture. The reaction was continued for 8 h at 120 °C. Samples were taken from melt mixture at a regular interval to monitor the conversion. The synthesised

polymer melt was then terminated by being cooled and quenched by the addition of benzoic acid (0.34 g, 2.80 mmol) in acetone. Following this, the polymer was isolated by precipitation into cold methanol for three times. The obtained polymer was a colourless viscous liquid material with 72.45% (5.83 g) yield.

5.2.2.2 Synthesis of Diblock Copolymers

Synthesis of mPEG-b-PεDL Block Copolymer

In a typical protocol for the synthesis of mPEG-b-PεDL copolymer, ε-DL (10.21 g, 60 mmol) was transferred to a microwave transparent vessel containing mPEG (5 g, 1 mmol) under a nitrogen atmosphere. The reaction vessel was then transferred to the cavity of CEM Discover microwave reactor with a maximum power of 300 Watts and operating at 2.45 GHz. A temperature program pre-set was set to 120 °C and commenced in order to melt and mix the reaction content uniformly. TBD (0.22 g, 1.8 mmol) was then separately dissolved in 500 µL of anhydrous acetone and added into reaction mixture *via* syringe to start the polymerisation once the set point temperature had been reached. For reaction termination and isolation see the Kinetic Experiment description below.

Synthesis of mPEG-b-PCL Block Copolymer

A similar procedure use employed to synthesise mPEG-b-PCL copolymers, ε-CL (5.70 g, 50 mmol) was added into the microwave vessel containing mPEG (5 g, 1 mmol). The reaction was heated to 120 °C and TBD (0.14 g, 1 mmol) was added into reaction to start the polymerisation as described above. For

reaction termination and isolation see the Kinetic Experiment description below.

Kinetic Experiments for the Synthesis of mPEG-b-PεDL Block Copolymer

For the kinetic studies, the reaction was "paused" by switching off the input microwave energy just long enough for samples to be taken from the polymerizing melt at a predetermined times. After the completion of the kinetic experiment, the reaction melts were cooled down and quenched by the addition of benzoic acid (0.34 g, 2.80 mmol) solution in acetone. The polymers were then isolated by being precipitated into cold methanol three times. This crude recovered copolymer was then dissolved in a small volume of acetone followed by re-precipitation in cold diethyl ether and the solvent residue was evaporated under vacuum. The recovered mPEG-b-PεDL copolymer was waxy material with 66.12% (10.05 g) yield while mPEG-b-PCL was a solid material with 88.34% (9.45 g) yield.

5.2.3 Determination of Critical Micelle Concentration (CMC) of Copolymers

The pyrene was used as a fluorescence probe in 1:3 fluorescence ratio methods for determination of critical micelle concentration[19] of mPEG-b-PεDL and mPEG-b-PCL copolymers. GraphPad Prism software (version 6.4) was used for analysing the results. Detailed procedure for CMC determination is given in chapter 2.

5.2.4 Preparation of Blank and Coumarin 6 loaded mPEG-b-PεDL and mPEG-b-PCL Micelles

In a typical protocol, mPEG-b-PεDL or mPEG-b-PCL (50 mg) and coumarin 6 dye (1 mg) were dissolved in acetone (5mL). This organic phase was then added dropwise to a continually stirring volume of HPLC water (10 mL) at a fix rate of 0.5 mL/min. The stirring was continued for 4 h at room temperature, after which the formulation was left to stand overnight in an open vial to ensure complete removal of acetone residues. This micelle solution was then passed through membrane syringe filter (pore size: 220 nm) (Millex-LG, Millipore Co., USA) to remove any aggregates. The formulation was then passed through PD10 desalting column (Sephadex G-25 Medium, GE Healthcare Life Sciences) to remove any small molecular weight impurities (<5K). A portion of the resulting cleaned micellar solution was freeze dried to calculate micelle recovery and dye content (% DyC).

The blank micelles were prepared by the same method where addition of dye was absent.

The nanoprecipitation of the dye was also performed following the same method as described above but where the copolymer was absent from the organic phase in order to determine the intrinsic solubility of the dye in water.

5.2.5 Characterization of the Micelles

The amount of coumarin 6 loaded in the micelles was estimated by dissolving a known amount of micelles (5 mg) in methanol followed by sonication and centrifugation. The supernatant was diluted appropriately with methanol and introduced to a UV-visible spectrophotometer at λ_{max} = 460 nm. A calibration curve was constructed over the quantification range of 2-20 µg/mL in methanol (Beckman Coulter DU 800 UV spectrophotometer) (Figure 5-1).

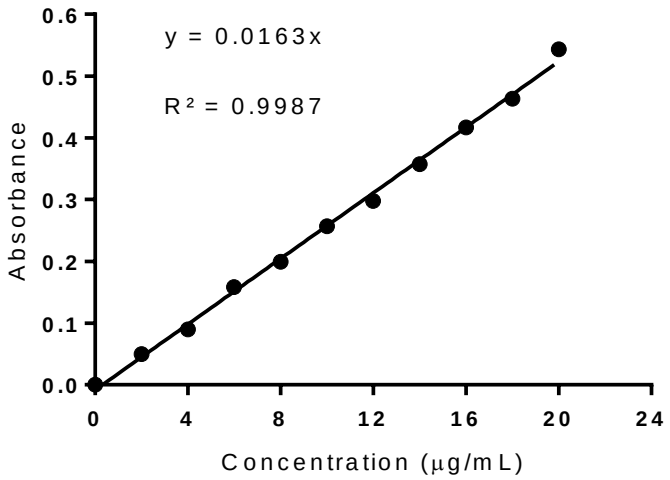


Figure 5-1 Standard calibration curve of coumarin 6 in methanol at wavelength (λ_{max}) of 460 nm.

Size, size distribution and polydispersity of the prepared micelles were determined by dynamic light scattering (DLS) method at a polymer concentration of 0.5 mg/mL in HPLC grade water using Malvern NanoZS instrument. Surface zeta potential was measured in HEPES 10mM buffer (pH-7.4) using the same instrument. The surface morphology and size were

confirmed by TEM images. The samples were imaged without staining of the samples on TEM grid. The size analysis on TEM images were performed using Image J software. The full experimental characterization procedures are given in chapter 2.

5.2.6 Cytotoxicity and Cell Uptake Study

The toxicity of the micelles was performed on C3A cells by fluorescent based 3 in 1 assay by the same procedure as described in chapter 3. All experiments were repeated in triplicate and results were reported as mean with standard deviations. GraphPad Prism 6 was used to analyze the data.

The cellular uptake study was performed on C3A cells according to the protocol described in chapter 3. All experiments were repeated in duplicate and the uptake was examined using Zeiss LSM880 confocal microscope.

5.3 Results

5.3.1 Measurement of Dielectric Properties of the Reagents

The dielectric properties of the reagents were evaluated to determine the ability of the materials to absorb microwave energy and convert this into heat at a given frequency (2.45 GHz). These properties are known to depend on the temperature and both physical and molecular nature of the materials. Thus the measurements were made for a temperature range of ambient to 140 ^{o}C, which included the target set point temperature. The dielectric constant (ε'), dielectric loss (ε'') and loss tangent (tan δ) were all assessed.

The plot of ε' as a function of temperature at 2.45 GHz (the ISM frequency at which the Discover Reactor operates) is shown in Figure 5-2.

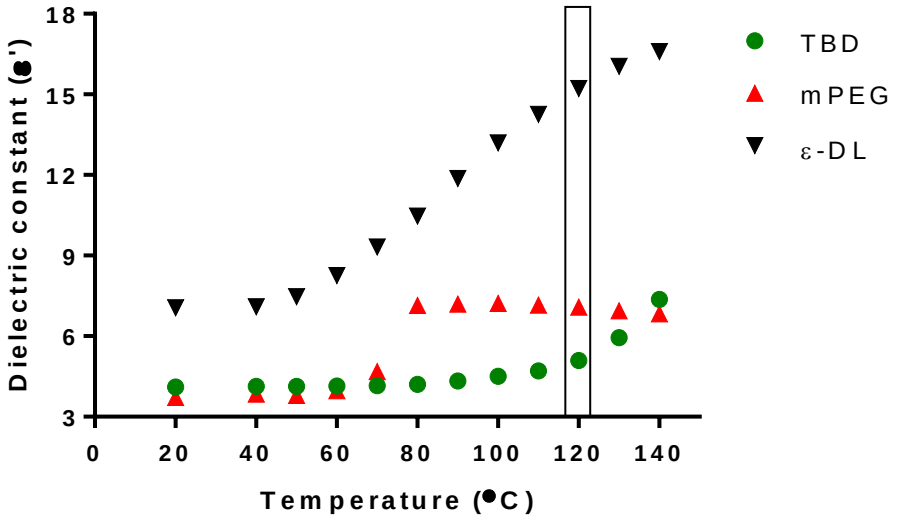


Figure 5-2 Dielectric constant (ε') of monomer, initiator and catalyst at various temperatures

The ε' was observed to increase as the temperature increased for all the materials. Indeed, the ε-DL monomer was found to exhibit significantly higher values compared to other reagents at selected reaction temperature of 120 °C. It indicates the higher microwave absorbing capability of the ε-DL monomer compared to other reactants. This might be due to polar ester bond of the monomer which might help in the absorption of microwave. The dielectric constant of ε-CL monomer was not determined as it has already been known to absorb microwave.[3] The selection of the reaction temperature also depended on the dielectric loss and loss tangent. The dielectric loss (ε'') against the temperature at 2.45 GHz is shown in Figure 5-3.

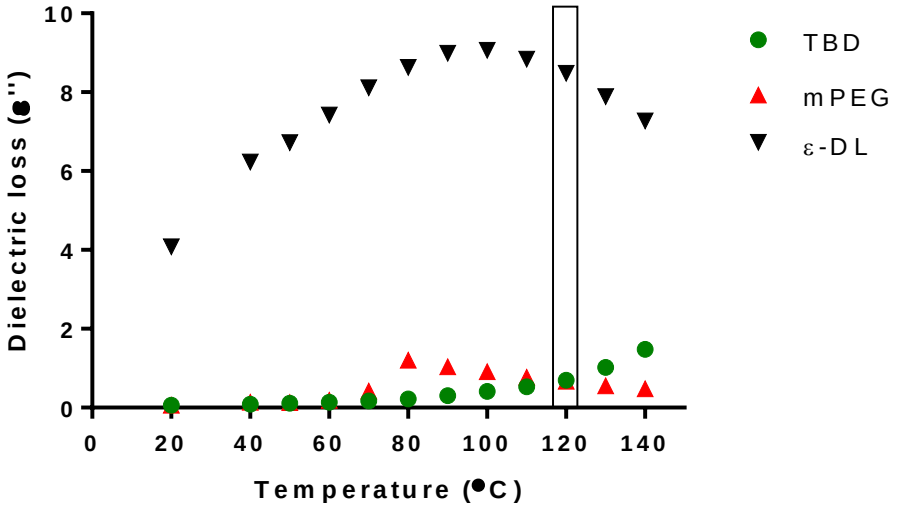


Figure 5-3 Dielectric loss (ε'') of monomer, initiator and catalyst determined at various temperatures

The ε-DL (reacting monomer) has shown to exhibit a significantly higher value of ε'' compared to other reacting materials. The ε'' of ε-DL monomer was observed to be increased with increasing the temperature upto 100 °C followed by decrease in the ε'' value. However, it showed around 12 times higher value of ε'' at 120 °C compared to the other reacting materials and thus can efficiency transfer absorbed microwave energy into the heat. The TBD also demonstrated an increased ε'' value with increasing temperature with a similar value point to that of the initiator found to be at around 120 °C. Thus, this was chosen as the reaction temperature as both these components vital for initiation both exhibit similar abilities to convert the stored energy they gain into heat. The loss tangents (tan δ) for starting materials at different temperatures at 2.45 GHz are shown in Figure 5-4.

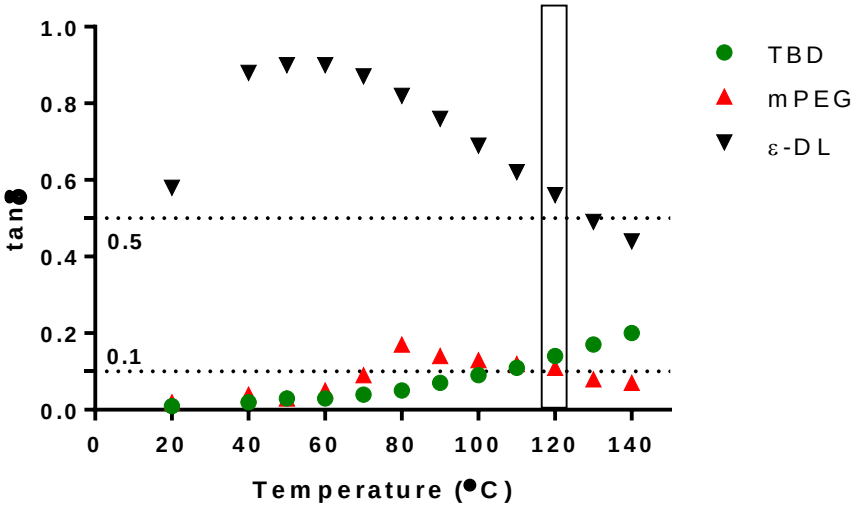


Figure 5-4 Loss tangent (tan δ) of monomer, initiator and catalyst at various temperatures

This property is calculated as a ratio of dielectric loss factor (ε'') to dielectric constant (ε') i.e. tanδ= ε''/ ε.' The monomers showed a tan δ > 0.5 up to 120 °C. The tan δ value for the initiator and catalyst was also found to increases with increasing the temperature. At 120 °C, the initiator and the catalyst showed tan δ ≥ 0.1 which is the point at which the materials are described as being microwave active or "lossy",[3] thus again underpinned the choice of 120 °C as the reaction temperature. Table 5-1 shows all the dielectric properties of the starting material at 120 °C.

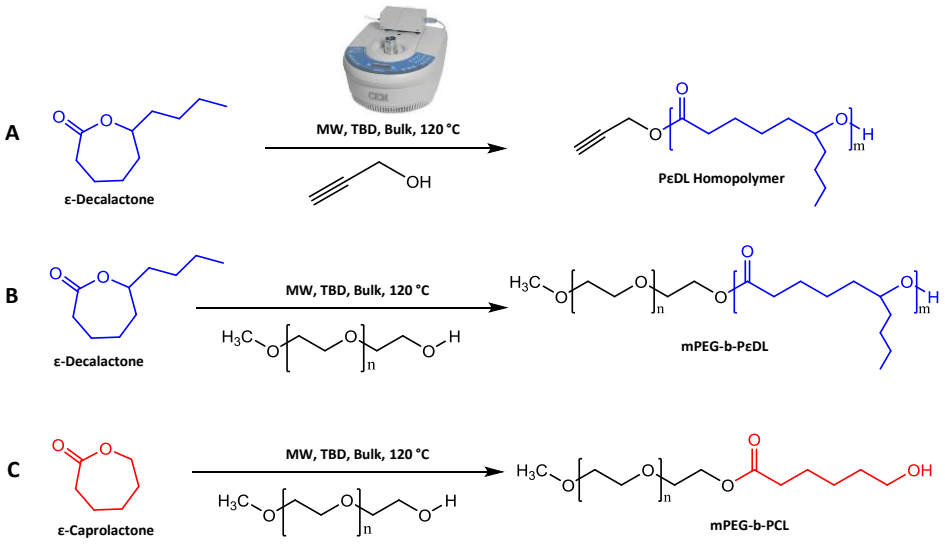
Table 5-1 Dielectric properties of all the starting materials at 2.45 GHz frequency at 120 °C

Materials	Dielectric constant (ε')[a]	Dielectric loss (ε'')[a]	Loss tangent (tan δ)[b]
mPEG 5000	7.1	0.7	0.1
ε-DL	15.2	8.5	0.6
TBD	5.1	0.7	0.1

[a] Determined by cavity perturbation technique
[b] Determined by formula tan δ= ε''/ ε

5.3.2 Microwave Assisted Ring Opening Polymerisation (MROP)

The results of the dielectric properties of the reagents were used to plan and interpret the results from the synthesis of polymer in microwave reaction. The polymers were synthesised in bulk to maximise the sustainability of the manufacturing strategy, i.e. no solvent was used reducing the VOC (volatile organic compounds) footprint of the procedure and minimising waste from the process. The synthetic route of the homopolymer and copolymers are depicted in Scheme 5-1



Scheme 5-1 Synthesis of ε-DL homopolymer (A), ε-DL copolymer (B) and ε-CL copolymer (C) catalysed by TBD in bulk using different initiators in MROP.

The microwave energy was introduced into the microwave vessel at the maximum power rating available from the reactor (300W) to rapidly increase the temperature to the target set point. The reaction temperature was measured using a fibre optic probe. The reaction mixture was observed to heat up almost instantly and reached to the experimental temperature of

120 °C within 50 sec. Figure 5-5 shows the power and temperature of the reaction against time for the first 50 sec in the microwave reactor. After this, a very low power level (between 1-30W) was needed to maintain the temperature.

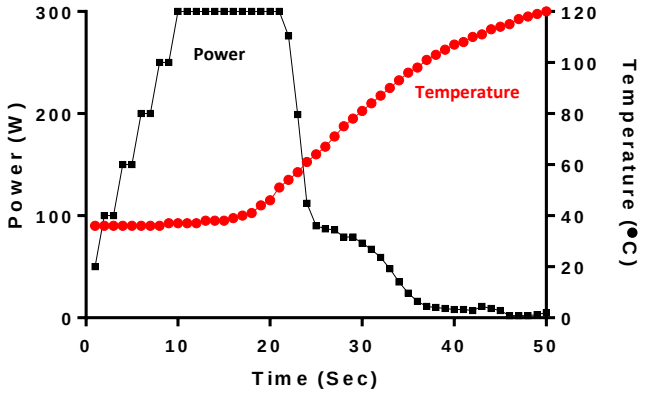


Figure 5-5 Microwave heating profile for the reaction mixture (ε-DL, mPEG and TBD) for 50 sec

The results of the microwave assisted ring opening polymerisation (MROP) of ε-DL and ε-CL on mPEG5k initiator using TBD are detailed in Table 5-2. The data of the conventional synthesis method described in previous chapter are also included so that they can be compared against those of the microwave based method to determine the relative efficacy of the two methods. The microwave method for ε-DL polymerisation showed an improvement on the polymerisation rate by reducing the reaction time by half compared to time required for the conventional heating. In practice this constitutes a reaction time saving of 6 h. By comparison, ε-CL polymerisation required only 2 min for get conversion to over 90% conversion compared to the 10 mins required in the conventional heating polymerisation method.

Table 5-2 Summary of experimental details and molecular weight obtained after ROP of ε-Decalactone and ε-Caprolactone using TBD as a catalyst.

Run	Heating Method	TBD Catalysts (mol%)	Polymer	[M]/[I][a]	Conversion (%)[b]	Time	T (°C)	Theoretical Mol. Wt. (g mol^{-1})	M_n^{NMR} ($gmol^{-1}$)[c]	M_n^{GPC} ($gmol^{-1}$)[d]	PDI[e]
1	Microwave	3	PεDL	70	94	6 h	120	12.0 K	11.2 K	6.0 K	1.07
2	Microwave	3	mPEG-b-PεDL	60	86	6 h	120	15.2 K	10.4 K	17.7 K	1.20
3	Microwave	2	mPEG-b-PCL	50	92	2 min	120	10.7 K	10.2 K	17.4 K	1.17
4	CH	3	PεDL	70	92	12 h	120	12.0K	11.0K	7.9K	1.09
5	CH	3	mPEG-b-PεDL	60	89	12 h	120	15.2 K	10.3 K	16.2 K	1.15
6	CH	2	mPEG-b-PCL	50	93	10 min	120	10.7 K	10.2 K	17.0 K	1.48

CH= Conventional hot plate heating [a]Monomer:Initiator ratio in feed; [b]Conversion determined by ^{1}H NMR; [c]Number average molecular weight (M_n) determined by ^{1}H NMR; [d]Number average molecular weight (M_n) determined by GPC; [e]Polydispersity index (M_w /M_n) determined by GPC

The kinetics of these reactions were then determined by conducting ^{1}H NMR analysis on samples removed at a regular intervals. The level of conversion that had been achieved was easily followed by comparing peak intensities of ε protons of ε-DL monomer both before and after conversion within the ^{1}H NMR spectrum as described in chapter 4 (Section 4.3.1). Figure 5-6 shows the kinetic data from the reaction when microwave energy was used as a heating source. The samples were taken at a regular interval (2 h) and the conversion was determined by ^{1}H NMR spectroscopy. The absence of TBD peaks in the purified polymer indicated the polymer was free from The apparent rate constant (k_p) for microwave and CH reactions for mPEG-b-PεDL synthesis were determined from gradient of the liner relationship obtained from plotting the log monomer conversion ratio ($In([M]_0/[M])$ against time (Figure 5-7). The k_p of ε-DL polymerisation in the CH method was determined to be 0.18 h^{-1}, whilst when microwave was used as a heating method it was observed to have been increased to 0.40 h^{-1}. In fact, nearly 80% monomer got converted in 4 h in the microwave experiment while it took nearly 10 h in CH for ε-DL polymerisation to reach the same point (Figure 5-6).

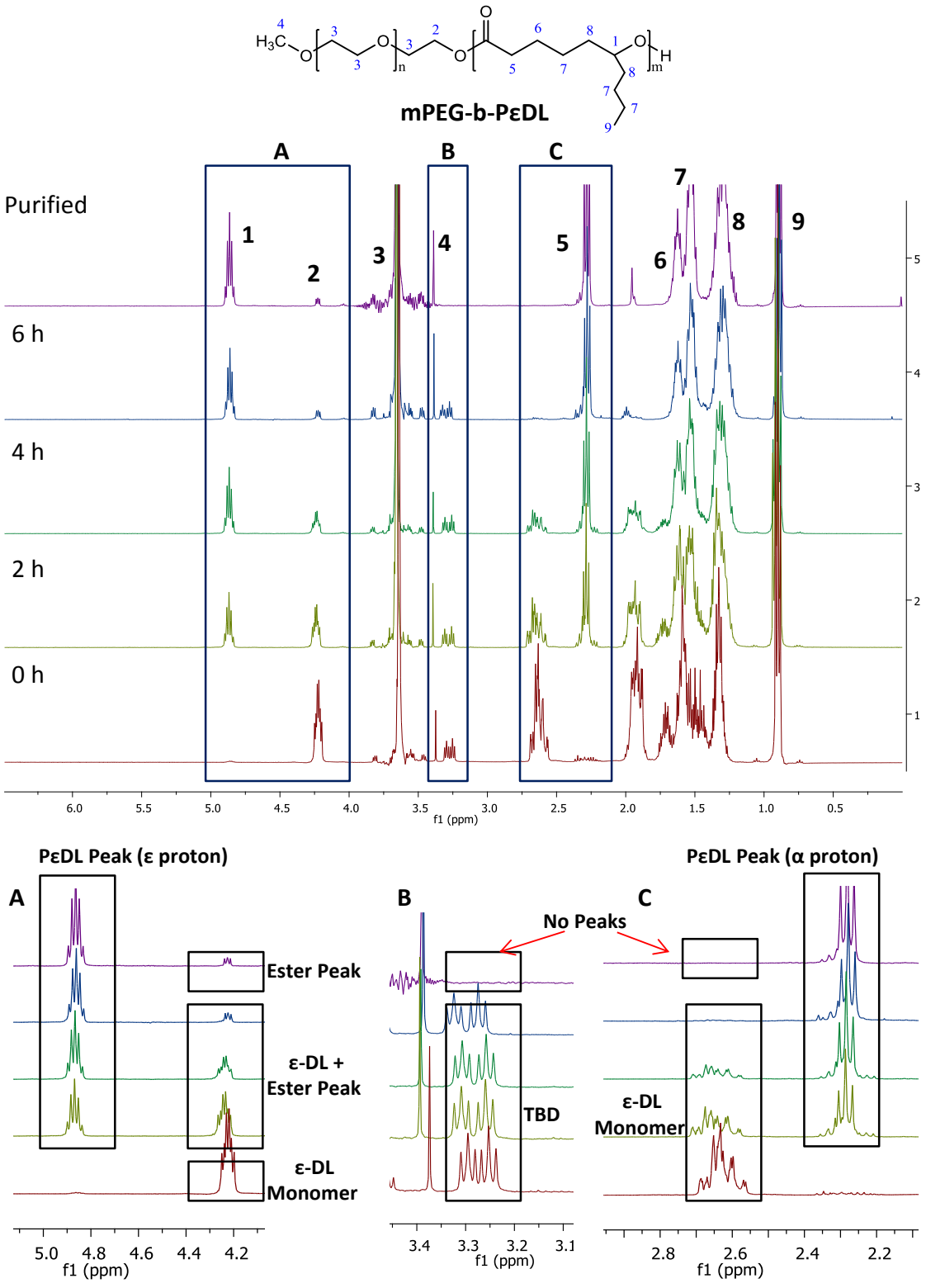


Figure 5-6 Kinetics behaviour of ε-DL polymerisation based on MROP

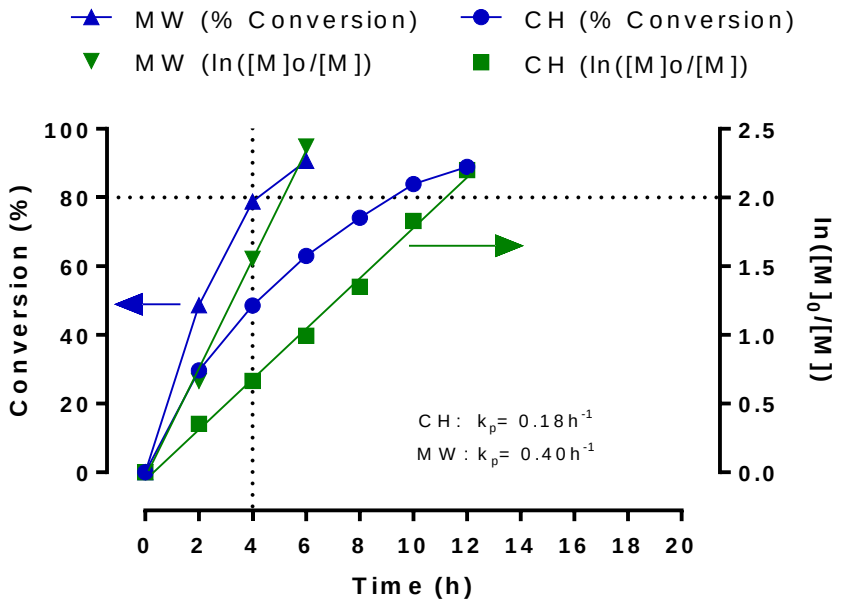


Figure 5-7 Reaction kinetic of ε-DL polymerisation on mPEG initiator using microwave and CH methods

The comparison of ε-DL polymerisation against ε-CL in microwave revealed that the ε-CL conversion took only 2 min to polymerize > 90 % of monomers whereas ε-DL needed 6 h for > 85 % of monomers conversion. Despite the higher of ε-DL (used high M/I feed ratio), the purified polymer showed lower degree of polymerisation (DP) (Table 5-2). A small shoulder in the GPC graph indicated some traces of impurity/by-product in the mPEG-b-PεDL copolymer (Figure 5-8). The traces of impurity were also observed when the same copolymer was synthesised by conventional heating method. The GPC analysis underestimated the M_n of PεDL homopolymer and overestimated the M_n of mPEG-b-PεDL copolymer compared to M_n estimated by ^{1}H NMR. Moreover, a higher PDI was observed for mPEG-b-PCL copolymer in CH method compared to MROP method (Table 5-2).

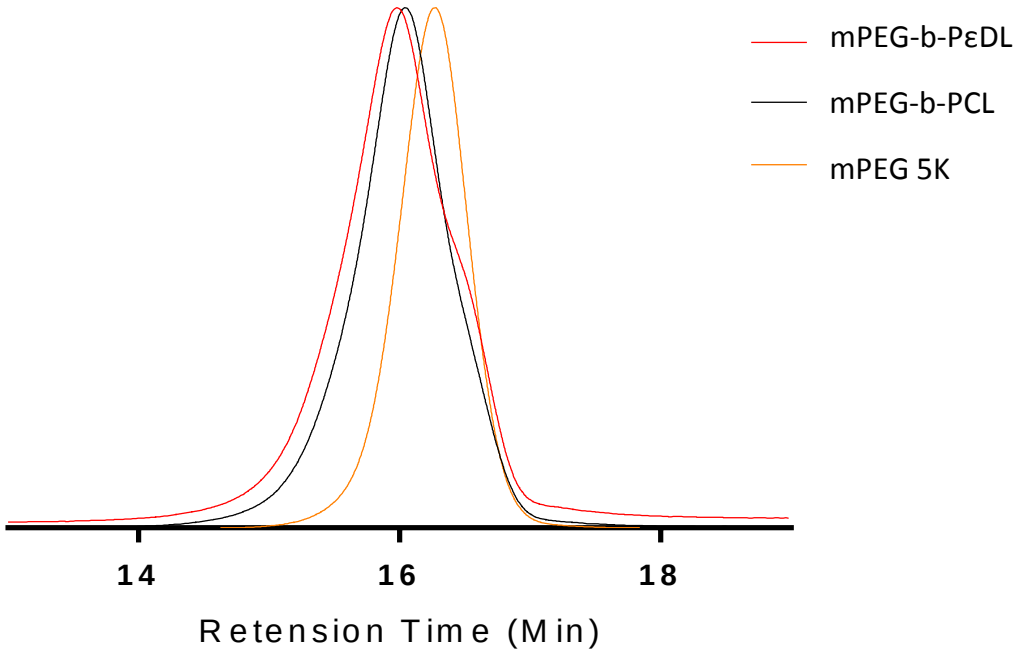


Figure 5-8 GPC traces of mPEG 5000, and synthesised copolymers made by MROP method

The ^{1}H NMR of copolymers was also determined in D_2O and compared with $CDCl_3$ to collect evidence for micelles formation. The peak signals of the protons of the hydrophobic blocks (PεDL and PCL block of copolymers) were found to be suppressed in D_2O where copolymers exist in micelles form (hydrophobic block surrounded by hydrophilic block). On the other hand the peak signals of the protons of hydrophobic blocks (PεDL and PCL block of copolymers) were present in the $CDCl_3$ where the copolymers exist as separate single chain entity (Figure 5-9).

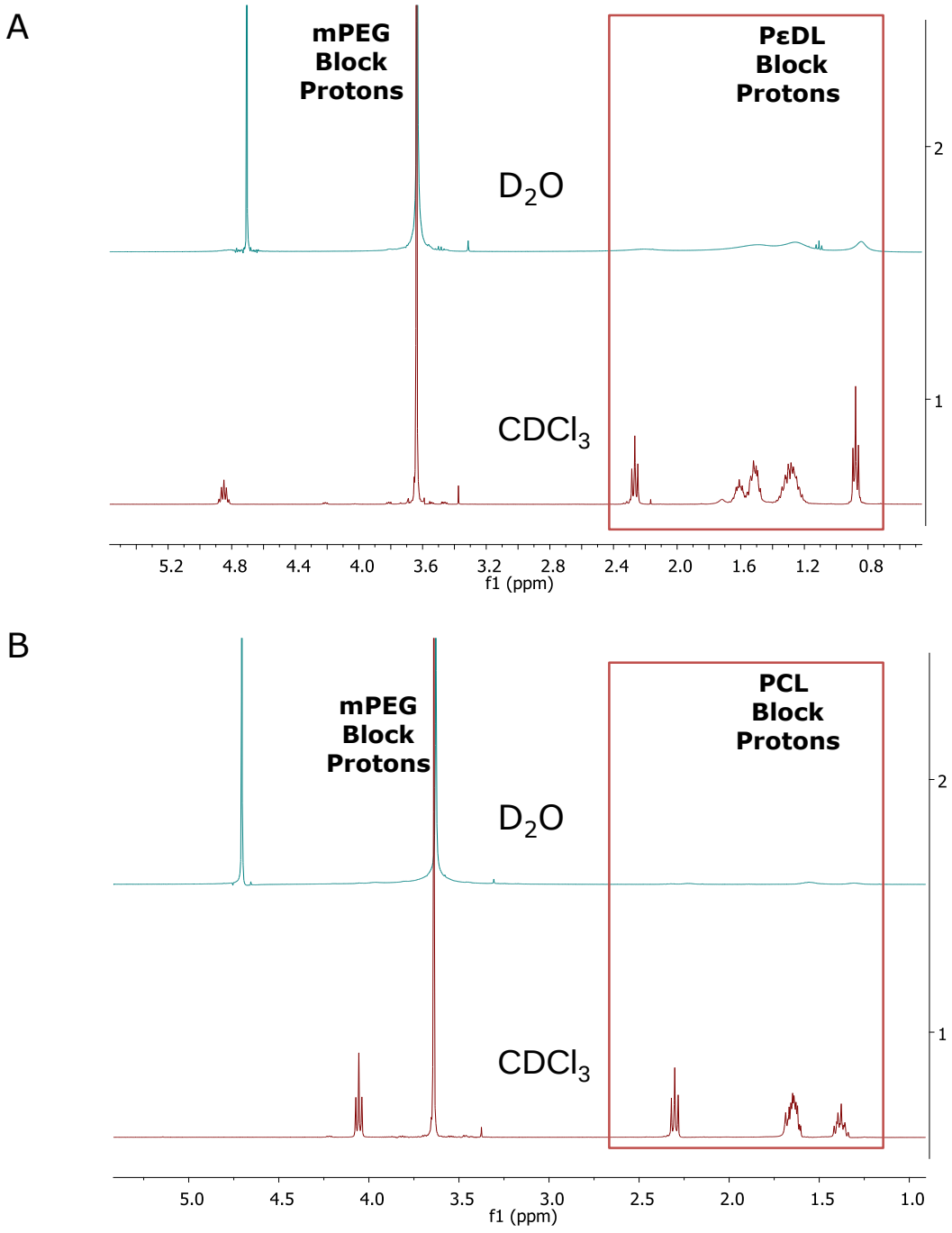


Figure 5-9 Comparison of ^{1}H NMR in D_2O and $CDCl_3$ solvent (A) mPEG-b-PεDL copolymer (B) mPEG-b-PCL copolymer

5.3.3 Determination of CMC of the Block Copolymers

Intensity ratio values (mean value) for peak 1 and 3 of fluorescence spectrum of pyrene acquired for different concentrations of polymers are given in Table 5-3.

Table 5-3 Intensity ratio values for peak 1 and 3 of fluorescence spectrum of pyrene acquired in different concentrations of polymers

Log C (mg/L)	Intensity Ratio (I_1/I_3)	
	(mPEG-b-PεDL)	(mPEG-b-PCL)
0.01	1.5851	1.5872
0.05	1.5658	1.5861
0.10	1.5545	1.5814
0.50	1.4519	1.5458
1.00	1.3683	1.5285
2.00	1.3446	1.3893
4.00	1.3340	1.3360
6.00	1.3432	1.2314
8.00	1.3445	1.2156
10.00	1.3351	1.2183
15.00	1.3364	1.2171
20.00	1.3375	1.2184
50.00	1.3342	1.2172

A graph containing the plot of the Log of the polymer concentration (mg/L) against the peak intensity ratio (i.e. of I_1 to I_3) for pyrene was used to determine the CMC. The curve obtained was fitted using a non-linear regression (Sigmoidal, 4PL, X is on log scale) to determine the point of inflection (IC50) which indicated an abrupt change in value and hence was attributed to be the CMC of the copolymer (Figure 5-10).

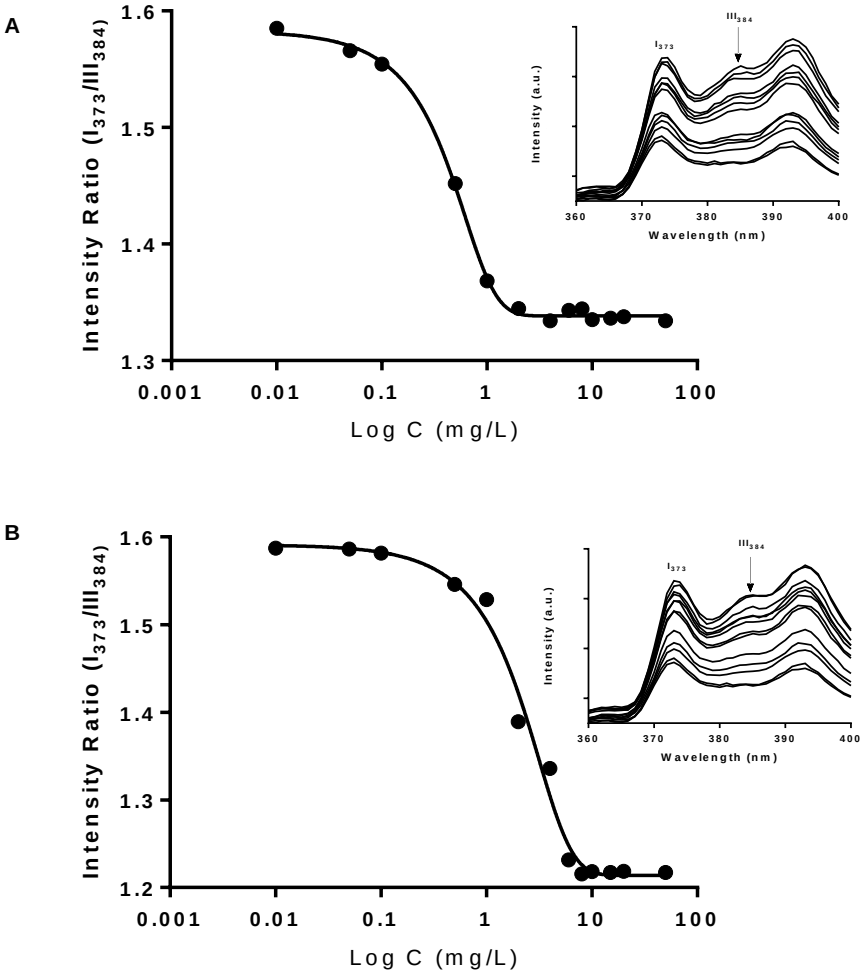


Figure 5-10 CMC plot for (A) mPEG-b-PεDL and (B) mPEG-b-PCL obtained by pyrene 1:3 peak ratio method.

A significant difference was observed between the CMC values for the copolymers ($P<0.05$, unpaired student's t test) containing the two lactone monomers (ε-DL and ε-CL). The CMC of mPEG-b-PCL copolymer micelles was observed to be more than double of the mPEG-b-PεDL equivalents (Figure 5-11).

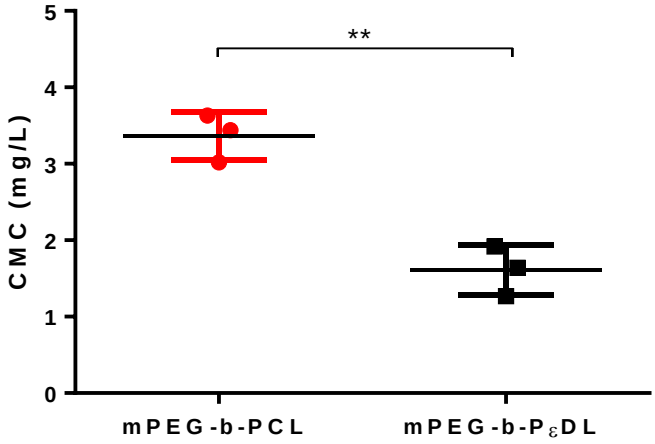


Figure 5-11 Comparison of 95% confidence interval (IC50) of the CMC. IC50 value was obtained by non-linear curve fitting of CMC plot (sigmoidal, 4PL).

5.3.4 Preparation and Characterization of Blank and Loaded Micelles

In order to use the copolymers as drug delivery vehicles, it is important to evaluate the loading capability and self-assembling properties of the two types of copolymer. A significantly higher dye loading was observed in mPEG-b-PεDL micelles compared to mPEG-b-PCL micelles. Although, the overall dye loading was low in both of the copolymers. In the assay used to determine the level of drug incorporated into the micelles, the intensity of the green-yellow colour in the formulation indicates the drug loading in the micelles. To gauge the base line colour that was attributed to the presence of the dye alone, the dye was precipitated in the water when the polymer was absent from the nanoprecipitation formulation which was observed to give rise to a transparent, clear solution upon filtration with a 0.22 μm filter (Blank formulation) (Figure 5-12).

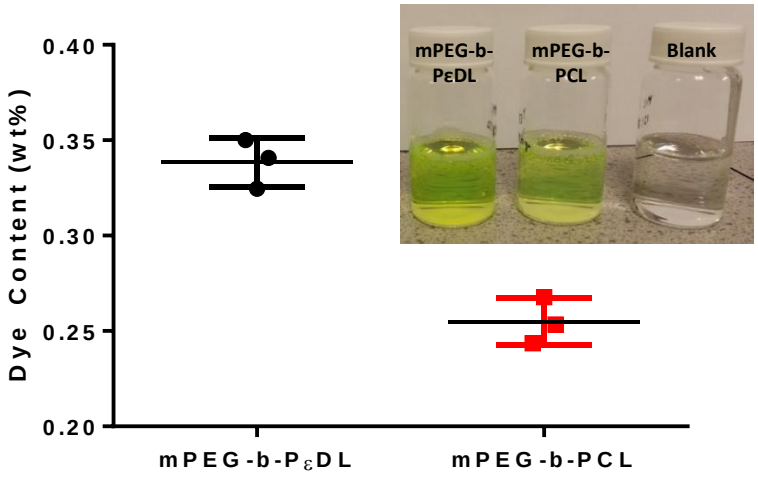


Figure 5-12 Coumarin 6 loading in different copolymers. Each point represents mean ± SD (n=3). A significant difference ($P < 0.05$, unpaired student's t test) was observed. Picture shows the micelle formulations. No dye was detected in blank where polymer was absent.

The self-assembling property of the copolymers was determined by subjecting them to analysis *via* TEM and dynamic light scattering (DLS) techniques (Table 5-4). The hydrodynamic volume of micelles made from mPEG-b-PεDL micelles was 38 nm which was significantly higher than the 31 nm recorded for the mPEG-b-PCL micelles. Furthermore, it was noted that the micellar size of both systems were not significantly changed by drug loading compared to unloaded micelles ($P > 0.05$, unpaired student's t test) of the same polymers. The samples were defined to exhibit a single peak in the DLS of narrow polydispersity, for both of the micelles formulations.

Table 5-4 Characteristics of empty and Coumarin 6 loaded block copolymer micelles

Polymer[a]	CMC (µg/mL)	Empty micelle		Dye Content (wt%)± SD	Coumarin 6 loaded micelles	
		Average Size (nm)[a]	PDI[b]		Average size (nm)[a]	PDI[b]
mPEG-b-PεDL	1.58[c]	38 ± 3[c]	0.13 ± 0.02	0.33 ± 0.12 [c]	40 ± 5 [c]	0.17 ± 0.02
mPEG-b-PCL	3.70	31 ± 3	0.15 ± 0.01	0.25 ± 0.15	32 ± 4	0.18 ± 0.02

[a] Intensity mean by Dynamic Light Scattering (DLS) Technique. [b] Polydispersity index (PDI) by DLS. [c] Significant difference from mPEG-b-PCL ($P < 0.05$, unpaired student's t test). SD=Standard deviation

TEM image of the empty micelles shows a uniform distribution of the spherical micelles for both of the copolymers with well-defined clear boundary. The size of the micelles of both the copolymers were <60nm analysed Image J software. There were no sign of aggregation seen in the micelles samples (Figure 5-13).

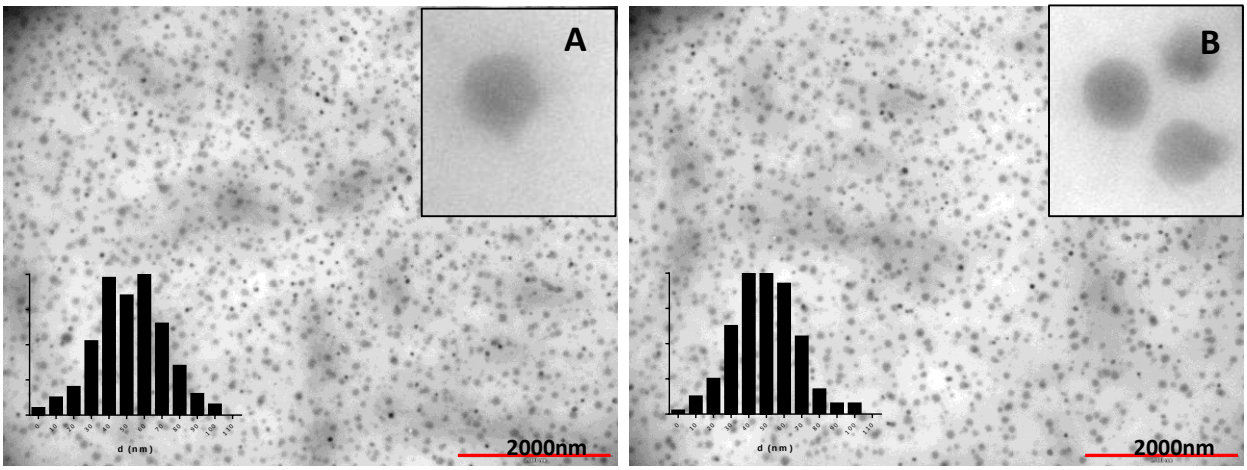


Figure 5-13 The TEM Images of empty micelles with size distribution histogram (using Image J software) and (A) mPEG-b-PCL micelles, (B) mPEG-b- PεDL micelles. The images were taken without staining. Scale bar – 2000nm.

5.3.5 Cytotoxicity and cell uptake study

The toxicity of the micelle was observed by determining the Alamar Blue, CFDA-AM, and Neutral Red dye uptake in the cells using fluorescent based method on C3A cells (human hepatocellular carcinoma). All three methods have shown the cell viability more than 80% in the concentration range from 4.6 to 300 μg mL^{-1} (Figure 5-14). Therefore, the micelles were considered as safe to be used for cell uptake study.

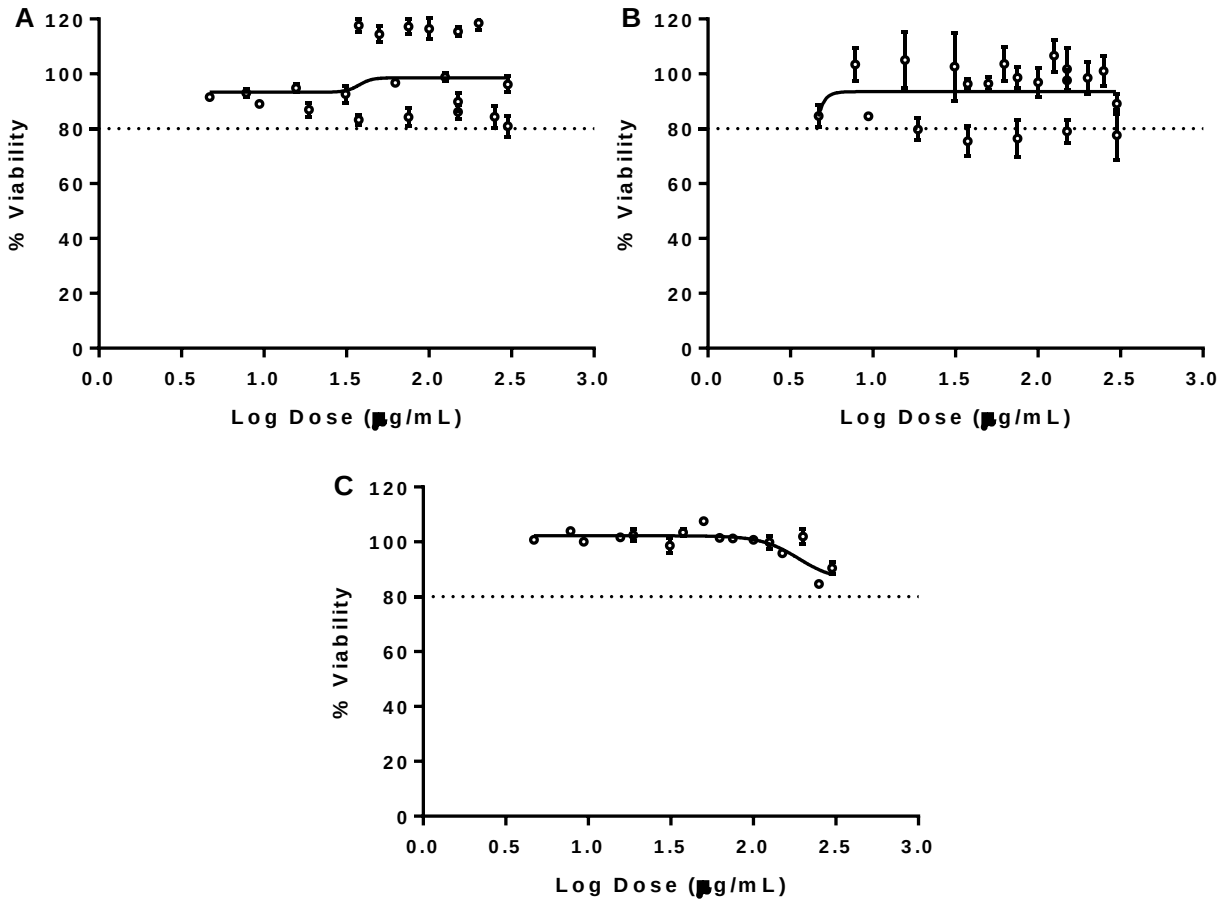


Figure 5-14 The C3A hepatocytes cell viability test following the exposure of mPEG-b-PDL micelles (at concentrations ranging from 4.6 to 300 µg mL^{-1}) for 24 h using Alamar Blue (A), CFDA (B) and Neutral Red (C) assays. Data are expressed as % viability ± SEM (n = 3 minimum).

The endocytic internalization of the dye loaded micelles was studied to evaluate their potential for use as vehicles for delivery of hydrophobic molecules inside the cells. The cell imaging of dye loaded micelles in C3A cell suggested that micelles were taken up by the cells in the early stage of study (within 10 min). The micelles were internalized progressively over the study time points (see Figure 5-15). The micelles were present inside the cells in cytosol and some of them are concentrated on the surface of the

nucleus while no particles were present inside the nucleus even after 1440 min of study time.

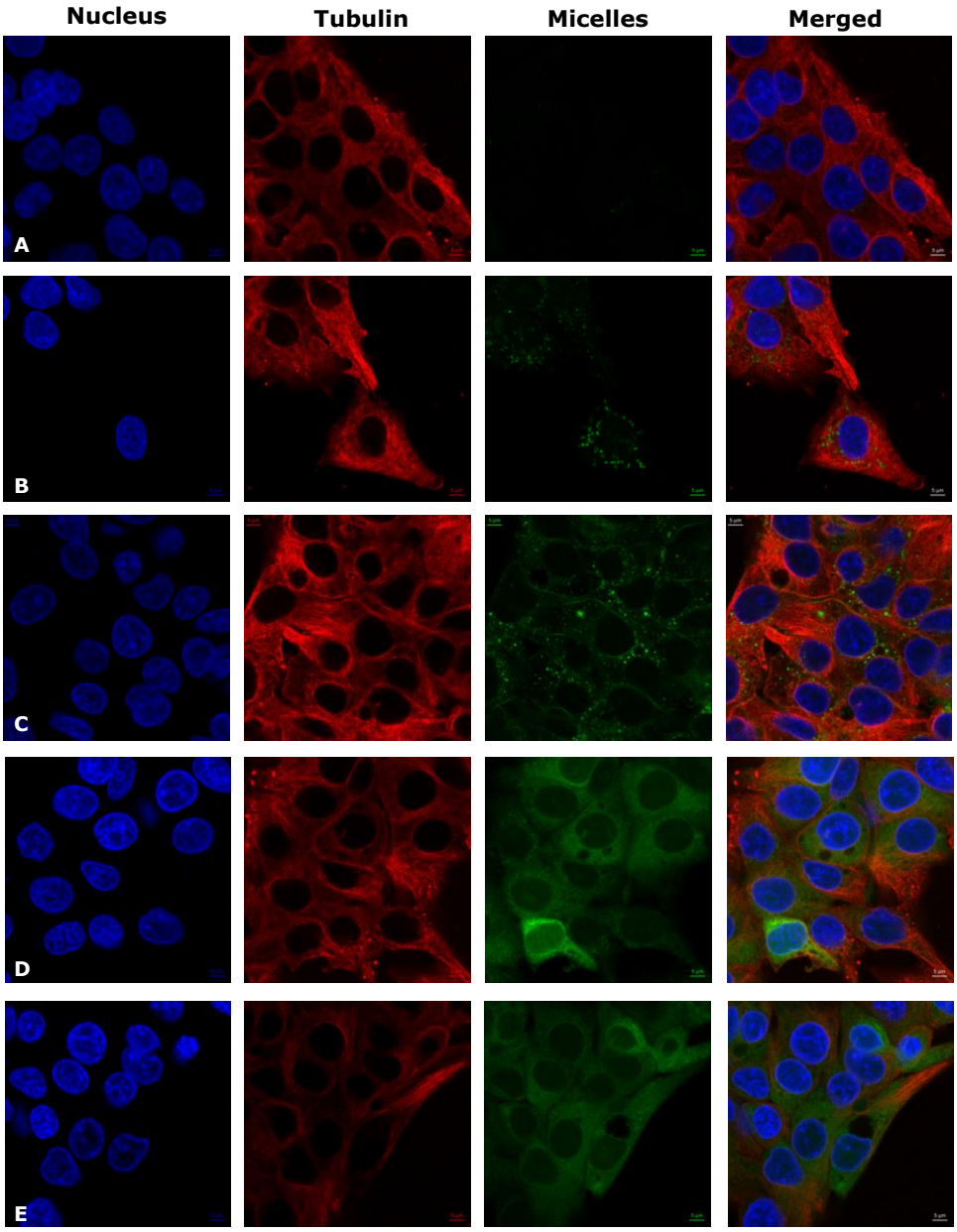


Figure 5-15 The time dependent uptake of coumarin 6 labelled mPEG-b-PεDL micelles by C3A (human hepatocellular carcinoma) cell lines. Cells were treated with cell medium (A) or micelles for 10 min (B), 60 min (C), 240 min and (D) 1440 min and then stained for the tubulin cytoskeleton (red) and nucleus (blue). The green colour showed by coumarin 6 loaded micelles.

5.4 Discussion

Microwave heating has been reported to provide the potential to deliver a clean, green and convenient method of heating, which often results in short reaction time with higher yields and reduced By-product formation. Hence, the copolymers based on renewable ε-DL and non-renewable ε-CL were synthesised by a microwave method and the characteristics of both the reactions and the final products were compared against those of conventional heating equivalents. It was proposed that the polar ester groups within the monomers would favours the absorption of the microwave energy and hence ensure that they could be heated in the reaction mixture uniformly, i.e. they would undergo selective heating throughout the entire volume of the reaction mixture. In so doing it would remove the potential for developing temperature gradients within the bulk of the reaction media. To determine the ability of the material to absorb microwave energy, the dielectric properties of the starting materials and the catalyst have been determined. These properties included the dielectric constant (ε'), dielectric loss (ε'') and loss tangent (tan δ). These properties are known to vary with temperature and enable a prediction to be made relative to the potential ability of the materials to both absorb microwave energy and convert it into heat at a given frequency (2.45 GHz – the operating frequesncy the the CEM reactor used). The ε-DL monomer was determined to have significantly higher dielectric constant (ε') (ability of a material to store absorb and

electrical potential energy) and dielectric loss (ε'') (ability of a material to convert electromagnetic energy into heat) with increasing the temperature when compared to the initiator and the catalyst. The ratio of these two components describes the loss tangent (tan δ= ε''/ ε) value which indicated the ability of the material to heat the reaction system. Based on its value, a compound may have: significant (0.1 < tan δ) or low (tan δ < 0.1) microwave heating capability. The microwave absorbing capabilities for monomer (ε-DL) was found to decrease as a function of temperature. However, it was optimum upto 120 °C where tanδ value was >0.5 indicating a high microwave absorbing capability. At the same temperature, the tan δ values of initiator and catalyst were found to increase as temperature increased also established a tan δ ≥ 0.1, which demonstrates that the initiator and catalyst also had a significant potential to contribute in the microwave heating of the reaction system. In short, at the selected reaction temperature (120 °C), all the reacting materials were predicted to have significant potential to contribute to the overall microwave heating and hence this was selected as a reaction temperature. The reaction was conducted in the bulk as the ε-DL monomer (liquid physical form) was able to dissolve the other reaction material and to make synthetic strategy more sustainable. The reaction temperature was reached within the 50 sec of the reaction mixture being introduced to the microwave reactor indicated a high efficacy of the starting materials to absorb microwave energy. The

copolymer of ε-CL was also synthesised. The dielectric property of the ε-CL had already been published and shown to be microwave absorbent (tanδ>0.1) at 120 °C.[3] Moreover, they had also shown that it was possible to accelerate the polymerisation of polymerised ε-CL in a microwave reactor.

The comparison of ε-CL polymerisation against ε-DL polymerisation in microwave revealed that the ε-CL conversion took only 2 min to polymerize >90% of monomers whereas ε-DL needed 6 h for >85% of monomers conversion. Being a structural analogue of ε-CL, it was anticipated that the ε-DL will react faster during MROP. However, a longer reaction time was needed to complete the conversion. This might be due to the presence of an extra butyl chain in the ε-position of biobased ε-DL monomer. This chain prevents the availability of alcohol by steric hindrance during MROP reaction. The other possible reason for the lower reactivity might be the generation of secondary alcohol upon opening of ε-DL ring on mPEG (1^{st} mer) which act as an initiator for further addition of monomers. Additionally the increased hydrocarbon character will make ε-DL more hydrophobic thus it may be less miscible with the more hydrophilic alcohol based initiators. Thus, ε-CL's faster reactions were attributed to a combination of (a) the absent of any alkyl chain thus reduced steric clutter around the reaction centre, (b) that it generates primary alcohol which can react faster compared to secondary alcohol on ε-DL and (c) it is more miscible with the initiators.

The comparison of the microwave against conventional hot plate heating method for ε-DL polymerisation revealed that the polymerisation in microwave requires just 6 h compared to 12 h for conventional hot plate heating method. The microwave can transfer energy directly to the reacting materials whereas CH involves the heating of the wall of the container by convection and conduction mechanism hence the core of the bulk material takes a longer time to achieve the required temperature. The apparent rate constant (k_p) was 2.25 times higher for microwave compared to CH method for ε-DL polymerisation revealing the higher capability of the microwave method. In this case the selective heating of the reaction components was proposed to overcome the steric barriers created by the presence of the hydrocarbon branch in this monomer or the lower reactivity of the secondary hydroxyl group. This conclusion was supported by the results for the ε-CL polymerisation in microwave method which proved to be very efficient where it took 2 min to convert >90% of the monomer to give copolymer with M_n^{GPC} 17.4 X 10^3 (PDI 1.17). By comparison, the CH method required 10 min to convert >90% of ε-CL to give M_n^{GPC} 17.0 X 10^3 with higher polydispersity (PDI 1.48). This indicates that the microwave was 5 times more efficient than CH method for ε-CL polymerisation. This also showed that by removing the steric clutter and/or providing a primary hydroxyl with higher reactivity produced an increased differential in the benefits obtained from selective microwave heating.

The stability of the micelles is an important aspect to be used as a delivery vehicle. Micelles are said to be thermodynamically stable if they have copolymer concentration above their CMC. CMC is a concentration where copolymer molecules begin to come together to from micelles due to hydrophobic-hydrophobic interaction forces. The CMC value for mPEG-b-PεDL micelles was observed to be lower compared to mPEG-b-PCL micelles. A similar results has also been illustrated where a lower CMC was noted for alkyl chain-substituted poly(lactide) copolymers than unsubstituted poly(lactide) copolymer.[20] However, a previous literature publication by Glavas *et al.* reported an opposite result to the one reported here; they observed a higher CMC for mPEG-b-PεDL micelle compared to mPEG-b-PCL micelles. However, they used a lower molecular weight of hydrophilic and hydrophobic block (2K each). Thus a lower CMC of the mPEG-b-PCL micelle in this case would be anticipated due to the crystallinity of the PCL core (2K) which acted as a driving force for self-assembly. On the other hand, the alkyl side chains in the PεDL core (2K) were postulated to disrupt the self-assembly process which gave a higher CMC for mPEG-b-PεDL micelle.[21] Our study involved higher molecular weight of the hydrophilic (5K) and hydrophobic blocks (5K) and hence higher overall molecular weight copolymers than those used by Glavas *et al.* Therefore, as the length of the hydrophobic block in the copolymer can change the crystallinity and hydrophobicity, it can affect the micelles CMC. Thus, the opposite results can

be explained by two reasons. The first reason might be the molecular weight of PCL in the copolymer which can affect the crystallinity of the core. The lower molecular weight PCL tends to crystallize more than the higher molecular weight.[22] This explains that the use of higher molecular weight PCL might reduce the crystallinity and hence there are less driving forces for self-assembly leads to higher CMC of mPEG-b-PCL micelles. The other reason might be the higher hydrophobicity of the PεDL core in mPEG-b-PεDL micelles due to higher molecular weight of PεDL block. The higher molecular weight PεDL can exert a higher hydrophobic phase separation driving force which can easily overcome the disruption effect of alkyl chain which can lead to the overall reduction in the CMC of the mPEG-b-PεDL copolymer. The study suggested that at higher molecular weight and their hydrophobicity characteristics acted as the dominant factors that define the CMC rather than the crystallinity. Previously, we have also shown a similar CMC pattern where mPEG-b-PδDL micelles showed lower CMC compared to mPEG-b-PCL micelles which confirms our hypothesis.[23]

In order to use the copolymers as delivery vehicles, it is important to evaluate the self-assembling property of the copolymer. The self-assembling properties of the copolymers were determined using ^{1}H NMR (in $CDCl_3$ and D_2O solvent), dynamic light scattering (DLS) and TEM techniques. The ^{1}H NMR spectrum of mPEG-b-PεDL in $CDCl_3$ showed peaks for both mPEG and PεDL blocks and indicated that the molecules act as a separate entities i.e.

copolymer molecules are not self-assembled to form micelles. However, the D_2O spectrum showed only mPEG peaks indicated the self-assembly of the copolymer where the PEG blocks were shielding the hydrophobic PεDL block. The same results has also been showed in previous studies with a smaller molecular weight copolymer.[21]

The DLS of the copolymeric micelles showed a single peak with low polydispersity index indicated the uniformity of the micelles formulation. The TEM image also showed uniformly distributed micelles with clear boundary for both of the copolymers indicated the formation of micelles. The sizes of the micelles determined by DLS and TEM (analysed ImageJ software) of both of the copolymers were <60 nm. The particles of <200nm are known to be less susceptible to reticuloendothelial system (RES) system.[24] The RES system is a part of immune system consists of monocytes and phagocytes which are responsible to remove foreign particles from the body. It showed that the obtained micelles size are less susceptible to RES system and hence can circulate for a longer period of time in the blood. The lower dye loading in both of the formulations could be related to a very high hydrophobicity of the dye which exerted a very high cohesive force between the dye molecules during nanoprecipitation. Therefore, as the dye-polymer interaction was less compared to dye-dye interactions, it resulted in the precipitation of most of the dye in the water. However, a higher loading in mPEG-b-PεDL micelles was observed compared to mPEG-b-PCL micelles. A higher core volume and

amorphous content in the mPEG-b-PεDL micelles might be the reason for higher loading. The 3 in 1 fluorescence method indicated that the polymeric micelles are less toxic to the C3A cells where less than 20 % of the cells died in the experimental conditions. It indicated that the micelles were not significantly affecting the metabolic activity, cell membrane integrity and lysosomal function of the cells. The uptake of the micelles was elucidated in the hepatic cell lines (C3A cell) as most of the micelles/particles are uptake by the liver cells.[25] Commonly, the hydrophilic particles are less efficient to internalization compared to hydrophobic nanoparticles.[26] However, the micelles were taken up by the cells very quickly in the early stage of the study. It indicates that the hydrophilic PEG surface of micelles was not providing enough shielding effect to prevent it from internalization. This might be related to the chain length of mPEG and hydrophilic/ hydrophobic ratio of the copolymer. The size of the micelles can also affect the internalization. It has been shown previously that the 50 nm polystyrene NP was internalized to higher extent compared to 500 nm polystyrene NP in hepatocytes cells.[27] Therefore, the smaller size of the micelles (<60 nm) could be a reason for higher internalization of the micelles within the cells.

5.5 Conclusions

The mPEG-b-PεDL copolymers have been successfully synthesised and compared with mPEG-b-PCL copolymer using TBD catalyst in MROP method. The conclusions of the results of the ROP synthesis was also supported by

reference to the dielectric data of the starting reaction materials. It was also shown that the microwave heating reduced the polymerisation time mPEG-b-PεDL copolymer by one half compared to conventional heating methods described in the last chapter which resulted in a reaction time reduction of 6 h. Also for the first time microwave acceleration of ε-CL ROP to produce mPEG-b-PCL copolymers using the TBD catalyst was demonstrated and shown capable of reducing the reaction time to 2 mins. We also demonstrated that the copolymers are able to self assebled in water to give micelles with amorphous (mPEG-b-PεDL) and semicrystalline (mPEG-b-PCL) cores. A lower CMC and smaller size of the mPEG-b-PεDL micelle illustrated the higher thermodynamic and kinetic stability of the micelles. The lower toxicity and time dependent uptake of the micelles into the cells demonstrate the capability of the polymer to be used as delivery vehicle. However, lower dye loading in the copolymer led to the use other drug molecules to realize the potential of the copolymer. Hence in the next chapter, the drug delivery potential of copolymer was evaluated using indomethacin as a model hydrophobic drug molecule.

5.6 References

1. X. M. Fang, C. D. Simone, E. Vaccaro, S. J. Huang and D. A. Scola, *Journal of Polymer Science Part a-Polymer Chemistry*, 2002, **40**, 2264-2275.
2. Z. J. Yu and L. J. Liu, *Journal of Biomaterials Science-Polymer Edition*, 2005, **16**, 957-971.

3. N. T. Nguyen, E. Greenhalgh, M. J. Kamaruddin, J. El Harfi, K. Carmichael, G. Dimitrakis, S. W. Kingman, J. P. Robinson and D. J. Irvine, *Tetrahedron*, 2014, **70**, 996-1003.
4. R. Nagahata, D. Sano, H. Suzuki and K. Takeuchi, *Macromolecular Rapid Communications*, 2007, **28**, 437-442.
5. S. Velmathi, R. Nagahata and K. Takeuchi, *Polymer Journal*, 2007, **39**, 841-844.
6. T. Nakamura, R. Nagahata, S. Suemitsu and K. Takeuchi, *Polymer*, 2010, **51**, 329-333.
7. C. Zhang, L. Liao and S. S. Gong, *Green Chemistry*, 2007, **9**, 303-314.
8. H. Stange, M. Ishaque, N. Niessner, M. Pepers and A. Greiner, *Macromolecular Rapid Communications*, 2006, **27**, 156-161.
9. H. Stange and A. Greiner, *Macromolecular Rapid Communications*, 2007, **28**, 504-508.
10. K. Kempe, C. R. Becer and U. S. Schubert, *Macromolecules*, 2011, **44**, 5825-5842.
11. R. Hoogenboom and U. S. Schubert, *Macromolecular Rapid Communications*, 2007, **28**, 368-386.
12. P. Kerep and H. Ritter, *Macromolecular Rapid Communications*, 2006, **27**, 707-710.
13. G. Sivalingam, N. Agarwal and G. Madras, *Journal of Applied Polymer Science*, 2004, **91**, 1450-1456.
14. Q. Xu, C. Zhang, S. Cai, P. Zhu and L. Liu, *Journal of Industrial and Engineering Chemistry*, 2010, **16**, 872-875.
15. H. Li, L. Liao and L. Liu, *Macromolecular Rapid Communications*, 2007, **28**, 411-416.
16. L. Q. Liao, L. J. Liu, C. Zhang, F. He and R. X. Zhuo, *Journal of Applied Polymer Science*, 2003, **90**, 2657-2664.
17. L. Liao, L. Liu, C. Zhang and S. Gong, *Macromolecular Rapid Communications*, 2006, **27**, 2060-2064.
18. C. Zhang, L. Liao and S. Gong, *Macromolecular Rapid Communications*, 2007, **28**, 422-427.
19. J. Aguiar, P. Carpena, J. A. Molina-Boĺıvar and C. Carnero Ruiz, *Journal of Colloid and Interface Science*, 2003, **258**, 116-122.
20. T. Trimaille, K. Mondon, R. Gurny and M. Möller, *International Journal of Pharmaceutics*, 2006, **319**, 147-154.
21. L. Glavas, P. Olsen, K. Odelius and A.-C. Albertsson, *Biomacromolecules*, 2013, **14**, 4150-4156.
22. M. A. Woodruff and D. W. Hutmacher, *Progress in Polymer Science*, 2010, **35**, 1217-1256.
23. K. K. Bansal, D. Kakde, L. Purdie, D. J. Irvine, S. M. Howdle, G. Mantovani and C. Alexander, *Polymer Chemistry*, 2015, **6**, 7196-7210.
24. C. Allen, D. Maysinger and A. Eisenberg, *Colloids and Surfaces B-Biointerfaces*, 1999, **16**, 3-27.

25. H. J. Johnston, M. Semmler-Behnke, D. M. Brown, W. Kreyling, L. Tran and V. Stone, *Toxicology and Applied Pharmacology*, 2010, **242**, 66-78.
26. N. S. Melik-Nubarov, O. O. Pomaz, T. Y. Dorodnych, G. A. Badun, A. L. Ksenofontov, O. B. Schemchukova and S. A. Arzhakov, *FEBS Letters*, 1999, **446**, 194-198.
27. K.-i. Ogawara, M. Yoshida, K. Higaki, K. Toshikiro, K. Shiraishi, M. Nishikawa, Y. Takakura and M. Hashida, *Journal of Controlled Release*, 1999, **59**, 15-22.

Chapter

6

Self-Assembly of Poly (ε-decalactone) based Copolymer Micelles for Delivery of Indomethacin

6.1 Introduction

The poor solubility of many drug candidates is one of the major hurdles in the formulation development of new drugs.[1] Around 70 % of new chemical entities are poorly soluble in aqueous media.[2] In the last few years, micelles have emerged as one of the major tools for solubilization and controlled delivery of many hydrophobic drugs.[3-10] Micelles are nanosized structures (10-100 nm) obtained by self-assembly of amphiphilic molecules above their critical micellar concentration (CMC) in water.[11-13] The hydrophobic part of the micelles forms a core which is surrounded by a hydrophilic outer shell, known as a corona.[14-16] The core-shell structure of micelles creates a cargo space for hydrophobic molecules. These cargo spaces have been used for drug loading in many studies.[17-20] The drug loading in the micellar cores can be affected by a number of factors. These includes the nature of core forming block, block length, polymer molecular weight, nature of drug and drug-polymer compatibility.[21] Many studies have shown that the drug-polymer compatibility is one of the major factors affecting drug loading into micelles.[22, 23] A polymer can act as a good solubilizer for a drug if they both have favorable interactions with each other and this enhances the drug loading. For instance, Yang *et al.* showed a higher doxorubicin loading in acid functionalized polycarbonate block copolymers due to the strong interaction of amine groups of the drug with the acid group of the polymer.[24] However, strong interactions can also prevent drug release from the core.

Therefore, it is important to optimize the formulation, such that a proper loading with desirable release kinetics can be achieved. A number of researchers have attached selected functional groups in block copolymer cores to facilitate strong interactions with drugs.[25] Marked improvements have been achieved for amphotericin B,[26] cisplatin[27] and doxorubicin (DOX)[28, 29] in terms of drug stability, loading and release property. One of the key parameters which may determine drug-polymer compatibility is the Flory-Huggins interaction parameter.[30, 31] A low value (ideally zero) of this parameter indicates a good interaction between drug and polymer. Several reports have shown the successful use of this parameter to determine the compatibility of a drug with polymer.[22, 23, 32]

In this chapter, a self assembled mPEG-b-PεDL polymer has been described for the solubilization and controlled release of indomethacin. The drug loading was optimized for different loading methods, use of organic cosolvent (acetone, THF and ethanol) and drug to polymer ratios during nanoprecipitation. The obtained results were compared with structurally similar mPEG-b-PCL polymers which have been utilised before for drug delivery.[33]

A drug-polymer compatibility study was also conducted by predictive computational approaches in micelles formed from the newly synthesised mPEG-b-PεDL copolymer and compared with mPEG-b-PCL copolymers for encapsulatioon and release of indomethacin. This has been accomplished by

estimating Flory-Huggins interaction parameters using the group contribution method (GCM). In general, a good compatibility should result in higher drug loading. In order to identify the dominant factor in drug loading and release, the predictive compatibility results were compared with experimental results to design rules for drug delivery systems.

A difference in the drug loading and drug release was expected for micelles with differences in the physical state of their core (amorphous or semicrystalline). Previous chapters have shown the amorphous nature of the mPEG-b-PεDL micellar cores compared to the semicrystalline mPEG-b-PCL core. In general, micelles with amorphous cores should enhance drug loading as drug molecules are reported to associate better with amorphous regions of the polymer. The butyl chain in the micelles core was expected to enhance the hydrophobic-hydrophobic interaction between drug and polymer which can lead to the higher solubilization of drug in micelles. However, the absence of electrostatic or hydrogen bonding functional groups in the polymer micellar cores were also predicted to prevent strong interactions between drug and polymer. Hence, these polymers were anticipated to have a good balance between drug-polymer association and release.

6.2 Methods

6.2.1 Determination of Solubility Parameters of Drug and Copolymers

The drug–micellar core compatibility was calculated by the Flory-Huggins interaction parameter given by:

$$\chi_{sp} = (\delta_s-\delta_p)^2 V_s/RT \quad (1)$$

Where χ_{sp} = Interaction parameter of solubilizate (drug) and core forming block (polymer hydrophobic block); δ_s = Solubility parameter of solubilizate (drug); δ_p = Solubility parameter of the polymer (core block); V_s = Molar volume of solubilizate (drug); R = Gas constant and T temperature in Kelvin.

The Hanson approach was used to calculate the partial solubility for estimation of the solubility parameter (δ) by eq (2).

$$\delta = (\delta^2_d + \delta^2_p + \delta^2_h)^{1/2} \quad (2)$$

where, δ_d, δ_p, and δ_h are the partial solubility parameters due to Van der Waals dispersion forces between atoms, electrostatic interactions or polarity, and hydrogen bonding between molecules, respectively. The partial solubility can be calculated using the group contribution method (GCM) obtained by the Hoftyzer Van Krevelen's method[34] using the expressions below.

$$\delta_d = \Sigma F_d/V \quad (3)$$

$$\delta_p = (\Sigma F^2_p)^{1/2}/V \quad (4)$$

$$\delta_h = (\Sigma E_h/V)^{1/2} \quad (5)$$

where F_d, F_p, and E_h indicates the specific functional group for dispersion forces (F_d), polar or electrostatic interactions (F_p), and hydrogen bonding (E_h) respectively. The values of these forces are available in the literature[35].

V refers to the molar volume which can be determine by the Fedos method[36]. Therefore the solubility difference (δ_s-δ_p) of drug and polymer can be estimated by

$$(\delta_s-\delta_p) \text{ or } \Delta\delta = [(\delta_s-\delta_p)^2_d + (\delta_s-\delta_p)^2_p + (\delta_s-\delta_p)^2_h]^{1/2} \quad (6)$$

Hence χ_{sp} is calculated using

$$\chi_{sp} = (\Delta\delta)^2 V_s/RT \quad (7)$$

Lower values $\chi_{sp,}$ suggest higher compatibility between drug and polymer. In the same way, compatibility is predicted to be highest when the solubility parameters of drug and polymer becomes equal (δ_s=δ_p). In other words low values of Δδ indicate good solubilization. The equation 7 also indicates that the interaction parameter depends on the molecular volume of the drug. Larger molecular volumes of the drug increase the interaction parameter value, hence will reduce compatibility with the polymer.

6.2.2 Preparation of Blank and Indomethacin Loaded Micelles

6.2.2.1 Dialysis Method

The dialysis method was used for copolymeric micelles preparation according to reported method with some modifications.[18] The block copolymer (50 mg) and indomethacin (4 mg, 1.1X 10^{-5} moles) was dissolved in 5 mL of organic solvents at room temperature. The organic phase was added into the water (10 mL) with stirring at a fixed rate of 0.5 mL/min using syringe pump. The

solution was stirred for 2 h followed by dialysis of the suspension for 24 h against 5 L of deionized water using cellulose dialysis membranes (molecular weight cut-off (MWCO): 1.2 X 10^4). The water was replaced at a predetermined time interval (6 h). The obtained formulation was passed through a membrane syringe filter (pore size: 220 nm) (Millex-LG, Millipore Co., USA) to remove any aggregates. A portion of the formulation was frozen and lyophilized to obtain freeze dried products. The same procedure was used for the preparation of blank micelles except that indomethacin was not added in the organic phase. The organic phase used for micellar preparations included acetone, tetrahydrofuran (THF) and ethanol (water miscible solvents).

6.2.2.2 Emulsion (O/W) Method

The emulsion method of drug encapsulation was used according to reported procedures with some modifications.[37] The loading was performed by dissolving polymer (50 mg) and drug (4 mg) in 2 mL of dichloromethane (DCM) (water immiscible organic solvent). To this solution, 10 mL of water was added with stirring and suspension was emulsified using probe sonication for 5 min. The DCM was evaporated by stirring the emulsified suspension at room temperature for 3 h. The obtained formulation was left overnight (open vial) in a fume cupboard to allow any residual solvents to evaporate. The micellar solution was then filtered through a membrane syringe filter (pore size: 220 nm) (Millex-LG, Millipore Co., USA) to remove

any aggregates. The drug loaded micelle formulation was then passed through a PD10 desalting column (Sephadex G-25 Medium, GE Healthcare Life Sciences) to remove any free drug and small molecular weight impurities (<5 K). A portion of the formulation was freeze dried to determine the drug content in the formulation. The blank micelle formulation was made by omitting the addition of drug in organic phase.

6.2.2.3 Nanoprecipitation

Micelles of the block copolymers were prepared by nanoprecipitation methods.[38] Briefly, copolymer (50 mg) and indomethacin (4 mg) were dissolved in the organic phase (5 mL) and added dropwise at a fix rate of 0.5 mL/min into HPLC water (10 mL) with stirring (1000 rpm). The solution was stirred for 4 h at room temperature and then left overnight for complete removal of acetone residue. The obtained micelles solution was passed through membrane syringe filter (pore size: 220 nm) (Millex-LG, Millipore Co., USA) to remove any aggregates. The formulation was then passed through a PD10 desalting column (Sephadex G-25 Medium, GE Healthcare Life Sciences) to remove any free drug and small molecular weight impurities (<5 K). The same procedure was used for the preparation of blank micelles except that indomethacin was not added in the organic phase. The organic phase used for nanoprecipitation included acetone, tetrahydrofuran (THF) and ethanol. A portion of the obtained micellar solution was freeze dried to calculate drug content (% DC).

6.2.3 Characterization of the Micelles

The amount of indomethacin loaded in the micelles was estimated by dissolving a known amount of micelles (5 mg) in methanol followed by estimation through UV-visible spectrophotometer at λ_{max} = 318 nm. A calibration curve was constructed over the quantification range of 5-50 µg/mL (Beckman Coulter DU 800 UV spectrophotometer) (Figure 6-1).

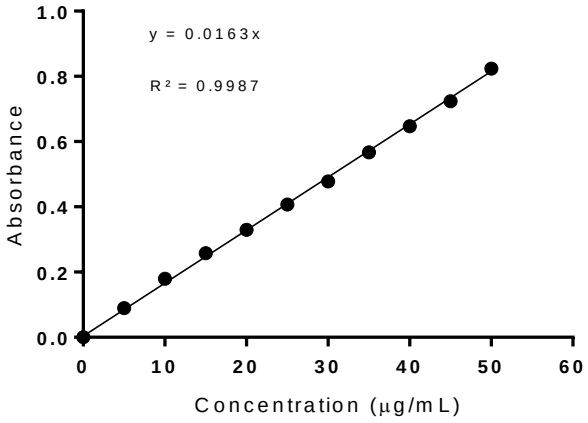


Figure 6-1 Standard calibration curve of indomethacin in methanol at wavelength (λ_{max}) of 318 nm.

Size, size distribution and polydispersity of the prepared micelles were determined by dynamic light scattering (DLS) at a polymer concentration of 0.5 mg/mL in HPLC grade water using Malvern NanoZS instrument. Surface zeta potential was measured in HEPES 10 mM buffer (pH-7.4) using the same instrument. The surface morphology and size were confirmed by TEM images. The samples were imaged without staining of the samples on TEM grid. The size analysis of TEM images were performed using Image J software. The full experimental characterization procedures are given in

chapter 2. All the measurements were performed on three different batches and the mean values were reported.

6.2.4 Stability Studies of the Micelles

The stability of the mPEG-b-PεDL micelles in HPLC water and PBS buffer was determined by measuring the size of the micelles after 4 weeks at room temperature. The buffer (10 mL) solution was evaporated to get the solid content of the PBS. The aqueous micelle solution (10 mL) was then added in the solid material and dissolved to obtain the micelles formulation in PBS. Size, size distribution and polydispersity of the prepared micelles were determined by dynamic light scattering (DLS) at polymer concentrations of 0.5 mg/mL in HPLC grade water or PBS buffer using a Malvern NanoZS instrument. The formulations were passed through a membrane syringe filter (pore size: 220 nm) (Millex-LG, Millipore Co., USA) before measuring the size of the micelles.

6.2.5 Degradation Study of Micelles

The degradation of empty mPEG-b-PεDL micelles was assessed in HPLC water (pH 7.4) and micelles formulation (in HPLC water) with *Pseudomonas cepacia* lipase (0.2 mg/mL). The micelle formulations were incubated at 37 °C. One vial from each set was collected at a predetermined time (30 days) and freeze-dried. The freeze-dried samples were then dissolved in chloroform, filtered, and analyzed by GPC to determine the change in molecular weight.

6.2.6 *In Vitro* Indomethacin Release Study

The *in vitro* time profile of indomethacin release was performed according to a reported method with minor modification.[39] An appropriate amount of freeze dried micelles, equivalent to 250 µg of indomethacin was redispersed in HPLC grade water (1 mL).The solution was transferred to dialysis tubing (Slide-A-Lyzer, 3.5 kDa, Thermo Scientific) and dialysed against 5 mL of phosphate buffer solution (PBS, 0.1 M, pH 7.4) at 37 °C. At a predetermined time intervals, the whole release media were taken as a sample and replaced with fresh media to maintain sink conditions. The samples were then freeze dried and dissolved in 1 mL of methanol to quantify drug by UV-visible spectrophotometry. Three control solutions (Control 'A', 'B' and 'C') were also prepared for comparison and analyzed by the same method given above. Control 'A' solution consisted of 250 µg of indomethacin dissolved in 1mL of phosphate buffer. Control 'B' consisted of 250 µg/mL of indomethacin solution in PBS in which 15 µL of mPEG-b-PεDL copolymer solution in acetone (stock: 250 mg/mL of mPEG-b-PεDL) was added. Control 'C' also consisted of 250 µg/mL of indomethacin solution in which 18 µL of mPEG-b-PCL copolymer solution in acetone (stock: 250mg/mL of mPEG-b-PCL) was added. Acetone in control solutions (Control 'B' and 'C') was removed by bubbling with nitrogen and volume was made up to 1 mL, if required.

6.3 Results

6.3.1 Solubility Parameters of Drug and Copolymers

The solubility parameters of indomethacin, PEG block and hydrophobic blocks of copolymers were calculated using the Hansen solubility approach using equation 1 given in the method section. The calculated values tabulated in table 6-1 indicated that the Van der Waals dispersion forces were nearly the same between copolymer segments (PεDL and PCL segments). The polarity and hydrogen bond formation ability was higher with the PEG segment as expected. The solubility difference (Δδ) was calculated by equation 6 using partial solubility parameters. The lowest value of this parameter was found for PCL cores (Δδ (PCL) = 4.47).

The interaction parameter (χ_{sp}) was then determined from the Δδ value using equation 7. Equation 7 also indicates the dependence of interaction parameter on molecular volume of the drug. Larger drug volume increased the value of interaction parameter, hence lowered the compatibility with polymer. The values for the solubility difference and interaction parameters are given in table 6-2. In our study, the interaction parameters were observed in the order of χ_{sp} (PεDL)> χ_{sp} (PEG)> χ_{sp} (PCL) which indicated the higher compatibility of the PCL compared to PεDL block of the copolymer.

Table 6-1 Calculated value of partial solubility parameters and total solubility parameters of copolymer segments and drug

Polymer segments and drug	Partial solubility parameter ($MPa^{1/2}$)			Molar Volume (cm^3/mol)	Total solubility Parameter δ_T ($MPa^{1/2}$)
	δ_d	δ_p	δ_h		
PεDL	17.05	3.00	6.54	163.20	18.50
PCL	17.66	4.97	8.42	98.50	20.18
PEG	17.17	11.11	9.12	36.00	22.85
Indomethacin	21.80	6.00	9.40	230.00	24.50

δ_d dispersion parameter; δ_p dipolar parameter; δ_h hydrogen bonding parameter; δ_T total solubility parameter

Table 6-2 Calculated values of solubility difference (δ_s-δ_p) and interaction parameter χ_{sp} between solute (drug) and polymer segments

Drug	(δ_s-δ_p) or **Δ** (PEG)	(δ_s-δ_p) or **Δ** (PCL)	(δ_s-δ_p) or **Δ** (PεDL)	χ_{sp} (PEG)	χ_{sp} (PCL)	χ_{sp} (PεDL)
Indomethacin	6.51	4.47	6.30	3.39	1.85	3.68

A stepwise calculation of various parameters is given in Appendix.

6.3.2 Preparation and Characterization of Blank and Indomethacin Loaded Micelles

The effect of the different methods on drug loading and the size of mPEG-b-PεDL micelles were evaluated by preparing micelles using nanoprecipitation, dialysis and emulsion methods (Figure 6-2). A slightly higher loading and larger sizes were observed for micelles prepared by the emulsion method compared to nanoprecipitation and dialysis ($P<0.05$, One way ANOVA). The emulsion method was included for comparison but for scale-up was not favorable as it required the use of toxic methylene chloride (International Conference on Harmonization (ICH) class 2 solvent). On the other hand, no

significant difference in loading and size was observed between the nanoprecipitation and dialysis methods where acetone was used as an organic phase ($P < 0.05$, One way ANOVA).

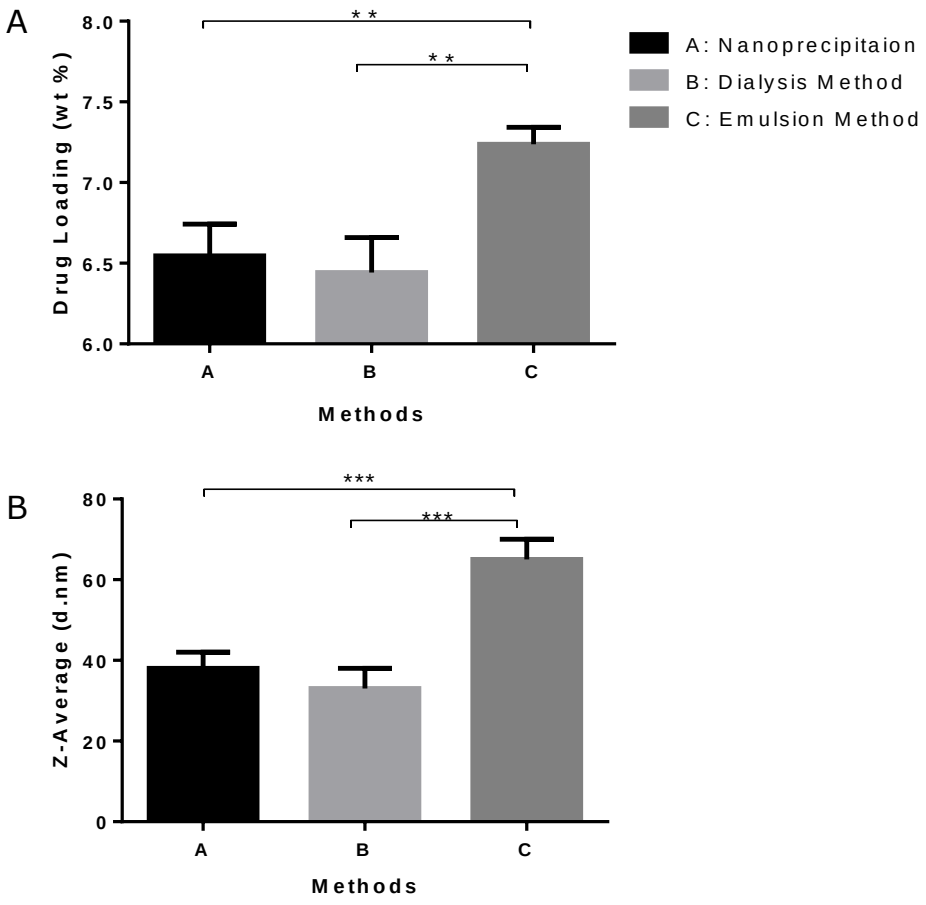


Figure 6-2 Effect of different methods on (A) drug loading and (B) average diameter of mPEG-b-PεDL micelles. A significant difference was observed between drug loading and micelle size for nanoprecipitation/Emulsion method and Dialysis/Emulsion method (***= $P < 0.001$, **= $P < 0.01$, One way ANOVA).

The effect of different solvents (acetone, ethanol and THF) on micelles formed by nanoprecipitation and dialysis was accessed by determining drug loading and size of the micelles made from mPEG-b-PεDL copolymers. A significant reduction in the drug loading was observed when ethanol was

used over acetone. However, no significant difference was observed when THF was compared against acetone in both of the methods (Figure 6-3).

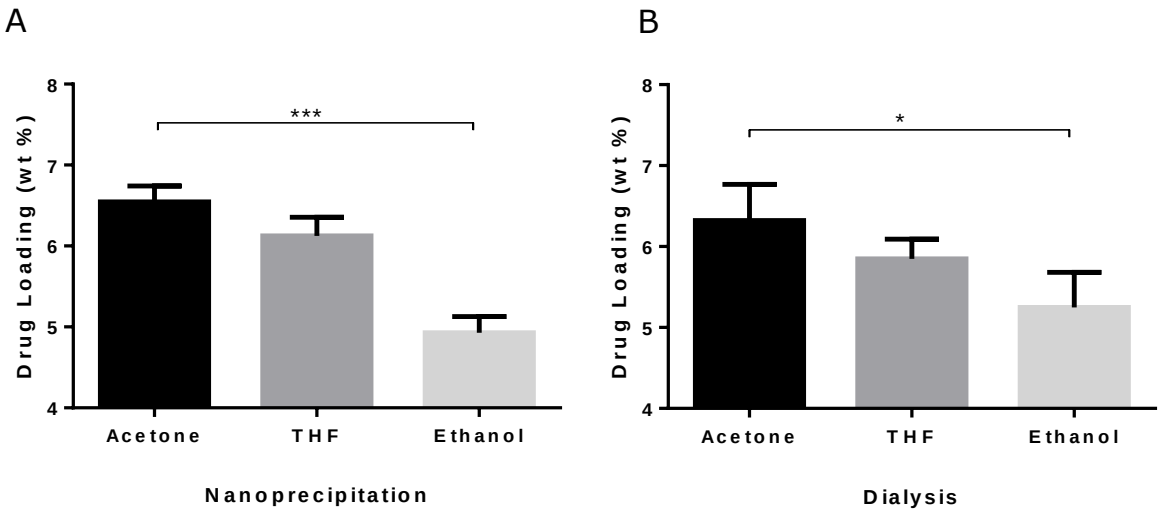


Figure 6-3 Effect of different solvents on (A) nanoprecipitation and (B) dialysis on drug loading in mPEG-b-PεDL micelles. Significant difference was observed between acetone and ethanol solvents (***= $P < 0.001$, *= $P < 0.05$, One way ANOVA).

No significant difference in size was observed between different solvents used in dialysis micelle formulation methods. However, a significantly larger size was observed for THF compared to ethanol and acetone solvents used in the nanoprecipitation method. A significant difference was also observed between dialysis and nanoprecipitation when THF was used as an organic phase ($P < 0.001$, student t test). Effects of different solvents on sizes of the mPEG-b-PεDL micelles made by nanoprecipitation and dialysis methods are given in figure 6-4. The effect of drug to polymer ratios (D/P ratios) during nanoprecipitation of mPEG-b-PεDL and mPEG-b-PCL copolymers was determined using D/P ratios of 4/50 and 8/50 (Figure 6-5).

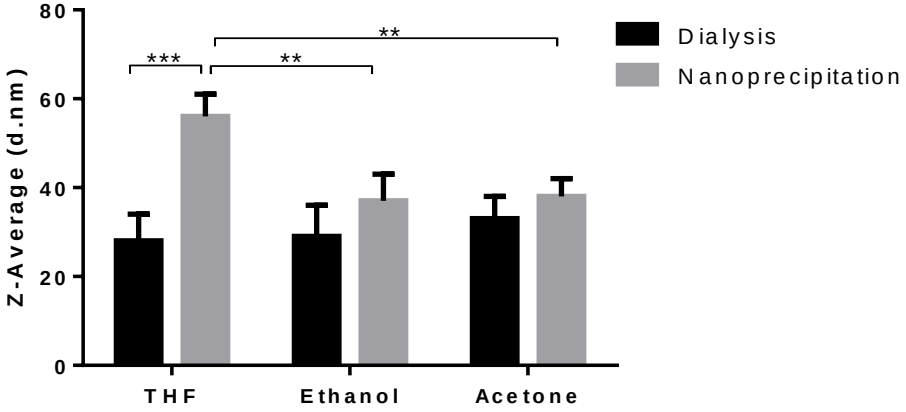


Figure 6-4 Effect of different solvents on sizes of the mPEG-b-PεDL micelles made by nanoprecipitation and dialysis methods. A significant difference was observed between solvents during nanoprecipitation (***= P < 0.001, **= P < 0.01, unpaired student's t test).

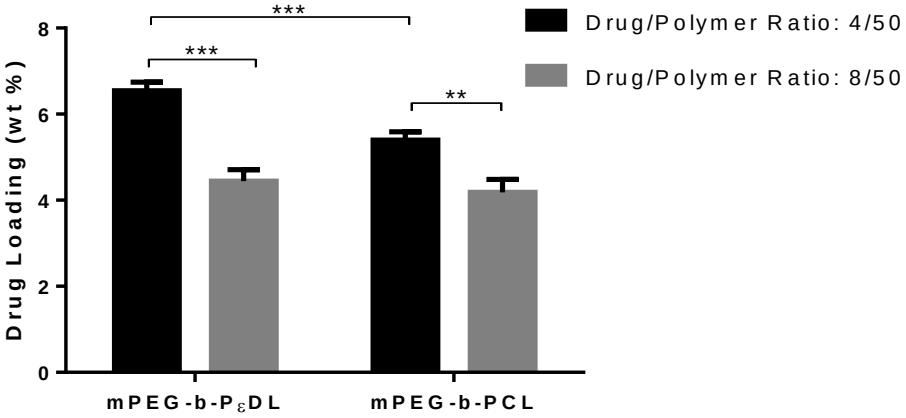


Figure 6-5 Effect of different drug to polymer ratios on drug loading in mPEG-b-PεDL and mPEG-b-PCL micelles. Significant difference in drug loading was observed for different polymers in different drug/Polymer ratios (***= P < 0.001, **= P < 0.01, unpaired student's t test).

A significantly higher drug loading was observed at D/P ratio of 4/50 compared to 8/50 ratio irrespective of any copolymers used during nanoprecipitation. A significant difference in loading was also observed when

mPEG-b-PεDL micelles were compared against mPEG-b-PCL micelles at D/P ratio of 4/50. Hence, nanoprecipitation at D/P ratio of 4/50 was considered as the optimum ratio and used further for micelle preparation and characterization for both of the polymers. The characterization data of the micelles made from mPEG-b-PεDL and mPEG-b-PCL copolymers by nanoprecipitation are given in table 6-3.

Table 6-3 Characterization data of blank and drug loaded micelles prepared from block copolymers.

Polymer	Z-average size (d/nm) (±SD) (Blank)	PDI (Blank)	Zeta Potential (mv) (±SD)	Z-average size (d/nm) (±SD) (Drug loaded)	PDI (Drug loaded)	Drug Loading (wt%) ±S.D.	Drug Encapsula-tion ±S.D. (%)
mPEG-b-PεDL	38 ± 2[a]	0.16 ± 0.02	-3.3 ± 1.3	39 ± 5	0.21 ± 0.02	6.55 ± 0.17[a]	81.10 ± 6.32[a]
mPEG-b-PCL	30 ± 3	0.18 ± 0.01	-1.9 ± 1.2	32 ± 4	0.20 ± 0.02	5.39 ± 0.49	66.14 ± 7.06

[a] Significant difference from mPEG-b-PCL ($P < 0.05$, unpaired student's t-test).

The percent micelles recoveries were determined after freeze drying of empty micelles and found in the range from 90 % to 95 %. The drug contents in loaded micelles were estimated in term of indomethacin/copolymer (wt%). Copolymeric mPEG-b-PεDL micelle was able to load 6.55 wt% whereas only 5.39 wt% drug was loaded by mPEG-b-PCL micelles. A significant difference was observed between the loading capabilities of the copolymers ($P < 0.05$, unpaired student's t test). In fact,

PεDL core enhanced the loading by 1.22 times compared to the PCL core of micelles. A significant difference was also observed between sizes of the mPEG-b-PCL with respect to mPEG-b-PεDL micelles (Figure 6-6).

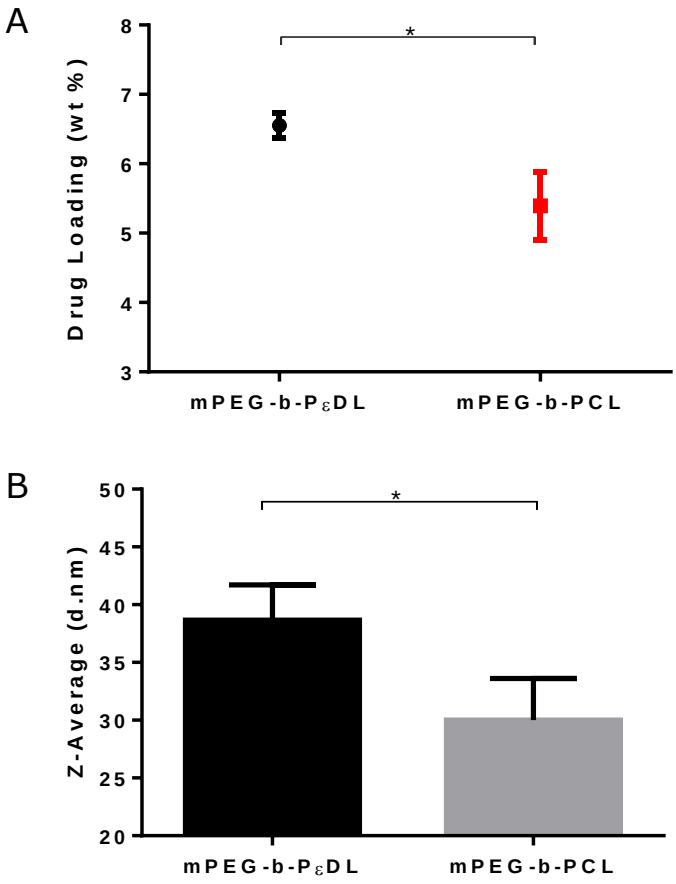


Figure 6-6 Nanoprecipitation of the copolymers (A) indomethacin loading (weight % to polymer) (B) Z- average size of the micelles. A significant difference (*= $P < 0.05$, unpaired student's t test) was observed between both of the copolymers for loading and size.

The Z-average diameter of mPEG-b-PεDL micelles was 38 nm determined in HPLC water. On the other hand, a significant reduction in the average size of the mPEG-b-PCL micelles (30 nm) was observed. The smaller size with narrow polydispersity indicated greater uniformity in the size. No secondary peaks were observed for either of the micellar formulations which indicated

that only one detectable population was made during nanoprecipitation. No significant difference in sizes was observed between blank and drug loaded micelles for both of the copolymers. Furthermore, no significant change in the micelle size was observed when micelles were stored in PBS for 4 weeks. The degradation of the mPEG-b-PεDL micelles was detected in presence and absence of the enzyme. The reduction in the M_n was significantly higher in the presence of enzyme (Figure 6-7).

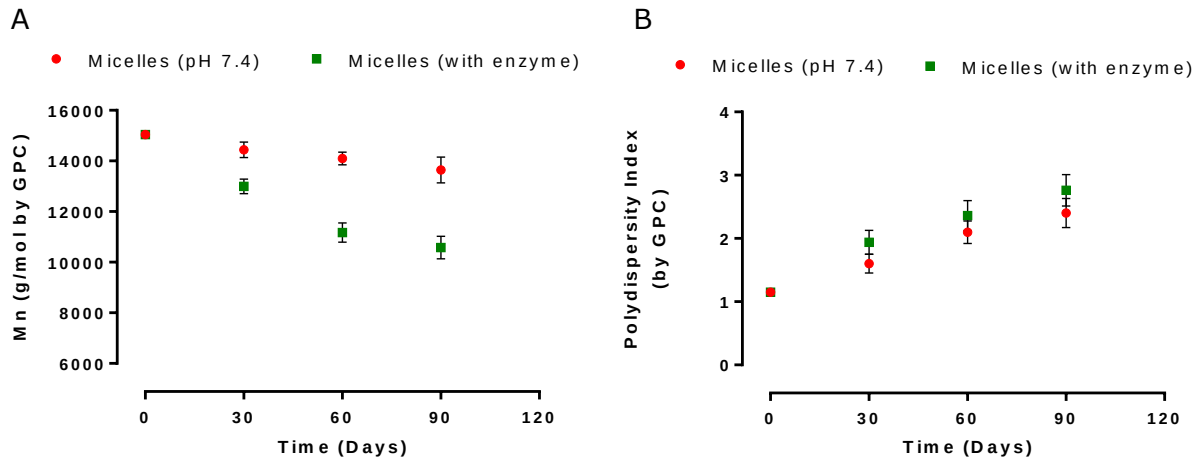


Figure 6-7 Loss in molar mass (M_n) of mPEG-b-PεDL copolymer (A) and polydispersity index (B) with time (days) in the presence and absent of *Pseudomonas cepacia* lipase (0.2 mg/mL) at 37 °C

The TEM images of the micelles showed the formation of uniformly distributed spherical micelles with a clear surface boundary. However, the analysis of TEM images (by Image J software) suggested the mean size to be <60 nm for both of the micelles formulation. The images did not reveal any sign of aggregation for either of the copolymers (Figure 6-8).

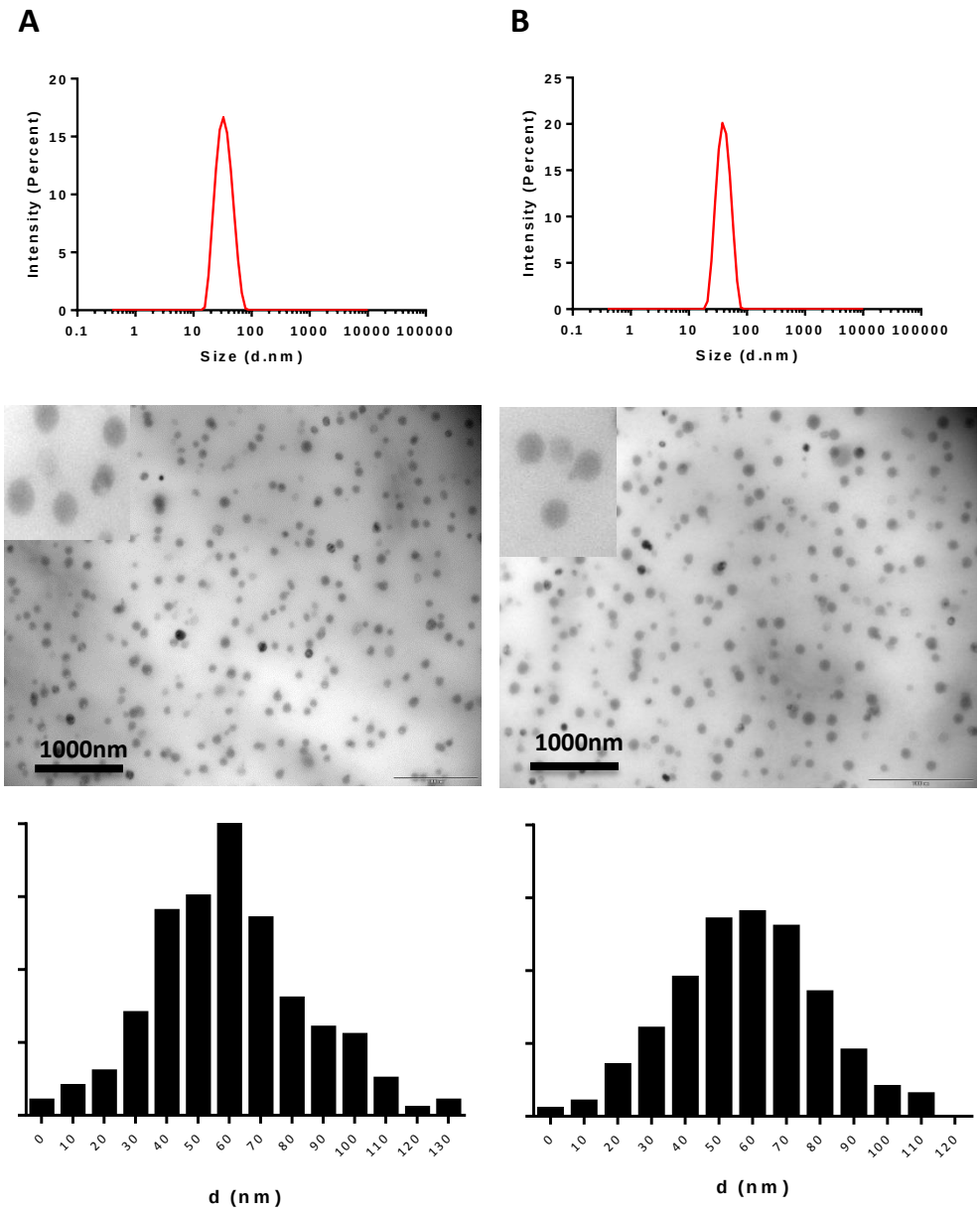


Figure 6-8 Micelle Size distributions by TEM Image and size distribution histogram (using Image J software) of empty (A) mPEG-b-PεDL micelles, (B) mPEG-b-PCL micelles. The images were taken without staining. Scale bar – 1000nm.

6.3.3 *In Vitro* Indomethacin Release

The percent cumulative release profile of indomethacin against time for different formulations and control systems is shown in figure 6-9. Control 'A'

which contains drug solubilized in PBS, showed a rapid drug release profile. A fast release of the free indomethacin (> 90 %) was observed across the membrane within 12 h. In contrast to rapid release from control 'A', indomethacin mixed with empty micelles of mPEG-b-PεDL (Control 'B') and PEG-b-PCL (Control 'C') in PBS took a longer period of time to cross the dialysis membrane, requiring 24 h for 90 % of the indomethacin to be separated from from control 'B' and 'C' micelles. There was no significant difference between control 'B' and control 'C' formulations in terms of time to retain indomethacin, but there was a significant difference observed for control 'A' with respect to control 'B' and control 'C' formulations.

In comparison, the drug loaded micelles showed sustained release characteristics regarding kinetics of drug transport across the membrane. A difference in the release profiles was observed between mPEG-b-PεDL and mPEG-b-PCL micelles. An initial rapid release was followed by a slow and sustained release phase from both of the formulations. The mPEG-b-PεDL micelles exhibited an initial burst release of 34 % in 6 h. This is followed by a sustained release phase (92 % in 120 h) where drug was slowly moved across the dialysis membrane into the release media. The mPEG-b-PCL micelle was able to hold the drug for a longer period of time with a significantly reduced burst release of the drug in comparison to mPEG-b-PεDL micelles. It exhibited a rapid release of 25 % in 6 h followed by 85 % in 120 h.

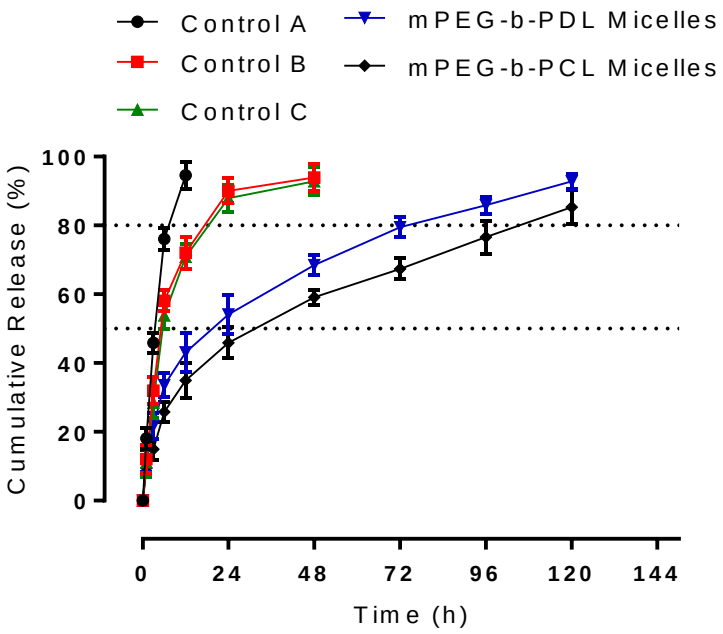


Figure 6-9 *In vitro* indomethacin release (%) from different test formulations in pH 7.4 PBS buffer solution at 37 °C. Each point represents mean ± SD (n=3).

6.4 Discussion

The potential of the mPEG-b-PεDL micelles for drug delivery was determined by loading a relatively hydrophobic drug indomethacin (log P = 4.25) and comparing results against mPEG-b-PCL micelles. The latter micelles have been widely investigated previously for encapsulation of hydrophobic molecules.[33] The formulations in this study were accordingly investigated for drug loading and size of the micelles. The loading capacities and sizes of mPEG-b-PεDL micelles were determined by emulsion, dialysis and nanoprecipitation methods. As expected, higher drug loadings and micelle size was observed for micelles prepared by the emulsion method. The water immiscible methylene chloride was used as an organic phase in the emulsion

method, and this solvent diffuses only very partially into water. This was predicted to prevent the desolvation of polymeric chains present in the methylene chloride droplets. In fact, the desolvation mainly occurs by the evaporation of organic phase. Hence, the addition of methylene chloride into the water produced concentrated organic phase droplets, containing polymeric chains and drug. This provided more opportunities for the drug to interact with polymer chains and hence precipitate together. The slower evaporation of organic solvent caused desolvation of the hydrophobic polymer blocks resulted in precipitation of larger size particles with more volume to accommodate the drug. However, the toxicity of the organic phase restricted us to adopt the method for micelle preparation any further. On the other hand, a water miscible solvent (acetone) was used during dialysis and nanoprecipitation method. Here, the organic phase could diffuse into the water phase, potentially to carry some of the polymer chain which on later stage of diffusion precipitated under conditions of greater polymer dilution to produce smaller block co-polymer micelles. Although no significant differences were observed when dialysis methods were compared against nanoprecipitation for drug loading and size, the long dialysis time persuaded us to use the one step nanoprecipitation method for both of the copolymers. Nanoprecipitation has been used previously for self-assembly of many similar copolymers hence this method was adopted as a 'one step' method for micelle preparation.[38, 41, 42] The size of the empty mPEG-b-PεDL

micelles (38 nm) was slightly higher compared to mPEG-b-PCL micelles (30 nm) ($P < 0.05$, unpaired student's t test). The calculated total volume of mPEG-b-PεDL micelles (amorphous PεDL cored) was 1.81 times higher compared to the volume of mPEG-b-PCL micelles (semicrystalline PCL cored). The volume was determined for the spherical micelles (detected by TEM) using formula of volume of sphere: $4\pi r^3/3$ (r determined by DLS). This may have been due to the amorphous nature of the PεDL core which can take up more volume compared to semicrystalline PCL core. A single population shown via DLS with low polydispersity for both the copolymers confirmed the relative uniformity in the micelles formulations. The stability of the micelles was also evaluated in PBS after 4 weeks of storage. No significant differences in the sizes indicated that the micelles were stable under these conditions. The morphology of the micelles was also confirmed by TEM, which showed mostly uniform spherical micelles. The micelles were well separated from each other indicating further the higher stability of the micelles conferred by the outer PEG corona even in the dry state. This suggested that micelles would not easily aggregate upon injecting in circulation, although the presence of multiple serum proteins in vivo might still be problematic for prolonged micellar stability. The size obtained from Image J software analysis of TEM images suggested the mean size to be less than 60 nm. The appropriate size along with non-aggregating characteristics of the micelles is important for *in vivo* stability and prolonged circulation of

drug delivery systems. Kim *et al.* showed that the size of block co-polymer micelles can be affected by the loading of drug within the cores[39]. However, in this case, no significant difference in size was observed, before and after drug loading in micelles. This illustrated that the specific loaded drug in the copolymer, i.e. indomethacin, did not influence the size of the micelles to a measurable extent. No sign of aggregation was observed upon dilution of micelles with PBS indicating the stability of the formulation for longer period of time. However, in the presence of an esterolytic enzyme, the polymer was degraded fast, suggesting that the micelles might be cleared from the body by enzymatic hydrolysis. A marginally higher drug loading was found with mPEG-b-PεDL copolymer (6.55 wt%) compared to mPEG-b-PCL copolymers (5.39 wt%). This might be due to the higher volume of the highly hydrophobic amorphous PDL core (1.81 times to PCL) compared to semicrystalline PCL core of the micelles. The drug transport profiles revealed sustained release characteristics of the micellar systems. Different controls were used to compare the release profile to indomethacin loaded micelles. Control 'A' represented indomethacin solution in PBS and hence no transport barriers existed except the dialysis membrane. On the other hand control 'B' and 'C' contained indomethacin solution in PBS but with empty micelles added in order to assess if indomethacin inherently partitioned into the micelles or associated with the micellar coronae. Indomethacin transport in these cases was slower compared to control 'A', which indicated IND was

interacting with the micelles. There was no significant difference observed between transport in the presence of control 'B' and control 'C' which showed that the IND was interacting in a similar manner with both of the empty micelles. In contrast to the control formulations, the indomethacin loaded micelles were able to delay the drug transport significantly and a sustained release pattern for a period of 120 h was found. A significant difference in indomethacin release was observed between PEG-b-PεDL and PEG-b-PCL micelles ($P < 0.05$, unpaired student's t test). The PEG-b-PεDL micelles exhibited burst release (34 % in 6 h) followed by a sustained release phase up to 120 h. On the other hand, PEG-b-PCL micelles were able to hold the drug for a longer period of time and reduced the burst release (25 % in 6 h) significantly. Approximately 80 % of drug was released in 72 h and 110 h for mPEG-b-PεDL and PEG-b-PCL micelles respectively. This indicated that the amorphous core of the mPEG-b-PεDL micelles was not able to hold the drug as compared to mPEG-b-PCL micelles with semicrystalline core. This result was expected as drug molecules might more easily move from the mobile chains of the PεDL core compared to those of the semicrystalline PCL core.

In order to collect more evidence, drug-polymer compatibility was calculated by determining Flory-Huggins interaction parameters. Indeed, the low values of the interaction parameter (χ_{sp}) of < 5 for all the segments of copolymers (mPEG, PεDL and PCL) suggested that the drug can interact with all the

segments. However, lack of the functional groups in the polyester copolymers reduced the possibility of any specific interactions like hydrogen bonding and ionic complex formation. This in turn indicates that dispersion forces will be involved in the drug-polymer interaction. However, as the relative values of dispersion parameters are similar [PCL (17.66)**>**PEG (17.17)**>** PεDL (17.05)], the strength of drug-copolymer interaction will be the same and hence, not make a proper distinction between polymer segments. Therefore, solubility differences were then calculated for determination of Flory-Huggins interaction parameters. The solubility difference (Δ) results showed the lower value for PCL (4.47) compared to PεDL (6.30) indicated the higher compatibility of the drug with PCL core. These results were also confirmed by determining interaction parameter (χ_{sp}). The PCL (χ_{sp} = 1.85) was found to have higher compatibility compared to PεDL (χ_{sp} = 3.68) and mPEG (χ_{sp} = 3.39). Theoretically, these values indicate that more drugs should encapsulate within the micelles with PCL core compared to PεDL core. Conversely, the indomethacin loading study revealed an overall higher loading in PεDL core (6.55 wt%) compared to PCL core (5.39 wt%). However, the comparison of indomethacin loading on the basis of per unit volume of the micelles revealed that the semicrystalline PCL cored micelle (mPEG-b-PCL) was able to load 1.5 times more compared to the amorphous PεDL cored micelle (mPEG-b-PεDL). This result illustrated the higher compatibility of the indomethacin with PCL core which obtained in

accordance with the solubility parameter calculations. It also demonstrated that the overall higher IND loading in PεDL core was obtained due to the amorphous nature of the core which increased the PεDL cored micelles volume by 1.81 times compared to the PCL cored micelles. This conclusion was also reinforced by a recent literature report where the core crystallinity of the PCL block was reduced by the incorporation of medium chain triglyceride (MCT) to enhance the loading of disulfiram (DSF), cabazitaxel (CTX), and TM-2 (a taxane derivative).[43]

The higher compatibility of the PCL core with indomethacin compared to the PεDL core suggested a slower release of drug from the mPEG-b-PCL micelles, and this was indeed observed in indomethacin release profiles. Also, the release can also be explained by the fact that PCL cores were expected to be semicrystalline hence less mobile to allow drug transport compared to amorphous PεDL core as explained earlier. The mPEG block, which was a common segment for both of the copolymers, showed a low interaction parameter value mPEG (χ_{sp} = 3.39). This also suggested compatibility between indomethacin and PEG. Although in micellar formulations the mPEG block would remain in the aqueous phase as a hydrated form, and hence have high energy costs for the drug to displace water and associate with it. The interaction parameters predicted from Flory-Huggins theory nevertheless suggested a binding possibility. The burst release in the first 6 h from micelles might be due to the loose interaction of

the indomethacin with mPEG at core-corona interface. Thus it might be expected that drug molecules might not only be in the core but also at the core-corona interface, and the association of indomethacin with micelles in the indomethacin transport studies with pre-formed empty micelles gave partial backing for this assertion.

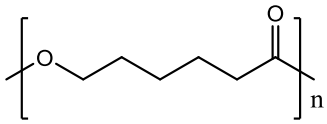
6.5 Conclusions

The drug delivery potential for the mPEG-b-PεDL micelles was evaluated and compared with mPEG-b-PCL micelles. We showed that the copolymers self-assemble in water to give non-aggregated nanosized micelles with amorphous (mPEG-b-PDL) and semicrystalline (mPEG-b-PCL) cores. The amorphous (PDL) core resulted in increased drug loading due to increased core volume. However, the determination of loading in term of per unit volume of the core illustrated the higher loading in PCL core which was in accordance with the Flory-Huggins interaction parameter. A sustained release pattern was also demonstrated by PDL core based micelles. However, a faster release form PDL core compared to PCL core illustrated the effect of core crystallinity on release properties. Therefore, the higher indomethacin loading and small size with sustained release characteristics of the mPEG-b-PDL micelles demonstrate the potential of the system to be used as a delivery vehicle.

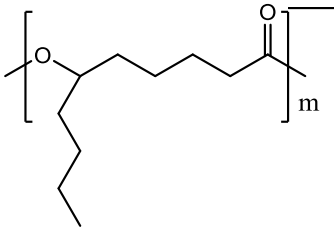
6.6 Appendix

Stepwise calculations for determination of solubility parameters of polymer segments and drug

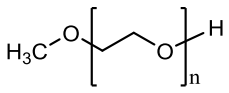
PCL Polymer

Fragments	Frequency	V^a ($cm^3\ mol^{-1}$)	Hansen solubility parameter[b]					
			F_d ($J^{1/2}\ cm^{3/2}\ mol^{-1}$)		$F_p{}^2$ ($J^{1/2}\ cm^{3/2}\ mol^{-1}$)		E_h ($J\ mol^{-1}$)	
COO	1	1x18	1x390	390	$(1x490)^2$	240100	1x7000	7000
CH_2	5	5x16.1	5x270	1350	$(5x0)^2$	0	5x0	0
		98.5		1740		240100		7000
			$\delta_d = F_d/V$		$\delta_p = (F_{pi}{}^2)^{1/2}/V)$		$\delta_h = (E_h/V)^{1/2}$	
			$\delta_d = (1740/98.5)$		$\delta_p = (240100)^{1/2}/98.5)$		$\delta_h = (7000/98.5)^{1/2}$	
			17.66 $MPa^{1/2}$		4.97 $MPa^{1/2}$		8.42 $MPa^{1/2}$	
			$\delta_T = (\delta_d{}^2+\delta_p{}^2+\delta_h{}^2)^{1/2}$		$(17.66^2+4.97^2+8.42^2)^{1/2}$		20.18 $MPa^{1/2}$	

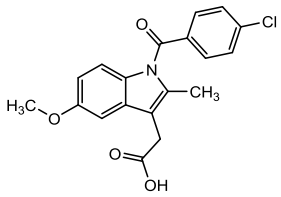
PεDL Polymer

Fragments	Frequency	V^a ($cm^3\ mol^{-1}$)	Hansen solubility parameter[b]					
			F_d ($J^{1/2}\ cm^{3/2}\ mol^{-1}$)		$F^2{}_p$ ($J^{1/2}\ cm^{3/2}\ mol^{-1}$)		E_h ($J\ mol^{-1}$)	
COO	1	18	1x390	390	$(1x490)^2$	240100	1x7000	7000
CH	1	-1	1x84	84	$(1x0)^2$	0	1x0	0
CH_2	7	7X16.1= 112.7	7x270	1890	$(7x0)^2$	0	7x0	0
CH_3	1	33.5	1x420	420	$(1x0)^2$	0	1x0	0
		163.2		2784		240100		7000
			$\delta_d = \sum F_d/V$		$\delta_p = (\sum F^2{}_p)^{1/2}/V)$		$\delta_h = (\sum E_h/V)^{1/2}$	
			$\delta_d = (2784/163.2)$		$\delta_p = (240100)^{1/2}/163.2)$		$\delta_h = (7000/163.2)^{1/2}$	
			17.05 $MPa^{1/2}$		3.00 $MPa^{1/2}$		6.54 $MPa^{1/2}$	
			$\delta_T = (\delta_d{}^2+\delta_p{}^2+\delta_h{}^2)^{1/2}$		$(17.05^2+3.00^2+6.54^2)^{1/2}$		18.5 $MPa^{1/2}$	

PEG Polymer

Fragments	Frequency	V^a ($cm^3\ mol^{-1}$)	Hansen solubility parameter[b]					
			F_d ($J^{1/2}\ cm^{3/2}\ mol^{-1}$)		$F^2{}_p$ ($J^{1/2}\ cm^{3/2}\ mol^{-1}$)		E_h ($J\ mol^{-1}$)	
O	1	1X3.8	1X100	100	$1X(400)^2$	160000	1X3000	3000
CH_2	2	2X16.1	2X270	540	$2X(0)^2$	0	2X0	0
		36.0		640		160000		3000
			$\delta_d = \sum F_d/V$		$\delta_p = (\sum F^2{}_p)^{1/2}/V)$		$\delta_h = (\sum E_h/V)^{1/2}$	
			$\delta_d = (640/36.0)$		$\delta_p = (160000)^{1/2}/36.0)$		$\delta_h = (3000/36.0)^{1/2}$	
			17.77 $MPa^{1/2}$		11.11 $MPa^{1/2}$		9.12 $MPa^{1/2}$	
			$\delta_T = (\delta_d{}^2+\delta_p{}^2+\delta_h{}^2)^{1/2}$		$(17.77^2+11.11^2+9.12^2)^{1/2}$		22.85 $MPa^{1/2}$	

Indomethacin

Fragments	Frequency	V[a] (cm^3 mol^{-1})	Hansen solubility parameter[b]					
			F_d ($J^{1/2}$ $cm^{3/2}$ mol^{-1})		F^2_p($J^{1/2}$ $cm^{3/2}$ mol^{-1})		E_h (J mol^{-1})	
Cl	1	1X24.0	1X450	450	$1X(550)^2$	302500	1X400	400
N	1	1X5.0	1X20	20	$1X(800)^2$	640000	1X5000	5000
O	1	1X3.8	1X100	100	$1X(400)^2$	160000	1X3000	3000
C=O	1	1X10.8	1X290	290	$1X(770)^2$	592900	1X2000	2000
COOH	1	1X28.5	1X530	530	$1X(420)^2$	176400	1X10000	10000
CH_3	2	2X33.5	2X420	840	$2X(0)^2$	0	2X0	0
CH_2	1	1X16.1	1X270	270	$1X(0)^2$	0	1X0	0
›C=	2	2X-5.5	2X70	140	$2X(0)^2$	0	2X0	0
Disubstituted phenyl ring	1	1X52.4	1X1270	1270	$1X(110)^2$	12100	1X0	0
Trisubstituted phenyl ring	1	1X33.4	1X1110	1110	$1X(110)^2$	12100	1X0	0
		230.0		5020		1896000		20400
			$\delta_d = \sum F_d / V$		$\delta_p = (\sum F^2_p)^{1/2} / V)$		$\delta_h = (\sum E_h / V)^{1/2}$	
			$\delta_d = (5020/230.0)$		$\delta_p = (1896000)^{1/2}/230.0)$		$\delta_h = (20400/230.0)^{1/2}$	
			21.8 $MPa^{1/2}$		6.0 $MPa^{1/2}$		9.4 $MPa^{1/2}$	
			$\delta_T = (\delta_d^2+\delta_p^2+\delta_h^2)^{1/2}$		$(21.8^2+6.0^2+9.4^2)^{1/2}$		24.5 $MPa^{1/2}$	

[a] Calculated from values reported by Fedors[36]
[b] Calculated from values and procedures described by Barton[40]

6.7 References

1. C. Rupp, H. Steckel and B. W. Mueller, *International Journal of Pharmaceutics*, 2010, **395**, 272-280.
2. Y. Lu and K. Park, *International Journal of Pharmaceutics*, 2013, **453**, 198-214.
3. G. Gaucher, M. H. Dufresne, V. P. Sant, N. Kang, D. Maysinger and J. C. Leroux, *Journal of Controlled Release*, 2005, **109**, 169-188.
4. M. L. Adams, A. Lavasanifar and G. S. Kwon, *Journal of Pharmaceutical Sciences*, 2003, **92**, 1343-1355.
5. H. M. Aliabadi, A. Mahmud, A. D. Sharifabadi and A. Lavasanifar, *Journal of Controlled Release*, 2005, **104**, 301-311.
6. H. M. Aliabadi, D. R. Brocks and A. Lavasanifar, *Biomaterials*, 2005, **26**, 7251-7259.
7. H. M. Aliabadi and A. Lavasanifar, *Expert opinion on drug delivery*, 2006, **3**, 139-162.
8. H. M. Aliabadi, D. R. Brocks, P. Mahdipoor and A. Lavasanifar, *Journal of Controlled Release*, 2007, **122**, 63-70.

9. B. A. Clements, J. Bai, C. Kucharski, L. L. Farrell, A. Lavasanifar, B. Ritchie, A. Ghahary and H. Uludag, *Biomacromolecules*, 2006, **7**, 1481-1488.
10. A. Mahmud and A. Lavasanifar, *Colloids and Surfaces B-Biointerfaces*, 2005, **45**, 82-89.
11. K. Letchford and H. Burt, *European Journal of Pharmaceutics and Biopharmaceutics*, 2007, **65**, 259-269.
12. X.-B. Xiong and A. Lavasanifar, in *Intracellular Delivery: Fundamentals and Applications*, ed. A. Prokop, 2011, vol. 5, pp. 251-289.
13. S. Elhasi, R. Astaneh and A. Lavasanifar, *European Journal of Pharmaceutics and Biopharmaceutics*, 2007, **65**, 406-413.
14. M. C. Jones and J. C. Leroux, *European Journal of Pharmaceutics and Biopharmaceutics*, 1999, **48**, 101-111.
15. X.-B. Xiong, Z. Binkhathlan, O. Molavi and A. Lavasanifar, *Acta Biomaterialia*, 2012, **8**, 2017-2033.
16. X.-B. Xiong, H. Uludag and A. Lavasanifar, *Engineering of Amphiphilic Block Copolymers for Drug and Gene Delivery*, 2009.
17. S. B. La, T. Okano and K. Kataoka, *Journal of Pharmaceutical Sciences*, 1996, **85**, 85-90.
18. I. L. G. Shin, S. Y. Kim, Y. M. Lee, C. S. Cho and Y. K. Sung, *Journal of Controlled Release*, 1998, **51**, 1-11.
19. Z. Song, R. Feng, M. Sun, C. Guo, Y. Gao, L. Li and G. Zhai, *Journal of Colloid and Interface Science*, 2011, **354**, 116-123.
20. H. S. Yoo and T. G. Park, *Journal of Controlled Release*, 2001, **70**, 63-70.
21. C. Allen, D. Maysinger and A. Eisenberg, *Colloids and Surfaces B-Biointerfaces*, 1999, **16**, 3-27.
22. A. Mahmud, S. Patel, O. Molavi, P. Choi, J. Samuel and A. Lavasanifar, *Biomacromolecules*, 2009, **10**, 471-478.
23. J. P. L. Dwan'Isa, L. Rouxhet, V. Preat, M. E. Brewster and A. Arien, *Pharmazie*, 2007, **62**, 499-504.
24. C. Yang, A. B. E. Attia, J. P. K. Tan, X. Ke, S. Gao, J. L. Hedrick and Y.-Y. Yang, *Biomaterials*, 2012, **33**, 2971-2979.
25. A. Lavasanifar, J. Samuel and G. S. Kwon, *Advanced Drug Delivery Reviews*, 2002, **54**, 169-190.
26. A. Lavasanifar, J. Samuel, S. Sattari and G. S. Kwon, *Pharmaceutical Research*, 2002, **19**, 418-422.
27. N. Nishiyama, Y. Kato, Y. Sugiyama and K. Kataoka, *Pharmaceutical Research*, 2001, **18**, 1035-1041.
28. M. Yokoyama, S. Fukushima, R. Uehara, K. Okamoto, K. Kataoka, Y. Sakurai and T. Okano, *Journal of Controlled Release*, 1998, **50**, 79-92.
29. K. Kataoka, T. Matsumoto, M. Yokoyama, T. Okano, Y. Sakurai, S. Fukushima, K. Okamoto and G. S. Kwon, *Journal of Controlled Release*, 2000, **64**, 143-153.

30. F. Gadelle, W. J. Koros and R. S. Schechter, *Macromolecules*, 1995, **28**, 4883-4892.
31. R. Nagarajan, M. Barry and E. Ruckenstein, *Langmuir*, 1986, **2**, 210-215.
32. P. J. Marsac, S. L. Shamblin and L. S. Taylor, *Pharmaceutical Research*, 2006, **23**, 2417-2426.
33. K. K. Bansal, D. Kakde, L. Purdie, D. J. Irvine, S. M. Howdle, G. Mantovani and C. Alexander, *Polymer Chemistry*, 2015, **6**, 7196-7210.
34. D. VanKrevelen, *Properties of polymers: their estimation and correlation with chemical structure*, Elsevier, Amsterdam, 1990.
35. A. Barton, *Handbook of Solubility Parameters and Other Cohesion Parameters*, CRC Press, Boca Raton, Florida, 2nd ed edn., 1991.
36. R. F. Fedors, *Polymer Engineering and Science*, 1974, **14**, 147-154.
37. V. P. Sant, D. Smith and J.-C. Leroux, *Journal of Controlled Release*, 2004, **97**, 301-312.
38. M. Gou, K. Men, H. Shi, M. Xiang, J. Zhang, J. Song, J. Long, Y. Wan, F. Luo, X. Zhao and Z. Qian, *Nanoscale*, 2011, **3**, 1558-1567.
39. S. Y. Kim, I. L. G. Shin, Y. M. Lee, C. S. Cho and Y. K. Sung, *Journal of Controlled Release*, 1998, **51**, 13-22.
40. *Textile Research Journal*, 1984, **54**, 138-138.
41. I. Y. Perevyazko, A. Vollrath, C. Pietsch, S. Schubert, G. M. Pavlov and U. S. Schubert, *Journal of Polymer Science Part a-Polymer Chemistry*, 2012, **50**, 2906-2913.
42. B. Kuldeep, K. Deepak, P. Laura, I. Derek, H. Steven, M. Giuseppe and A. Cameron, *Journal*, 2015, **6**, 7196-7210.
43. J. Gou, S. Feng, H. Xu, G. Fang, Y. Chao, Y. Zhang, H. Xu and X. Tang, *Biomacromolecules*, 2015, **16**, 2920-2929.

Chapter

7

Conclusions and Future Work

7.1 Conclusions

In the present thesis, polyesters were synthesized by polycondensation and ring opening polymerizations. The synthesized polymers were characterized and evaluated for properties important for commercial and biomedical applications.

In chapter three, the synthesis of polyester polymers was described by melt polycondensation methods. The effect of phenyl content on polymer properties (e.g. crystallinity) and nanoparticle properties (e.g. size, dye loading) was evaluated and it can be concluded that increasing the phenyl content in the polymer changed its properties from semi-crystalline to amorphous. The dye loading of the polymer was also dependent on the phenyl content of polymer. In addition, the study also provided the information about the stability and degradability of the P02 (Pluronic coated and uncoated) nanoparticles. The low cellular toxicity and efficient cell uptake were advantages found with the selected polymer (P02 polymer). However, the high polydispersity of the polymers, the use of non-renewable monomer, tedious method of synthesis and the overall low loading of the dye directed us to use more efficient ring opening polymerizations of renewable ε-decalactone monomers to generate polyesters for potential biomedical applications.

Chapter 4 described the ring opening polymerization (ROP) of renewable decalactone monomers (ε-DL and δ-DL) by conventional heating (CH) methods using mPEG initiator in conjunction with TBD as an organic catalyst to replace $Sn(Oct)_2$. The copolymer of non-renewable ε-CL was also synthesized for a proper comparison. The TBD route showed efficient catalytic activity compared to $Sn(Oct)_2$.The study also suggested that the alkyl chain of the decalactone reduced the polymerization rate. Moreover, a significant difference in the reaction temperature was observed for seven membered ε-DL monomer (120 ^oC) compared to six membered δ-DL monomer (50 ^oC) confirming the effect of ring size on polymerization.

Chapter 5 described the improvement in ε-DL polymerization by utilizing MROP reactions to replace conventional ROP. The dielectric measurements of the reagents indicated that all the reaction materials absorbed microwaves at the selected reaction temperature of 120 ^oC. Microwave based ROP reduced the polymerization time of ε-DL by half compared to conventional hot plate ROP method. The data also demonstrated that the copolymers were able to self-assemble into water to give micelles with amorphous (mPEG-b-PεDL) and semicrystalline cores (mPEG-b-PCL). A higher thermodynamic and kinetic stability was confirmed by lower CMC and smaller size of the mPEG-b-PεDL micelles. The synthesized mPEG-b-PεDL copolymer micelles also showed a lower toxicity and time dependent uptake

into C3A cells which demonstrated the potential of the copolymer for future drug delivery applications.

A preliminary drug delivery investigation of the mPEG-b-PεDL copolymer micelles was described in chapter 6. Indomethacin (IND) was chosen as a model drug, and it was found that an overall higher loading by wt % of IND occurred in the amorphous core of mPEG-b-PεDL copolymer micelles compared to mPEG-b-PCL copolymer micelles. However, estimation of the IND loading per unit core volume of the micelles suggested that the PCL core was able to load 3.57 times more compared to the PεDL core which was consistent with predicted Flory-Huggins interaction parameters. It is likely that the overall higher IND loading in PεDL core was obtained due to the amorphous nature of the PεDL regions which increased the interior volume by 1.81 times compared to the PCL core. The sustained release pattern obtained from mPEG-b-PεDL copolymer micelles along with the higher loading suggesting the possible utility of the synthesized copolymer in the biomedical field.

7.2 Future Work

The work presented in the thesis provides useful preliminary data for the novel polymers. Future work might include the following points:

- The ROP of decalactones with different sizes is required to understand the effect of size and alkyl chains on reaction kinetics and polymer properties.
- Improvements in the MROP synthesis method is needed to establish by controlling the process parameters in pilot scale production to ensure the widespread use of MW based polymerization technology.
- One polymer cannot be used for all drugs for drug loading. For instance, a huge difference in the loading was observed for coumarin 6 dye (0.33 wt%) compared to indomethacin (6.55 wt%) in mPEG-b-PεDL micelles. Hence, the drug delivery aspects of the poly(decalactone) copolymers needs to be explored with other hydrophobic drugs to establish the copolymer as a delivery vehicle.
- Full degradation profiles of the poly(decalactone) copolymers are required prior to *in vitro* and *in vivo* studies.
- The uptake mechanisms and polymer toxicity profiles are required in a range of human cell lines for better understanding of the delivery vehicle.
- Finally, the potential of the poly(decalactone) copolymers is needed to established by performing *in vivo* study particularly the bio-distribution study on tumor (KB cells induced) bearing athymic mice models by injecting micelles formulation (anticancer drug loaded) with or without tagged folic acid (FA) ligand.